Contract No. DA-36-039-SC-78902

TIROS I METEOROLOGICAL SATELLITE SYSTEM

FINAL COMPREHENSIVE TECHNICAL REPORT

Volume I

Prepared for the

U.S. ARMY SIGNAL RESEARCH AND DEVELOPMENT LABORATORY

FORT MONMOUTH, N. J.

and the

NATIONAL AERONAUTICS AND SPACE ADMINISTRATION

WASHINGTON, D. C.

ASTRO-ELECTRONICS DIVISION
DEFENSE ELECTRONIC PRODUCTS
RADIO CORPORATION OF AMERICA
PRINCETON, N. J.

AED-339

Issued July 1, 1961

PREFACE

This Final Comprehensive Technical Report on the TIROS I Meteorological Satellite System includes, within practical limits, detailed discussions of the development, design, test, and operation of those portions of the system which were contracted to the Astro-Electronics Division of the Radio Corporation of America under Contract Number DA-36-039-sc-78902. These portions include the satellite, in its entirety, and the major part of the (ground based) Command and Data-Acquisition Stations.

Five identical satellites, and three essentially-similar sets of ground-station equipment were fabricated for the TIROS I project. However, specific units are discussed only where differences in handling, scheduling, or operation are of importance. Other discussions can be considered to apply to the No. D-3 satellite, which was placed into orbit on 1 April 1960.

Volumes of data were taken during the design and environmental test periods; only typical and most significant data are reproduced here because of space limitations.

A bibliography of technical reports and other publications which contain more detailed and supporting information, is given at the end of this report.

* *

The TIROS Exploratory Meteorological (Experimental) Program came into being as a result of the efforts of the Ad Hoc Committee on Meteorology, set up in June 1958, by the Advanced Research Projects Agency (ARPA) to plan a meteorological satellite program. This committee included, among many specialists, representatives from Rand Corporation, Army Ballistic Missile Agency, Office of Naval Research, U.S. Army Signal Research and Development Laboratory, National Advisory Committee for Aeronautics, Air Force Cambridge Research Center, U.S. Weather Bureau, University of Wisconsin, and the Astro-Electronics Division of RCA.

The RCA-TIROS I Project was one phase of the over-all Program, which, in April 1959, came under the management of the National Aeronautics and Space Agency. Technical direction to this project was given to the U.S. Army Signal Research and Development Laboratory.

Other organizations which cooperated in the systems concepts, and, later, in system operation, include the U.S. Weather Bureau; Air Force Cambridge Research Center, and its consultant, Allied Research Associates; Air Weather Service; U.S. Navy Research Weather Facility; the U.S. Naval Photo-Interpretation Center; the U.S. Signal Corps; the U.S. Air Force Ballistic Missile Division; Space Technology Laboratories; and Douglas Aircraft Company.

CONTENTS

VOLUME I

Section		Page
Preface		iii
	PART 1. INTRODUCTION	
I	Background of the TIROS Program	I-1
II	System Implementation	II-1
	PART 2. DEVELOPMENT AND DESIGN	
I	System Studies	I-1
	A. General Studies	I-1
	B. Launch and Orbit Considerations	I-7
	1. Introduction	I-7
	2. Photocoverage Analysis	I-7
	a. Limitations of Photocoverage	I-7
	b. Initial Analysis	I-10
	c. Detailed Pre-launch Analysis	I-10
	3. Satellite Orientation with Respect to the Sun	I-17
	a. Sun Angle	I-17
	b. Fraction of Time in the Sun	I-18
	4. Adjustment of Launch Time to Obtain Optimum Photocoverage	I-19
	a. Calculation of Launch Time vs. $\Delta\phi$	I-19
	b. Establishment of Optimum $\Delta\phi$ and Launch Time Tolerance	I-22
	5. Contact Time Between the Satellite and Ground Stations	I-23

CONTENTS (Continued)

Section		Page
	6. Accessibility of Various Ground Areas for Remote Picture-taking	I-25
	7. Actual Orbit Achieved	I-26
	C. Satellite-Ground Communication	I-28
	1. General Considerations	I-28
	2. Selection of Transmission Parameters	I-29
	3. Definition of Symbols	I-29
	4. TV Subsystem Propagation	I-30
	5. Beacon Subsystem Propagation	I-31
	6. Command Subsystem Propagation	I-31
II	Analysis of Environmental Effects	II-1
	A. Thermal Considerations	II-1
	B. Dynamics Considerations	II-2
	1. General	II-2
	a. Sun-Follower	II-3
	b. Change of the Moment of Inertia	II-3
	c. Slow-Down of the Camera Assembly Only	II-3
	C. Optical Considerations	II-5
III	Component Design	III-1
	A. Satellite Components	III-1
	1. Standardization and Reliability	III-1
	2. TV Picture Subsystem	III-2
	a. General	III-2
	b. Functional Description	III-3
	(1) TV Cameras	III-4
	(2) Magnetic Tape Recorder	III-24
	(3) TV Transmitters	III-38
	(4) Command Receivers	III-43
	(5) Programming and Control System	III-44
	3. The Telemetry and Tracking Subsystem	III-44

CONTENTS (Continued)

Section		Page
	a. General	III-44
	b. Functional Description	III-44
	c. Telemetry Sensors	III-44
	(1) General	III-44
	(2) Development	III-47
	(3) Testing of the Temperature Sensor	III-48
	(4) Sensor Evaluation	III-49
	d. Telemetry Switch	III-49
	(1) General	III-49
	(2) Functional Description	III-49
	e. Beacon Transmitter (Subcarrier Oscillator Section)	III-51
	(1) General	III-51
	(2) Functional Description	III-52
	f. Beacon Transmitter (R-F Section)	III-54
4.	Reference Indicator Subsystems	III-54
	a. North Indicator	III-54
	(1) General	III-54
	(2) Sun-Sensor Electronics	III-55
	(3) Sun Sensors	III-65
	b. Attitude Indicator	III-72
	(1) General	III-72
	(2) Basic Requirements	III-73
	(3) Development	III-73
	(4) Subsystem Design	III-76
	(5) Tests	III-78
	(6) Evaluation	III-81
5.	Electrical Power Supply Subsystem	III-83
	a. General	III-83
	b. Development of Subsystem Concepts	III-83
	c. Power - Source Specifications	III-88

CONTENTS (Continued)

Section		Page
	(1) Solar Cells	III-88
	(2) Storage Cells	III-91
d.	Voltage Regulator Specifications	III-93
e.	Solar-Array Power-Availability Studies	III-93
	(1) Total Energy Calculation	III-93
	(2) Spectral Transmission Loss Resulting from Glass Cover and Coating	III-96
	(3) Power Loss Caused by Diodes	III-96
	(4) Series-Paralleling Losses	III-97
	(5) Micrometeorite Bombardment Effects	III-98
	(6) Effects of Temperature and Storage-Battery Voltage Variations	III-98
	(7) Deterioration of Output Power with Increasing Temperature	III-98
	(8) Energy Transfer Efficiency	III-99
f.	Development of Protection Circuits	III-100
	(1) General	III-100
	(2) Regulators	III-105
	(3) Load Protection Fuses	III-111
g.	Final Design	III-111
h.	Storage-Battery Procurement and Evaluation	III-112
	(1) General	III-112
	(2) Comprehensive Storage Battery Test Program	III-119
i.	Solar-Cell Test Program	III-126
	(1) Physical Inspection	III-126
	(2) Electrical Tests	III-127
	(3) Assembly and Light Tests	III-128
	(4) Final Test	III-130
	VOLUME II	
6.	Antenna Subsystem	III-145
a.	General	III-145
b.	Functional Description	III-145
c.	Development	III-145

CONTENTS (Continued)

Section		Page
	(1) Initial Development	III-145
	(2) Transmitting Antennas and R-F Coupling Matching Networks	III-149
	(3) Antenna for Command Receiver	III-169
	d. Tests	III-170
	(1) Final Radiation Pattern Measurements on Full-Scale Model	III-170
7.	Dynamics Control	III-176
	a. Introduction	III-176
	b. The Precession Damping Mechanism	III-176
	(1) Design Analysis	III-179
	(2) Experimental Results	III-179
	(3) Comparison of Experimental Versus Analytical Results	III-189
	(4) Functional Description	III-190
	c. The Despin (Yo-Yo) Mechanism	III-191
	(1) Design Analysis	III-191
	(2) Functional Description	III-192
	d. The Spin-Up Rockets	III-193
	(1) Rocket Design	III-194
	(2) Rocket Test Requirements	III-196
	(3) Rocket Test Results	III-196
	(4) Functional Description	III-197
8.	Satellite Structure	III-198
	a. General	III-198
	b. Design Criteria	III-198
	c. Design Details	III-201
	d. Vibration Analysis	III-207
	e. Test	III-207
	(1) Static Loading Test	III-209
	(2) Dynamic Vibration Test	III-213

CONTENTS (Continued)

Section		Page
9.	Thermal Design	III-214
a.	General	III-214
b.	Analysis of the Heat Flow Problem	III-214
(1)	Thermal Sources	III-214
(2)	Radiation Input	III-215
(3)	Thermal Response of the Satellite	III-215
(4)	Thermal Energy Equations	III-217
c.	Development of Suitable Surfaces and Surface Coating	III-222
d.	Experimental Verification of Thermal Design	III-226
e.	Actual Determination of Satellite Temperature	III-227
10.	Integration of Satellite Components	III-228
a.	Subsystem Integration Problems	III-228
b.	Mechanical Integration	III-228
B.	Ground Station Components	III-230
1.	Introduction	III-230
2.	Functional Description	III-231
3.	Physical Configuration	III-233
4.	The Satellite Command and Control Equipment	III-234
a.	General	III-234
b.	Functional Operation	III-235
c.	Master Clock	III-238
(1)	General	III-238
(2)	Functional Description	III-239
d.	Control Tone Generator	III-239
e.	Remote Picture Time Set	III-239
f.	Antenna Programmer	III-239
(1)	General	III-239
(2)	Functional Description	III-241
g.	Program Selector and Power Control Unit	III-243
h.	Relay Power Supply	III-243

CONTENTS (Continued)

Section		Page
	(1) General	III-243
	(2) Functional Description	III-244
	i. Command Transmitter and Transmitter Control Panel	III-244
	j. Command Programmer	III-248
	(1) General	III-248
	(2) Functional Description	III-250
	k. Clock Set-Pulse Demodulator	III-252
	(1) General	III-252
	(2) Functional Description	III-253
5.	Data Receiving Components	III-255
	a. Introduction	III-255
	b. TV Receivers	III-255
	c. Beacon and Telemetry Receivers	III-255
	d. Diversity Combiners	III-256
	(1) General	III-256
	(2) Functional Description	III-256
6.	Data Processing and Display Components	III-258
	a. General	III-258
	b. Functional Description	III-259
	c. Display and Video Amplifier	III-261
	(1) General	III-261
	(2) Functional Description	III-263
	d. Sawtooth Generator and Deflection Amplifier	III-264
	(1) General	III-264
	(2) Functional Description	III-268
	e. Horizontal Sync Separator	III-268
	(1) General	III-268
	(2) Functional Description	III-270

CONTENTS (Continued)

Section		Page
	f. TV - FM Demodulator	III-272
	(1) General	III-272
	(2) Functional Description	III-273
	g. Tape and Computer Control	III-274
	(1) General	III-274
	(2) Functional Description	III-275
	h. Monitor Control	III-278
	i. Sun-Angle Computer	III-278
	(1) General	III-278
	(2) Functional Description	III-281
	j. Calibrator	III-286
	(1) General	III-286
	(2) Functional Description	III-291
	k. Attitude Pulse Demodulator	III-296
	(1) General	III-296
	(2) Functional Description	III-296
	l. Elapsed Time Counter - Scanner	III-299
	(1) General	III-299
	(2) Functional Description	III-301
	7. Ground Station Antenna System	III-303
	8. Tape Recorders	III-303
	9. Events Recorder	III-304
	a. General	III-304
	b. Functional Description	III-304
C.	Satellite Checkout Equipment	III-304
	1. Introduction	III-304
	2. Development and Design	III-304

CONTENTS (Continued)

Section		Page
	3. Functional Description	III-305
	4. Operational Checks for the TIROS I Satellite	III-306
	5. Checks Made on the Go, No-Go Equipment	III-307
	6. Antennas and R-F Propagation	III-307
	D. The Image Enhancement Console	III-308
	1. Introduction	III-308
	2. Equipment Design	III-308
	a. General	III-308
	b. Image Enhancement Console	III-309
	(1) Mechanical Construction	III-309
	(2) Optics and Electronics	III-312
	c. The TIROS Tape Readout Equipment	III-317
	(1) The Tape Loop	III-317
	(2) Peripheral Equipment (Record Mode)	III-318
	(3) Peripheral Equipment (Playback Mode)	III-318

VOLUME III

PART 3. TESTS

I	Test Philosophy	I-1
II	Subsystem Tests	II-1
	A. Component Tests	II-1
	B. Satellite Subsystem Tests	II-2
	1. Specific-Performance-Evaluation Tests	II-2
	a. Despin Tests	II-2
	b. Antenna Pattern Measurements	II-7
	c. Camera Light Threshold Measurements	II-7
	d. Solar Cells and Battery Tests	II-7

CONTENTS (Continued)

Section			Page
		e. Magnetic Field Tests	II-8
		f. Structural Loading Tests	II-8
		g. Thermal Tests	II-8
	2.	Environmental Test	II-10
		a. Philosophy	II-10
		(1) Prototype Satellite - Component Test	II-11
		(2) Prototype Satellite Tests	II-11
		(3) Flight Satellite Component Tests	II-11
		(4) Flight Satellite Test	II-11
		b. Equipment and Performance Evaluation	II-11
III	System Tests		III-1
	A.	Satellite System Tests	III-1
	1.	Qualification Tests	III-1
	2.	Standard Performance-Evaluation Test Philosophy	III-2
	3.	Vibration Test	III-2
		a. General	III-2
		b. Structure Vibration Test	III-2
		(1) Method of Testing	III-2
		(2) Procedure	III-3
		c. Satellite Vibration Test	III-4
		(1) Equipment	III-4
		(2) Procedure	III-7
	4.	Final Check before Shipment to Cape Canaveral	III-10
		a. General	III-10
		b. Alignment	III-10
		(1) Wide and Narrow-Angle Camera Systems	III-11
		(2) North Indicator System	III-15
		(3) Horizon Scanner	III-15
		(4) Balancing and Moment of Inertia	III-16

CONTENTS (Continued)

Section		Page
	5. Chronological History of the Satellites	III-23
	a. T-1/T-1A Prototype Satellite	III-23
	(1) Video Linearity Check	III-26
	(2) Power Supply Measurements	III-28
	b. T-2 Prototype Satellite	III-29
	c. D-1 Flight Model Satellite	III-34
	d. D-2 Flight Model Satellite	III-36
	e. D-3 Flight Model Satellite	III-36
	f. Test Program Results	III-38
	B. Ground Station System Tests	III-39
	PART 4. FIELD OPERATIONS	
I	Scope	I-1
II	Princeton Ground Station	II-1
III	Cape Canaveral Support	III-1
	A. Pre-Launch	III-1
	1. Introduction	III-1
	2. Satellite Preparation	III-2
	B. Launch	III-3
	C. Post-Launch	III-4
IV	Washington, D.C. Control Center	IV-1
	A. Introduction	IV-1
	B. Pre-Launch	IV-1
	C. Launch	IV-2
	D. Post-Launch	IV-2
V	Kaena Point (Hawaii)	V-1
	A. Introduction	V-1
	B. Equipment Installation	V-2

CONTENTS (Continued)

Section		Page
	C. Training	V-3
	D. Station Operation	V-4
VI	Fort Monmouth	VI-1
	A. Introduction	VI-1
	B. Training Program	VI-2
	PART 5. REFERENCES AND APPENDICES	
	References	1
	Bibliography	3
	Distribution List	7
Appendices	A. Calculation of Sun Angle and Fraction of Time in Sun for Circular Orbit	A-1
	B. Teletype Message from NASA Containing Orbital Data	B-1
	C. RCA-AED Environmental Test Specification (TSP-T1-100B)	C-1
	D. Theoretical Analysis of the Team Precession Damping Mechanism	D-1
	E. Stress Analysis, Lower Plate Assembly	E-1
	F. Analysis and Calculating to Prove Despin Air Drag	F-1
	G. Measurement of Ratio of Absorptivity of Sunlight to Thermal Emissivity	G-1
	H. Radiation Inputs to the TIROS I Satellite	H-1
	I. RCA-TIROS Specifications for Structure and Component Finishes, Including Solar Cell Coatings (SP-1000)	I-1
	J. Analysis and Calculations of Static and Dynamic Balance Requirements	J-1
	K. Analysis of Temperature-Sensing Circuits	K-1

LIST OF ILLUSTRATIONS

VOLUME I

Figure		Page
	PART 2. DEVELOPMENT AND DESIGN	
1	Characteristics of Breakdown Potential	I-1
2	Solar Spectrum	I-3
3	Radiation Belt	I-3
4	Co_{60} Radiation Test	I-4
5	Simulated Micrometeorite Bombardment	I-6
6	Simulated Micrometeorite Bombardment	I-6
7	Orbit of TIROS I Satellite and Its Effect on Photocoverage	I-8
8	Cross Section through Plane of Orbit	I-8
9	Narrow-Angle Camera Latitude Extent of Photocoverage versus Days after Launch with Distortion the Only Limiting Factors	I-12
10	Narrow-Angle Camera Latitude Extent of Photocoverage versus Days for a 1 April 1960 Launch with Distortion and 20 Degrees Solar Elevation the Limiting Factors	I-12
11	Wide-Angle Camera Latitude Extent of Photocoverage versus Days after a 1 April 1960 Launch	I-13
12	Narrow-Angle Camera Latitude Extent of Photocoverage versus Days after Launch with a 20 Degrees Change in Right Ascension of Sun from Normal Point ($\Delta\phi$)	I-13
13	Wide-Angle Camera Latitude Extent of Photocoverage versus Days for a 1 April 1960 Launch with Approximately 20 Degrees Change in Right Ascension of Sun from Normal Point ($\Delta\phi$)	I-15
14	Geometrical Limits of Latitude Extent of Photocoverage of Narrow-Angle (NA) and Wide-Angle (WA) Cameras versus Days after Launch	I-15
15	Portion of Orbit Useful for the Narrow-Angle and Wide-Angle Cameras Based on the Extent of the True Anomaly versus Days after Launch	I-16

LIST OF ILLUSTRATIONS (Continued)

Figure	Title	Page
16	Portion of Orbit Useful for the Narrow-Angle and Wide-Angle Cameras Based on the Extent of True Anomaly versus Days after Launch	I-16
17	Degrees of True Anomaly Per Minute of Flight versus Orbit Altitude	I-17
18	Alpha Angle between Sun Vector and Spin Axis for Various Days after 1 April 1960 Launch and Various Right Ascensions of Sun from Normal Point Angles ($\Delta\phi$)	I-18
19	Fraction of Time in Sun (Ψ) versus Days after Launch for 1 April 1960 Launch	I-19
20	Fraction of Time in the Sun (Ψ) for Various Orbit Altitudes	I-20
21	Period, Orbital Advance, and Orbits per Day versus Orbit Altitudes	I-21
22	Launch Time (GMT) versus Right Ascension of Sun from Normal Point($\Delta\phi$)for an East Longitude of Normal Point(ΨN)of 43.97 Degrees	I-22
23	Right Ascension of Sun from Normal Point($\Delta\phi$)and Launch Time versus Day of Launch and the Earlier Launch (Minutes after 0500 EST) versus Date of Launch	I-23
24	Ground Contact Time versus Longitude of Ascending Node	I-24
25	Availability of Ground Areas for Photocoverage, TIROS I	III-131
26	Observed Motion of the TIROS I Spin Vector	I-27
27	Angle Alpha versus Days after Launch	I-28
28	TV Picture Subsystem, Block Diagram	III-3
29	Wide-Angle TV Camera and Associated Electronics Package	III-4

LIST OF ILLUSTRATIONS (Continued)

Figure	Title	Page
30	TV Camera System, Block Diagram	III-5
31	TV Camera System, Schematic Diagram	III-133
32	Waveforms, TV Camera Electronic Circuits	III-135
33	Auxiliary Sync Generator, Schematic Diagram	III-137
34	Tape Transport	III-25
35	Magnetic Tape Recorder, Block Diagram	III-26
36	Decoupling Circuit, Schematic Diagram	III-31
37	Essential Parts of the Tape-Transport Mechanism	III-31
38	Recorder Motor Power Supply, Schematic Diagram	III-34
39	Recorder Delay and Power Converter, Schematic Diagram	III-34
40	Video Modulator and Head-Drive Amplifier, Schematic Diagram	III-35
41	Video Amplifier and Mixer, Schematic Diagram	III-35
42	Sun Position Gate and 10-kc Oscillator, Schematic Diagram	III-36
43	Sun Position Playback Amplifier and Head-Drive Amplifier, Schematic Diagram	III-37
44	Optimum Frequency Response of Record Heads	III-37
45	Video Modulator Linearity Curve	III-39
46	Video Playback Amplifier Response Curve	III-39
47	Playback Amplifier Temperature Characteristics	III-39
48	TV Transmitter, Schematic Diagram	III-139
49	The Telemetry and Tracking Subsystem, Block Diagram	III-45

LIST OF ILLUSTRATIONS (Continued)

Figure	Title	Page
50	Response Speed of Test Thermistor in Vacuum	III-48
51	Telemetering Switch with Drive and Voltage Reference Circuitry, Schematic Diagram	III-50
52	Voltage Dependence of SCO Input Due to SCO Input Parameters	III-52
53	30-mw Transmitter and Subcarrier Oscillator, Schematic Diagram	III-53
54	Sun-Sensor Unit Locations on Satellite Baseplate	III-56
55	Sun-Angle Data Chain, Block Diagram	III-56
56	Sun-Sensor and Electronics Pulse Shapes	III-58
57	Sun-Sensor Electronics, Block Diagram	III-60
58	Preamplifier, One-Shot Multivibrator and Summing Circuit, Schematic Diagram	III-62
59	Light-Beam Positions versus Output Waveforms (Nominal)	III-63
60	Sun-Sensor Input and Output Pulses	III-63
61	Satellite Coordinates	III-66
62	Sensor Alignment Requirements	III-67
63	Sun-Angle Sensor Orientation	III-67
64	Experimental Sun-Sensor Unit	III-68
65	Modified (coded) Solar Cell	III-69
66	Sun Sensor Housing, Exploded View	III-70
67	Sun Sensor Housing, Cutaway View	III-70
68	Attitude Indicator Data Chain, Block Diagram	III-72
69	Horizon Scanner, Block Diagram	III-76

LIST OF ILLUSTRATIONS (Continued)

Figure	Title	Page
70	Horizon-Scanner Filter, Schematic Diagram	III-76
71	Horizon Pulse Shaper, Schematic Diagram	III-77
72	Nominal Characteristics of Horizon-Pulse Shaper Output Pulse	III-78
73	Power Supply Subsystem, Block Diagram	III-84
74	Early Power Supply Circuit, Simplified, Schematic Diagram	III-86
75	Power Supply Circuit of Early 1960	III-87
76	Power Supply, Functional Block Diagram	III-88
77	TIROS I Satellite Showing Solar-Cell Location	III-94
78	Spin-Axis/Sun-Vector Relationship	III-95
79	Solar-Cell Interconnection, Block Diagram	III-97
80	Plot of Average Solar-Cell Temperatures	III-99
81	Plot of Energy Available to Load	III-101
82	Plot of Pre-Launch Alpha Variations	III-101
83	Plot of Pre-Launch Sigma Variations	III-102
84	Storage-Battery Fuse Circuit, Schematic Diagram	III-103
85	Storage-Battery Circuit with Diodes Added, Schematic Diagram	III-103
86	Fuse Board, Schematic Diagram	III-104
87	Battery Protection Circuits, Schematic Diagram	III-106
88	Charging-Current Limiter Circuit Configurations	III-107
89	Voltage Regulators, Block Diagram	III-109
90	Voltage Regulators, Schematic Diagram	III-110

LIST OF ILLUSTRATIONS (Continued)

Figure	Title	Page
91	Power Control Units, Schematic Diagram	III-141
92	Cut-Open View of F-Cell	III-114
93	Positions at which Storage Cells were Cut to Determine Connection Integrity	III-116
94	Location and Dimensions of Crimped Grooves	III-117
95	Solar-Cell Assembly Configurations	III-129
	VOLUME II	
96	R-F Coupling and Matching Network, Block Diagram	III-146
97	Plot of Scale-Model Impedance Measurements (108 Mc)	III-152
98	Scale-Model Impedance Measurements (235 Mc)	III-153
99 (a)	R-F Coupling and Matching Network, Schematic Diagram	III-157
(b)	R-F Coupling and Matching Networks	III-159
100	108-Mc Balun	III-163
101	108-Mc Diplexer	III-163
102	235-Mc Balun	III-163
103	235-Mc Diplexer	III-163
104	Dipole Transmitting Antenna Assembly	III-166
105	Comparison of Radiated-Field Components, 108 Mc (Actual Satellite)	III-172
106	Total-Power Radiation Pattern, 108 Mc (Actual Satellite)	III-172
107	Comparison of Total Power Radiation Pattern, 108 Mc (Actual Satellite versus Full-Scale Model)	III-173
108	Comparison of Total-Power Radiation Pattern, 108 Mc (Actual Satellite versus Full-Scale Model)	III-173
109	Comparison of Radiated-Field Components, 235 Mc (Full-Scale Model)	III-174

LIST OF ILLUSTRATIONS (Continued)

Figure	Title	Page
110	Total-Power Radiation Pattern, 235 Mc (Full-Scale Model)	III-174
111	Pattern Coordinate System	III-175
112	Yo-Yo Despin Mechanism	III-177
113	TEAM Precession Damping Mechanism: (a) Outlines of Details, and (b) Photograph	III-178
114	Spin-Up Rockets Mounted on TIROS I Baseplate	III-179
115	TEAM Precession Damping Mechanism Coordinate System	III-180
116	Friction Data for the TEAM Precession Damping Mechanism	III-185
117	TEAM Precession Damping Mechanism Test Equipment for Checking Analytical Design Derivations	III-187
118	Final Speed Ratio versus Total Despin Mass for Several Satellite Inertias	III-192
119	Yo-Yo Despin Mechanism (Hooks, Cable, and Attachments)	III-193
120	Installation of Payload Rocket	III-202
121	Baseplate Assembly	III-202
122	Structural Assembly	III-203
123	Results of Vibration Analysis	III-209
124	A TIROS I Housing in Place on the Structural Loading Test Fixture with the Strain Gage Instrumentation is Located on the Bench at the Right	III-210
125	Mass Distribution Plates on Satellite Baseplate	III-211
126	Mylar Pressure Bag	III-211
127	Steady-State Temperatures for a 100% Sun Orbit, with $\beta = 0$, as a Function of α which is the Angle between Satellite Spin Axis and the Sun Vector	III-221

LIST OF ILLUSTRATIONS (Continued)

Figure	Title	Page
128	Day-Night Temperature Variation for a 70% Sun Orbit, as a Function of α	III-221
129	Day-Night Temperature Variation for a 68% Sun Orbit, as a Function of Angle α	III-221
130	Schematic of Direct Measurement of α/ϵ Apparatus	III-223
131	Effect of Coating upon the Effective Emissivity of Solar Cells	III-225
132	TIROS I Ground Complex, Functional Diagram	III-230
133	Primary Ground Station Components, Simplified Block Diagram	III-232
134	Ground Station Components	III-321
135	Satellite Command and Control Equipment, Racks 1 and 3	III-236
136	Satellite Command and Control Equipment, Rack 2	III-236
137	Satellite Command and Control Equipment, Block Diagram	III-237
138	Master Clock and WWV Receiver, Front View	III-240
139	Master Clock, Block Diagram	III-240
140	Master Clock, Schematic Diagram	III-323
141	Programmer, Front View	III-242
142	Antenna Programmer, Block Diagram	III-242
143	Antenna Programmer, Schematic Diagram	III-325
144	Program Selector and Power Control Unit, Front View	III-244
145	Program Selector and Power Control Unit, Schematic Diagram	III-245

LIST OF ILLUSTRATIONS (Continued)

Figure	Title	Page
146	Relay Power Supply, Front View	III-246
147	Relay Power Supply, Block Diagram	III-246
148	Relay Power Supply, Schematic Diagram	III-247
149	Command Programmer, Front View	III-249
150	Command Programmer, Block Diagram	III-251
151	Command Programmer, Schematic Diagram	III-327
152	Clock Set-Pulse Demodulator, Block Diagram	III-253
153	Transmitter Control Panel and Clock Set Pulse Demodulator, Schematic Diagram	III-254
154	Beacon and Telemetry Receivers, Block Diagram	III-256
155	Probability Distribution of Transmission Efficiency	III-257
156	Diversity Combiner, Block Diagram	III-259
157	Diversity Combiner, Schematic Diagram	III-260
158	Data Processing and Display Components, Block Diagram	III-261
159	Video Monitor Rack	III-262
160	Display and Video Amplifier, Block Diagram	III-264
161	Frequency Response of 60-Cps Chopper	III-265
162	Frequency Response of Chopper Stabilized D-c Amplifier	III-265
163	Display and Video Amplifier, Schematic Diagram	III-329
164	Sawtooth Generator Circuit, Functional Diagram	III-267
165	Sawtooth Generator Waveforms	III-267
166	Deflection Amplifier, Functional Diagram	III-267

LIST OF ILLUSTRATIONS (Continued)

Figure	Title	Page
167	Horizontal Circuits, Sawtooth Generator and Deflection Amplifier, Block Diagram	III-269
168	Sawtooth Generator and Deflection Amplifier, Schematic Diagram	III-331
169	Horizontal Sync Separator, Block Diagram	III-271
170	Horizontal Sync Separator, Waveforms	III-271
171	Horizontal Sync Separator, Schematic Diagram	III-333
172	TV-FM Demodulator, Block Diagram	III-274
173	TV-FM Demodulator, Schematic Diagram	III-335
174	Video Control and Power Rack	III-275
175	Tape and Computer Control, Block Diagram (2 parts)	III-276
176	Tape and Computer Control, Schematic Diagram	III-337
177	Monitor Control, Schematic Diagram	III-339
178	Sun-Angle Computer, Front View	III-280
179	Sun-Angle Computer, Block Diagram	III-282
180	Sun-Pulse Waveforms and Significant Timing	III-283
181	Sun-Angle Computer, Logic Diagram (12 sheets)	III-341
182	Index 40-kc Tone Generator, Schematic Diagram	III-284
183	Index 70-kc Tone Generator, Schematic Diagram	III-284
184	Index 40-kc Tone Demodulator, Schematic Diagram	III-285
185	Index 70-kc Tone Demodulator, Schematic Diagram	III-285
186	Readout Control Gate, Schematic Diagram	III-286
187	Video Test Pattern	III-289

LIST OF ILLUSTRATIONS (Continued)

Figure	Title	Page
188	Calibrator, Block Diagram	III-365
189	Composite Video for One Line	III-293
190	Calibrator, Schematic Diagram (2 sheets)	III-367
191	Attitude Recorder Rack	III-296
192	Attitude Pulse Demodulator, Block Diagram	III-297
193	Attitude Pulse Demodulator, Schematic Diagram	III-371
194	Elapsed Time Counter-Scanner, Block Diagram	III-300
195	Checkout Equipment, Simplified Block Diagram	III-305
196	Checkout Equipment, Block Diagram	III-373
197	Checkout Programmer, Schematic Diagram	III-375
198	Checkout Command Transmitter, Schematic Diagram	III-377
199	The Image Enhancement Console Equipment	III-309
200	The Image Enhancement Console with Front Access Doors Open	III-310
201	The TIROS Tape Readout Equipment	III-311
202 (a)	The Hard Copy (Flying Spot) Scanner Assembly	III-313
202 (b)	The Scanner Optical-Ray Diagram	III-313
203	The Scanner and Video Circuits, Block Diagram	III-313
204	Typical Image Waveforms	III-315
205	The TIROS Tape Readout Circuits, Block Diagram	III-317

LIST OF ILLUSTRATIONS (Continued)

VOLUME III

PART 3. TEST

Figure		Page
206	The Yo-Yo (Despin) Mechanism Field Test Fixture for Satellite Engineering Test Model Testing	II-4
207	Facsimile of Brush Recorder Chart Run No. 31, Date: 22 July 1959	II-4
208	Results of Yo-Yo (Despin) Mechanism Test for Satellite Engineering Test Model Testing	II-5
209	Final Speed Ratio versus Total Despin Mass for Several Vehicle Inertias	II-5
210	Yo-Yo Despin Mechanism Field Test Fixture for Satellite Prototype (T-1 and T-2) Testing	II-6
211	Despin Test System Used for Prototype (T-1A and T-2) Testing, Block Diagram	II-6
212	Solar-Cell Test Fixtures (a) Indoor Fixture, (b) Outdoor Fixture	II-9
213	Magnetic Field Drag Test Cylinder	II-9
214	48-Inch Vacuum Chamber	II-10
215	Vibration Test Equipment, Block Diagram	III-5
216	Calidyne Vibration Machine	III-6
217	TIROS I Special Shipping Container	III-12
218	Camera Alignment Fixture for TIROS I Satellite	III-13
219	Polar-Chart Target for Camera No. 2 (Wide-Angle Lens)	III-13
220	Dynamic Balancing Equipment	III-18
221	Dynamic Balancing Displacement Pickup, Schematic Diagram	III-18
222	Balance Planes for Dynamic Unbalance Tests	III-19
223	Vector Diagram of Unbalance Forces	III-19
224	Test Arrangement for Moment of Inertia About Spin Axis	III-21

LIST OF ILLUSTRATIONS (Continued)

Figure	Title	Page
225	Test Arrangement for Moment of Inertia Normal to Spin Axis (Bifilar Suspension)	III-22
226	Output Characteristics (I-V Curve) of Top-Surface Solar Cells of No. T1-A Satellite	III-27
	PART 5. REFERENCES AND APPENDICES	
A-1	Cross-Section of Unit Sphere in Plane of S and L Vectors	A-3
A-2	Geometric Relationship for Determining Sun Angle (α) and Fraction of Time in Sun (Ψ)	A-3
D-1	TEAM Precession Damping Mechanism Coordinate System	D-3
E-1	Flange Stress at Station R of Satellite Baseplate	E-3
E-2	Timoshenko's Loading (Sinusoidal Load Simply Supported)	E-3
E-3	Section Properties of Baseplate Radial Ribs	E-6
E-4	Bending Moments Envelope; 1 g Deadweight	E-7
E-5	Baseplate Rib Section (Determination of Stress and Margins of Safety)	E-6
F-1	Displacement of Yo-Yo Despin Mechanism Weights and Cables (When Unwinding)	F-10
F-2	Displacement of Yo-Yo Despin Mechanism Weights and Cables (When Fully Extended)	F-10
F-3	Displacement of Yo-Yo Despin Mechanism Weights and Cables (Upon Release)	F-16
G-1	Rate of Temperature Change Versus Fourth Power of the Sample's Temperature (Iridized Aluminum). Straight Lines are Fitted to the Experimental Points. The a/e Ratio is Calculated from the Difference in the Intercept; t is Calculated from the Slope.	G-8

LIST OF ILLUSTRATIONS (Continued)

Figure	Title	Page
G-2	Dependence of a/e Ratio Measurement on the Vacuum Around the Sample	G-9
J-1	Satellite Dynamic - Balance Vector Diagram	J-3
J-2	Equivalent Couple with Lumped Masses	J-3
J-3	Dynamic Balance Limits Versus Satellite Inertia Ratio	J-7
K-1	Temperature - Voltage Relationship of Simple Sensor Circuits (I)	K-2
K-2	Temperature - Voltage Relationship of Simple Sensor Circuits (II)	K-2
K-3	Temperature - Voltage Relationship of Conductance - Compensated Sensor Circuit	K-5
K-4	Temperature - Voltage Relationship of Active Compensated Sensor Circuit	K-5
K-5	Temperature - Voltage Relationship with Different β Values in CR_t and R_t Legs	K-10
K-6	Theoretical Temperature - Voltage Relationship of Final Sensor Circuit Design	K-10
K-7	Actual Temperature - Voltage Relationship of Final Sensor Circuit Design, Obtained During Tests	K-11
K-8	Temperature Versus SCO Frequency Relationship of Final Sensor Circuit Design	K-11

PART 1. INTRODUCTION

SECTION I. BACKGROUND OF THE TIROS PROGRAM

The TIROS Program was established to obtain, through the medium of satellites, meteorological data that will assist scientists throughout the world in their search for a better understanding of the factors that control the world's weather.

TIROS is an acronym for Television (and) Infra-Red Observation Satellite, which is descriptive of the basic instrumentation planned for TIROS. Only the television sensors were ready at the time scheduled for the TIROS I launch, so the infra-red instrumentation was withheld for the next satellite in the series. TIROS I was the first United States satellite to carry an internal-scan, programmable television system and, therefore, equipped to return detailed cloud-cover pictures of a large percentage of the earth's area.

The concept of using satellites as weather observers is not new, and considerable study relating to its general feasibility and proposed design parameters had been conducted for some years. Also during this period, projects dealing with satellite feasibility and design had been advancing at RCA, keeping step with the constantly increasing capabilities of rocketry. In mid-1958, an Ad Hoc Committee on Meteorology was created by the Advanced Projects Research Agency (ARPA) to help formulate the design objectives for a meteorological satellite program. It was found that a satellite already under development at RCA lent itself to ready modification for a meteorological observer, and this project was then redirected toward the meteorological objectives under the name: TIROS I.

RCA was assigned the responsibility of developing the satellite structure and its instrumentation, as well as the ground-based equipment required to complement the satellite's operation, and to assist in the operational support to assure the success of the project.

SECTION II. SYSTEM IMPLEMENTATION

The implementation of a satellite-borne, television-equipped, meteorological observation satellite was limited (from a practical standpoint) by instrumentation (state-of-the-art); and temporal, budgetary, and range safety problems.

Since TIROS I was a meteorological experiment, exploratory in nature, compromises in the requirements one would set for an operational satellite were possible. However, the desire for the maximum exploitation of the potentials of a meteorological orbiter led to a system of considerable complexity. Since TIROS was part of a meteorological experiment, and was not a satellite experiment per se, state-of-the-art techniques were to be used to the greatest extent possible. Missile-range firing restrictions were such that the best orbit obtainable from a geographical coverage standpoint was in the neighborhood of 50-degrees inclination. This would provide coverage, over a period of time, of a global belt lying between 50-degrees north latitude and 50-degrees south. Within this area, communication with a ground station would be limited to a 10-minute (nominal) interval. Constant ground contact was, obviously, impractical; a data storage and (fast) readout system, therefore, was indicated. Although constant observation of the areas under the orbiting satellite would have been desirable, the TV cameras required an earth or cloud luminance which could be provided only by incident sunlight. It was not, therefore, too restricting to plan on a spin-stabilized satellite, with the spin axis (and parallel TV-camera axes) fixed in space, and facing the earth during only a portion of each orbit. However, launch time and injection had to be planned to have the cameras facing sunlit portions of the earth --- at least for a major portion of the satellite's early life. The carrier rocket assigned for the TIROS I launch defined (implicitly) the weight and (orbital) altitude limits. The resulting weight and space limitations on the instrumentation, and the unique requirements encountered in adopting earth-type components for space use, engendered some highly-advanced state-of-the-art designs.

The use of a wide-angle and a narrow-angle TV camera is discussed in Part 2, Section II: Optical Considerations. The observations of areas in the order of 700 miles on a side would give much-desired information on large-scale cloud and weather systems. However, "close-ups" of about a 10 to 1 ratio would permit observation of specific cloud types, and show details of cloud patterns not easily obtainable from other types of observations.

To return to the problem of ground-station contact, it was planned to incorporate a dual-function instrumentation sequencing system aboard the satellite --- one that would control all instrumentation (in real time) by direct command from the ground, and would also control the instrumentation at other times upon receipt of pre-programmed information stored in the satellite. Thus, the number of ground stations could be severely limited

(actually, two were used), and all "business" could be transacted with the satellite during the time of ground-station contact -- "business" refers to stored-data readout, direct picture-taking and readout, and programming of the satellite instrumentation control for future "remote" operation. (The actual techniques are highly refined, and are detailed later in this report.)

A spinning satellite maintains no simple orientation reference to the earth, and the geographical orientation of the cloud photographs is essentially random. A reference can be derived if the attitude of the spin axis with respect to the earth is known, as well as the angle between the camera and the sun (a "fixed" reference), for each picture taken. Ingenious systems, also described later in this report, were included to perform these functions.

In order to monitor the behavior of the satellite and its instrumentation, a telemetry system which would report various temperature and voltage parameters was felt necessary. This information was transmitted periodically, over the tracking-beacon transmitters.

To maintain a source of electrical power, a bank of storage batteries was carried aboard the satellite, and a solar-cell energy converter was included to maintain the batteries in a state of charge.

It was found feasible to utilize stations of the Minitrack network to track the satellite and receive the continuous flow of (spin-axis) attitude data. This information was forwarded to a clearing agency: the N.A.S.A. Space Control Center, at Washington, D.C. Data received (and partially processed by the ground stations) also was sent to this Space Control Center which, in turn, collected from the participating agencies and sent back to the ground stations, data for future programming of the satellite. The TIROS ground complex is discussed more specifically in the section on Field Operations.

PART 2. DEVELOPMENT AND DESIGN

SECTION I. SYSTEM STUDIES

A. GENERAL STUDIES

The constraints and deleterious effects of the environment on a satellite had to be considered in designing TIROS I. Early in the developmental program, the major constraints were identified and their effects studied. Thermal, dynamic, and optic considerations are discussed in Section II, following. Other constraints considered are discussed here.

Corona Discharge (Arc-over). The breakdown potential (see Figure 1) for a gas of atmospheric composition drops to 300 volts for a product of pressure (p) and gap distance (d) which equals 0.6; where p is in mm Hg and d in cm. At satellite altitudes, this product pd is so small as to pose no problem. In the ascent, however, conditions may be realized wherein arc-over could occur. Considerations, therefore, relative to the ascent phase, must include the possibilities of reduced voltages, encapsulation, or initiation of operation after orbit has been obtained.

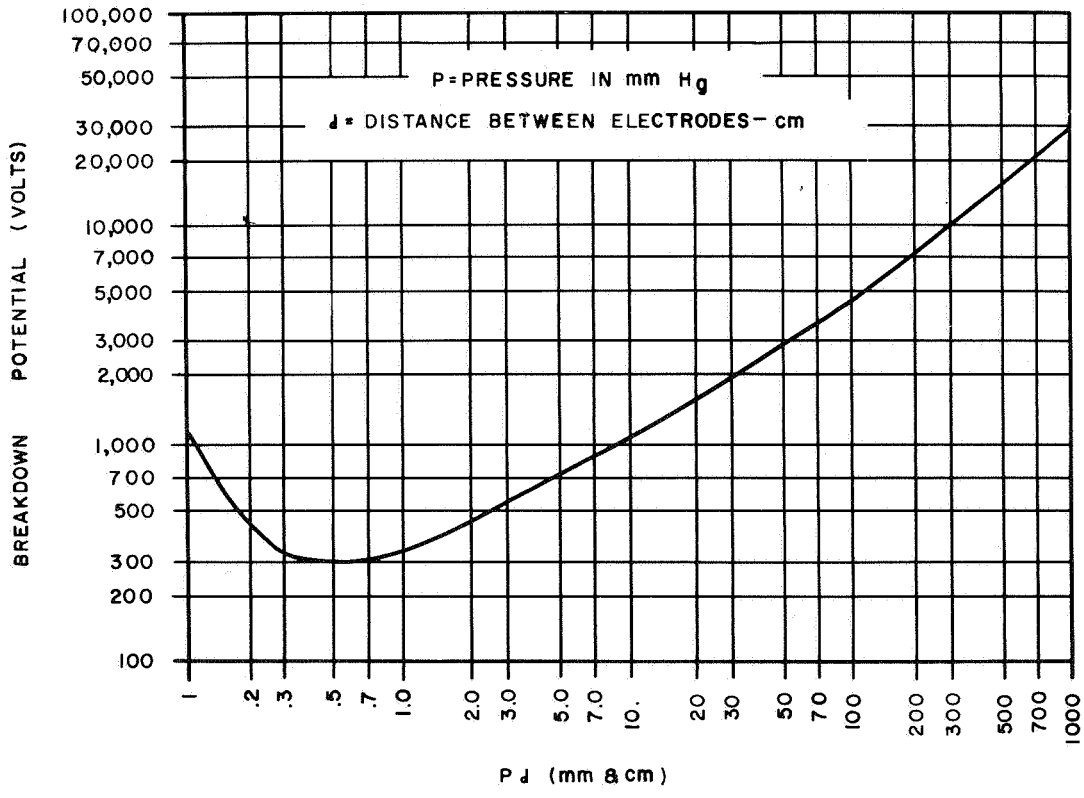

Figure 1. Characteristics of Breakdown Potential

Explosive Decompression. Explosive decompression may occur in component containers in which an arbitrary pressure is maintained, when the external pressure drops sufficiently. In addition, puncture of the container by micrometeorites would create an outward rush of air with possible deleterious effects on component supports.

Boiling and Leakage Through Seals. Boiling points of liquids are greatly lowered at the pressures associated with satellite altitudes. At the temperatures and pressures encountered, many fluids boil and seep out of their containers. This effect may be enhanced by differential thermal expansion with consequent loosening of seals and gaskets. The condition of zero gravity at low pressures adds the complication that escaping fluids continue to move in the direction of their escape. Loss of heat transfer medium (by micrometeorite puncturing of pressurized containers) could cause components to reach temperatures which would result in malfunctioning.

A typical example, which was studied at RCA-AED, arises in connection with the use of anti-friction bearings for rotating members. Under normal atmospheric conditions it is possible to use conventional ball bearings lubricated with low-temperature and low-volatility oils. At reduced pressures, however, outgassing presents an insurmountable problem not only through the loss of lubricant, but also in the possibility of redeposition of the lubricant on elements which would be adversely affected.

Solar Radiation. Figure 2 indicates the solar spectrum above the earth's atmosphere, which fairly closely approximates that of a 6000°K black body. Of greatest interest in terms of radiation damage to materials is the ultra-violet and X-ray region. The flux in this region constitutes approximately 9 percent of the total solar emission. Superimposed on the solar photo-emission spectrum is the Van Allen Radiation Belt of electron and/or proton fluxes. The general characteristics of the radiation belt are shown in Figure 3. The numbers refer to counts of high-energy particles per cm per steradian per sec. Latest satellite probes are revising upwards both the intensity values and the extent of the belts. The maximum flux occurs in the soft X-ray region of 50 kev electrons; the higher energy particles lie beyond 75 mev in the energy spectrum. With the aid of the Signal Corps, RCA-AED conducted radiation damage tests of materials which were being considered as possible surface coatings for satellite thermal control and for thermal protection of the silicon solar cells used for power generation on satellites.

Figure 2 shows the spectral regions, the dosages applied, and the types of materials investigated. It is of interest to note that a full spectrum analysis must be made since it was found, in several cases, that materials only showed effects in but one of the three regions, and these were not the same region for different materials. The dosages for the ultra-violet and X-ray tests are effectively a year's input of the radiation belt maximum intensity. A typical result which has interest for image sensors is shown in Figure 4. On the right is a control glass slide which was not irradiated. On the left is a plastic-coated slide irradiated by an 800,000-roentgen dosage of a Co_{60} source. The radiations are gamma rays of 1.1 and 1.3 mev. It can be seen that the plastic has browned under the radiation and, as would be expected from the penetrating gamma rays, the browning is a volume effect (the thicker the material the greater the browning).

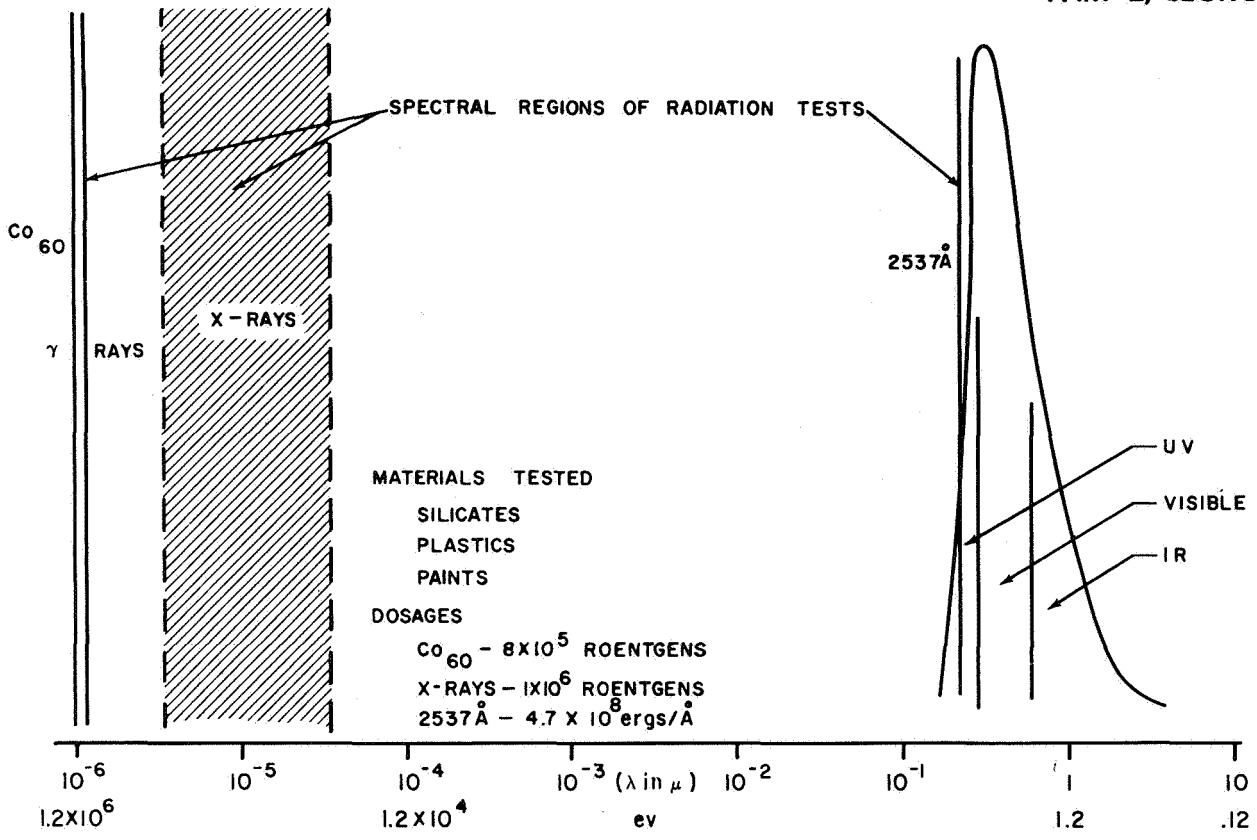

Figure 2. Solar Spectrum

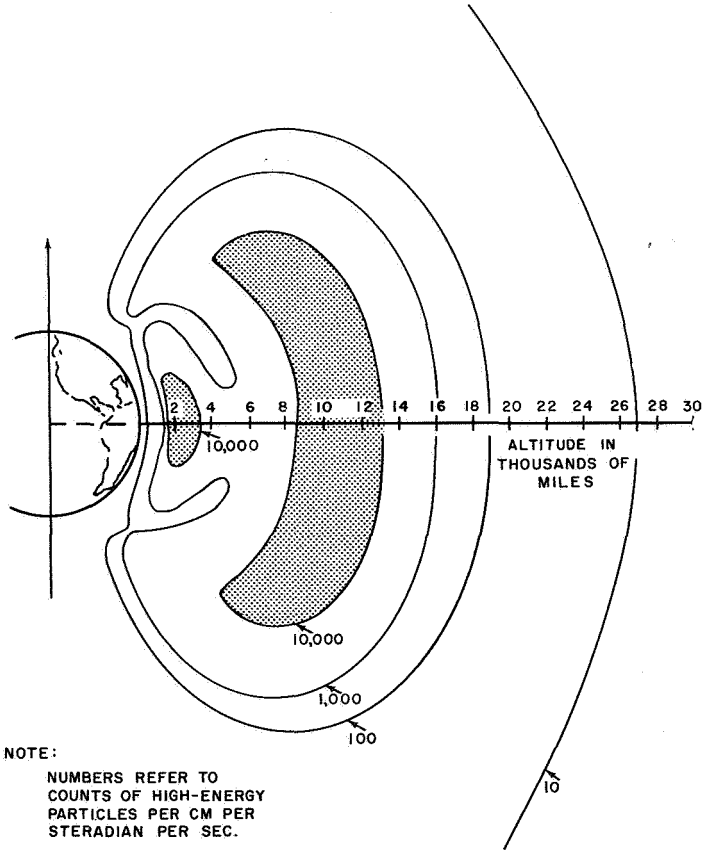

Figure 3. Radiation Belt

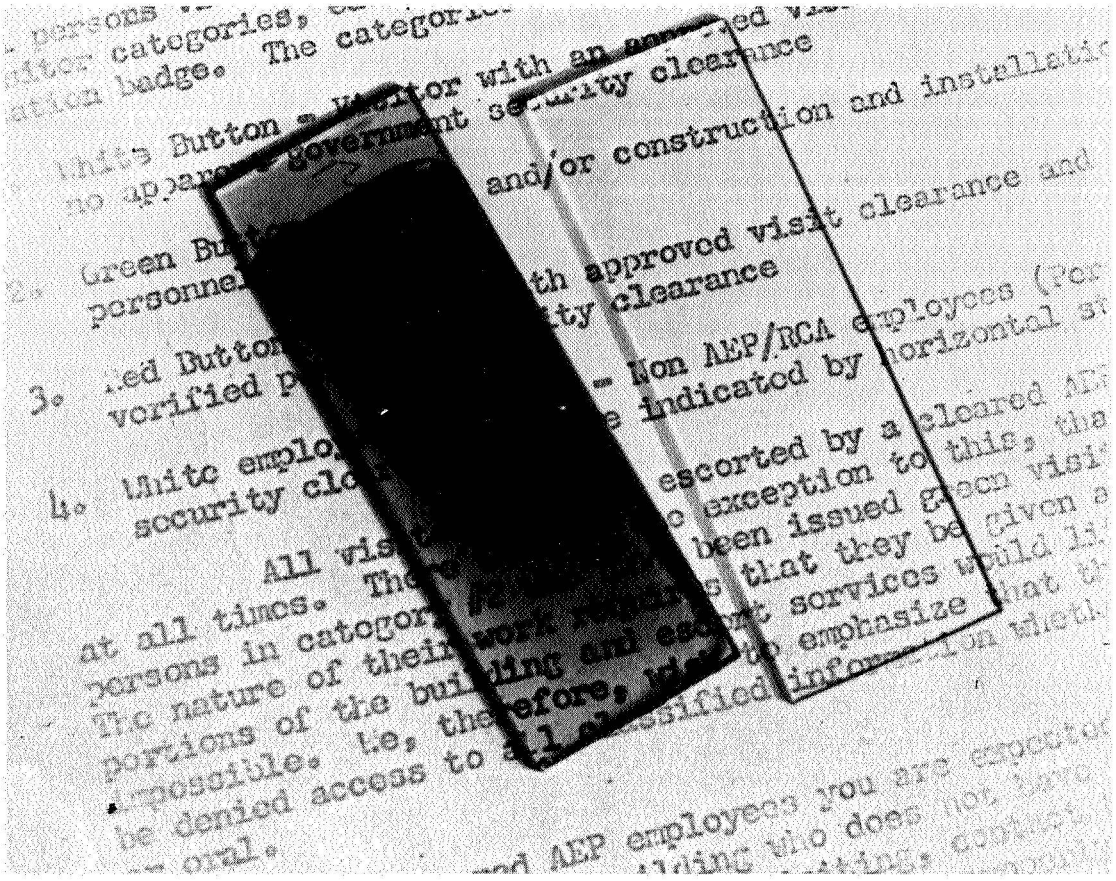

Figure 4. Co_{60} Radiation Test

Unfortunately, this was common slide glass; lens glass was not tested. If a particular glass does exhibit browning per unit thickness, then the multiple lens system of camera optics, using such glass, would suffer very large losses in transmission.

Solid Particles. Meteors having masses greater than 1 gram can penetrate skin thicknesses of 0.040-inch aluminum on impact. Smaller micrometeorites will sandblast a surface, and hence, will create changes in surface optical and radiative properties which will change equilibrium temperature distributions on the satellite.

Evidence up to and during the TIROS I project on meteorite distribution at satellite altitudes appears to fluctuate widely. Microphone impact measurements on the 1958 α, and 1958 γ and on the 1959 Paddle Wheel satellite showed a mean flux rate of 10^{-3} to 10^{-2} particles /m^2 sec with diameters greater than 3 μ. Russian data, on the other hand, seemed to indicate counts of 90 to 100 particles/m^2 sec with diameters of at least 10 μ. This was 10,000 to 100,000 times greater than the American measurements indicate. Recent data indicated that the Russian data have been revised downward to a much closer agreement with the American data. A second type of measurement of micrometeorite activity is the grid-wire experiments, wherein a grid wire is ruptured when an impact from a micrometeorite larger than a preassigned diameter is received. For Explorer I (1958) not more than one (and perhaps none) of the wire gauges were broken during the lifetime of the telemetering system. For Explorer III no grid wires were broken between

the launch dates 26 March 1958 and 6 May 1958. Between 6 May 1958 and 7 May 1958 two grids were fractured. It is perhaps advisable at this point to quote Jet Propulsion Laboratory External Publication, No. 538.

> "This occurrence* was followed by an interesting series of happenings. On May 8 and 9 erratic behavior was observed in one of the telemetering channels on the low-power transmitter. After 0415 G.M.T. on May 9 no signal at all was observed from this transmitter. During May 10 and 11 the Minitrack receiving stations indicated intermittent operation of the high-power transmitter, and after May 11 no further signals were received for several days. After a period of a few days both transmitters returned to operation. However, the low-power transmitter carried no telemetry signal, and the operation of the interrogated beacon was intermittent.
>
> "The coincidental failure of these two transmitters is curious. The two units operated quite independently with separate circuitry and separate power supplies. It was expected that they might have similar lifetimes, but failure of both within one or two days of each other simply from coincidental power failures is not very likely."
>
> "One other item of information must now be introduced. All of the micrometeorite data before this time were taken in a period of normal background activity. No meteor showers were encountered. However, the shower Eta Aquarides, which has been associated with Halley's Comet, occurs during the early part of May, reaching its most intense activity on about May 5. It is therefore very suggestive that the fracture of two wire gauges and the very nearly coincident failure of two independent radio systems followed within a few days of the predicted time of this meteor shower. It is reasonable to speculate that some sort of internal damage was caused by impact of meteorites."

More information came from an IRBM sent up in May, 1959. Here, there were 8 grid wires positioned on each side of the payload. The telemetry signals were functioning quite normally when suddenly within a few seconds all 8 grids on one side were fractured. The fluctuations in reported micrometeorite activity thus appears to be the actual state of affairs rather than measurement errors.

Figures 5 and 6 indicate the results of work by Standford Research Institute in bombarding a lucite and glass disc with steel particles ranging in size from less than 3 μ to 25 μ with velocities in the order of 18,000 ft/sec.

The surface of the glass disc is badly shattered with a resultant 25-percent decrease in transmission, whereas the lucite has absorbed the particles and reformed around them with negligible transmission loss.

*Fracturing of two Explorer I grid wires between 6 May and 7 May 1958.

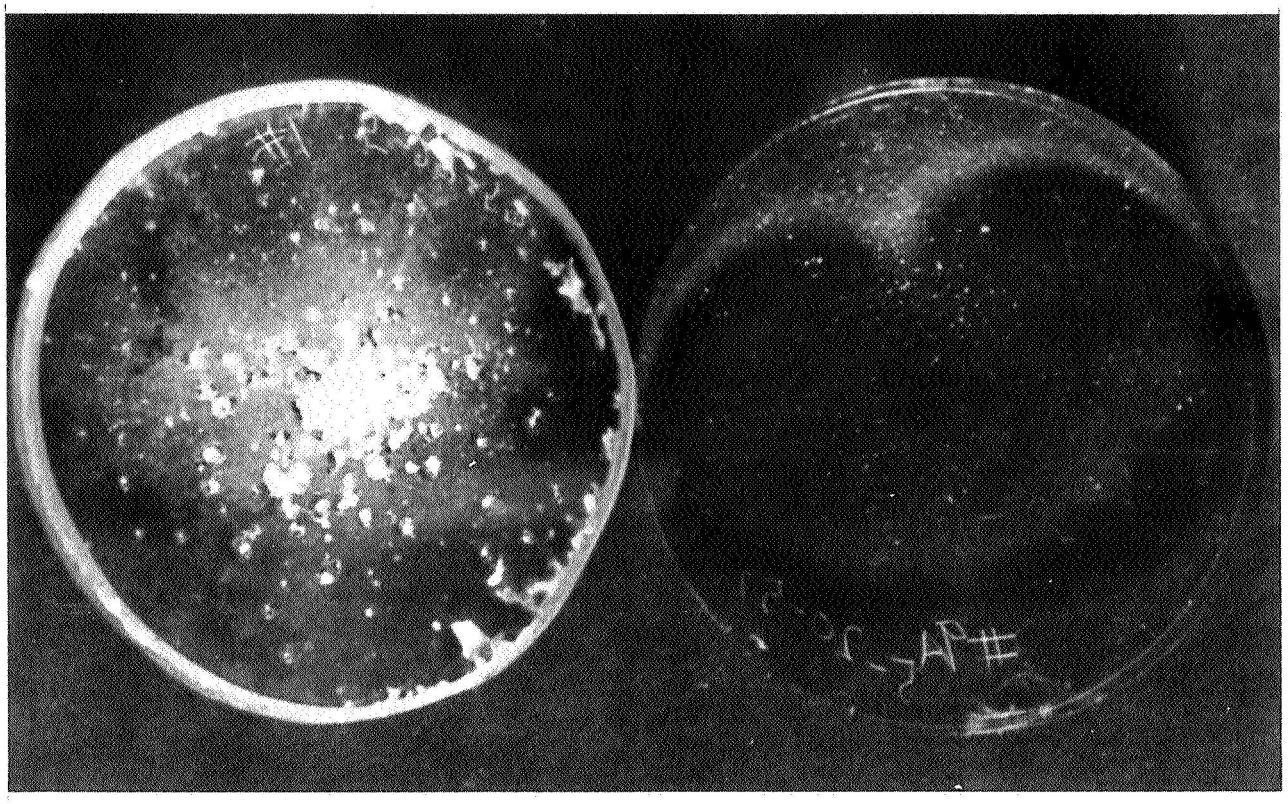

Figure 5. Simulated Micrometeorite Bombardment

(159) 92 The reaction between hydrogen peroxide and ammonia
K. B. MIRONOV

(158) 65 The influence of the nature of the cations and anions on the solubility of titanium tetrachloride in salt melts
L. A. TSIOVKINA and M. V. SMIRNOV

(163) 67 On the mutual influence of ions in aqueous solutions
L. S. LILICH

(169) 69 The solid phases crystallising in the system Na_3PO_4-Na_2SO_4-H_2O at high temperatures (200-350°)
M. I. RAVICH and L. F. YASTREBOVA

(182) 75 Physico-chemical analysis in the nitric acid treatment of phosphates. the quater-
[illegible]$_2O$-N_2O_5-H_2SiF_6-H_2O at 60°
A. V. RUSAL[illegible] d S. Ya. SHPUNT

(19[illegible]) 81 The [illegible] for the ternary system H_2O-KCl-$CaCl_2$ from the [illegible] perature [illegible] freezing [illegible] 300°
[illegible]AN and [illegible] KUZNETSOV

(205) 8[illegible] hydroly[illegible] s in the HF-NH_4F_2-H_2O system
[illegible]d Yu.[illegible] BUSLAEV

(21[illegible]) [illegible]tainmen[illegible] of equilibrium distribution of micro-component between [illegible] phases
[illegible]SEV

(220) 9[illegible] [illegible]tree prep[illegible]ration of radi[illegible]emically pure yttrium-90
N. [illegible]NKO

(225) 94 Mea[illegible]ement of t[illegible] solubilities of oxides of silver in alkali solutions by radioactive tracer method
[illegible]A and N. A. BALASHOVA

(227) 95 Instantaneous coprecipitation of traces of caesium with Prussian blue
M. KYRSH and O. E. ZVYAGINTSEV

Brief communications

(230) 97 Measurement of the saturated vapour pressure of anhydrous lanthanum chloride by the radioactive tracer method
An. N. NESMEYANOV and L. A. SAZONOV

(231) 98 The measurement of the saturated vapour pressure of lithium chloride
An. N. NESMEYANOV and L. A. SAZONOV

Figure 6. Simulated Micrometeorite Bombardment

It is not meant to imply that bombardment shown here constitutes the mass and velocity distributions of micrometeorites in space, but rather that the qualitative damage effects are dependent on the hardness of the object undergoing the bombardment. The extension of these results to camera optics is obvious but the solution is not. Substitution of plastic lenses would probably create more problems from radiation and outgassing than would be solved in terms of micrometeorite damage.

Dissociated Gases. At satellite altitude, the constituents of the atmosphere are dissociated. Atomic oxygen will react with heavy metals such as iron, copper, and silver, and with many organic materials. Consideration should therefore be given to the avoidance of materials that do not form adherent oxide layers. In cases such as electrical contacts, where oxide formation is intolerable, the use of noble metal coating or atmospheric shielding is indicated.

Atomic (nascent) nitrogen poses a problem only where exposed metals are at high temperatures.

At satellite altitudes, the concentration of ozone is negligibly low and does not constitute a hazard.

B. LAUNCH AND ORBIT CONSIDERATIONS

1. Introduction

An accurate method of predicting the photographic coverage of the earth's cloud cover, as a function of the orbit and time after launch, was required in order to: (1) properly evaluate the capability of the satellite, (2) establish a basis for determining the operational sequence, duration, and time of photography, (3) develop video and communication traffic estimates, and (4) optimize the orbit and launch parameters. Furthermore, it was necessary to be able to predict the contact time versus orbit position relationship between the satellite and the ground stations because this criteria also affected operational planning and traffic estimating. This contact time versus orbit position relationship data could also be used to evaluate the efficiency of the proposed ground station sites.

2. Photocoverage Analysis

a. Limitations of Photocoverage

The geometric relationship of the TIROS I satellite in orbit and its effects on photocoverage is shown in Figure 7 and a cross section through the plane of orbit is shown in Figure 8. The normal point (NP) is that point on the earth's surface at which the orbiting satellite's cameras would point straight down. The satellite will not pass over this NP unless that point lies in the plane of the orbit. The NP can also be defined as the intersection of the line (radius) drawn from the earth's center in the direction of and parallel to the spin axis of the satellite. The spin axis of the satellite is fixed in space by the satellite's rotation about its axis in a manner similar to that of a gyroscope.

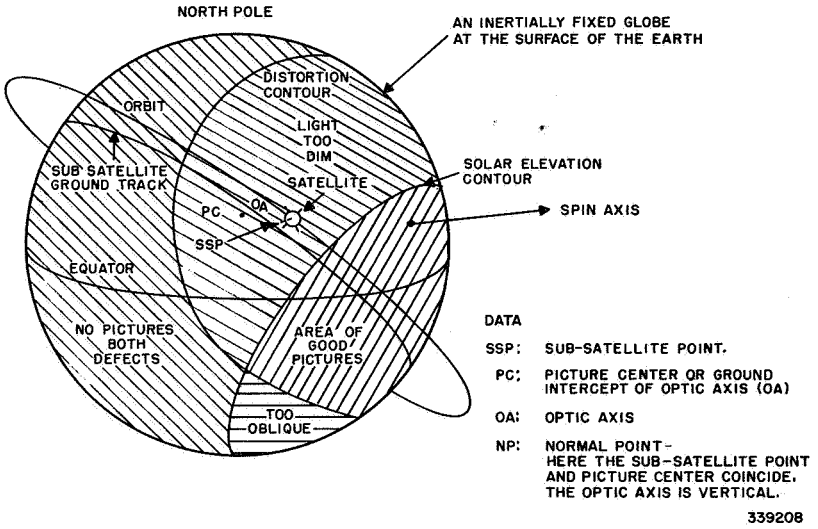

Figure 7. Orbit of TIROS I Satellite and its Effect on Photocoverage

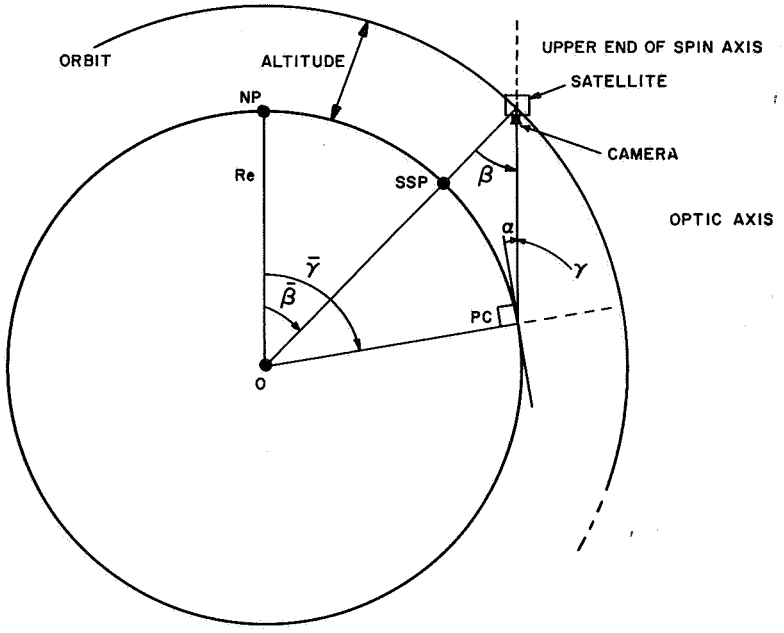

DATA:

$\bar{\gamma}$ LIMITING ARC FROM NORMAL POINT TO PICTURE CENTER

γ ZENITH ANGLE OF SATELLITE AT PC

$\bar{\beta}$ LIMITING ARC FROM NP TO SUBSATELLITE POINT

β NADIR ANGLE FROM NADIR TO CAMERA AXES

α ELEVATION ANGLE OF SATELLITE AT PC

NP NORMAL POINT

PC PICTURE CENTER

O CENTER OF EARTH

SSP SUB-SATELLITE POINT

Re EARTH RADIUS

339209

Figure 8. Cross Section through Plane of Orbit

As the satellite moves in its orbit, the angle of incidence α of the camera's optic axis upon the surface of the earth varies. As this angle (α) decreases, foreshortening of the field of vision becomes an important distortion, and the increase in slant range reduces the picture resolution. For each camera, a minimum angle of incidence (α), known as the distortion limit, was specified to limit these effects.

The distortion limit was generated by constructing a small circle (with a radius limited by the minimum incidence angle) on the surface of the globe about the normal point. Whenever the ground intercept of optic axis (also called the picture center, PC), fell within the distortion circle (also called the contour), the distortion constraint was adequately satisfied.

Good photography is also dependent upon the solar illumination of the surface of the earth. Solar illumination is perpendicular to the surface of the earth only at the subsolar point, and becomes progressively more oblique as the distance from the subsolar point increases. To be able to accurately predict the area of usable illumination, a circle was constructed with radius equal to the maximum permissible solar zenith angle. For the solar illumination contour, because the distance of the sun from the earth approaches infinity, the limiting radius is equal to the maximum permissible solar zenith angles.

Photocoverage, therefore, was confined to those areas which fell within both the distortion and illumination contours simultaneously. These areas were expected to undergo a slight change over a period of weeks due to the annual motion of the sun. The intersection of the orbit and these areas was expected to change more rapidly because of the regressive motion of the orbital plane. At launch, the subsatellite ground track would bisect the distortion circle because the normal point was expected to lie on or near the orbit ground track. Therefore, the launch time selected would provide the information for properly positioning the orbit with respect to the sun and assure adequate illumination of the ground track in the low distortion area of the day of launch. As the orbit regressed with time, the orientation of the subsatellite ground track would be expected to move partly or even completely out of the area of possible picture-taking and then later reintersect the area.

The angles that define the boundaries of photocoverage and the radii of the limiting circles for both the wide-angle and narrow-angle cameras are listed in the following table. Figure 8 illustrates the plane geometric relationships for determining the radii of the limiting circles.

Early in the photocoverage analysis only, the useful approximation was made that the subsatellite point and picture center point coincided. (This is equivalent to zero satellite altitude.) Then, whenever the subsatellite point fell within the area of the distortion and illumination contours, pictures were possible. This assumption was more conservative than assuming the picture center to be within the contour limits.

Camera	Boundary	Minimum Elevation	Circle Radius
Narrow	Distortion	20°	55°
	Illumination	18.6°	71.4°
Wide	Distortion	0°	90°
	Illumination	0°	90°

Other picture-taking constraints considered were the effects of the actual length of the arc of the subsatellite ground track within the available photocoverage area, the solar power input limitations of the satellite, and the interaction of the maximum satellite clock delay with the chosen orbit and with the ground readout station sites. The effects of these constraints are discussed in detail in subsequent paragraphs.

b. Initial Analysis

Early in the TIROS I program, maps and globes of the earth were used to predict photocoverage capabilities for a radial and an axial camera for a few days after launch of the satellite. Later, the radial camera was eliminated and only a prediction history of the axial cameras (picture center points) was required. For photocoverage prediction purposes, the axial cameras were assumed to be centered on the subsatellite point (SSP). (This is equivalent to zero satellite altitude.) This assumption was more conservative than if the picture center was assumed to be within the contour limits. In addition, the cameras were considered to be capable of picture-taking whenever the SSP was sufficiently illuminated and the obliquity of the camera axes, with respect to the ground, was within the prescribed distortion limit.

Generation of the photocoverage history was accomplished by choosing a particular initial orientation of the orbit ground trace (subsatellite ground track) with respect to the solar illumination contour and distortion contours. The extent of the area available for photocoverage was then tabulated by latitude, true anomaly, time, and other desired criteria. The orbital trace over the ground was then moved to correspond to the next orbit of interest and the tabulation repeated. Detailed information of the early photocoverage analysis is contained in RCA-AED Technical Memos 233-11, 233-20, and 233-23.

c. Detailed Pre-Launch Analysis

During the year prior to launch, the various approximations of the initial photocoverage analysis were deleted and more exact calculations were performed on a computer. Histories of the latitude extent of photocoverage were made for a period of 100 days after launch based on various orbital altitudes, inclinations, and for various times of launch.

As in the graphical method previously explained, a particular orientation of the orbit with respect to the illuminated area at launch was assumed. The chosen normal point lay, of course, on the launch orbit. The ground intercept of the optic axis of the cameras was calculated, as required, to define its intersection with the distortion limit contours and solar illumination limit contours whenever they fell within the distortion limit contours. One orbit each 3-1/2 days, with the regression of the orbit nodes considered, was sufficient to determine the outline of the photocoverage patterns.

The latitudes at the beginning and end of photocoverage of each orbit were computed and plotted for both northbound and southbound directions of satellite travel. This procedure was adopted in order to clarify the graphical presentation of latitudinal coverage, because separation of the two directions of travel gives the effect of unfolding the otherwise complex photocoverage boundaries into simple repetitive patterns.

The abscissa of the graph (Figures 9 through 14) is used to represent time in days after launch. The lower half of ordinate axis is the latitude at which photocoverage begins or ends for northbound travel of the orbiting satellite; the upper portion is for southbound travel. The latitude calibrations are arranged so that the northern extremes of travel are at the center of the graph while the southern extremes of travel are at the top and bottom. The latitudes, when the direction of travel of the picture center reverses, were also computed within the illumination and distortion contours. The satellite can then be said to move from bottom to top across the graph at any date of interest. The various boundaries encountered define the type and extent of photocoverage.

In most cases, separate figures were drawn for the wide-angle and narrow-angle cameras because of the complexity of the photocoverage patterns. The following designations are used in the illustrations:

WA	Wide-angle camera
NA	Narrow-angle camera
D	Distortion boundary
SUN	Illumination boundary
IN	Inward crossing of a boundary by the satellite into a region more favorable for picture-taking
OUT	Outward crossing to an area less favorable
TO or TURNOVER	Locus of latitude at which the picture center reverses its direction to travel from north to south or vice versa

The turnover curves (Figures 12 and 13) are mirror-imaged about the center of the page. When the picture center point is progressing upward and encounters a turnover curve, its direction of travel changes; therefore, the picture center point jumps immediately to the mirror image of its location and proceeds upward.

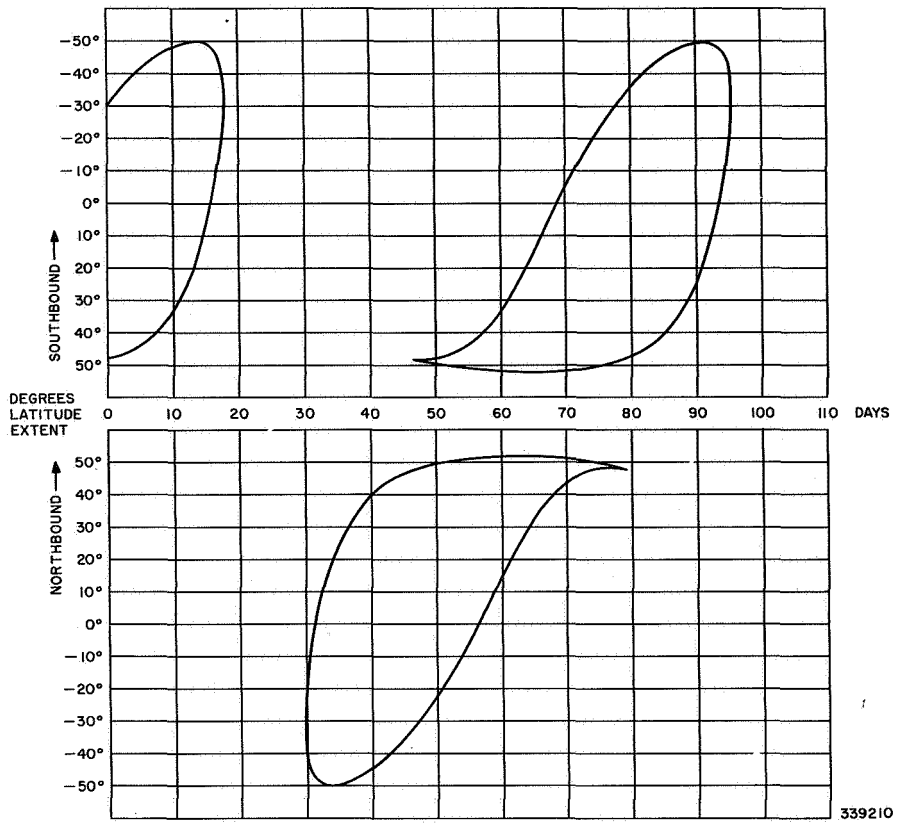

Figure 9. Narrow-Angle Camera Latitude Extent of Photocoverage versus Days after Launch with Distortion the Only Limiting Factors

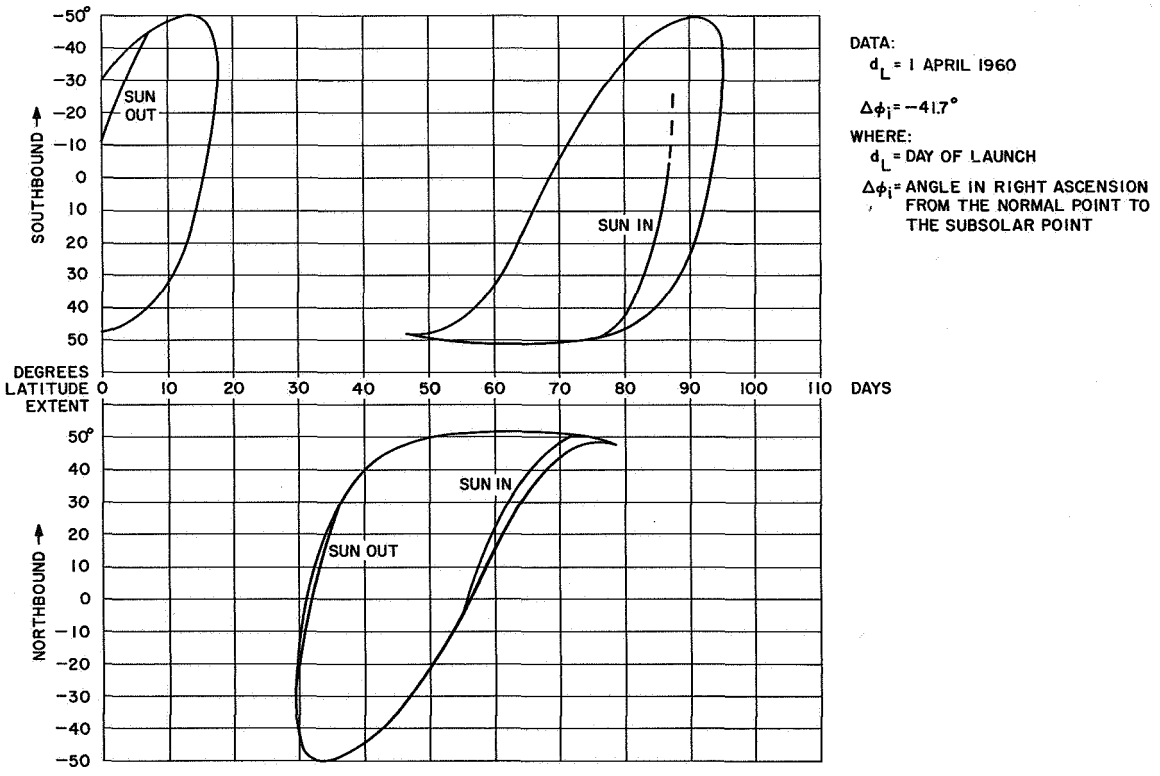

Figure 10. Narrow-Angle Camera Latitude Extent of Photocoverage versus Days for a 1 April 1960 Launch with Distortion and 20 Degrees Solar Elevation the Limiting Factors

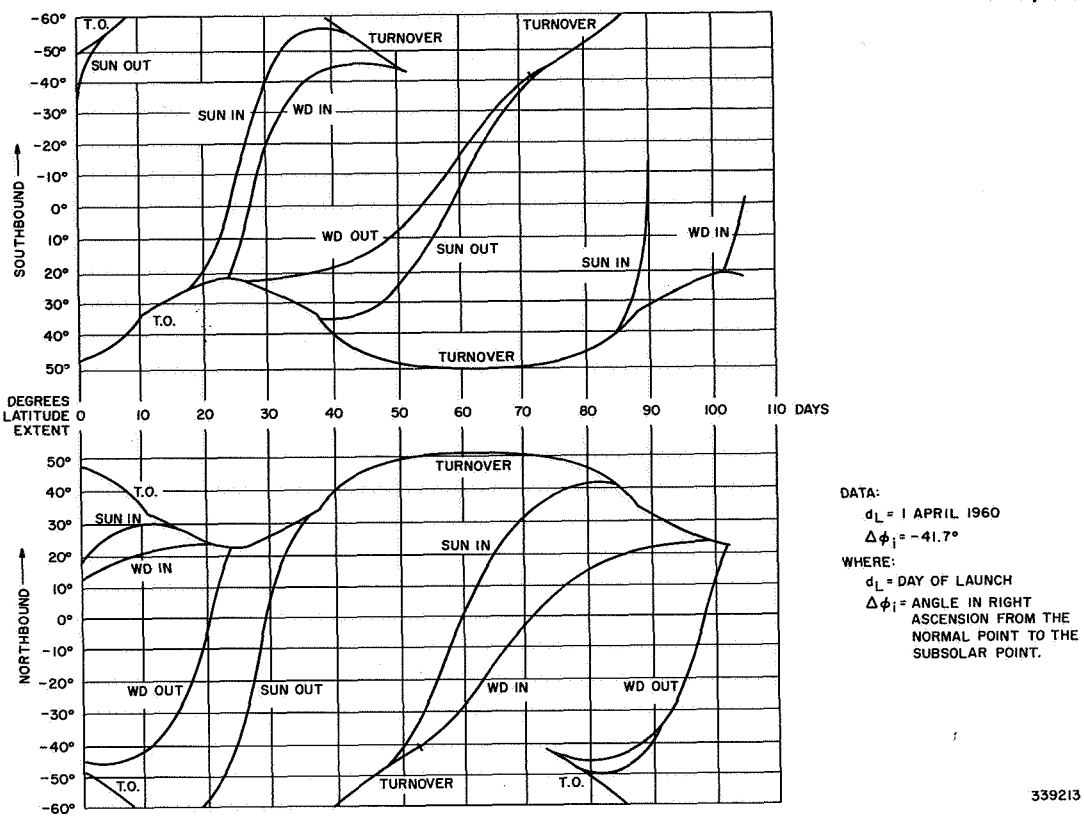

Figure 11. Wide-Angle Camera Latitude Extent of Photocoverage versus Days after a 1 April 1960 Launch

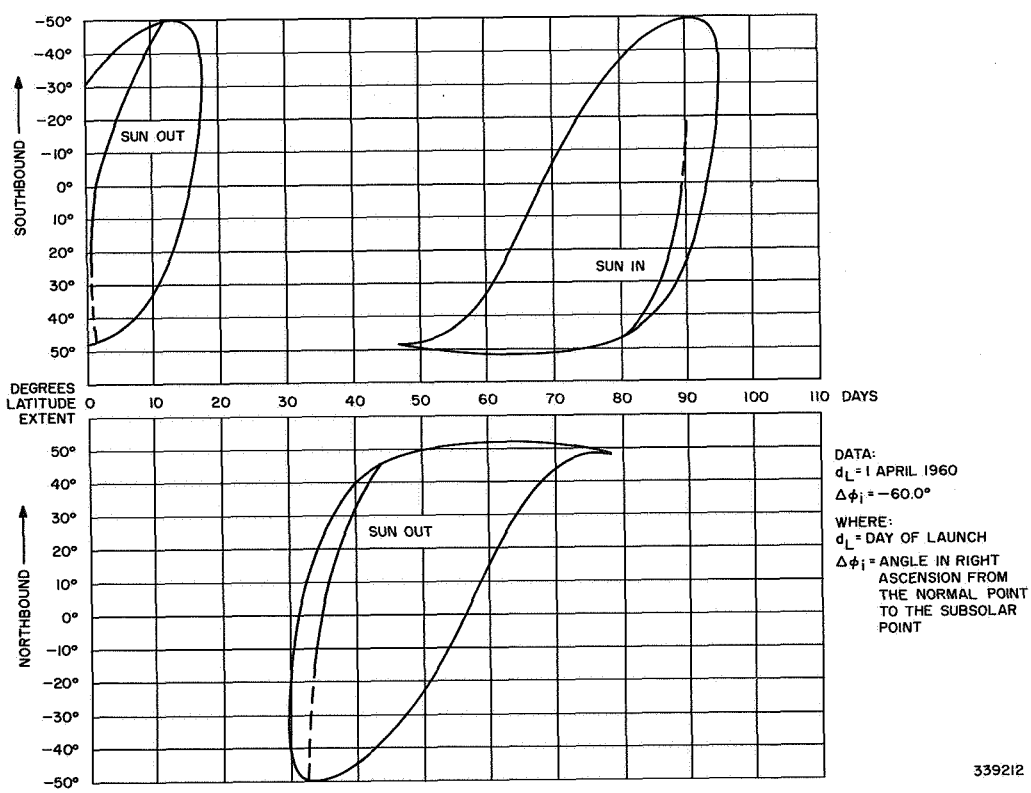

Figure 12. Narrow-Angle Camera Latitude Extent of Photocoverage versus Days after Launch with a 20 Degrees Change in Right Ascension of Sun from Normal Point ($\Delta\phi$)

The one orbit examined at each point selected in time is taken as representative of all orbits on that day. As the earth rotates under the orbit plane, bands of area will be available for data acquisition between the latitudes specified by the latitude extent curves. Essentially all of the area of the band will be visible above 30 degrees latitude, a substantial part of the band area will be useable between 30 degrees North and 30 degrees South.

The latitude extent of photocoverage for the narrow-angle camera when distortion was the only limitation is shown in Figure 9. The restriction of 20 degrees solar elevation as the limit of useful illumination for an 1 April 1960 launch was added for the narrow-angle camera in Figure 10 and the wide-angle camera in Figure 11. The effect of a 20 degrees change in right ascension of the sun from the normal point ($\Delta \phi$) on the latitude extent of photocoverage is shown in Figure 12 for the narrow-angle camera and in Figure 13 for the wide-angle camera. The assumed orbit in Figures 10 through 13 was circular and direct with an altitude of 380 nautical miles and an inclination of 48.3 degrees.

Figure 14 shows the latitude extent of a proposed orbit which was selected in order to prevent impact with the European landmass by the Thor-Able vehicle hardware or, possibly, the final stage and satellite combination. A southeast launch from Cape Canaveral was proposed, so that the impact zone would be only in the South Atlantic. The consequences of such a launch would be that the normal point would fall at approximately 20 degrees latitude. Only the distortion limits are shown. Assuming that the satellite had a fixed spin axis orientation, the Northern Hemisphere coverage would be rather oblique. The radius of the distortion circle for the narrow-angle camera was fixed at 70 degrees; and, for the wide-angle camera at 90 degrees. The inclination of this orbit was reduced from 48.3 degrees to 30 degrees, thus limiting the photocoverage to latitudes not much greater than 30 degrees in the same hemisphere in which the normal point lies. The maximum view from the subsatellite point to the horizon, if visible, is about 24 degrees of arc; therefore, the picture center may be as much as 24 degrees north or south of the subsatellite point, a considerable extension of latitude photocoverage. It is not quite correct to assert that the edges of the field of view of the wide-angle camera will always provide this extent of photocoverage because of the considerable lens distortion and the slightly poorer lens resolution at the field edges.

The orbit finally planned for the TIROS I satellite was, as originally specified, a northeast launch from Cape Canaveral. The orbit was reshaped so that the 3-sigma probability impact zone for the upper stages and payload in case of malfunction was within the Bay of Biscay and not on the European landmass. This orbital choice reestablished the normal point in the Northern Hemisphere and assured excellent photocoverage of the areas of principal meteorological interest. The orbit finally planned was the following:

Altitude:	380 nautical miles
Inclination:	48.3°
Launch Azimuth:	46.5°

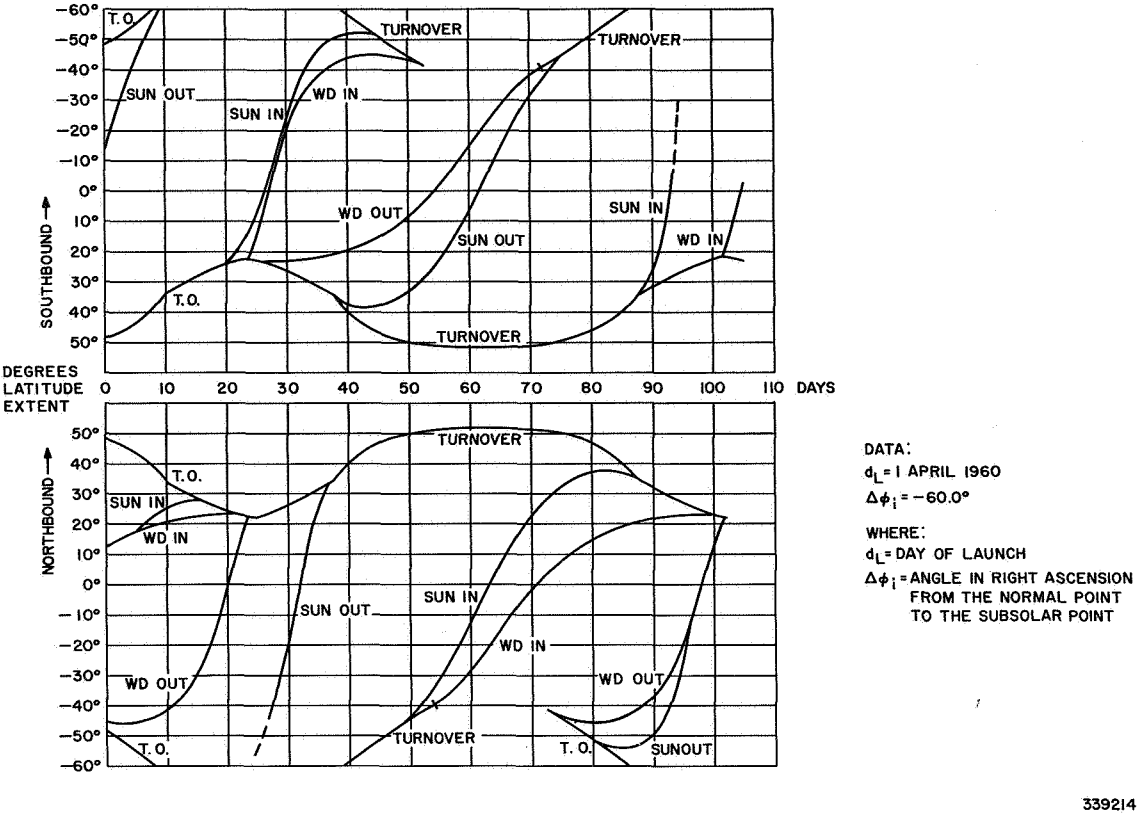

Figure 13. Wide-Angle Camera Latitude Extent of Photocoverage versus Days for a 1 April 1960 Launch with Approximately 20 Degrees Change in Right Ascension of Sun from Normal Point ($\Delta\phi$)

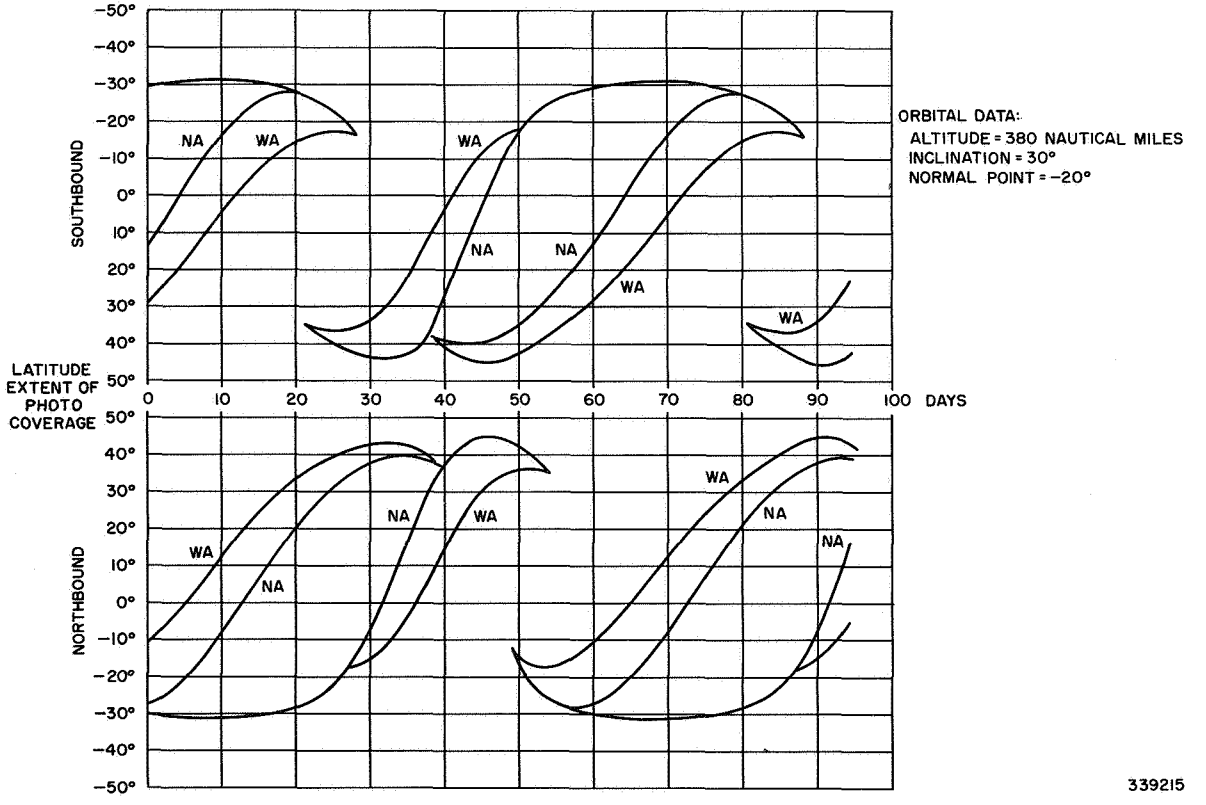

Figure 14. Geometrical Limits of Latitude Extent of Photocoverage of Narrow-Angle (NA) and Wide-Angle (WA) Cameras versus Days after Launch

Coast Period: 423.9 sec.

Time to Injection: 731.1 sec.

Normal Point:

Latitude: 20.0° North

Longitude: 43.97° East

Of particular interest is the comparison between the wide-angle and narrow-angle camera when the right ascension angle at launch between the normal point and subsolar point was varied. The principal effect seemed to be a lateral (time) shift in the illumination derived boundaries to latitude extent. This effect was a determinant in choosing a launch time.

Another measure of photocoverage availability was the history of the true anomaly or arc along the orbit, which was contained within the zone suitable for picture-taking, as a function of days after launch. The portion of orbit useful for the narrow-angle and wide-angle cameras versus days after launch for two specific launch orientations is shown in Figures 15 and 16. Since the remote picture-taking function was of 16 minutes duration and the satellite moved at 3.64 degrees per minute (See Figure 17, Degrees of True Anomaly per Minute of Flight versus Orbit Altitude), at least 58.2 degrees were required at an altitude of approximately 440 miles to make full use of length of the remote picture sequence. It is obvious from Figures 15 and 16 that the narrow-angle camera could be predicted to have little or no favorable periods for picture-taking from approximately 15 to 30 days after launch. This was confirmed by the latitude extent

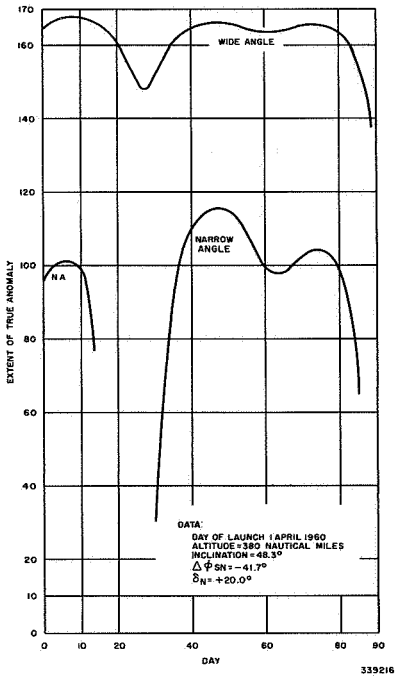

Figure 15. Portion of Orbit Useful for the Narrow - Angle and Wide - Angle Cameras Based on the Extent of the True Anomaly versus Days after Launch

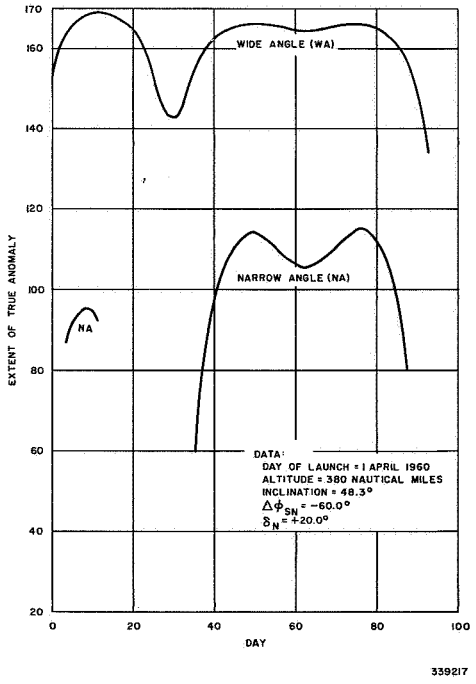

Figure 16. Portion of Orbit Useful for the Narrow - Angle and Wide - Angle Cameras Based on the Extent of True Anomaly versus Days after Launch

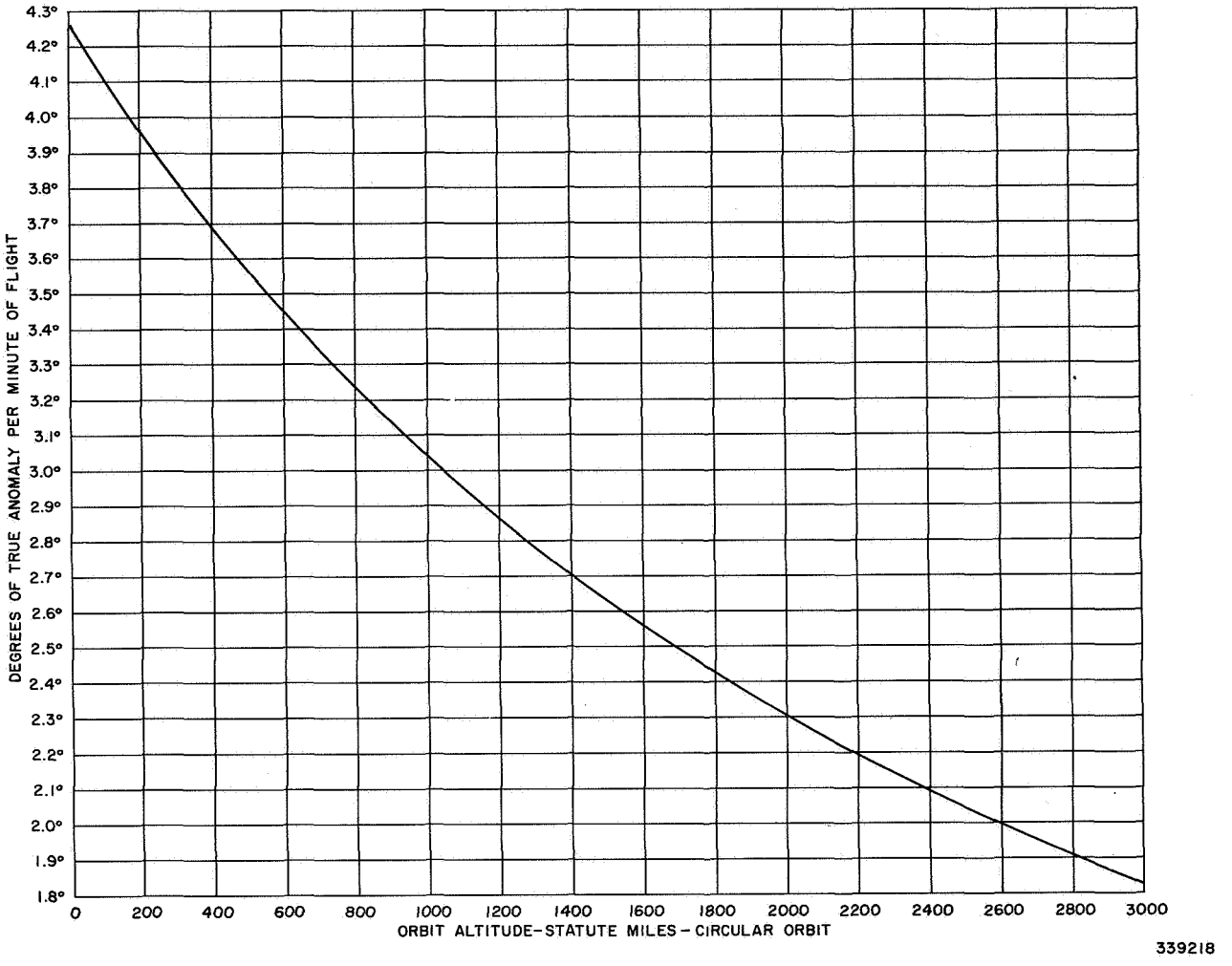

Figure 17. Degrees of True Anomaly Per Minute of Flight versus Orbit Altitude

curves, Figures 10 and 11. The wide-angle camera, in contrast, had a slight dip in the useful arc length at that time, but would have ample and continuous utility until day 90. This can also be confirmed on inspection of the latitude extent curves shown in Figures 11 and 13.

3. Satellite Orientation with Respect to the Sun

a. Sun Angle

The angle between the upper spin axis and the direction to the sun is defined as the sun angle (α). This angle was based on the assumption of a fixed spin axis direction, and its history was calculated as a function of launch orientation and time after launch. Refer to Appendix A for the method of calculating the sun angle.

The history of the sun angle is shown for three launch orientations for the final TIROS I prelaunch orbit as a function of days after launch in Figure 18. The launch time parameter ($\Delta \phi$) is the angle in right ascension from the normal point to the subsolar point (positive to the east).

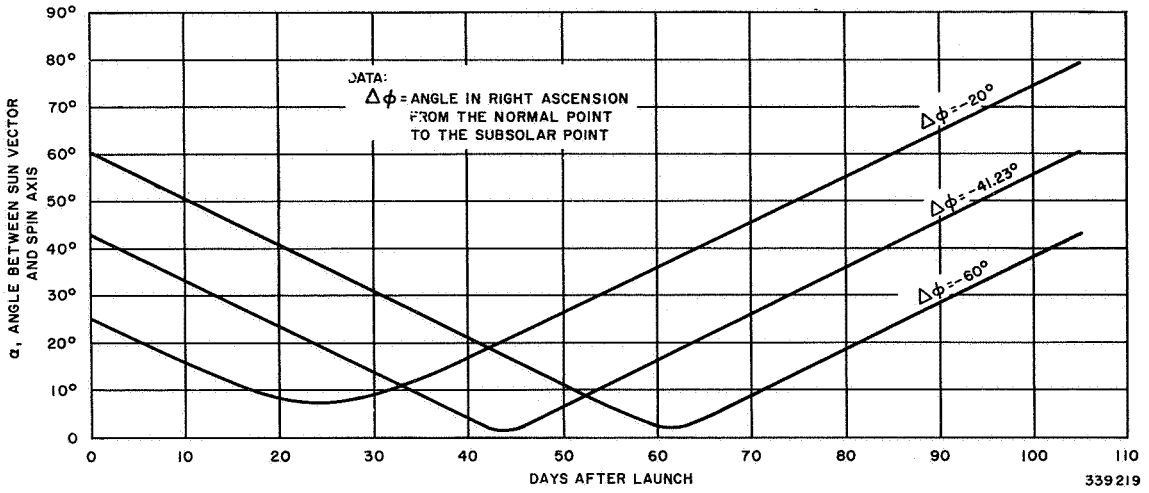

Figure 18. Alpha Angle between Sun Vector and Spin Axis for Various Days after 1 April 1960 Launch and Various Right Ascensions of Sun from Normal Point Angles ($\Delta\phi$)

The sun angle was an important factor in the satellite North Indicator subsystem and solar cells. The North Indicator (or sun angle) Subsystem reported the rotational phase of the satellite with respect to the sun by telemetering the output of the sun-angle sensor units. The slit provided for each sun-angle sensor unit was only one degree wide in the direction of rotation, and 60 degrees wide in the axial direction so that the sun was expected to be visible to the sensors until the sun angle dropped below 20 degrees.

The solar power input and thermal equilibrium were also controlled by the sun angle. A low sun angle would cause the sun to shine almost directly on the top of the satellite and only slightly on the sides, causing the sides and baseplate of the satellite to become relatively cold and the top to become too hot. The elevated temperature of the top decreased the efficiency of the relatively few solar cells exposed to the sunlight and thus tended to decrease the solar power input. The power input to the solar cells also tended to vary with the projected area, and was expected to diminish with both low and high sun angles. A broad flat maximum of available power was expected for sun angles of between 30 and 60 degrees.

b. Fraction of Time in the Sun

The fraction of time in the sun, as calculated in Appendix A was primarily a function of the orbit altitude, angular inclination, and initial orientation of the orbit with respect to the sun. Three histories of fraction of time in the sun versus days after launch for various launch conditions are given in Figure 19. The effect of launch time variations ($\Delta\ \phi$) as shown was primarily a time shift in the patterns. Furthermore, every second maximum reaches 100 percent time in the sun, while the other maximum was substantially lower for the orbit. This effect was due to the ecliptic with respect to the equator. The sun time history was, therefore, sensitive to the launch data as well as the launch time.

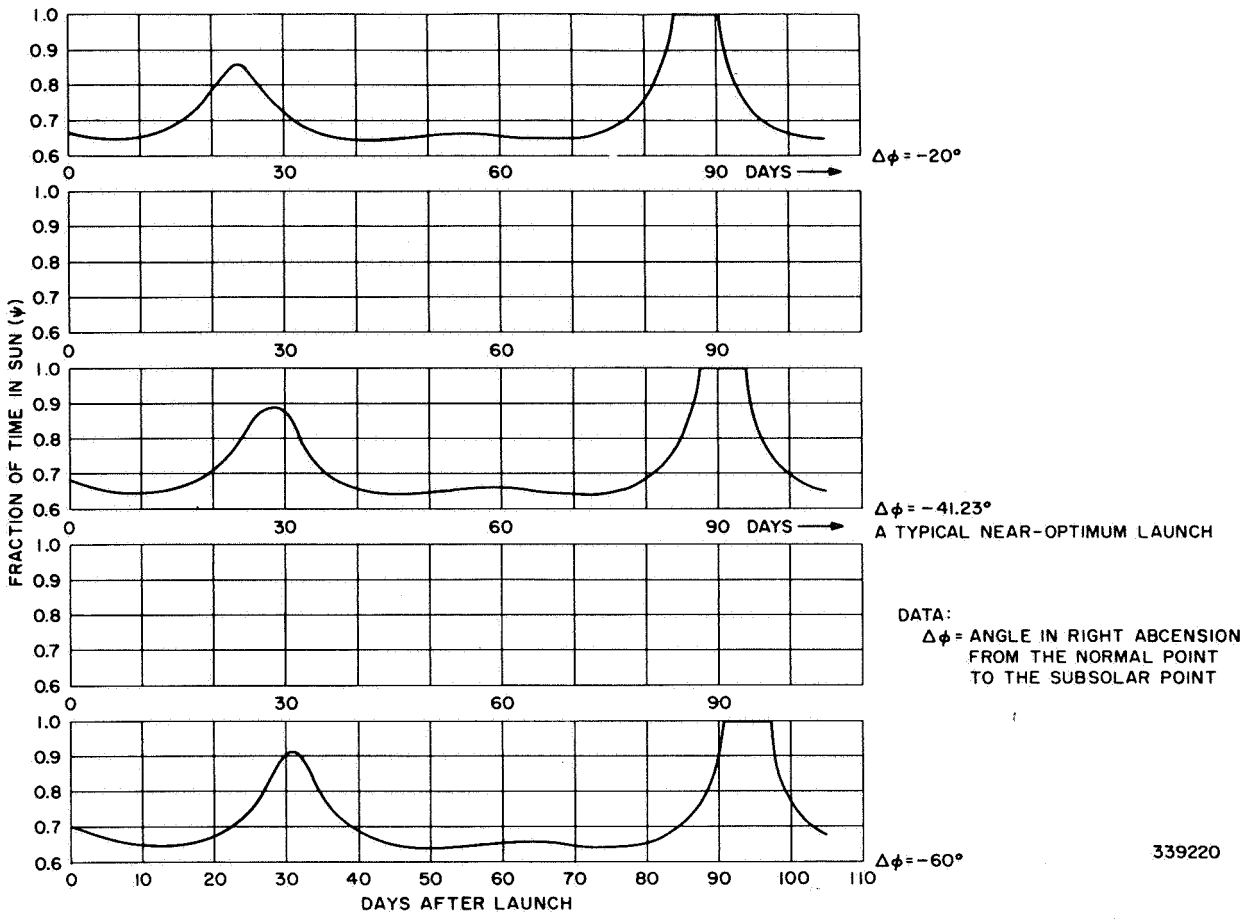

Figure 19. Fraction of Time in Sun (ψ) versus Days after Launch for 1 April 1960 Launch

Minimum fraction of time in the sun as a function of orbit altitude for any circular orbit is shown in Figure 20. The maximum time in the sun depended on the inclination as well as altitude and had an upper limit of 1.0, although for low altitude and low inclination orbits, this may never have been achieved.

4. Adjustment of Launch Time to Obtain Optimum Photocoverage

a. Calculation of Launch Time VS $\triangle\phi$

Time of launch is directly specified by $\Delta\phi$, the angle in right ascension from the normal point to the subsolar point. The time interval from launch to injection was given as 731 seconds; the longitude of the normal point as 43.97 degrees East; and the period as approximately 98.6 minutes (from Figure 21, Period, Orbital Advance and Orbits per Day versus Orbit Altitude).

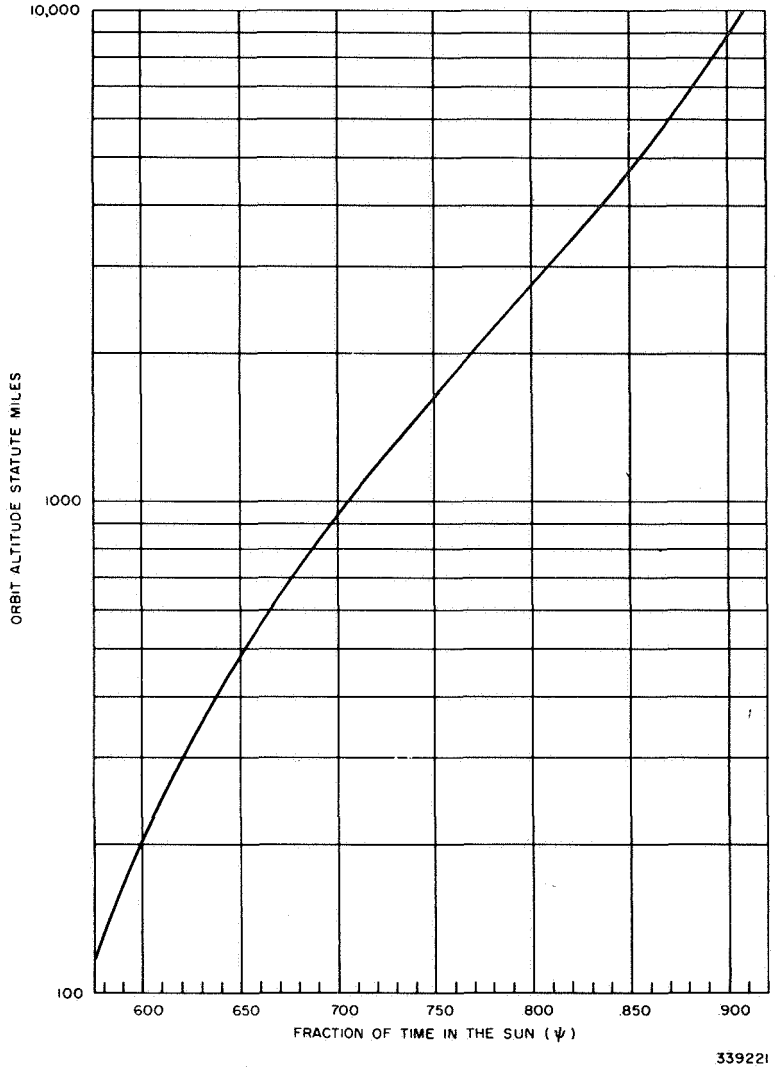

Figure 20. Fraction of Time in the Sun (ψ) for Various Orbit Altitudes

The launch time* required to produce a specified $\Delta\phi$ was found as follows:

L_Z = GMT time of launch

= time of crossing the NP - time of flight

$$= 12 - \left(\frac{\psi N + \Delta\phi i}{15}\right) - 0.60$$

$$= 8 \text{ hours and } 28.2 \text{ minutes } \frac{\Delta\phi i}{15}$$

*The "equation of time" term represents the positional difference between the "fictitious" mean sun on which Greenwich Mean Time is based, and the observed sun. This term will cause the optimum time to vary slightly with launch date. For this date, the term is approximately -4 minutes, i.e., the launch should be approximately 4 minutes later than calculated. The time tolerance of ±30 minutes on launch can easily contain such minor variations, so the term was ignored.

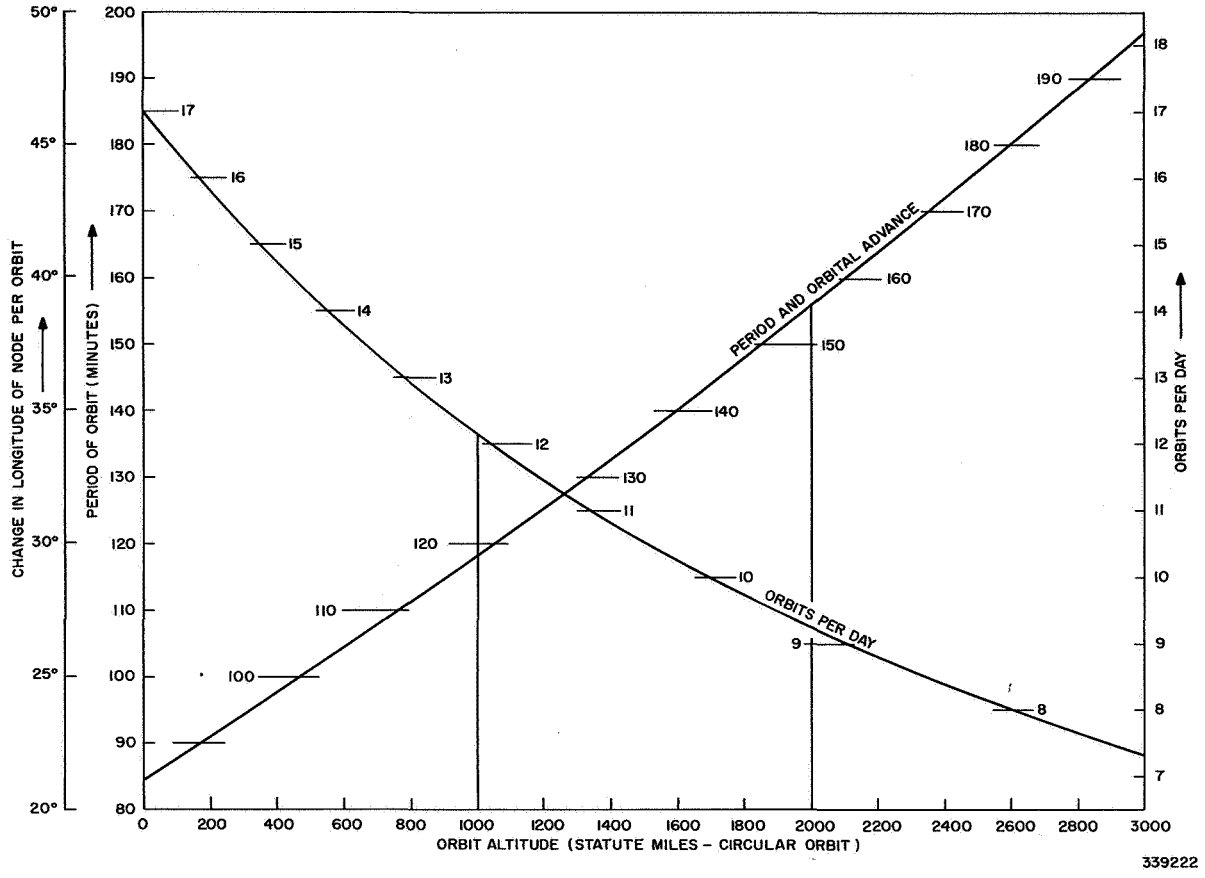

Figure 21. Period, Orbital Advance, and Orbits per Day versus Orbit Altitude

Where:

time of crossing normal point = $12 - \left(\frac{\psi N + \Delta\phi i}{15}\right)$

ψN = East Longitude of NP

$\Delta\phi$ = right ascension from NP to the sun

time of flight = time from launch to NP $\cong 0.60$ hours

The GMT and EST launch time to produce various $\Delta\phi$'s are listed below:

$\Delta\phi$	GMT	EST
-41.7°	11:15	6:15 AM
-60°	12:28	7:28
-20°	9:48	4:48

The relationship between $\Delta\phi$ and the GMT launch time is shown in Figure 22 for an East Longitude of the NP (ψN) of 43.97 degrees.

b. Establishment of Optimum $\Delta\phi$ and Launch Time Tolerance

It was apparent on inspection of the portion of the useful orbit for the narrow-angle and wide-angle cameras based on the extent of true anomaly versus days after launch (Figures 10 through 16) and the latitude extent of coverage graphs (Figures 10 through 13) that a launch time sufficiently late in the day to produce a $\Delta\phi$ of - 60 degrees would cause a rather severe loss of remote photographic capability in the Southern Hemisphere for the first few days after launch. It was also observed that a launch time sufficiently early to produce a $\Delta\phi$ of -20 degrees would cause the sun angle to drop below 20 degrees, thereby cutting off the North Indicator Subsystem at an unreasonably early date. (See Figure 18, α Angle Between Sun Vector and Spin Axis for Various Days after Launch and Various $\Delta\phi$ i Angles.) Between -20 degrees and -60 degrees would be a reasonable compromise, however.

It was then decided that a reasonable criterion for selection of launch time would be the attainment of the same sun angle 90 days after launch as that of the day of launch. An appropriate calculation was made to obtain the relationship in Figure 23, Right Ascension of Sun from Normal Point ($\Delta\phi$) Versus Date of Launch and the Earliest Launch (Minutes after 0500 EST) Versus Date of Launch. For April 1, the optimum $\Delta\phi$ was given as -41.5 degrees; the corresponding launch time as 11:14 GMT, or 6:14 A.M. EST (5:00 + 30 + value from Figure 23). The allowable tolerance on alignment of the spin axis with its intended position due to launch time error was set at ± 7.5 degrees or ± 30 minutes.

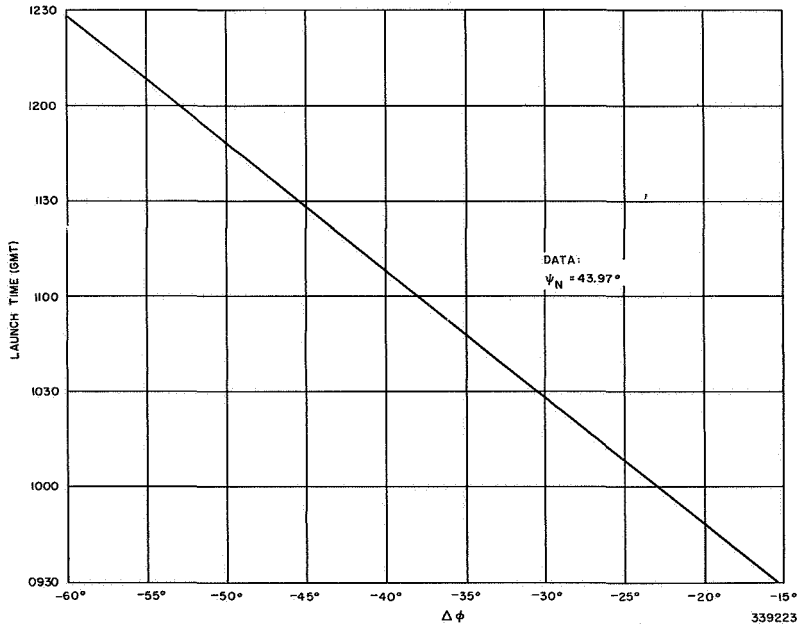

Figure 22. Launch Time (GMT) versus Right Ascension of Sun from Normal Point ($\Delta\phi$) for an East Longitude of the Normal Point (ψN) of 43.97 Degrees

This specified the launch interval as 5:44 to 6:44 A.M. EST, a 1-hour interval, which was well within the boundaries of permissible launch time due to the possible loss of coverage or early demise of the North Indicator Subsystem.

5. Contact Time between the Satellite and Ground Stations

An important system design consideration was the time available for contact between each ground station and the satellite. For a power-limited system, the contact had to be long enough to allow the transmission of the required information at the bandwidth which would be provided. This time also controlled the numbers of direct pictures to be expected from the satellite.

The contact time per orbit and the number of orbits contacted each day were functions of the orbital parameters such as altitude, inclination, eccentricity, and longitude of ascending node; and of such ground station parameters as latitude, longitude, and minimum antenna elevation angle at which contact would be efficiently provided. For any orbit and each ground station of interest, it was possible to calculate or graphically construct a curve of time in view above some specified minimum antenna elevation as a function of ascending node longitude. Part of the calculation would be made graphically. The contour around each ground station, defining subsatellite points at which the satellite would just be visible at the minimum antenna elevation for the altitude specified, was a small circle. This circle could be plotted on a polar sterographic or Mercator map projection. The useful part of the ground track of the satellite over a rotating earth was plotted on a sheet of tracing paper using the map grid for coordinates. The orbit track was then calibrated in degrees of true anomaly or in minutes of flight time from the ascending node of the orbit.

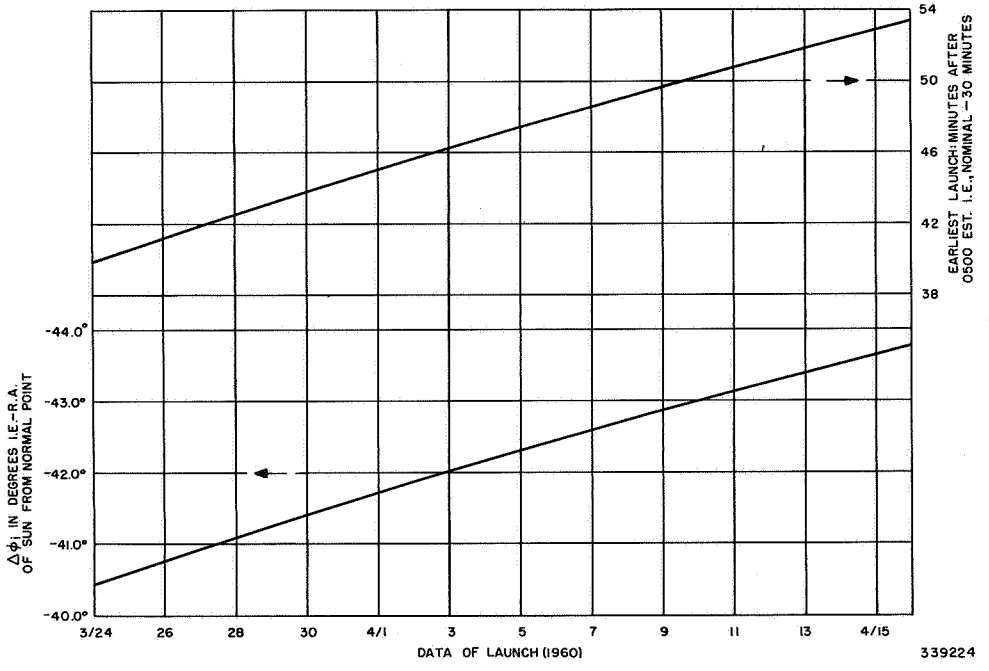

Figure 23. Right Ascension of Sun from Normal Point ($\Delta\phi$) and Launch Time versus Day of Launch and the Earlier Launch (Minutes after 0500 EST) versus Date of Launch

The orbit track overlay was then placed over the map of ground station elevation angle contours and the ascending node aligned with a desired longitude. The time of arc within contact was then read off between the two track intersections (if any) with each elevation contour and tabulated for plotting against longitude. The ascending node was then moved to a new longitude and the process repeated. The semi-graphical process was fast and convenient for circular orbits only. The ground track of the satellite and the elevation contours were mostly conveniently calculated by machine or hand, and then plotted. Contact time for an elliptical orbit was much more difficult to analyze by this method. Machine computation seemed more desirable than graphical means.

The iterative computation to solve for the points of intersection between a circular orbit trace and the minimum elevation contours for several ground stations was programmed on a computer. Figure 24 gives the results of this analysis for the TIROS I orbit and ground stations. Four ground stations are included: Kaena Point, Hawaii; Cape Canaveral, Florida; Fort Monmouth (Deal), New Jersey; and RCA-AED at Princeton, New Jersey.

For the same orbit, the shape of the curves was a function of the latitude and minimum antenna elevation of each ground station. If the satellite passes completely to the north of the coverage circle, as in the case of Hawaii, the coverage curve takes the form of two separate humps. As the ground stations are located further North, the valley between the humps is filled in more and more, and the humps move closer together in longitude of ascending node, as can be seen from the curves for Cape Canaveral and Fort Monmouth (Deal). Finally, though not shown here, the hump has only one peak which becomes shorter and narrower as the ground station moved above the maximum latitude to which the satellite could travel, i.e., the inclination of the orbit).

ORBIT DATA
ALTITUDE 380 N.MI. CIRCULAR
INCLINATION 48.3° DIRECT
PERIOD 98.85 MINUTES
ORBITS PER DAY 14.6
WESTWARD ADVANCE OF NODE
LONGITUDE PER ORBIT 25.03°
DEGREES TRUE ANOMALY PER MINUTE 3.64

SITE DATA	LAT	LONG	MIN EL	NMI SLANT RANGE	CONTACT RADIUS	ORBITS T>4 MIN
FT. MONMOUTH, N.J.	+40°184417	−74°056750	2.5°	1518	23.4°	6-7
RCA-AED PRINCETON, N.J.	+40.291027	−74.560861	5.0°	1388	21.2°	6-7
HAWAII	+21.563306	−158.24037	2.5°	1518	23.4°	6
CAPE CANAVERAL	+28.468333	−80.540000	2.5°	1518	23.4°	7-8

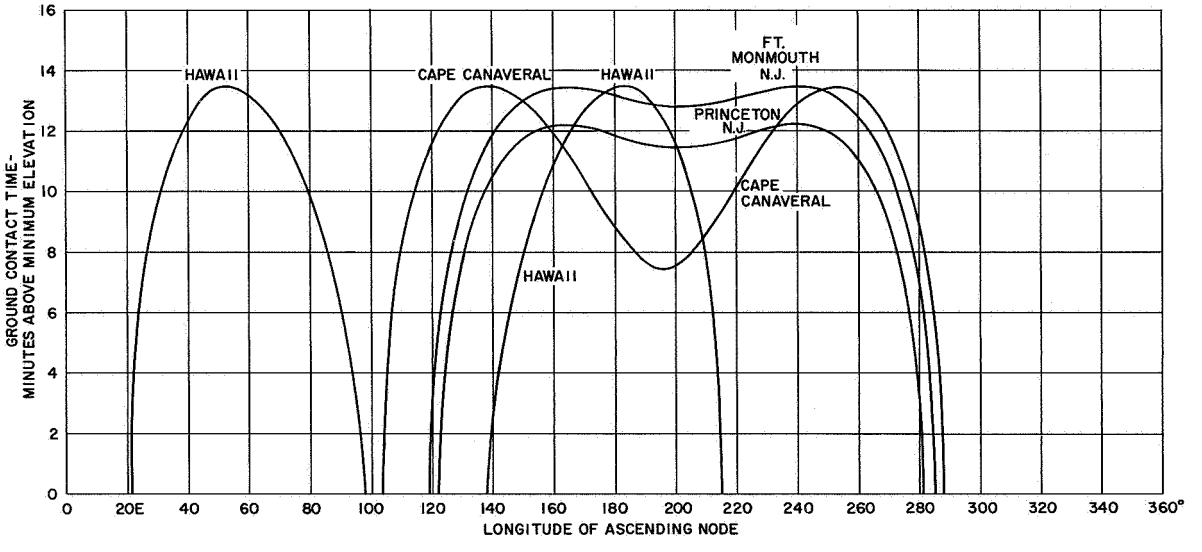

339225

Figure 24. Ground Contact Time versus Longitude of Ascending Node

It must be noted that one of the two periods of usefulness of the Hawaii station coincides completely with the useful period of the Fort Monmouth station. Such overlap could have been avoided by a different selection of ground station sites (to give the maximum number of orbits contacted per day).

The number of orbits which could be contacted per day with the Hawaii-Fort Monmouth combination of stations was 9 to 10. The useful duration of such contacts averaged 9 to 10 minutes, which was ample time for direct playback and clock set functions whenever they were required simultaneously. If the satellite system was limited in duty cycle due to insufficient solar input, programming could be reduced to the necessary level. If not, a generous contact capability was assured.

Due primarily to the rotation of the earth during the orbital period, successive ascending nodes occurred approximately 25 degrees farther westward in longitude than the preceding node. It is obvious from inspection of Figure 24, Longitude of Ascending Node Ground Contact Time versus Longitude of Ascending Node, that contact would be missed on one orbit in the daily sequence between the end of the Fort Monmouth contacts and the beginning of the left set of contacts at Hawaii. There would be a second and longer period of no contacts after the left set or second set of contacts at Hawaii, before the next day's sequence began at Fort Monmouth.

6. Accessibility of Various Ground Areas for Remote Picture-Taking

One of the more interesting facets of the photocoverage prediction problem was the determination of the ground areas which would be seen by the satellite. Figure 25,§Availability of Ground Areas for Photocoverage, TIROS I, is a Mercator world map showing the principal TIROS I ground stations and various coverage zone boundaries. The nearly circular contours about each ground station show the minimum duration of contact which a satellite would have with that ground station if the subsatellite ground track passed tangent to or within the contour. Direct contact, (i.e., direct and immediate transmission to the ground station of TV pictures not stored within the satellite) was possible whenever the subsatellite point fell within the 0 minute contour. The subsatellite ground track was a sinewave-like curve centered on the equator. Its northbound crossing of the equator, called the ascending node, could occur at any longitude. The zone boundaries shown as dashed lines are segments of ground tracks. (A similar but larger map and a movable clear orbit track overlay were furnished to each ground station and TIROS Technical Center, and were used as prediction and programming tools.)

The accessibility of a ground area for photocoverage depended upon the number of passes that the satellite made over the area in question and the time that had elapsed since the satellite last passed over a ground station. The remote program delay clock in the satellite had a maximum delay of approximately 5 hours. Therefore, the beginning of remote coverage could be delayed up to 5 hours after the passage of the satellite over a ground station where the clock was set and started.

If the ascending node of the orbit occurs at Longitude 280 degrees East (80 degrees West Longitude), this would be the first orbit of the daily sequence of orbits contacted by the ground stations as the earth rotated. Fort Monmouth ground station could program the

§This illustration is printed on a fold-out page located at the end of this volume.

cameras to take pictures somewhere on the orbit before the next ground contact. Remote pictures could be taken over the North Atlantic, Europe, etc., wherever illumination and distortion permit, until the satellite re-enters the Fort Monmouth photocoverage circle. The ability to take pictures in an area once every orbit is here defined as full remote coverage for that direction of travel (northbound or southbound) although in general a particular ground point would be visible twice a day at most.

For certain ascending node longitudes, the orbit would pass between the coverage circles without contacting either station. Therefore, remote pictures could not be taken once per orbit in the zones visible to the satellite along that part of its path, but rather once in the entire 2 (or more) orbit periods. This was defined as low availability for the direction noted. An orbit was missed regularly in the daily sequence, passing between Fort Monmouth coverage and Hawaii coverage. Thus, there was a much longer interval (4 or 5 orbits) between the last orbit contacted by Hawaii in each daily sequence of contacts and the first orbit contacted by Fort Monmouth on the following day. The clock could initiate the remote sequence only during the first 5 hours of this gap. Therefore, certain areas of the earth's surface were not available at all in a particular direction of travel. Two small areas, one near 49 degrees North Latitude at 20 degrees East Longitude, the other near 49 degrees South Latitude at 200 degrees East Longitude (160 degrees West Longitude), could not be flown over by the satellite taking remote-mode pictures at any time. This loss of coverage was not a serious limitation, especially because the wide-angle camera often could see the horizon, up to 24 degrees of arc away from the sub-satellite point. The orbit inclination and the distortion and illumination criteria, as already discussed, were the primary limitations to photographic coverage.

7. Actual Orbit Achieved

The final objectives, as previously explained, for the TIROS I orbit were: circular orbit, altitude 437.4 statute miles, inclination 48.3 degrees; payload vertically (normal point) at 20.0 degrees North Latitude, and 43.97 degrees East Longitude (59.9 degrees right ascension and 20.0 degrees declination). The orbit finally achieved had an apogee altitude of 467.01 statute miles, a perigee altitude of 430.5 statute miles and an inclination of 48.387 degrees. The normal point was located at 18.0 ± 2 degrees North Latitude and 62.2 ± 2 degrees right ascension.

The most significant deviation from the pre-launch predictions was in the orientation of the spin axis, which was assumed to be stationary in the pre-launch photocoverage predictions. Observation of the satellite in orbit showed that it moved in declination and right ascension after launch. A study to observe the spin axis motion of the TIROS I satellite under the influence of magnetic, gravitational, and eddy current torques was conducted at RCA-AED. Figure 26 shows the observed track of the spin axis and the track computed from the model. The results show that, for the proper choice of the satellite's magnetic moment, theory and actual operation are in close agreement. With the exception of the effect of the motion of the spin axis, all the predictions of photographic coverage were successful with respect to orbital parameters.

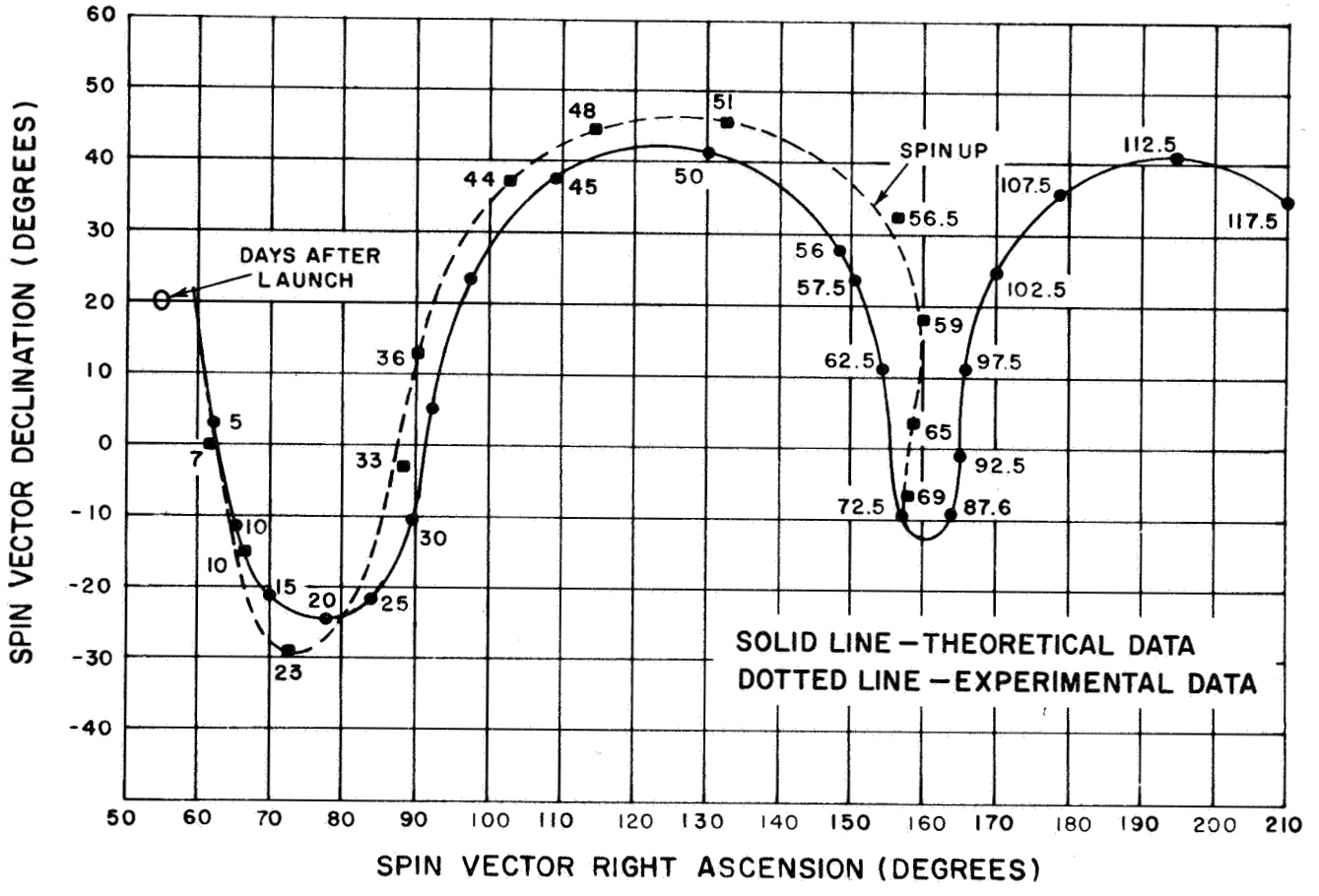

Figure 26. Observed Motion of the TIROS I Spin Vector

Since the launch occurred at 6:40 A.M. EST, nearly the last minute of the allotted hour from 5:44 to 6:44 A.M., on 1 April 1960, the Normal Point or spin axis celestial coordinates achieved were from 16.0 degrees to 19.8 degrees (North) declination and 60.2 degrees to 64.1 degrees (East) right ascension. (A confirming teletype message from W. R. Bandeen of NASA dated 5 July 1960 is reproduced in Appendix B.) The right ascension from the normal point to the sun ($\Delta\phi$ i), therefore was approximately 10.8 degrees - 62.1 degrees or 51.3 degrees ± 2.0 degrees. Predictions were made immediately after launch by interpolating between the predictions made for -41 degrees and -60 degrees $\Delta\phi$ i. The later predictions were rendered invalid after a few weeks because of the motion of the spin axis. This was first noticed as a discrepancy in picture location and attitude, but it affected sun angle as well. The sun angle achieved remained substantially above the predicted values due to this drift. (See Figure 27, Angle α versus Days after Launch.) The sun-angle subsystem continued to work during the useful life of the satellite instead of exhibiting the expected dead period due to low sun angles.

Since the horizon scanner system was not useful as means of determining the satellite attitude (because the field of view was to wide, the spectral response sometimes caused spurious signals and the ground station computer programming was not flexible enough to handle this data), it was necessary to infer attitude from any available data. It was possible to determine attitude from the wide-angle photographs, and the sun angle from temperature and voltage telemetry. For a discussion of attitude determination from photographs, refer to Allied Research Associates, Inc. "A Manual of Emergency

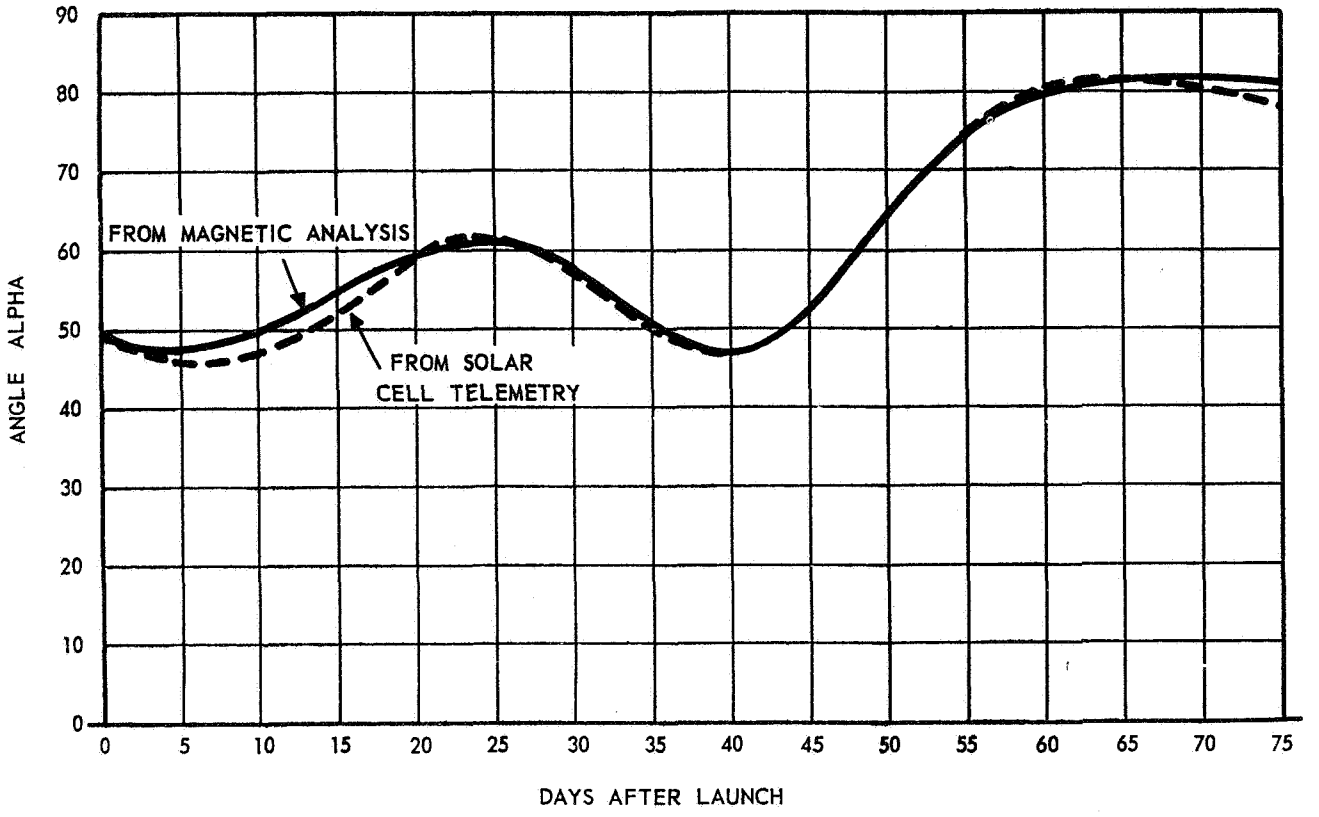

Figure 27. Angle Alpha versus Days after Launch

Computation Procedures for the Immediate Operational Use Program of Project TIROS," and RCA-AED Technical Memo 310-13 titled "A Satellite Picture Rectification Device" dated 12 December 1958.

C. SATELLITE-GROUND COMMUNICATION

1. General Considerations

Since the primary mission of TIROS I was the transmission of cloud photographs, the satellite to ground communication link for transmitting this data received considerable study. The usual trade-off of power, bandwidth and data rate were considered together with those system limitations inherent to existing subsystems. The basic system finally evolved from many compromises and considerations of limitations in various parts of the system. The basic data rate was chosen such that the 500 line picture was read out in 2 seconds. This gave a maximum video frequency of 62.5 kc. Due to the requirements for low frequency recording, the video signal was used to frequency modulate an 85 kc subcarrier before recording on tape. This subcarrier in turn was used to frequency modulate the TV transmitter.

The radio-frequency for the TV transmission was chosen to lie in the 215- to 260-Mc telemetry band due to the existence of 60 ft. parabolic receiving antenna systems and

associated FM receivers. This band also represented a good choice between lower frequencies with increased cosmic noise and the higher frequencies where state-of-the-art transmitters were less available. Having chosen the bandwidth, carrier frequency and antenna gain, the required transmitter power was a reasonable value. The design criterion for the TV-FM circuit was that a minimum carrier-to-noise ratio of 12 db, with some margin, be available at maximum slant range. The final choice of these various factors gave a margin of about 10 db above the FM threshold with a 2-watt FM transmitter. The maximum slant range was based on a minimum angle above the horizon of five degrees. The choice of the 200-Mc band also was influenced by the need for a nearly isotropic antenna radiation pattern on a vehicle structure roughly a wavelength in diameter at this frequency.

The tracking beacon frequencies of 108.00 and 108.03 Mc were chosen to conform with existing Minitrack facilities. These frequencies also allowed use of existing transistors, with proven performance in the Explorer and Vanguard systems. While the availiable power output of these devices was limited to the 10 to 100 mw range, the use of narrowband receiving systems allowed use of these relatively low power transmitters. In addition to tracking, the beacon transmitters also were used to transmit the slow-speed telemetry data which measured the performance of the orbiting system.

In addition to the requirements for transmission of TV and tracking data, a "command" radio circuit was required to control the satellite functions. Due to the use of AM command transmitters at existing Minitrack stations, the same system and frequency band were chosen for TIROS I. The choice of frequency band was again influenced by feasibility of antenna structure on the satellite and by existing ground transmitters, plus the limitation of transistors for the satellite borne command receiver. Due to the extreme reliability desired for the command functions, a large margin of power (200 watts) was provided in the command transmitter.

In general, the calculated system performance was realized in the TIROS I radio transmission system. (Reference 19)

2. Selection of Transmission Parameters

The calculation of radio propagation parameters for TIROS I were based on the following characteristics:

Maximum elevation:	400 nautical miles
Maximum slant range (5 degrees above horizon):	1435 nautical miles

3. Definition of Symbols

P_T: transmitter power output db above 1 watt (dbw)

G_T: gain of transmitting antenna over isotropic (db)

L_T: coupling or line losses, transmitting system (db)

G_R: gain of receiving antenna over isotropic (db)

L_R: coupling or line losses in receiving system (db)

P_L: path loss between isotropic antennae (db)

P_R: signal power received by matched load (dbw)

P_N: noise power received by matched load (dbw)

F: receiver or preamplifier noise figure (db)

T_A: antenna temperature (°K)

T_e: receiver noise temperature referred to input: $T_0(F-1)$

T_0: IRE reference temperature = 290°K

B: system bandwidth (cps)

K: Boltzmann's constant (1.38×10^{-23} joules/°K)

4. TV Subsystem Propagation

For this system the desired criterion was that the i-f carrier to noise should be above the FM threshold at maximum range. The FM threshold was taken as 12 db rms carrier to rms noise in the 500 kc bandwidth i-f. Early tests on the TIROS I TV Picture Subsystem showed that excellent video pictures were received at this i-f ratio which corresponded to 21 db peak black to peak white signal to rms noise ratio.

To account for the fact that circular polarization was used in the TV transmitter, while linear polarization was used to receive the signal, a loss of 3 db is indicated by $G_T = -3$ db. The use of 3 db noise figure preamplifiers was assumed, and the antenna temperature due to cosmic noise was estimated to be 620°K at 235 Mc.

The following calculations then indicate a carrier-to-noise ratio of 21 db at maximum range or a margin of 9 db over threshold. A sixty-foot parabolic receiving antenna and a 2-watt carrier were assumed.

$$P_R = P_T + G_T - L_T + G_R - L_R - P_L$$

$$P_R = +3 -3 -1 +29 +0 -149$$

$$P_R = -121 \text{ dbw}$$

$$P_N = K (T_A + T_e) B$$

$$P_N = -142 \text{ dbw}$$

$$C/N = -121 + 142 = 21 \text{ db}$$

5. Beacon Subsystem Propagation

In this system, the transmitter output was about 30 mw; the polarization loss was zero, since H and V outputs were combined; and a 10-db gain receiving antenna was assumed. The i-f bandwidth assumed was 10 kc; and the receiver noise figure itself, 3 db. These constants result in an 8 db carrier-to-noise ratio in the wide i-f channel (i.e., 10 kc). However, in the narrow telemetry filter of 200 cps bandwidth, an improvement of about 14 db results. In the telemetry recorder, a 10-cps low-pass filter again increases the S/N ratio, so ample margin is obtained. In addition, at some stations, higher-gain receiving arrays were used. T_A was estimated as 1830°K and T_o = 290°K.

$$P_R = P_T + G_T - L_T + G_R - L_R - P_L$$

$$= -15 + 0 - 1 + 10 - 0 - 142$$

$$P_R = -148 \text{ dbw}$$

$$P_N = K(T_A + T_e)\, B$$

$$= -156 \text{ dbw}$$

C/N in 10 kc i-f channel = -148+156 = +8 db

S/N in 5 kc audio channel* = +8 db

S/N in 200 cps filter = 8+10 log 5000/200 = 22 db

6. Command Subsystem Propagation

For this circuit, a 200-watt transmitter was used. A one db loss was allowed for lines and coupling circuits; a 12 db transmitting antenna gain was used; a 3 db loss was allowed for linear polarization at the receiver; an addition 3 db loss was allowed for the effect of paralleling two receivers on the single receiving antenna. The carrier-to-noise ratio is calculated for the 40 kc i-f channel of the command receiver with a noise figure of 10 db. The tone filters used in the vehicle varied in bandwidth; however, calculations refer to a nominal 1 kc bandwidth filter. Ample margin is derived from this combination of factors.

$$P_R = P_T + G_T - L_T + G_R - L_R - P_L$$

$$= 23 + 12 - 1 - 3 - 3 - 144$$

$$= -116 \text{ dbw}$$

$$P_N = KT_oBF = 148 \text{ dbw}$$

C/N in 40 kc i-f channel = -116 + 148 = 32 db

S/N in 20 kc audio channel* = 32 db

S/N in 1 kc audio channel = 32 + 10 log 20,000/1000 = 45 db

* The C/N ratio for a 10 kc i-f is the same as the S/N ratio for a 5 kc audio channel. The C/N ratio for a 40 kc i-f is the same as the S/N ratio for a 20 kc audio channel.

SECTION II. ANALYSIS OF ENVIRONMENTAL EFFECTS

A. THERMAL CONSIDERATIONS

The temperature-control problem for TIROS I was that of maintaining an acceptable range of temperatures in a non-homogenous mass which: (1) would be in direct sunlight for part of an orbit, and be shadowed (by the earth) for the remaining part, and (2) while illuminated, would have one surface always facing toward the sun (although at a varying angle), and an opposite surface facing away from it. An allowable temperature variation between 0° and 50°C within the satellite was set mainly by physical limitations of the instrumentation, while solar cell energy-conversion characteristics set a requirement for the lowest possible temperature at the housing outer surfaces. Allowable satellite weight and design-simplicity considerations dictated the use of passive temperature control techniques.

The over-all temperature control problem involved three main areas: analysis of the heat-flow problem, development of suitable surfaces and surface coatings to obtain desired absorptivity to emissivity ratios, and finally, experimental verification of the satellite's thermal-design acceptability. Factors that entered into the treatment of the three-dimensional satellite structure, as contrasted with a simple surface, were:

1. Thermal conduction and radiative coupling among the various component masses of the satellite,
2. Distribution of the internally-generated heat,
3. The thermal time constants of the several masses, and
4. The influences of the satellite geometry on the effective radiative properties of various surfaces.

The governing equation is that of heat conduction; but this equation could not be solved rigorously because of intractable boundary conditions. However, as has since been proven, models and approximate solutions provided sufficiently accurate information for satisfactory thermal analysis and design.

A series of studies (discussed in Part 2, Section III: Thermal Design) resulted in a "compromise" design, lying between two extreme philosophies for thermal control: the adiabatic, or "thermos bottle" design, in which the interior instrumentation is thermally isolated from the exterior satellite surfaces; and the isothermal design, in which all of the parts of the satellite are in such good thermal contact that the entire satellite can be assumed (at any one time) to be at one temperature. The structure and contents would

be so designed as to provide: (1) the maximum possible radiant energy interchange between a single-layer top skin and the satellite interior; (2) a single-layer, segmented, side skin, electrically, but not thermally, insulated from the top skin; and (3) a single-skin (stiffened) baseplate; the latter two for minimum thermal resistance between inner and outer surfaces. The thermal condition of all components would be monitored to determine if special localized treatment would be necessary.

The actual design, then, proceeded on this basis; it is discussed in detail in Part 2, Section III: Component Design.

B. DYNAMICS CONSIDERATIONS

1. General

One of the early problems that had to be solved in the development of the TIROS I satellite was that of adequate dynamics control (orientation and spin control). Predictions of camera coverage were based on a fixed spin-axis orientation in space, which would be maintained by spin stabilization. The satellite had to rely mainly on initial momentum for maintaining its spin rate. In addition, a strong possibility existed that the spin axis of TIROS I would "wobble" (nutate or precess) about the initial orientation when the satellite separated from the final-stage rocket. Because the spin and optical axes are not parallel during nutation, the magnitude and duration of nutation could greatly affect the usefulness of the entire mission by smearing the camera image.

By proper selection of the ratio of principal moments of inertia and an internal energy absorber, a spin-stabilized satellite can be made to spin without "wobble" or precession about the desired spin axis. Studies of dynamics control techniques made during satellite projects preceding TIROS laid the groundwork for the design of the TIROS devices. The first satellite proposed to carry a TV camera into orbit was limited in its dimensions by the rocketry available at the time of its development. It was necessary, in this first design, to orient the camera optical axis along the longitudinal axis of a rod-shaped structure approximately 5 inches in diameter. A spinning structure prefers to spin about the line around which the mass of the body has its maximum moment of inertia. For the rod-shaped body, this is a line perpendicular to the longitudinal axis of the rod.

The carrier rocket for this satellite received a spin around its longitudinal axis (of approximately 750 rpm) during launch, for stabilization. Upon satellite separation, a disturbance causing a component at right angles to its spin axis would cause the satellite to precess.

This oscillation builds up if there is any energy dissipated (such as heat due to mechanical bending) in phase with the precession oscillation. The system finally ends up spinning around its axis of maximum moment of inertia, and appears to be tumbling. Explorer I proved this theory when it actually tumbled due to the whipping of the crossed dipole antennas which were used for the 108.00-Mc beacon. To counteract this problem, an "active" damping system for this type of satellite was devised to produce mechanical friction which would be out of phase with the precession oscillation. This method

required that there be a net power gain by the system, derived, in this case, from the chemical batteries. The system would spin true about its longitudinal (rod) axis with such a device.

A decision to change the mission of the original satellite resulted in assignment of a different missile system (Juno II) which permitted a greater satellite weight and more favorable configuration. However, it was still not possible to achieve a ratio of moments of inertia which would provide a disc-shaped, stabilized system. A new optical system was called for, which dictated a much lower satellite spin rate because of the high-camera-resolution requirement. A slowdown from an initial 450 rpm spin rate to as slow a rate as would still maintain enough angular momentum for stabilization (i.e., about 10 rpm) was planned. The means to achieve optical-axis orientation were extensively analyzed and the following methods were considered.

a. Sun-Follower

This method required the camera to be attached to a platform which counter-rotated, with respect to the outer frame of the satellite, at a rate which immobilized the optical axis. The sun was to be used as a fixed reference during the picture-taking period.

b. Change of the Moment of Inertia

This method, by increasing the moment of inertia, would change its inertia from a rod to a disc, thereby assuring spin stabilization at the required 10 rpm.

c. Slow-Down of the Camera Assembly Only

This would be done during the picture-taking part of the orbit by transferring the camera momentum to a high speed flywheel.

Method b. was finally selected. Detailed dynamic analyses of satellite slow down and of the elimination of precession were made. Selection was made of a cable-reel slow-down mechanism, using weights in a manner similar to the balls on a fly-ball governor. This design would solve both problems of speed slow-down and conversion from rod to disc characteristics while the satellite was in orbit.

The weights (in this case, the satellite batteries) at the ends of four cables would be slowly let out (due to centrifugal force) to a distance of six feet. In the process of increasing the moment of inertia, this would (in a momentum conservation system) slow down the angular speed. By keeping the four extended batteries and cables (under tension from centrifugal force) as part of the overall mechanical system, the total satellite system would be converted from a rod to a disc-shaped body. The dissipation of energy released from the flexing of the cables due to any precession would cause the oscillation to damp out, as in a stable disc-shaped system, keeping the configuration axis, spin axis, and optical axis properly aligned. A prototype was built and tested at RCA. Computer studies of this system indicated that the final orientation of the satellite would be reached

in less than one-quarter of an orbit, so that it would be capable of transmitting pictures during its first orbit.

Another change in the missile system (this time, the Juno IV) permitted a reproportioning of the satellite structure to a pill-box shape, approximately 42 inches in diameter and 19 inches high. Since the rocket's upper stage used liquid propellent, and was equipped with guidance control, no spin was needed for stabilization during the launch phase. Consequently, the satellite could be placed into orbit at the spin rate needed for orbital altitude stabilization, consistent with picture-taking requirements (10 rpm). The despin weights and cables requirement was thereby eliminated, resulting in a much simpler system.

A second change in the mission requirement of the satellite was directed (in mid-1958) to that of a meteorological observer. Independent TV camera and magnetic recording systems, and "scanning" infrared observation systems were to be provided. This new arrangement required an increase of spin rate to 12 rpm.

Again, a change in the missile system (to the THOR) required reconsideration of the spin rate problem. The final stage of the THOR missile system used solid fuel, and was spin-stabilized at 120 rpm. Therefore, it would be necessary to slow down the spin rate of the satellite in orbit from 120 rpm to 12 rpm. Once again, the weight and cable despin system was considered. It was found unnecessary to maintain the extended weights and cables as part of the satellite system, because no conversion of the ratio of moments of inertia from rod to disc was required. A simpler system was evolved, in which weights and cables wrapped around the satellite housing are allowed to fly out under the influence of centrifugal force at the initial angular velocity, and then are released to continue into space, carrying with them sufficient momentum to slow down the spin rate to 12 rpm. A photograph of the "Yo-Yo" installation on the satellite is shown in Figure 112. The ten-fold spin-speed reduction was to be accomplished by about 2-1/2 pounds of equipment. (This "Yo-Yo" type of despin mechanism, was originally used by Jet Propulsion Laboratory on Pioneer IV.)

The earth's magnetic field acting upon magnetic materials in the satellite eventually reduces its spin rate below the desired minimum acceptable value of 9 rpm. A number of small "spin-up" rockets, whose firing was controlled from the ground, were equi-spaced around the periphery of the satellite to compensate for spin slow-down. By firing a pair of opposed rockets from ground control a spin-up of 3 rpm could be accomplished.

In addition to the consideration of spin-rate control, means for quickly damping out any precession or nutation introduced into the satellite upon its injection into orbit were studied. It is true that if a damper were left out of a spin-stabilized satellite it would eventually end up spinning about the desired axis. The disadvantage to this method is length of time (a few weeks) for the satellite to become stabilized. Furthermore, if it would be disturbed by any outside influence, such as a meteorite, precession would again render it ineffective for a considerable duration of time even if a vital spot was not damaged.

Because TIROS I (or any other satellite) is not infinitely rigid, this damping action is present. Each point of the precessing satellite structure is subjected to a sinusoidal force of a magnitude that is a function of its position. This indicates that cyclic shear stresses are acting throughout every portion of the vehicle, which would result in minute deflections of adjacent particles of structure. Since the structure has hysteresis we would again have one-way flow of energy. The main disadvantage as pointed out previously is that this flow would take too long and be nearly impossible to check by either calculation or measurement. An analysis of the parameters involved in precession resulted in the design of a novel tuned energy-absorption mass (TEAM) damping mechanism. This mechanism is illustrated in Figure 113. It consists of two masses, 180 degrees apart sliding vertically on the inside of the satellite, which convert the kinetic energy of precession to thermal energy by friction. When all of the kinetic energy is converted to thermal energy, the satellite is spin-stabilized. The advantages of this design are:

1. Each sliding mass need be only one-thousandth of the satellite's mass,
2. Alignment of the spin axis with the optical axis is attained within a tolerance of ± 0.5 degree, and
3. The time to reach this alignment from an initial value of ± 2.5 degrees is about one minute (based on a 120 rpm initial spin rate).

The details of the design and functioning of the TIROS I dynamics control devices are discussed in Part 2, Section III: Dynamics Control.

C. OPTICAL CONSIDERATIONS

Although the design of predecessor satellites is reflected, to a large extent, in the design of many portions of the TIROS satellite, the optics required for the meteorological mission (as contrasted with the missions of previous designs) was completely unrelated. Relatively simple, refractive optics were found to be adequate on the basis of the required quality of coverage (i.e., resolution) and area of coverage. These parameters were dictated by the meteorological utility demanded of the satellite, and stemmed principally from work done at Blue Hill Meteorological Observatory. (Reference 1)

An initial specification calling for three cameras, each having a different angle of view, was soon changed to two cameras, having angles of view (and resolutions) in the neighborhood of a 10 to 1 ratio. The wide-angle camera was to cover an area approximately 725 miles on a side;* the narrow-angle, approximately 63 miles. From an altitude of 400 nautical miles the wide-angle camera, with a resolution of approximately 1.3 miles, would permit photography of major cloud systems; while the narrow-angle camera, with a resolution of approximately 0.127 miles, would permit photographic discrimination between single cloud elements, and, thus, identification of cloud forms.

*Because of the spherical geometry involved, a rigorous specification of coverage area is quite complex. Simple relations drawn between camera angles and coverage may, therefore, be misleading.

The usefulness of the TV camera is measured not only in terms of the dimensions of the scene it is capable of resolving, but also in the minimum illumination required for an exposure. Typical vidicon operation permits the following operating conditions: with 0.03 ft-candle-seconds impinging on the photoconductor through the lens, an image bright enough to produce a good picture on a television screen will result with an effective lens aperture ratio of F/2, and a 1 millisecond exposure. A scene illuminance of 480 foot-lamberts is required by the specifications. The cameras were capable of linear operation over a scene-illuminance range of 100 to 14,000 foot-lamberts. The maximum highlight brightness which could be encountered in space was estimated to be 11,000 foot-lamberts; therefore, vidicon saturation would not occur. Photography, then, is practicable at any time when the position of the satellite with respect to the sun and the "subject", or scene, is favorable; and when minimum illumination of the scene by the sun exceeds this value.

For best definition of clouds and cloud masses, a somewhat different spectral response is desired than that for normal earth photography. Sensitivity restricted to the red, orange, and yellow parts of the spectrum was found to give superior results. Consequently, a vidicon with high sensitivity along the yellow to red portion of the spectrum was developed for TIROS, and the optical (lens) system incorporated a "yellow" filter (with a cut-off below 5000 Å) to provide an optimum spectral range. The two lenses selected for TIROS I were essentially off-the-shelf items. The wide-angle lens of 5.33 mm focal length, was supplied by the Elgeet Optical Company; the narrow-angle lens, of 40 mm focal length, was supplied by the Goertz Optical Company. However, both were modified by the manufacturers for the TIROS application by the elimination of unnecessary components, ruggedization, incorporation of the spectral filter, and adaptation for satellite mounting.

SECTION III. COMPONENT DESIGN

A. SATELLITE COMPONENTS

1. Standardization and Reliability

Reliability was considered a paramount factor from the start of the TIROS I project, through the design and development phase, the parts procurement program, the construction phase and final testing. In the design of TIROS I, provisions were made for separate TV camera channels in the satellite which were completely independent of each other operationally. Furthermore, redundancy was incorporated in the provisions for programming the direct and remote modes of operation. The satellite power supply was isolated into three separate portions, which normally operated with paralleled output. These portions were so protected that if any portion became disabled or malfunctioned, it would have no adverse effect on the two remaining portions. This factor of safety guaranteed continued, if limited, operation of the satellite.

Each TIROS I ground station contained duplicate programming racks, with either capable of being a back-up for the other within switch-over time (with the possible loss only of clock-setting accuracy).

When designing the subsystems, the quality control evaluation of parts for reliability was the foremost factor in their selection. The selection of parts and components was based to a large extent on reliability analyses performed by the Central Engineering Department of RCA, composed of engineering specialists in reliability. All standard parts that became stock items were purchased only after the recommendation of this group. To further ensure parts reliability, all parts were derated below the ratings specified by the manufacturer. Quality control inspection was conducted on each vendor item upon delivery, to ascertain whether they conformed to RCA specifications.

Special procurement parts specifically designed for TIROS I (including parts manufactured by RCA) were also checked for conformance to the reliability requirements. Some of these items, such as the ground-based tape recorders and spin-up rockets, were inspected by RCA engineers and vendor engineers at the vendor's facilities.

During development and design, reviews were held with engineering consultants and field technicians to determine the design effectiveness and reliability for components, subsystems, and the system in its entirety. As a result of these reviews, recommendations for improved reliability were incorporated into the system. As soon as parts were incorporated into functional components, all pertinent data on their performance was recorded, and this information was made available to responsible personnel who, when

persistent malfunctions were indicated, took the necessary steps to prevent their recurrence. Furthermore, all space hardware was subjected to severe environmental tests to ensure that it met reliability requirements.

The effectiveness of the standardization and reliability program was proven by the fact that the majority of reliability objectives were met.

The few failures and malfunctions that occurred had no adverse effect on the over-all objectives of the program. Two minor ground-station malfunctions, which were easily corrected, occurred during post-launch operations.

2. TV Picture Subsystem

a. General

The satellite-borne portion of the TV picture subsystem consists of two essentially equivalent channels, each having five functional components. Together, these five components performed the primary task of the TIROS I satellite, which was to take pictures of the earth's cloud cover at appropriate times, store the data when necessary, and transmit the data to the ground stations upon radio command from the ground.

The five functional systems which comprise the satellite portion of the television picture subsystem are as follows:

1. The TV camera
2. The tape recorder
3. The TV transmitter
4. The command receiver
5. The programming and control equipment

TV pictures are taken by a wide-angle and a narrow-angle vidicon camera, each of which is mounted on the satellite baseplate pointing down parallel to the spin axis. The narrow-angle and wide-angle TV pictures are sequentially transmitted by the TV transmitters to the ground stations, where they are received by TV receivers and associated electronics, recorded on a magnetic tape recorder and presented as a video display.

This subsystem is capable of two modes of operation, direct and remote. In the direct mode of operation, the TV pictures are taken at 10 or 30 second intervals upon command from the ground station and are transmitted to the ground station directly, as they are taken. The direct mode of operation is used when the satellite is within communication range of the ground stations. In the remote mode of operation, a series of 32 pictures are taken at 30-second intervals, by each camera; the time at which the series is started is preset by ground radio command, in the satellite programmer. The pictures are stored by the two video tape recorders until the satellite is again within communication range of a ground station, at which time they are played back and transmitted to the ground station upon command.

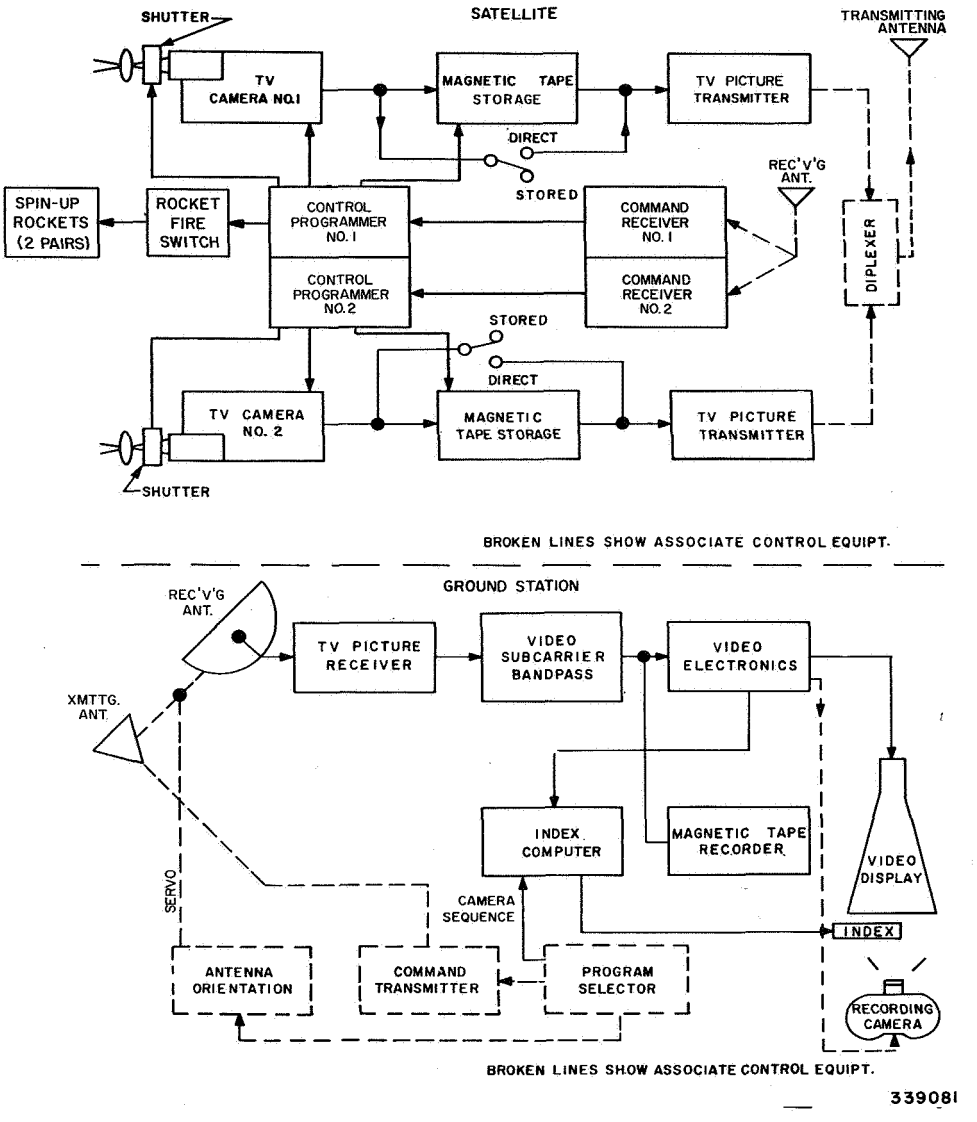

Figure 28. TV Picture Subsystem, Block Diagram

b. Functional Description

A block diagram of the TV picture subsystem is shown in Figure 28. Command signals are transmitted from the ground by the command transmitter which is controlled by the program selector. These signals are received simultaneously by the two command receivers in the satellite and fed directly to the two control programmers. According to the command signal, the control programmer either stores the command for the remote mode of operation, or applies the command directly to the cameras to start the picture-taking for the direct mode of operation. The programmer also controls the outputs of the TV cameras. In the remote mode of operation, the camera outputs are applied to the magnetic tape recorders for application as modulation to a subcarrier or for storage and subsequent playback (upon command from the ground station), at which time the tape-recorded data is played out into the TV transmitter. In the direct mode of operation, the camera video output is applied to the tape recorder electronics, again as modulation to a subcarrier generated there, and is then applied directly to the TV

transmitter for transmission to the ground station. (The auxiliary control unit in the satellite also controls the firing of the spin-up rockets through the rocketfire switch).

The TV transmitter signal is received, at the ground station, on two receivers which are connected for polarization diversity. The video subcarrier is then separated from the sun-angle signals (which are transmitted by the TV transmitters) by the video subcarrier bandpass filter. The video is then applied to the video electronics, the output of which is presented as a video display on a kinescope. It is also applied directly to a recorder for storage. A recording camera is used to photograph the kinescope display and a picture identification code (camera and picture numbers). The picture identification code is derived from the video electronics and processed by the index computer for presentation on the index display.

(1) TV Cameras

(a) General

Two independent vidicon camera systems were used on the satellite, each consisting of the camera optics and associated electronics. These camera systems were specially designed and built by RCA for satellite meteorological observation service. The function of the cameras is to optically collect an image of the earth's cloud cover and convert the image to an electrical video signal which can be processed and transmitted to the ground stations.

The cameras, one of which is shown in Figure 29, were identical units, except for the lenses. A wide-angle lens, which provided a 104° field of view and a surface picture approximately 725 miles square, was used on one camera; a narrow-angle lens, which provided a 13° field of view and a surface picture approximately 63 miles square was used for the other camera. The wide-angle and narrow-angle cameras provided ground resolution of approximately 1.3 and 0.127 miles per scan line, respectively. A 500 line per frame scan was used for the vidicons. They were scanned at a line rate of 250 cps (non-interlaced) with a frame rate of 0.5 cps (2 seconds per frame).

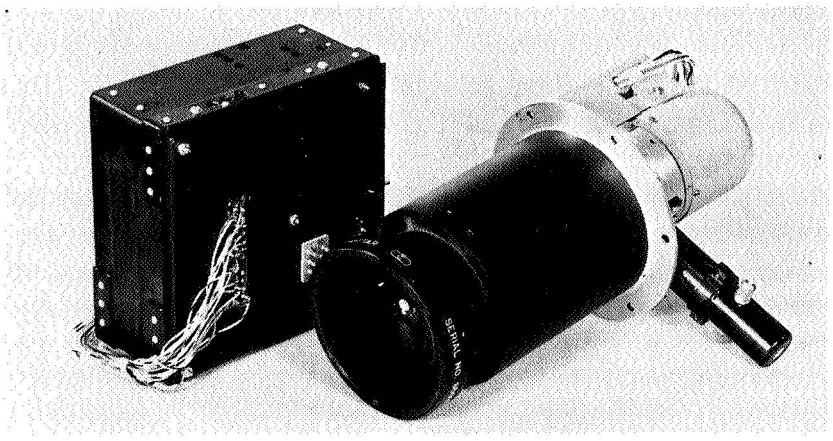

Figure 29. Wide-Angle TV Camera and Associated Electronics Package

(b) Functional Description.

A block diagram of the TV Camera is shown in Figure 30. The camera lens focuses the light gathered from the viewed scene onto the one-half inch vidicon. This tube has a useful diagonal of 0.354 inch; the scanned area is an 0.250 inch square. Reticle lines are superimposed upon the photoconductor surface in order to show a black cross at the center and small corner markings defining a 3/16 inch square. The reticle markings are used for optical-mechanical calibration and linearity determination.

The light pattern collected on the vidicon is scanned by an electron beam which discharges the photoconductor, causing a signal proportional to the light intensity to flow in the target lead. A subminiature Type 5904 tube is used for the video preamplifier. A cathode follower configuration is employed to transform the low-level video signal from the extremely high impedance level at the target to a sufficiently low value for transmission through a cable to the transistorized video amplifier.

The TV camera housing contains the lens, vidicon, yoke, and shutter. The video preamplifier is constructed in a small case which is mounted at the side of the camera in order to keep the target-signal lead as short as possible and thus minimize noise pickup and avoid high frequency losses due to shunt capacitance. All of the other electronics, with the exception of the sync generator, are located in an adjacent camera electronics package.

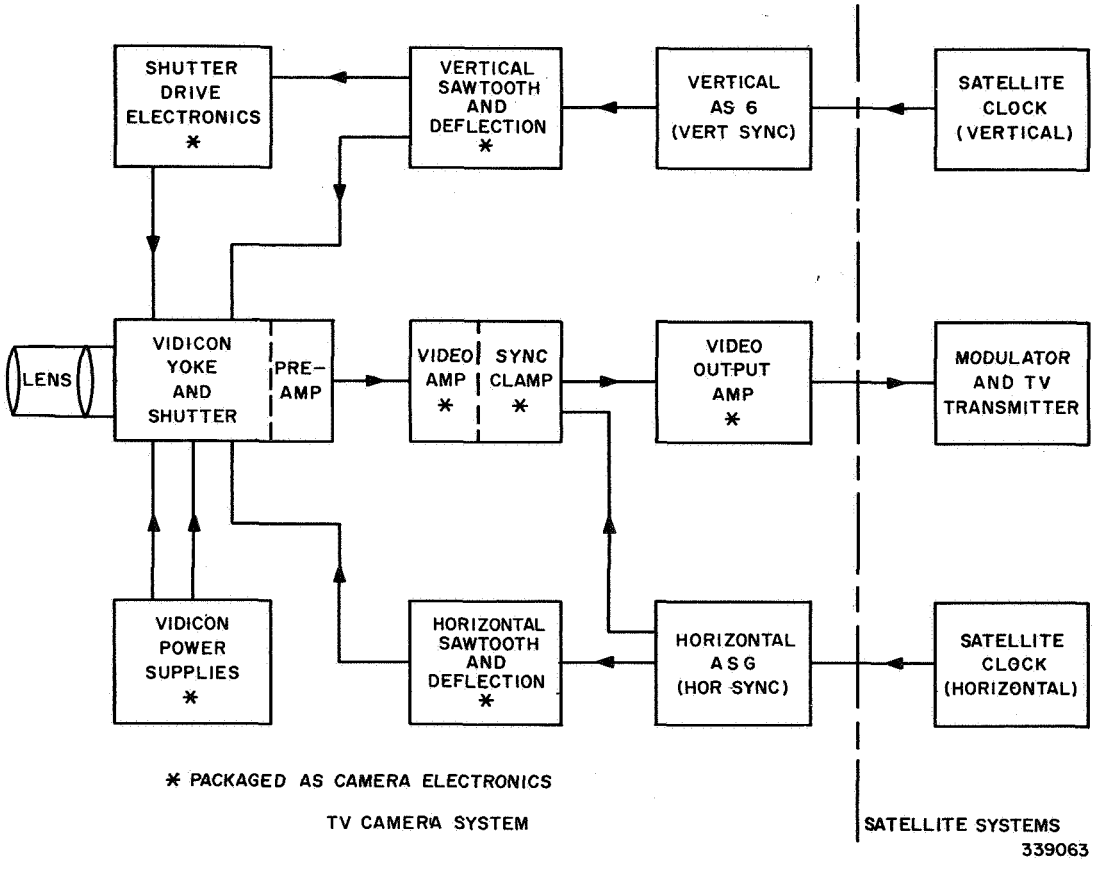

Figure 30. TV Camera System, Block Diagram

The low-level video signal is amplified by a four stage a-c coupled, transistor video amplifier. The d-c level is restored by means of a synchronized clamp which operates at the horizontal rate. A three stage d-c amplifier inserts horizontal sync pulses and amplifies the composite signal to the proper dynamic range for the video modulator contained in the recorder subsystem. The modulated subcarrier is then either put on magnetic tape for later transmission (remote operation), or is fed directly to the TV transmitter for immediate transmission (direct operation).

Several important components of the camera electronics, not directly in the video signal path, are the deflection circuits, the vidicon power supply, and the shutter-drive electronics. A horizontal deflection saw-tooth waveform is generated at a rate of 250 pps and is synchronized by the horizontal sync pulses. This sawtooth voltage is amplified and applied to the horizontal deflection yoke. Symmetry (centering) and amplitude (size) controls are included for initial camera set-up. A similar circuit generates the vertical-deflection sawtooth waveform, which is also synchronized but at the 0.5 pps vertical rate. The amplified deflection voltage is then applied to the vertical winding of the yoke. Centering and size controls are included to permit the position of the scanned area to be changed to accommodate the individual vidicon that may be installed.

The vidicon power supply contains a regulated dc-dc converter to provide high voltages, and a current regulator for the focus coil and filament currents. The voltages supplied are -20 to -30 volts for the control grid, +20 to +30 volts for the target, +250 volts for electrostatic focus, and +300 volts for grid number two. A current regulator supplies 100 milliamperes ±1% for the magnetic focus coil and the vidicon heater which is connected in series. The other bias voltages and preamplifier heater and plate voltages are obtained from the -24.5 volt supply common terminal to the entire vehicle.

The shutter used in the camera is a focal-plane traveling-slit type which is driven by a moving coil in a magnetic field. The exposure time is nominally 1.5 milliseconds. Power to the shutter coil is supplied by switching the coil terminals to -26 volts and ground with power transistors. The terminals are reversed every other operation, causing the shutter to move from left to right, then right to left on succeeding operations. The shutter actuation is synchronized with the leading edge of the vertical blanking pulse so that the exposure is completed before the beginning of the sweep (i.e., the end of blanking).

The master timing pulses are obtained by dividing the 18 kilocycle signal from the clock oscillator to obtain the 250 pps horizontal and the 0.5 pps vertical rates. The clock pulses trigger the respective horizontal and vertical auxiliary sync generators which, in turn, provide synchronizing pulses to the camera system. Either or both auxiliary sync generators will "free-run" with reasonable stability and provide approximately correct horizontal and vertical rates in the event of clock failure. Direct mode pictures may then be commanded when the satellite is within range of a command and data acquisition station.

(c) Optics

1. Development. Design of a TV camera for satellite installation was started at RCA quite some time before the beginning of the TIROS project, when the desirability of a slow (two-second) scan system became apparent. The meteorological mission of TIROS I required redesign, to the greatest extent, of the camera optics. Research was undertaken to determine the requirements for photographing the earth and cloud cover from high altitudes. Several studies were made in such areas as contrast ratios between various types of cloud formations and surfaces, effects of various reflections of various surfaces on nadir sky brightness, and cloudhaze scattering and absorption properties. Photographs, at various cloud-background ratios, were taken from high altitude with different combinations of film and filter types. Measurements which were made by the U.S. Air Force, at an altitude of 100,000 feet, with a Littrow Spectrograph, were used as a data source to determine sky luminence and surface illumination caused by solar and skylight. These were studied in an effort to determine the most desirable camera characteristics.

Both one-half inch and one-inch vidicons had been developed for the earlier TV satellite programs. An early evaluation indicated that the one-half inch vidicon would be the better choice for the TIROS project because it was found to have sufficient resolution and required less operating power and space and weighed less than one-inch vidicon. Also, it had been indicated by the meteorological interests that a vidicon with surfaces which were sensitive at the red end of the color spectrum was required, and a one-half inch vidicon with this characteristic could be readily placed in development at the RCA Tube Division, Lancaster, Pa. This vidicon was to be used with a red filter to provide high sensitivity at the red end of the spectrum and to cut off the response below the red wavelengths (5 millimicrons). The meteorologists later indicated that they also wanted sensitivity in the orange and the yellow parts of the spectrum; at this time a Bausch and Lomb Y10 yellow filter was used to replace the red filter.

Throughout the TIROS I project, the vidicon was subjected to vibration and other environmental tests and studies. As a result, structural changes were made to ruggedize the vidicon.

Late in the program, the U.S. Weather Bureau decided that it would be necessary to have corner and center reticles engraved on the inside of the vidicon to aid in picture identification and orientation. This rendered the vidicons, which had already been made, usless. However, the reticles provided for fixed optical alignment which permitted electrical change of size and centering on the raster. That is, when calibrated optically, the relationship between distance on the ground and the distance between the reticles on the vidicon would be maintained regardless of electrical changes of the raster.

The mechanical rotary shutter, developed for an earlier TV system, was evaluated for use on the TIROS I program. It was found unsuitable because its vibration produced microphonics in the vidicon, and could not be properly synchronized. The commercially available American and German shutters were investigated and found too unsuitable from the life expectancy standpoint. The desired life expectancy goal for the shutter was 200,000 operations. At this time, work was started at RCA-AED to develop a magnetically operated shutter. To provide a backup for the RCA development program, the General Time Corporation was given a contract to develop a shutter based on some of their design ideas. This contract resulted only in some initial investigations of a mechanical-trigger type of shutter which was unsatisfactory because its operation was unreliable and did not have a sufficient life expectancy. The work at RCA had also been continued during this time and resulted in a relatively simple, solenoid operated, focal-plane shutter which provided the required life expectancy.

Originally, the TIROS Satellite was to contain three TV cameras which were to be identical except for lens angles. A camera with a wide-angle (104°) lens was to be mounted radially (pointing perpendicular to the spin axis), and cameras with medium (70°) and narrow-angle (12°) lenses were to be mounted on the baseplate pointed down parallel to the spin axis.

A considerable amount of time was spent investigating the availability of lenses (particularly wide-angle lenses) which would meet the satellite requirements. Also, requests for proposals were sent to many of the known lens manufacturers and meetings were arranged at manufacturer's plants to discuss lens requirements. (Ref. 2, 3, and 4)

(d) Electronics

1. Development and Design

a. General. Initial camera system specifications as envisioned in the TIROS program are contained almost exactly in the tentative specifications for the television cameras of the RCA JUNO Meteorological Satellite. (Ref. 5) This specification describes a three-camera system. The TIROS System utilized only two; a wide-angle or low resolution camera, and a narrow-angle or high resolution camera. The wide-angle camera described in the referenced specification is indicated as a radial camera. However, for TIROS, the wide-angle camera was axially aligned along an axis paralleled to that of the narrow-angle camera. The specifications for the vidicon, for the camera input and output, for the synchronizing pulses, for the video amplifier and other requirements in the specifications, pertains directly to the TIROS System. This document served the initial specifications for TIROS Camera Systems Development. Most of the initial studies and analyses performed for the TIROS type of video system had already been completed during the preceding satellite project.

An extensive vidicon selection and testing program was undertaken. The vidicons were pre-tested at the (RCA) manufacturing source. However, final acceptance, including temperature runs, were made at the Astro-Electronics Division of RCA. The deflection yoke for the TIROS camera system was a ruggedized version derived from similar yoke developed earlier by RCA. The camera mechanical design was more or less straightforward with no particular difficulties.

Mounting of the wide-angle lens presented somewhat of a problem because of its weight; the majority of the weight was concentrated at the end of the lens away from the mounting surface. A tubular structure, surrounding the lens and supporting the lower end, was fastened to the camera housing to form a solid structure which was capable of transmitting loads to the baseplate. As a result of early vibration testing on the satellite, triangular braces, which reached down to the bottom end of the wide-angle lens housing, were added to the satellite structure. This stiffened the lens in a horizontal direction and eliminated some of the critical vibration resonances.

The camera system video amplifier chain consists of three units: The video preamplifier which is installed on the camera housing, the video amplifier, and the clamp and video-output amplifier. The latter two are installed in the camera electronics box. The video preamplifier was located on the camera housing. A separate auxiliary sync generator, which provides the vertical and horizontal sync signals, was contained in a separate housing which was mounted on a TV transmitter.

The following paragraphs describe the development and design of the TV camera circuits. The schematic diagrams of the camera electronics and the auxiliary sync generator are shown in Figures 31§ and 33§, respectively. Figure 32§ shows the waveforms obtained at the points indicated in Figure 31. These waveforms are also indicated by their identifying numbers in the circuit description paragraphs (e.g., WF No. 20).

b. Video Preamplifier. A considerable amount of experimentation and testing was conducted during the design stage of the camera to determine the type of preamplifier configuration to be used with it. The problem arose because the output impedance of the vidicon is very high; thus, it is susceptible to interference and noise pickup. At the same time, a high degree of high-frequency loss in the signal would be caused by stray capacitance of the leads, unless care was exercised in the layout of the unit. A low-impedance output from

§ These illustrations are printed on fold-out pages, located at the rear of this volume.

the preamplifier was desired, on the other hand, for stability. The most important consideration, however, was the low noise requirement that was imposed upon the preamplifier because of the very low signal levels obtained from the vidicon output.

Several circuit configurations were considered and tested. The most promising one was a circuit which utilized a subminiature, Type 5904 vacuum tube, connected as a cathode follower. It was superior to any transistor circuits which were tried at that time because its signal-to-noise ratio was better by approximately 16 db.

This circuit was chosen for the final design. In the final configuration this preamplifier exhibited an input impedance of 1.8 megohms and an output impedance of 2.2 kilohms. The cathode-follower configuration was desirable for proper impedance match; its voltage gain of 0.85 was acceptable.

The selected subminiature tube type was subjected to extensive environmental testing which included vibration, static acceleration, shock, thermal, and life tests. In addition, the tubes were tested for microphonic characteristics. None of the tube samples used in the tests failed.

c. Video Amplifier. The requirements of the video amplifier dictated a rather special circuit design. It had to be a low-noise unit, and was to be capable of providing a voltage gain of at least 1000. The lower limit of its passband was required to extend below 10 cycles per second. It was to have a uniform response (without peaking) up to about 70 kc, with frequency roll-off at the higher end of the spectrum to limit the noise in the output. It was to have a good stability characteristic with temperature change, and be capable of providing at least a 5-volt output without clipping.

To meet these requirements, a special transistor configuration was developed which utilized four, nearly identical, d-c coupled, PNP-NPN transistor pairs in each stage. The salient features of these pairs were good electrical and thermal stability, an extremely uniform response over the complete passband, freedom from distortion, and wide dynamic range. In addition, the low output impedance of this configuration made it conveniently adaptable to a cascaded circuit.

The first two stages are very similar, employing a large amount of negative feed-back. As a pair, they exhibit a 1.3 kilohm input impedance and 1.1 kilohm output impedance with a gain of approximately 11. The second pair is similar to the first pair, but the third pair incorporates some changes in order that a gain control may be

inserted. The input and output impedances and maximum gain are similar to the first two pair. The fourth pair is modified in order to handle a larger dynamic range.

Four of these stages are used in the video amplifier. The amplifier and input circuit have a flat response from a few cycles per second to about 300 kc. Peaking is used to compensate for the high-frequency roll-off of the input circuit. A special roll-off filter is used to limit the bandwidth to 100 kc. It has a gain of 1200 and can tolerate signal amplitudes as high as eight volts at the output (only a 4-volt output is required). It has negligible change of gain with the change in temperature and can operate with a change of over 20% in supply voltage before any significant change in the output can be noticed.

d. Clamp Driver. The purpose of the clamp driver is to provide pulses of equal amplitude and opposite polarity of sufficiently low impedance for clamp switching during blanking periods. This was achieved through the use of a balanced-load phase splitter (Q301). The pulses (WF Nos. 20 and 21) are provided at the collector and emitter loads of the transistor and are a-c coupled to the clamp. No difficulties of any type were experienced with this circuit during any of the tests.

Because the spectrum of the video information extends to zero frequency, some type of d-c restoration was necessary at the output of the a-c coupled amplifier used with this camera. A keyed clamp was used to provide this d-c restoration. This clamp consists essentially of a capacitor (C402) connected to a diode switch (CR404 and CR405) which is connected to a fixed voltage source. The clamp is keyed (synchronized) during the horizontal blanking time by the horizontal sync pulse. The d-c level to which the video is clamped is determined by a resistor-thermistor circuit which was designed to duplicate the temperature characteristics of the vidicon. The switch closes during blanking periods and the capacitor charges to the potential of the voltage source. The switch is opened during the readout period, leaving the stored charge across the capacitor until the next blanking period, at which time the cycle is repeated.

Unless the charge across the clamp capacitor remains constant during the line period, a certain shading of the video information results. That is, the impedance level of the circuitry which the clamp works into has to be rather high so that the clamp capacitor would not be discharged to any higher degree than desired.

A special high impedance circuit (Q402 and Q403) was designed to follow the clamp. It consists of a d-c coupled bootstrap amplifier

with an input impedance of several megohms and unity gain. With this design, no appreciable shading was detected during the tests.

e. Deflection Amplifier Circuits. There are two deflection circuits per camera; one for horizontal and one for vertical deflection. Each circuit consists of two sections; the sawtooth generator and the deflection amplifier. Both circuits are identical except for the difference in time constants in the sawtooth generators and coupling networks between the sawtooth generators and deflection amplifiers.

Each sawtooth generator consists of a constant current source (Q206 for vertical and Q304 for horizontal) charging a capacitor of suitable size. The values for charging currents and capacitors were selected to provide the sawtooth waveforms (WF Nos. 11 and 25) of desired linearity. The outputs (WF Nos. 16 and 31) are coupled into d-c amplifiers which drive the horizontal and vertical windings of the yoke.

Considerable effort was devoted to the development and selection of the deflection amplifier circuits. The major problem with the deflection circuits was that of keeping the output d-c levels and the amplitudes of the output waveforms of both sawtooth generators and deflection amplifiers constant over the specified temperature ranges. This was necessary because the d-c levels determine centering, and the sawtooth amplitudes determine the size and the aspect ratio of the picture.

Three basic types of deflection circuits were developed. The first circuit which was tried was a simple, single-ended output amplifier. This circuit was found to be unsatisfactory, because during early tests, it was found that this simple configuration was very dependent upon the amplitude of the supply voltage and the ambient temperature. It also exhibited an excessive change in centering with line voltage variations, and centering-control adjustments caused variations in the output amplitude which resulted in changes of picture size.

A second type of deflection circuit was then tried. This circuit employed a direct-coupled d-c amplifier with a single-ended emitter follower at the output to drive one side of the yoke. The other side of the yoke was returned directly to the first stage emitter, to provide extensive d-c feedback. This circuit exhibited very good stability with respect to line voltage variation. A development model of this feedback deflection amplifier was tried in the actual camera circuit and some difficulty was encountered in establishing centering. This amplifier was capable of operation at both the 0.5 cycle per second vertical rate and at the 250 cycle per second horizontal rate. One unsolved problem, however, was the continuous variation of the output amplitude with centering control which caused the picture

size to change when the centering was varied. Also, an intolerably large change in centering with temperature variations was exhibited by this circuit. An attempt was made to insert temperature stabilization.

In the final state of development, the feedback type deflection amplifier did meet the specifications for size and centering variations. However, it was felt that this did not provide the desired performance and did not leave enough margin for long term stability and/or deterioration due to the space environments.

A new type of deflection amplifier was designed. It employed a complementary symmetry output stage working against a d-c regulated voltage circuit, so that no direct current flowed through the deflection yoke during zero signal conditions. This complementary configuration exhibited desirable stability with temperature in that both transistors and Zener diodes, which were used to hold the voltage constant on the other side of the yoke, all drifted in the same direction and at approximately the same rate with temperature.

D-c stability of the sawtooth generators was obtained by providing for the complete discharge of the capacitors C302 and C604 to constant voltages during the blanking periods. The balance was set up in a bridge circuit, so that no direct current flowed through the deflection yoke during zero signal conditions. The inherent change of gain of the transistors with the change in temperature was compensated for through the use of special compensating silicon diodes (CR210 and CR304) in the base circuits of the sawtooth generators (Q206, Q304). The purpose of the diodes is to decrease the charging currents (and hence to decrease the amplitudes of the waveforms) of the respective sawtooth generators with increase in transistor gain. In addition to this, the output from the horizontal sawtooth generator is d-c coupled to its deflection amplifier. This minimizes d-c drift problems in the output.

Some difficulty was experienced with the silicon PNP output transistor. The state of silicon PNP development was lagging considerably behind the corresponding NPN development at the time the circuits were designed. A particular transistor in use exhibited internal open conditions at approximately -10°. This was found to be a manufacturing defect which affected nearly the entire batch which had been purchased. These were replaced with a coaxial transistor by the same manufacturer. A slight tendency for size change with temperature was also exhibited. However, several of the transistor-types were changed. The final configuration represented the best compromise of temperature and voltage stability with over-all circuit performance.

Each camera was tested, in its final form, in a vacuum and over the specified temperature ranges, and it was found that the maximum change in frame size, aspect ratio, and centering was less than ±2.0% and some of the units remained within ±1.0% limits.

f. Blanking Mixer. Requirements for the blanking mixer were to combine vertical and horizontal sync pulses to provide mixed blanking for the cathode of the vidicon. This was achieved through the use of an OR gate in the base circuit of Q203. The output of the transistor was clipped to a constant voltage level by two Zener diodes in series. This provided a train of pulses (WF No. 5) of constant amplitude. No problems were associated with this circuit under any test conditions at any time.

g. High-Voltage Power Supply. Several high-voltage low current sources were required for proper operation of vidicon pick-up tubes. Approximately 300-volts d-c was the highest voltage required. The high-voltage power supply utilized a standard dc-dc converter. Two negative and three positive voltages were provided by the high-voltage power supply. One negative voltage was for the vidicon control grid; the other was a small sampling of this voltage which was provided for telemetry. The positive outputs (approximately +300 volts) were for the vidicon target, the vidicon electrostatic focus grid 3 and the vidicon grid 2.

An earlier version of the vidicon high-voltage power supply utilized a high-voltage regulator on the output side. However, handling voltages in the order of 300 volts with a transistorized voltage regulator proved to be extremely difficult with the transistor devices then available. Considerable trouble was experienced, particularly in the temperature compensation range since the stabilizing element used for the high voltage regulator was a series string of Zener diodes (which have high temperature coefficients when manufactured for the high-voltage ranges). This resulted in a cumulative error in the output voltage which was caused by the voltage change across individual reference diodes. Considerable effort was expended in an attempt to compensate for this voltage change. However, the output regulator had to be replaced by an input regulator and a low impedance, high-voltage source. A three-transistor series regulator was then designed to regulate the input voltage. With this configuration, the power supply output voltage remained within the specification limits for all variations for supply voltage and ambient temperature. This regulator also isolated sharp transients, caused by the dc-dc converter, from the other loads in the satellite.

Functionally, the high voltage power supply consists of three separate circuits:

1. The regulator
2. The oscillator
3. The rectifier

The primary winding of the transformer, in conjunction with two power transistors comprises an oscillator circuit. The two transistors (Q104 and Q105) are connected in a regenerative feedback circuit which oscillates at a frequency of approximately 770 cps (WF Nos. 1 and 2). The voltage (WF Nos. 3 and 4) induced in the secondary winding of the transformer is rectified by a full-wave bridge rectifier and is filtered by an RC filter. The input voltage to the converter is controlled by the three-transistor series voltage regulator.

h. Focus-current Regulator. To protect the vidicon heater from the current surge which is common to all indirectly heated devices, a heater current regulator was needed. The requirements for the heater current regulator were to maintain a load of current of 100 milliamperes ±1%, over both the temperature and input voltage ranges. Concurrently, a similar problem existed for regulation of the current in the focus coil in order to maintain the electronic focus of the vidicon within narrow limits. This was necessary in order to maintain high over-all resolution. The proper range of operation for the focus coil was also in the 100 milliampere region. A considerable power saving could be realized by operating the focus coil at exactly 100 milliamperes and adjusting the other electrode voltages for optimum focus at 100 milliamperes; the vidicon filament could then be operated in series with the focus coil. The amplitude of the current could then be controlled by a single regulator with a two to one saving in regulator losses, when compared to a two-regulator configuration.

Work was started on a combination focus current and vidicon filament current regulator. The major problems were the vidicon heater resistance, which changed from cold to hot operation, and the resistance change of the yoke with environmental temperature changes.

Another difficulty in regulating this current under given conditions was that the voltage drop across the focus coil, vidicon heater and the current sampling resistor was too high for a given supply voltage. (The focus coil resistance increases nearly 25% to 25°C.) Because of this large voltage drop, only a few volts were available at the focus current regulator transistor (Q202).

Early work in 1958 resulted in a regulator with an over-all regulation of approximately ±5%, of which 2-1/2% was attributed to temperature variations and approximately 2% to line voltage variations. The major problem in the temperature stabilization of the regulator was found to be the germanium power transistor used as a series regulating element. Tests indicated that some type of thermal compensation would be required to maintain the current output within the required limits at extreme temperatures.

A later design, developed in 1959 in an attempt to solve the temperature problem, incorporated a medium-power, PNP, silicon transistor as the series element. Because of the relatively lagging state of development of PNP devices at that time, however, this transistor caused an additional problem because of its low direct-current gain at high collector currents.

The transistor gain and temperature problems were compensated for by the addition of a d-c coupled, transistor amplifier to drive the series regulator transistor (Q202). A small resistor (R202) was added, in series with the regulator to serve as a sensing device for current changes. The error-voltage signal is applied to the base of Q201, through the thermistor temperature compensating network. The vidicon filament and focus current and the temperature error signals are amplified by Q201 and applied to the base of regulator transistor Q202 to effect regulation. A double Zener diode reference network was included in the emitter circuit of Q201 to minimize the effects of line voltage variations.

This final regulator design provided the required 1% current regulation over the required temperature range. However, at this time, the input voltage was supplied through the vehicle voltage regulator rather than directly from an unregulated source. This reduced the input voltage variation requirements of the current regulator because the vehicle regulator provided an input voltage (24.5 v) which was nearly constant (±1%).

i. Vidicon. Special attention was devoted to the selection and test of the vidicon tube because this was the most important component of the TV camera. A special program was initiated at RCA to develop and produce a certain number of ruggedized 1/2-inch vidicons which would operate at a two-second scan rate, be sensitive enough to operate with a 1.5 millisecond exposure, have an extremely wide dynamic range, and have sufficiently high output to provide signal-to-noise ratio of at least 25 db when used in conjunction with a transistorized amplifier.

An extensive test program was organized after the first few tubes of the desired type were obtained. The vidicons were tested under severe conditions of vibration, acceleration, shock, and temperature variation, and were life tested.

The tubes were selected on the basis of sensitivity, uniformity of output, persistence, microphonics, spot concentration on target, warm-up period, variation of the output with temperature, and amount of dark current. Several problem areas were discovered and design was corrected accordingly. A new mesh ring design was introduced to reduce mesh microphonics. The assembly consists of a ring with a square hole instead of the customary round hole. Tests showed that with this configuration, mesh microphonics were reduced at least 50 per cent in amplitude. The vibration tests indicated that the getter welding method was not dependable in some cases and the getter design was changed to increase dependability.

At the end of the project, the vidicon was improved to a point where it possessed ample sensitivity with excellent uniformity, dynamic range, and negligible microphonics under ordinary operating conditions. The tube could withstand over a 100 g, 11 millisecond shock. The test samples operated satisfactorily after having been shaken at 20 g level of band limited noise (20 cps to 2000 cps) for three hours continuously. Life test data, taken over approximately a one-year period, shows a heater life of approximately 4000 hours.

j. Dark Current Compensation. One of the problems which was encountered in the vidicon operation was an inherent presence of a leakage current in the load. This is called the "dark current", and it occurs because the semiconductor used for the target material is not a perfect insulator in the absence of light. Therefore, a certain amount of beam current leaks into the load through the target, when the face plate is not exposed to the light. The amount of dark current varies with the change in temperature; it also varies between tubes. It appears on the output as a d-c level superimposed upon the video signal; therefore, it changes the brightness of the video. The voltage level, to which the video information is clamped, must be adjusted to compensate for this brightness change in the video. In addition, to compensate for the thermal variation of the dark current, the clamp voltage must be temperature controlled in inverse proportion to the change in dark current. This is achieved by a special thermistor network (R420 and R411). The transfer characteristic of the network is adjusted for each individual vidicon to be used with the particular camera circuit. Therefore, several thermal runs are required on each camera, for this purpose alone, to assure the stability of the video level with the change in ambient temperature.

k. Shutter. A shutter with an exposure time of 1.5 milliseconds and a tolerance of ±0.25 millisecond was required by the initial specifications. A mechanical, rotating type shutter was developed as an initial attempt to meet this requirement. This shutter consisted of two slotted discs, which were rotated at different speeds so that the vidicon would be exposed each time the slots were aligned. This method was discarded because it required excessive power to constantly revolve the disc while the camera was operating, and was difficult to synchronize the vertical sweep with the shutter pulse. Also, vibrations, which were produced by the gear train, caused microphonics in the vidicon. To replace the rotating-disc shutter, a shutter which operated on an entirely different principle was developed. This shutter consisted of a plate with a vertical slot which traveled across the face of the vidicon, perpendicular to the horizontal scan lines, in a manner similar to a standard focal-plane shutter. The shutter exhibited good optical efficiency and in general, appeared to have desirable characteristics.

A method of driving this shutter back and forth across the face of the vidicon, was then needed. A moving coil arrangement, similar to a loudspeaker voice coil with large excursion limits, was designed. The shutter was attached to the moving coil which was placed in the space surrounding an axial magnet so that a direct current applied to the coil would drive it in either direction, depending on the polarity of the current. The coil was of a single layer solenoid configuration, which was printed on a machined form. The pitch of the winding was varied to provide a constant shutter travel rate, with a slight fall-off at the end of the travel.

A circuit to provide controlled driving current to the shutter coil was developed. The first approach was to switch the drive current with a double-pole, double-throw relay which served as a reversing switch. The current to the coil was controlled by a transistor switch which determined the amplitude and duration of current while the relay determined the direction of the current flow. In this manner the coil with its attached shutter could be driven first in one direction and then in the other.

Considerable opposition to the use of a relay for this application was encountered because of its life expectancy. Because the relay operated once for each shutter operation, it was thought that the life of the relay would be a limiting factor in circuit reliability, and for this reason, a new circuit was designed.

A second method was devised to drive the shutter in which one side of the shutter coil was permanently connected to a source of -13 volts, and the other side was alternately connected to -26 volts or to ground, by turning on one of two transistor switches. Because

the voltage across the coil was one-half of that used for the first design, the number of turns of the coil had to be increased to retain the same number of ampere turns. Increasing the turns on the coil proved to be somewhat difficult, because of space limitations, and a third method of driving the coil was devised. In the third (final) circuit, four power transistors were connected in a bridge configuration, with opposite nodes of the bridge connected to -26 volts and to ground. The shutter coil was connected to the other two nodes of the bridge. By closing an opposite pair of transistor switches, the coil could be connected from the supply voltage to ground. Alternating the pairs of transistors through which the current flowed to the coil, reversed the force on alternating cycles. The satellite control, shutter-command pulse was used to trigger a bi-stable flip-flop once for each shutter pulse. One positive and one negative going output of the flip-flop were used to turn on the appropriate pair of power transistors through an isolation amplifier and a differentiation circuit. The output current pulse through the shutter coil is between 60 to 70 milliseconds in length and has an amplitude of 2.5 amperes. In this final shutter coil configuration, sliding brushes were used to convey the current to the coil. The setting of the brush pressures proved to be quite critical, and considerable effort was required to develop the proper technique.

When installed in the TV camera, the shutter blade accelerated quickly, traveled across the face of the vidicon at a nearly constant speed, and was stopped at the end of travel by a silicon-rubber bumper. The design exposure time of 1.5 milliseconds was consistently obtained. Some variations were noted between individual units. However, each shutter maintained its characteristic exposure time after repeated cycling and aging. Life tests were performed on the shutters, and the lifetimes proved to be adequate for satellite operation. An experimental shutter, which was subjected to life tests, performed 500,000 operations, with only 15 percent change of speed.

1. Auxiliary Sync Generators (ASG). The auxiliary sync generator (shown schematically in Figure 33) was added to the camera-circuit design to rectify system problems which were discovered during the payload integration phase of the satellite prototype testing. The master clock originally provided both vertical- and horizontal-synchronizing pulses at a precise rate, derived by frequency division from the 18-kilocycle oscillator. The vertical-sync pulse was derived from one frequency divider for the remote picture-taking cycle and from a different circuit for the direct picture phase. The direct picture circuits provided a 200 millisecond pulse and the remote picture circuits provided a 100 millisecond pulse. Because the vertical pulse width determines vertical blanking time, the

picture size differed between the two modes of operation. The horizontal pulse was found to be slightly above ground potential in one case and below that level in the other. Because the sync pulse was injected into a direct-current amplifier, the video reference level shifted somewhat between the direct and remote modes. The horizontal deflection circuit also exhibited a tendency to change centering when this voltage reference shifted between the direct and remote modes.

(1) Horizontal Auxiliary Sync Generator. The horizontal ASG consists of a free running multivibrator with provision for synchronizing the repetition rate with the 250 pps master clock output. The free run rate was set at 238 pps for reliable triggering. The output pulse width was 321 microseconds positive going to ground from -24.5 volts.

A ten to one reduction in average power was achieved by using a complementary PNP-NPN circuit with both transistors on during the pulse output portion of the cycle and both off during the remainder of the cycle. Upon initial application of power, the NPN transistor Q2 is turned on by the bias network R8, R7, CR3, and R10. This allows the PNP transistor Q1 to turn on, charging capacitor C3 with Q1 base current through R5 and CR2. As Q1 turns on, a portion of its collector current charges C2 through R4, CR3, and the base of Q2, and saturates Q2 in the on condition.

The output pulse is taken from the collector of Q1, which remains near ground potential for the pulse duration. The base current in Q1 decreases as C3 charges, until this current can no longer maintain saturation. Q1 starts to turn off, ending the charging current through C2. The voltage across R10 starts to reverse and cuts off Q2. Q2 cuts off Q1 as C3 starts to discharge through R3, R12, and R6 reversing the voltage across R3.

The off time is determined by the amount of current flowing into C2 as it discharges through the power supply and R1, R2, R4, R7 and R8. As the voltage on C2 nears zero, but before it can reverse polarity, the current through R8 and R7 flows through CR3 and the base of Q2. This turns Q2 on and the cycle is repeated. The on time may be varied by changing R5 or C3; the nominal setting provides a 321 microsecond pulse width. The repetition rate is locked to the 250 pps clock rate by differentiating the clock pulses with C1 and R2, clipping the negative spikes with CR1, and triggering Q2 through C2, R4, and CR3 with the positive spikes.

(2) Vertical Auxiliary Sync Generator. A complementary multivibrator is also employed for the vertical rate portion of the auxiliary sync generator. The pulse repetition time is set at 2.40 seconds for the free-run rate. In normal operation the vertical output is locked to the vehicle clock vertical pulse at a 2.00 second rate. The output pulse width is 100 millisecond ±5 per cent and is independent of the width of the driving pulse. The output level remains at -24.5 volts during the off time and is positive-going to ground for the output pulse. The incoming clock sync pulse is inverted and differentiated before triggering the multivibrator.

The PNP transistor Q4 is connected to supply a small amount of "on" bias when power is applied. As Q4 turns on C5 starts to charge through R20 and CR5. This provides base current for the NPN transistor Q5, which turns on and allows the base current through Q4 to increase, charging C6. Both transistors rapidly reach saturation and an output pulse is provided at the collector of Q4. The on state is maintained until C5 charges sufficiently to begin to cut off base current to Q5. As Q5 goes out of saturation, C6 stops charging and begins to discharge through R19, R17, and R26. This reverses the emitter-base voltage at Q4 and cuts it off. Q4, in turn, cuts off Q5 as C5 begins to discharge. The off condition remains until the forward base bias on Q4 regains control from the discharge current of C6. Q4 switches on turning Q5 on and repeats the cycle.

The vertical rate is normally locked to the clock output. Incoming clock sync pulses are inverted and differentiated by Q3 and C7. The resulting trigger turns Q4 on before the free-run time has elapsed.

Temperature effects upon the germanium PNP transistor are compensated for by the thermistor R27 and Zener diode CR6. The voltage to which C6 charges is then varied to offset the increased leakage exhibited by Q4 during high temperature operation. R27 and CR6 were added after the system integration and system thermal vacuum tests disclosed a +60°C temperature on the ASG circuit board. The heat was generated by the TV transmitter, upon which the ASG unit was mounted. During extended system operation with transmitter power on, the transmitter temperatures exceeded +75°C. Thermal insulation between the transmitter and ASG reduced the heat transfer considerably. The temperature compensation modification to the circuit further reduced the possibility of spurious pulses at the higher temperatures. As modified, the ASG will operate normally at temperatures up to +60°C. In practice the temperature never exceeds +50°C.

The ASG provides the TV camera subsystem with a standardized source of synchronizing pulses during all modes of operation. (Previous differences in sources had caused size and centering discrepancies to appear between the direct and remote modes of operation.) The ASG will also provide direct and horizontal sync pulses to the camera system in the event of vehicle clock malfunction.

2. Packaging. The camera electronics circuits (with the exception of the preamplifier which was mounted on the camera housing and the auxiliary sync generator which was mounted on the TV transmitter) were mounted on six printed circuit boards within a metallic box. The six boards were mounted parallel to each other and perpendicular to a "mother board" which contained the interconnecting wiring and terminals for connections to other systems on the vehicle. The first board contained the high-voltage power supply and an input regulator. The second board contained the focus- and filament-current regulator, blanking mixer, and the vertical-deflection sawtooth generator and deflection amplifier. The third board contained the clamp driver, the horizontal-sawtooth generator, and the horizontal-deflection amplifier. The fourth board contained a sync-drive circuit, the synchronous clamp, video output amplifier and the video telemetry circuitry. The fifth board contained the four pair main video amplifier. The shutter actuation circuits were contained on the sixth board. The terminals from the six boards were soldered to the mother board at one end and supported at the other end by the aluminum box. This box completely enclosed the camera electronics, except for the terminals and access holes to the various centering and gain controls which were required to be accessible for initial alignment of the camera electronics. The dimensions of the box were 6 by 6 by 3 inches. It was originally designed to lie on the flat side and be bolted to the satellite baseplate in this manner. However, space considerations, during the mechanical integration, required that the camera electronics box be mounted in the upright position. Some minor redesign, to enable the box to stand on one end and withstand environmental vibration, was required after the systems vibration tests. Several additional straps were added in order to strengthen the box mechanically.

3. Test. All cameras of the TV camera subsystem were designed and tested to meet the TIROS environmental test specifications. (Ref. 6)

Performance of the camera circuitry in its final form was not affected in any way by the vibration or vacuum testing. The only exceptions to this were the vidicon and the preamplifier tube.

The camera electronics was relatively immune to the vibration testing (that is, within the specifications indicated previously) because of the mechanical construction of the unit and because solid-state components

were used in the design. The application of conformal coating to all of the components and the use of special heat conducting compound, in places where there was sufficient amount of electrical power dissipated to cause local heating of those components, resulted in uniform heat redistribution. The cameras did not depend upon the cooling properties of the air. Therefore, the operation in a vacuum caused no additional problems.

In addition to the environmental tests performed on the cameras, each camera was subjected to several thermal runs to check the performance of the circuits and to compensate, or correct if necessary, for any deviations from desired results. During the tests the following were monitored and investigated:

1. Focus stability.
2. Change in picture size.
3. Change in aspect ratio of the frame.
4. Centering stability in horizontal and vertical directions.
5. Change in dark current content.
6. Change in video amplitude.
7. Vidicon sensitivity.
8. Vidicon resolution.
9. Change in noise content in the output.
10. Target material storage persistence.
11. Vidicon warm-up time period.

Only after these requirements were met were the cameras subjected to further environmental testing.

After satisfactory completion of all of the tests, the flight cameras were mounted on the satellite, which in turn was subjected to proper environmental testing. After this, the cameras were again subjected to final inspection and calibration. This made the cameras flight-ready. The flight calibration included the following:

1. Optical focus set for uniformity. A collimator was used for this purpose.
2. Electrical focus checked.
3. Frame size checked. It was ascertained that the horizontal and vertical sweeps were adjusted to cover the desired target area.

4. Aspect ratio checked. The horizontal and vertical sizes were made identical.

5. Vertical and horizontal centering checked. It was ascertained that the frame was centered properly within the vidicon target area.

6. Target erase time checked. The bias on grid No. 1 of the vidicon was checked. The bias on this grid controls the beam current of the vidicon which, in turn, determines the time interval required to discharge the target from the previous image and prepare it for the next exposure.

7. Light calibration. Response of the camera to various light intensities was checked and the gain of the video amplifier was set to provide a desired transfer characteristic. The light response of each camera was recorded.

8. Sync amplitude adjusted. It was ascertained that the sync amplitude represented 25 per cent of the composite maximum signal output from the camera.

9. Warm-up time checked. The warm-up time was required to be below 26 seconds. That is, the camera had to be warmed up before the first picture was taken.

10. Signal-to-noise ratio was checked at the output of the camera.

11. Microphonics of the vidicon were checked.

12. The camera assembly was visually inspected.

(2) Magnetic Tape Recorder

(a) General

Two magnetic-tape recording and playback units, each having two separate channels, were included in the TV camera system to record the wide- and narrow-angle TV pictures and the sun-angle signals when the satellite was out of communications range of a ground station. (The over-all unit is henceforth referred to, for simplicity, merely as the tape recorder.) Each tape recorder included associated electronic circuits through which the camera video and the sun-angle signals are processed both in the direct and remote modes of operation. The outputs of the electronic circuit are mixed and applied directly to the TV transmitter as composite modulation in the direct mode of operation or recorded individually and mixed during playback in the remote mode of operation.

The tape recorders were specially designed by RCA for satellite operation. Their main characteristics are high stability and reliability, and small size, weight, power consumption. Each recorder basically consists of a specially designed tape transport and the associated electronics, which includes a d-c to a-c converter for motor power supply, and a motor control circuit.

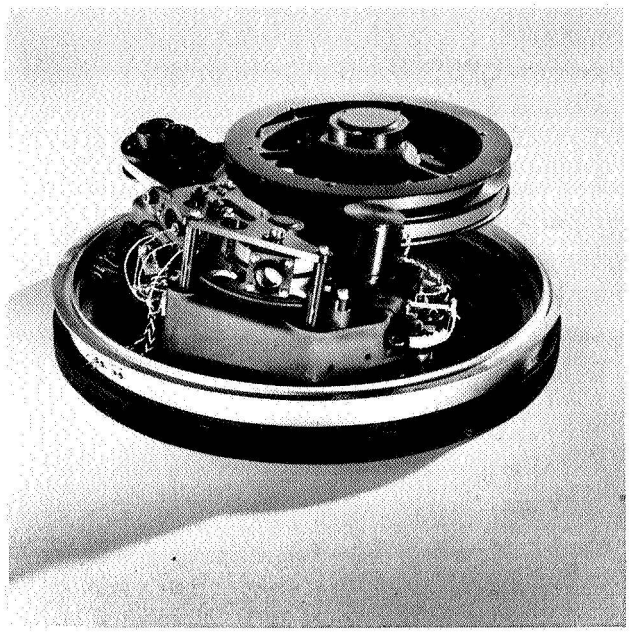

Figure 34. Tape Transport

(b) Functional Descriptions

The tape transport, shown in Figure 34, contains the tape storage reels, tape driven motor and mechanisms, one record and one playback head (each with two channels), a permanent-magnet erase head, and an "end-of-tape" sensing switch. The motor drives both reels simultaneously through a specially designed constant-tension mechanism. In the remote mode of operation, the drive motor is started and the tape is conveyed, past the record head, from the inside reel to outside reel. During playback, the tape is conveyed, past the playback head, from the outside reel to the inside reel. The data is played back in "inverted" form. The erase head is so located, in relation to the record and playback heads, that the tape is erased after playback, and is again erased (traveling in the reverse direction) before being re-recorded.

The recorder electronics, shown in block diagram form in Figure 35, is used in both the Direct and Remote modes of satellite operation to process both the video and sun-angle signals.

In the direct mode of operation, the video signal is received from the television cameras and used to modulate the 85-kc subcarrier oscillator ± 15 kc, with the tip of sync at 100 kc. The FM signal is then supplied to the mixer, which combines the FM video signal with the sun-angle signal and applies it to the transmitter. In the direct mode of operation, the sun-angle signal is used to trigger the gate and the 10-kc oscillator which feeds the mixer directly.

In the remote mode of operation, the frequency modulation by the video signal is the same as in the direct mode of operating, but the signal is used to drive the head-drive amplifier, which applies the signal to the magnetic tape. After storage of the signal, the video playback amplifier receives the signal from the playback head

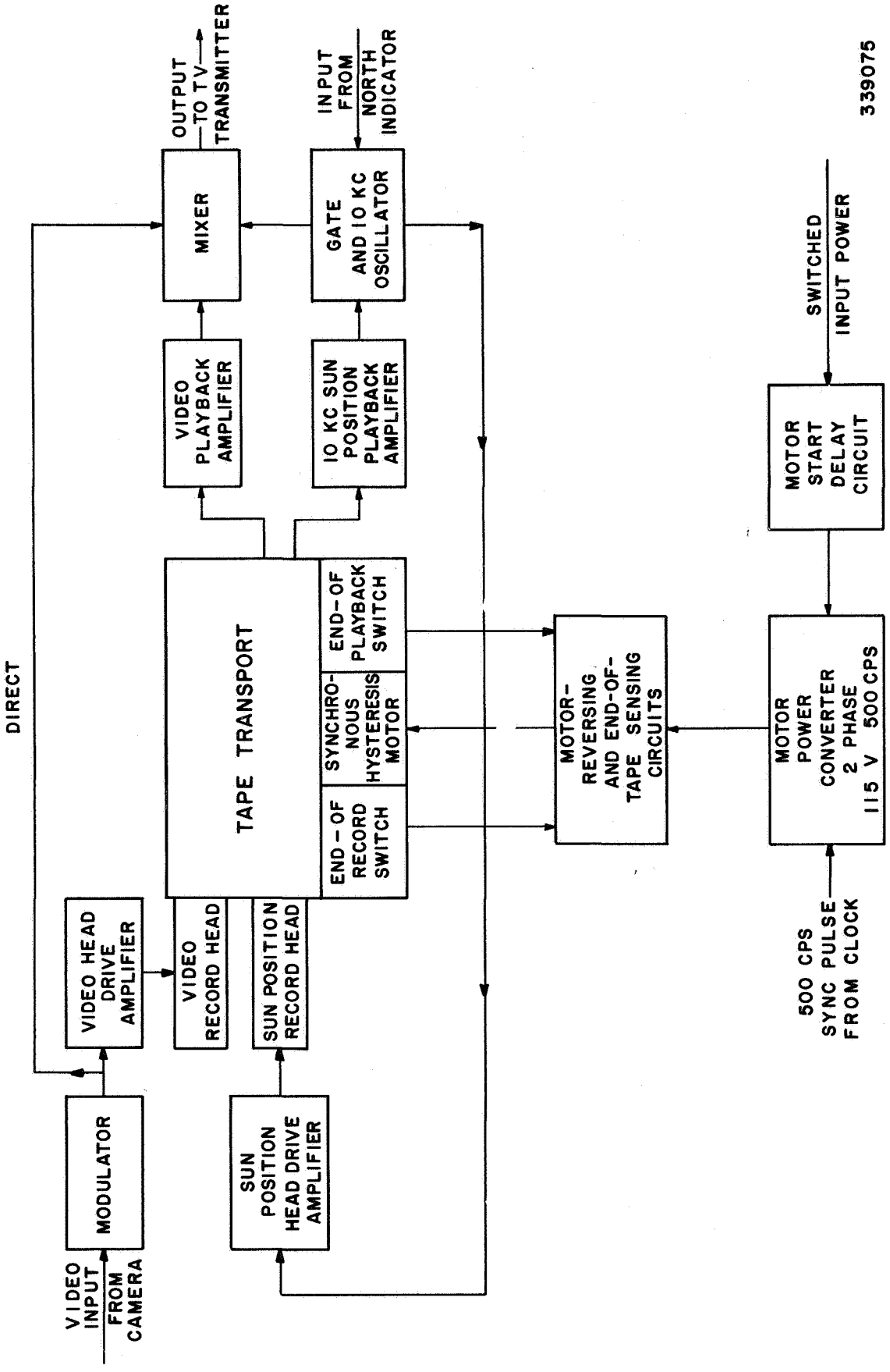

Figure 35. Magnetic Tape Recorder, Block Diagram

and amplifies it, equalizes it, and feeds the signal to the mixer. The gate and 10-kc oscillator are triggered from the sun-angle indicators, as in the direct mode of operation, but the gated signal is fed to the 10-kc head-drive amplifier which records the 10-kc burst on the tape. After magnetic storage, the 10-kc bursts are amplified in the 10-kc playback amplifier, rectified, differentiated, and used to retrigger the gate and 10-kc oscillator, which then feeds its signal to the mixer as in the direct mode of operation.

The power converter and motor controls circuit provides a-c power for the drive motor. The recorder is controlled by switching the power to the individual circuits and no signal leads are switched.

(c) Signal Storage Requirements

At the start of the program a search for an existing recorder to meet the requirements for satellite application to do the job was fruitless. The combination of requirements of quality, reliability, light weight, low power consumption, and ruggedness were not available in any known recorder. However, an RCA design of several years previous to this time, which had several of the sought-for virtues, appeared amenable to fairly rapid redevelopment to meet the subsystem objectives.

It was necessary for the recorder to be light enough not to account for a large percentage of the satellite's total weight. It must be rugged enough to withstand the acceleration and vibration of launch. Unattended operation of the recorder in orbit meant the recorder must be reliable with simplicity of operation. The limited power available in a satellite meant a recorder with low power consumption. The tape recorder was required to store and playback 32, two-second-scan, 500-line television pictures, with minimum deviation from the quality of directly transmitted cloud pictures.

1. Original Specifications

a. Transport

Tape Capacity:	400 ft. long, 3/8 inch wide; 1.5 mils thick polyester
Tape Speed:	50 inches/second
Motor:	synchronous hysteresis
Drive:	rubber tire riding on motor shaft
Reel Take Up:	constant tension "negator" spring coupling between reels
Base Casting:	aluminum

b. Electronics

Video System

Type of system:	FM
Input:	video (0 to 62.5 kc) amplitude 0 to 4 v peak
Subcarrier Oscillator:	center frequency 85 kc ± 15 kc deviation ± 3 per cent overall stability.
Head Drive Amplifier:	18 to 20 ma P-P into 1 mh magnetic recording head.
Playback Amplifier:	input 1 mv P-P, output 3.6 v P-P equalized to provide ± 2 db overall response from entire recording system.

Sun Position System

10 kc Oscillator:	10 kc ± 1 per cent at 0.4 v P-P output.
Gate Circuit:	20 db on-off ratio triggered via 20 v square wave 2k Ω source impedance. Two triggers one from sun position circuits other from 10 kc playback amplifier.
10 kc Playback Amplifier:	input 1 mv P-P at 10 kc; output -20 v d-c when 10 kc is present.
Output Mixer:	The function of this stage is to take the 3.6 v P-P from the video playback amplifier and add it to 0.4 v P-P from the gated 10 kc giving a total of 4 v P-P output to the television transmitter.

Power Converter

Output:	512 cps 110 v 2 phase
Input:	28 v dc unregulated
	13-volt 312-microsecond pulse from clock.
Auxiliary functions:	motor reversing, motor on and off, and end of tape control.

2. Final Specifications. The final specifications for the recorder system are contained in "Specifications for the RCA TIROS Exploratory Meteorological Satellite System (TSP 100 dated July 1, 1959).

3. Design Analysis. A video bandwidth of 62.5 kc was required for the 500 line, 2-second scan television picture. Direct* recording of video signals was not desirable for several serious reasons. First, the low-frequency response of a magnetic recording system is very poor. If the signal is equalized externally, the low-frequency noise becomes objectionable; non-linearity of the overall process is also a problem. Level fluctuations (such as magnetic drop outs) are also troublesome in direct recording of video because they appear as picture information in the final picture.

To overcome these limitations, a frequency-modulated carrier system was chosen for this application. With this system, non-linearity of the magnetic medium is tolerable if the carrier frequency is higher than the highest video frequency. Reproduction of the subjectively important low-frequency portion of the video band is excellent, even though the carrier frequency is in a region of mediocre magnetic performance. Reproduction of the higher video frequencies is good because the lower side-bands they produce fall into a frequency band of high magnetic performance.

The bandwidth requirement for the transmitter to send the stored pictures to the ground station was approximately 150 kc. This determined the upper side band limit of the frequency modulated video signal. A carrier frequency of 85 kc with a deviation of ± 15 kc gives a first order video side band up to 147.5 kc. The frequency spectrum of the signal to be recorded, allowed the selection of a magnetic tape speed of 50 inches per second. At this speed and for the number of pictures to be recorded (32), the length of tape required was approximately 400 feet, allowing some time for the recorder to accelerate and coast between pictures. The use of brakes to reduce this length was considered at the start of the project, but was discarded in favor of simplicity.

Obtaining the required tape-speed stability was the difficult part of the development task. Although available modern high-quality instrumentation recorders were capable of providing the tape motion stability necessary, the basic problem in designing a transport for use in a satellite was to duplicate such performance with a mechanism which was several orders of magnitude reduced in size, weight, volume and power consumption. In addition, the transport was required to be able to withstand the stresses of launching and the rigors of the space environment in which it was expected to operate, and to be reliable enough

*Amplitude modulated, as opposed to frequency modulated.

to operate unattended throughout its expected life. To save space, the tape reels were mounted coaxially and adjacent to each other. To reduce power consumption, the energy used to unwind one reel was used to wind the other. For speed control a frequency-locked supply voltage was used to drive a synchronous-hysteresis motor. For ruggedness, a sound mechanical design was used and the components were supported by a cast frame.

(d) Development

The tape recorder electronic circuits were developed in accordance with the initial concepts and no major change of design or approach was required. Only several component changes were required during the course of the development.

When the tape transport was integrated into the system, it exhibited a 7-cps jitter and a ± 5 per cent speed variation from one end of the tape to the other. This instability caused difficulties with the video sync at the ground stations. The required stability was achieved by replacing the rubber tire drive with a Mylar belt of the type developed by the U.S. Army Signal Research and Development Laboratory. The recorder power supply imposed a large 512-cps variation on the vehicle power supply. To isolate this signal from the rest of the system, L-C decoupling circuits were added in the d-c power input leads. R-C decoupling circuits (Figure 36) were added to all leads which connected the electronic circuits to the satellite supply. Sprague Type HK disc capacitors were initially used for phase shift in the power converter, but they began to fail after the units were in service for a relatively short period of time. When the vendor was consulted about this failure, it was revealed that these capacitors had been derated from the original 1000-vdc rating to 500 vdc after this capacitor type had been recommended for this application. It was derated because, at higher voltages, a carbonized path formed, over the ceramic dielectric and under the coating, from one capacitor plate to the other. This effect was a direct function of time, which indicates why the failures occurred only after the power supplies had been in operation. On the basis of this finding, Sprague Vitamin-Q capacitors, rated at 1000 vdc, were chosen to replace the defective Type HK capacitors.

The shaft upon which the tape reels were mounted developed a radial crack during development-model shock tests and, although it did not break off completely, it was later replaced by a larger, stronger shaft.

(e) Functional Description

1. Tape Transport. The basic tape-handling mechanism (Figure 37) consists of a capstan, an idler, and two coaxial reels mounted in a triangular configuration. The reels are coupled to each other by means of an assembly of constant-tension springs, and the idler and capstan are angled in such a way as to aid the tape in moving from the plane of one reel to that of the other. The drive mechanism consists of a 400-cycle synchronous-hysteresis motor which is coupled to the

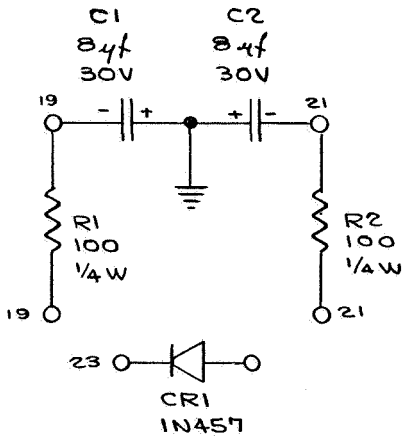

1170746-

FOR LIST OF PARTS SEE DWG

1172798 SHT 2 "A" SIZE

Figure 36. Decoupling Circuit, Schematic Diagram

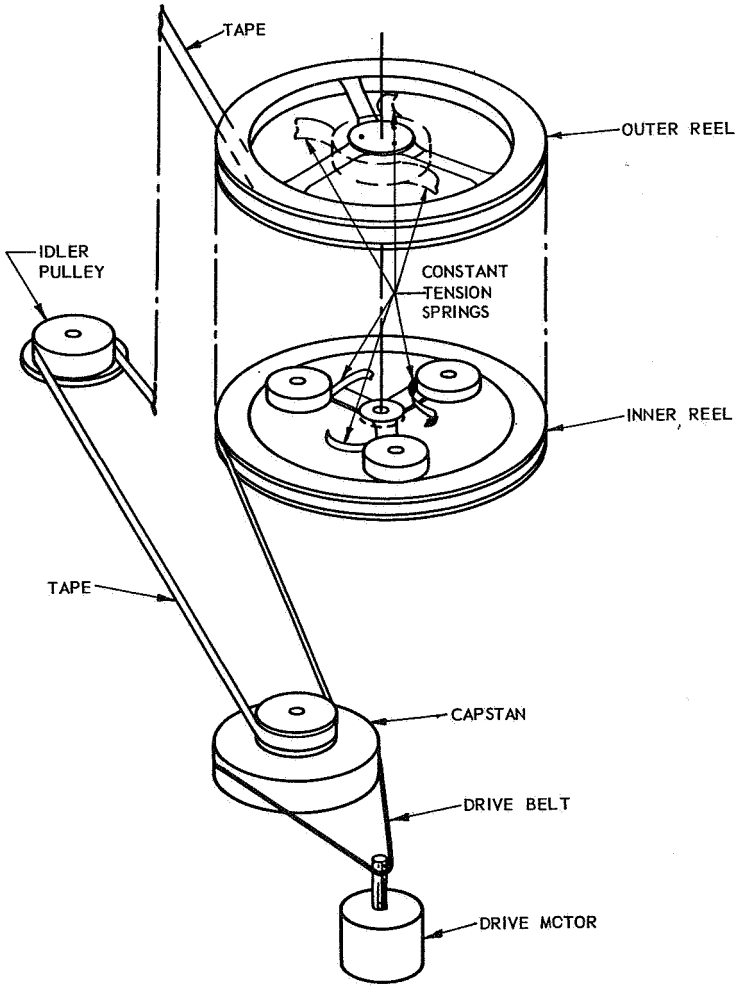

Figure 37. Essential Parts of the Tape-Transport Mechanism

capstan by means of an endless polyester film belt, 0.001-inch thick. Operation of the transport is as follows: the motor drives the capstan, the capstan pulls the tape, and the tape pulls the supply reel. The take-up reel is then pulled by the supply reel because the two reels are coupled to each other. Both reels do not move in perfect unison; there is relative motion between them. The constant-tension springs permit this relative motion while still maintaining constant tension on the tape. The most important feature of this design is the spring coupling between the reels. This configuration made the low power consumption (12 watts, a-c) characteristic of the recorder possible because very little power was required for developing tape tension; the virtually perfect constancy of tension on the tape made a major contribution to tape motion stability. The inherent reliability of such a tensioning mechanism provided, to a large degree, for the reliability of the entire transport. The spring assembly does, however, have one slight disadvantage. The transport was required to be relatively large compared to the volume of tape it carried, because of the large diameter reels that were required. The reels were of a large diameter so that the differential radius, that is, the difference in radius between an empty reel and a fully-loaded reel, was small compared to the mean radius.

The differential radius was required to be small for three reasons. First, it determined the number of relative turns of the two reels; this number had to be kept small so that the constant-tension spring capacity, which was required, was kept reasonably small. Second, the spring capacity, which depends directly on the differential radius, determined the range of load variation that the spring assembly reflected back to the driving motor. Third, because the transport was to be operated in both directions, the "belt theorem", regarding belting over pulleys in non-parallel planes, was satisfied only when both reels were equally loaded. Therefore, the differential radius had to be kept small enough to permit proper tape tracking to be maintained with only a slight crown on the capstan and idler.

The most smoothly rotating member of any tape transport is usually the member with the highest stored kinetic energy. In this case, it was the rotor of the synchronous-hysteresis motor, which rotated at 12,000 rmp. Consequently, it was this motion which dominated the actual movement of the tape, and tight coupling between the motor and capstan was desirable. An endless polyester film belt, 0.001-inch thick was used to provide a low-compliance, high-traction coupling. This belt introduced no measurable motion errors of its own.

Bearing friction of all rotating members was kept low by the use of ball bearings exclusively. Each bearing was pre-loaded to remove all residual play. The bearings were lubricated with a silicone grease.

The transport is capable of operating over a temperature range of 0°C to 50°C for extended periods, and no component part shows sensitivity to temperature within the range for which the transport was designed.

Although the transport was installed in a pressurized container inside the TIROS satellite, it is also capable of operating in a vacuum.

2. Electronics

a. Motor Power Converter. The Motor Power Converter (Figure 38) supplies the two-phase, 110-v, 512-cps power to the synchronous-hysteresis motor on the transport. It also provides end-of-tape control and motor reversing auxiliary functions. The converter is basically a two-core, multivibrator type converter with a feedback winding from the output transformer to the drive transformer. The free-running frequency of the circuit is set slightly below the desired 512-cps output frequency. A 512-cps sync signal from the clock is supplied to the drive transformer to lock the converter at that frequency. (Figure 39)

b. Recorder Motor Power Supply. The end-of-tape switching is accomplished by a piece of metalized tape at both ends of the tape. The metalized tape closes a circuit when it rides over the two end-of-tape sensing bars and turns on a transistor. The transistor, in turn, energizes an end-of-tape relay, which removes power from the converter circuit. The motor is reversed by a relay which merely reverses one pair of leads in the motor winding.

c. Video Modulator and Head-Drive Amplifier. The functions of the video modulator and head-drive amplifier (Figure 40) are to receive the amplitude-modulated video signal from the camera and use it to frequency-modulate a subcarrier oscillator. The resulting frequency-modulated signal, in turn, is supplied to the head-drive amplifier for recording, or to the mixer for direct transmission.

d. Video Playback Amplifier and Mixer. The Video Amplifier and Mixer (Figure 41) receives the signal from the playback head amplifier, equalizes it, adds it to the 10-kc sun pulse in the mixer, and supplies 4.0 v pp to the transmitter. In the direct mode of operation, the subcarrier signal is applied from the modulator, directly to the mixer instead of from the playback head.

e. Sun Position Gate and 10-kc Oscillator. The functions of the sun-position gate and 10-kc oscillator (Figure 42) are to provide a 10-kc signal for recording sun pulses, provide a 10-kc signal for transmission of sun pulses to the mixer, and to gate the 10-kc signal for direct transmission recording and playback.

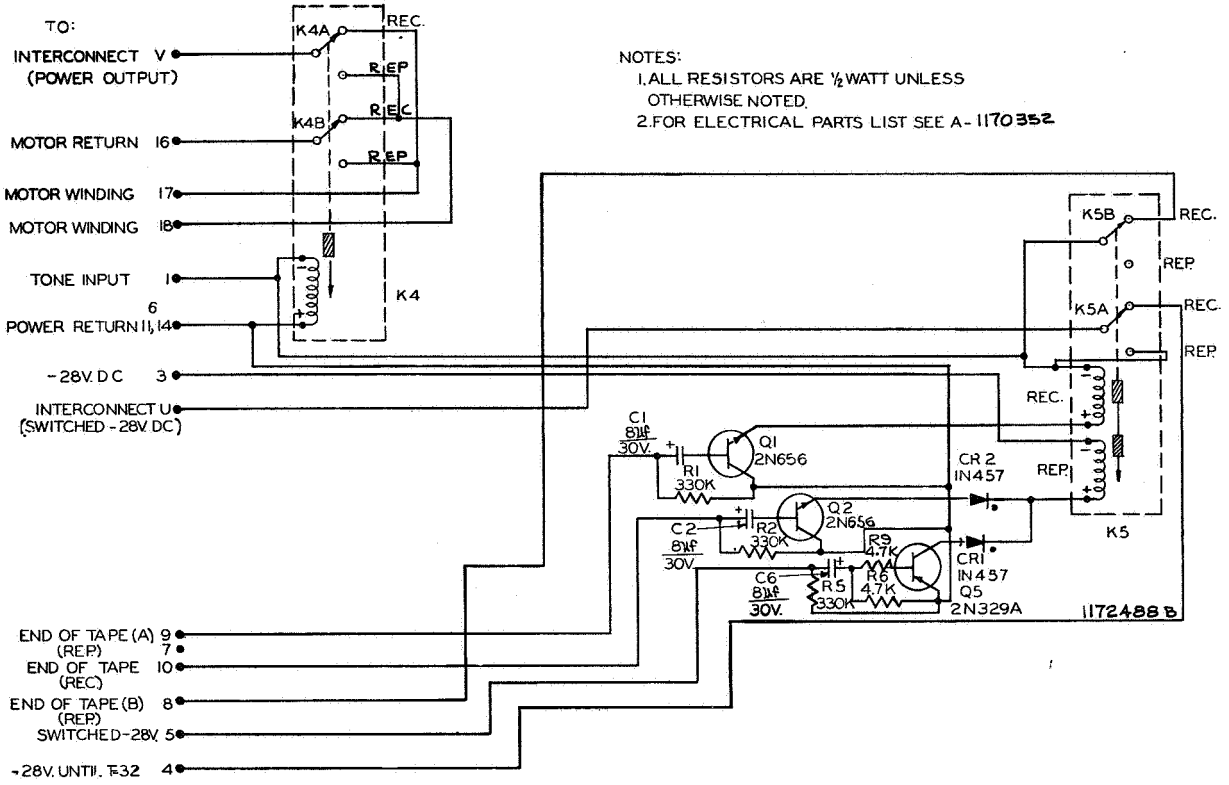

Figure 38. Recorder Motor Power Supply, Schematic Diagram

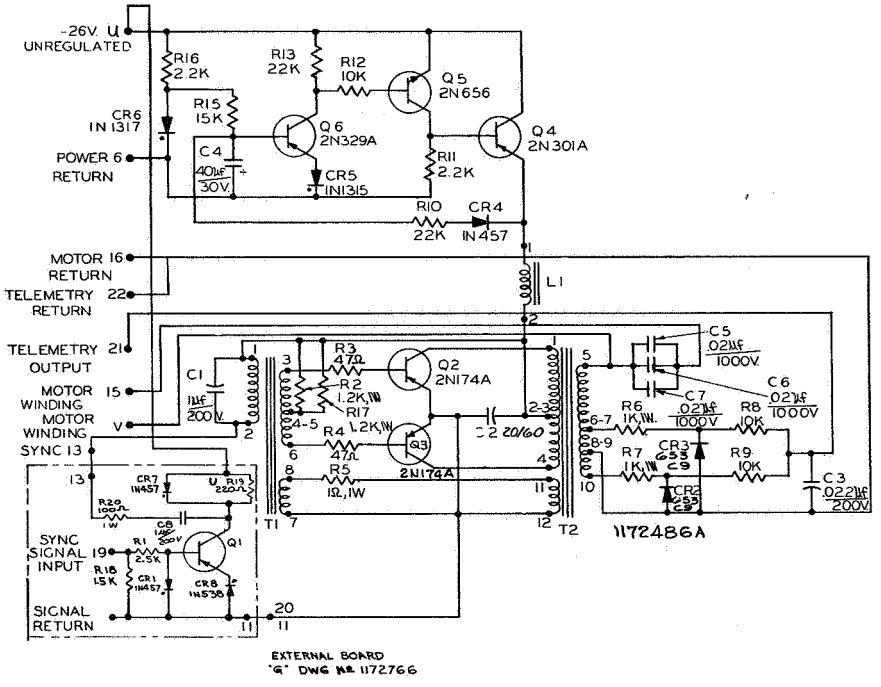

NOTES:
1. ALL RESISTORS ARE ½ WATT UNLESS OTHERWISE NOTED.
2. FOR ELECTRICAL PARTS LIST SEE A- 1170349

Figure 39. Recorder Delay and Power Converter, Schematic Diagram

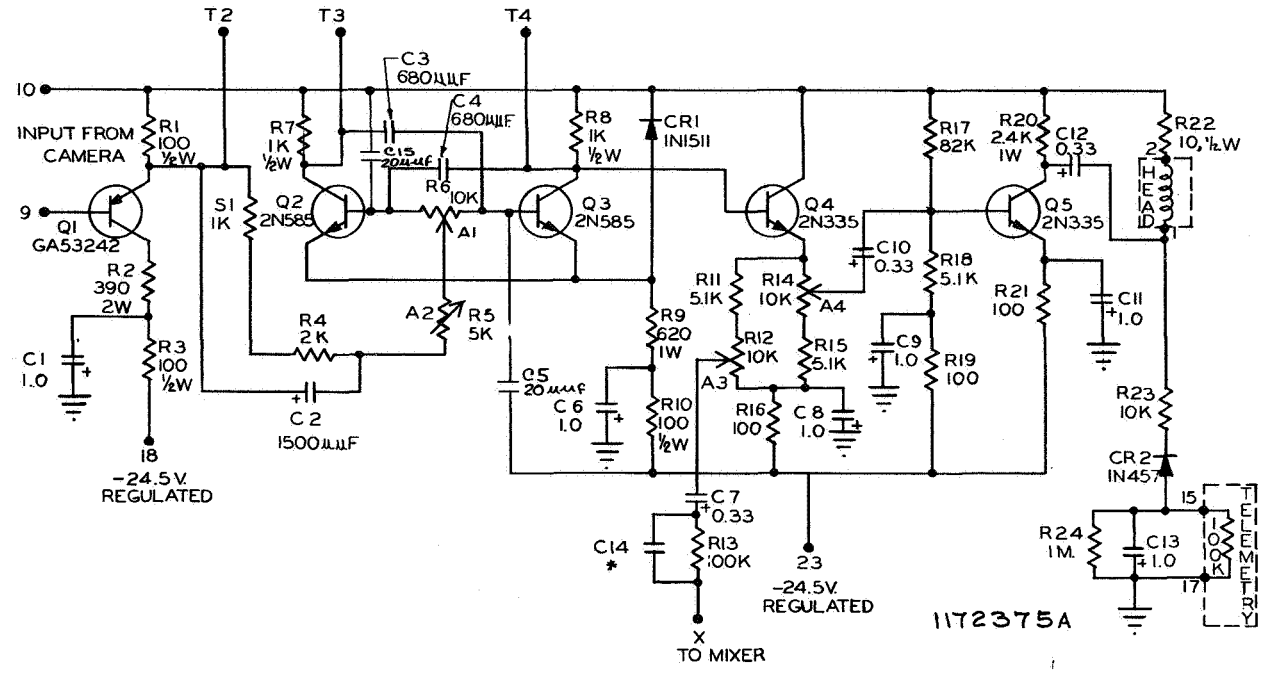

NOTES:

1. RESISTANCE VALUES ARE IN OHMS & ¼WATT EXCEPT AS NOTED.
2. FOR ELECTRICAL PARTS LIST SEE A-1170275

* 3. C14 SELECTED DURING TEST

Figure 40. Video Modulator and Head-Drive Amplifier, Schematic Diagram

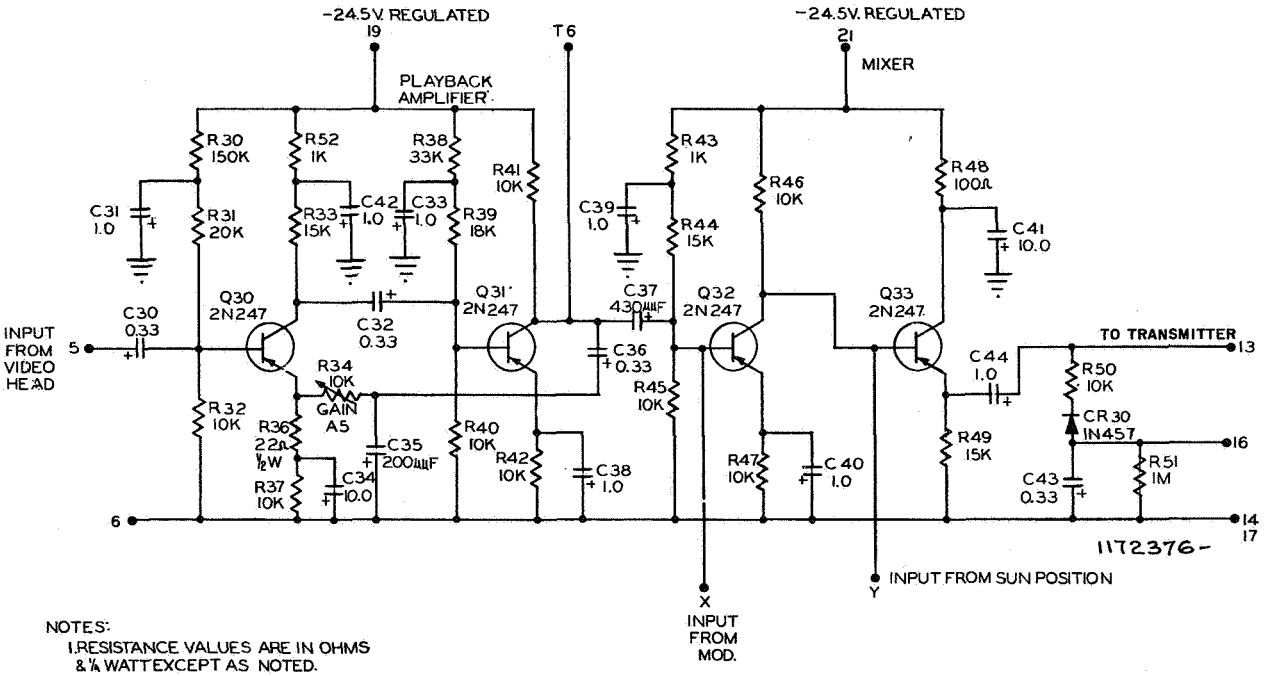

NOTES:

1. RESISTANCE VALUES ARE IN OHMS & ¼ WATT EXCEPT AS NOTED.
2. FOR ELECTRICAL PARTS LIST SEE A-1170276

Figure 41. Video Amplifier and Mixer, Schematic Diagram

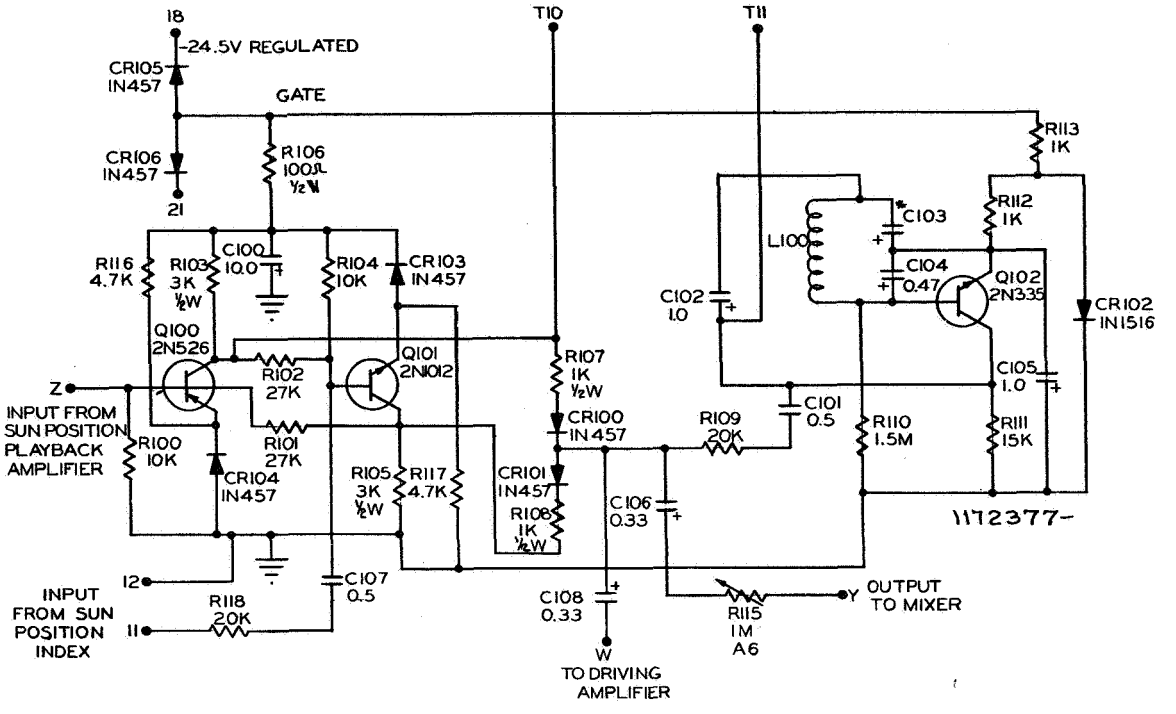

NOTES:
1. RESISTANCE VALUES ARE IN OHMS & ¼WATT EXCEPT AS NOTED.
2. FOR ELECTRICAL PARTS SEE A-1170277
3. *C103 SELECTED TO SET FREQUENCY OF 10 KC OSCILLATOR.

Figure 42. Sun Position Gate and 10-kc Oscillator, Schematic Diagram

f. Sun Position Playback Amplifier and Head-Drive Amplifier. The sun position playback amplifier and head-drive amplifier (Figure 43) circuits supply the head current which is required to record the 10-kc pulses on the tape, amplify the 10-kc pulses recorded on the tape, rectify them, filter them, and differentiate them.

(f) Tests

Each part of the tape recorder was given its individual mechanical and electrical test in addition to the standard unit vibration, shock, and vacuum thermal test.

On the transport the items checked were wow and flutter, speed drift, acceleration time, and optimum frequency response of the magnetic heads. The wow and flutter measured was 0.03 per cent rms from 0.5 to 250 cps. The speed drift in all cases was less than ± 0.5 per cent. The maximum acceleration time was 0.5 second at room temperature. A typical optimum frequency response curve of the heads is shown in Figure 44.

All power converter units were individually subjected to temperature tests at three different temperatures. These tests were made during a five minute run at each temperature with the units electrically connected to a motor which was outside of the test chamber. Typical results of these tests are listed in the following table.

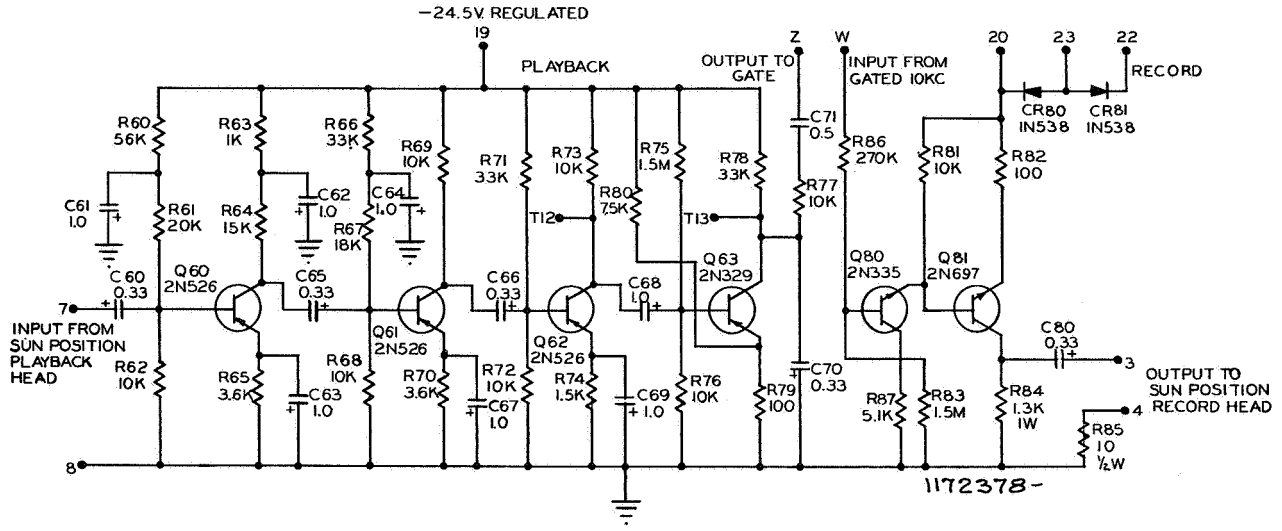

NOTES:
1. RESISTANCE VALUES ARE IN OHMS & ¼ WATT EXCEPT AS NOTED.
2. FOR ELECTRICAL PARTS LIST SEE A-1170278

Figure 43. Sun Position Playback Amplifier and Head-Drive Amplifier, Schematic Diagram

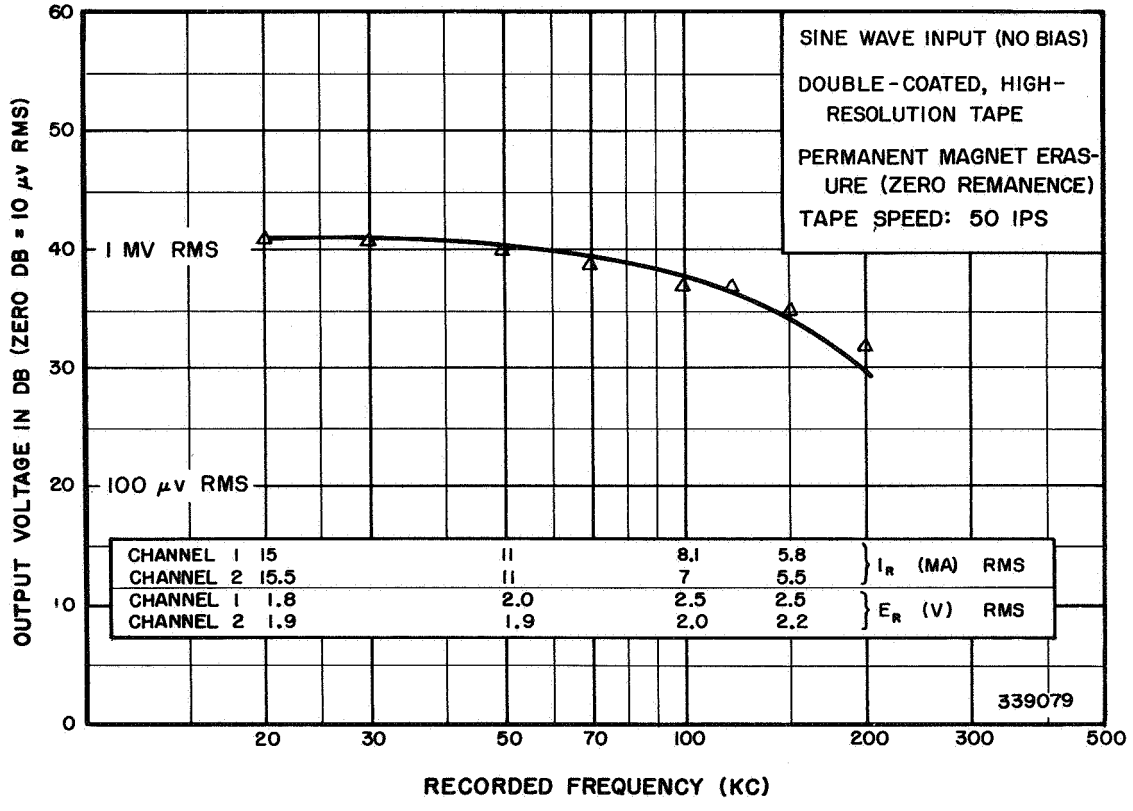

Figure 44. Optimum Frequency Response of Record Heads

POWER CONVERTER TEMPERATURE TESTS (at Pressure of 4×10^{-5} mm Hg, min.)			
	+23°C	+60°C	-10°C
Input Current at 28 v	Maximum 0.95A Average 0.90A	1.0 0.96	0.95 0.90
Input Voltage for Sync Operation at 500 ~	18 v to 33 v	18 v to 33 v	18 v to 33 v
Input Frequency for Sync Operation	480 ~ to 700 ~	475 ~ to 700 ~	475 ~ to 700 ~
Minimum Sync Voltage	3 v peak	3 v peak	3 v peak
Sync Pulse Width	270 to 1000 microseconds	270 to 1000 microseconds	270 to 1000 microseconds
Power Delay Time	1.1 to 1.3 seconds	1.1 to 1.3 seconds	1.1 to 1.3 seconds

The additional recorder electronics tests were for the modulator linearity, subcarrier oscillator frequency stability, input frequency vs. modulator deviation, video playback amplifier frequency response, maximum gain, signal-to-noise ratio, gain vs. temperature, and stability of the 10-kc oscillator.

A typical modulator linearity curve is shown in Figure 45. The subcarrier oscillator frequency stability from -20°C to 70°C was better than ± 2 percent. The input frequency vs. deviation curve for the modulator is flat from d-c to 62.5 kc. The video playback amplifier response is shown in Figure 46. The maximum gain of this amplifier was 73 db. The signal-to-noise ratio, using peak-to-peak signal and rms noise was 50 db. A typical gain vs. temperature curve is shown in Figure 47. The 10-kc oscillator stability was better than ± 0.5 percent from -20°C to +65°C.

(3) TV Transmitters

(a) General

Two identical FM transmitters were included in the satellite to transmit the TV camera video and sun-angle signals to the ground stations. One transmitter was used for the narrow-angle camera and the other was used for the wide-angle camera. The (same) sun-angle signals were transmitted by both transmitters, simultaneously with the video signals.

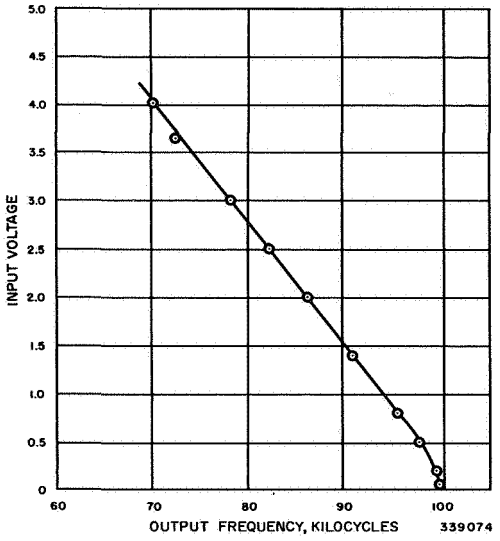

Figure 45. Video Modulator Linearity Curve

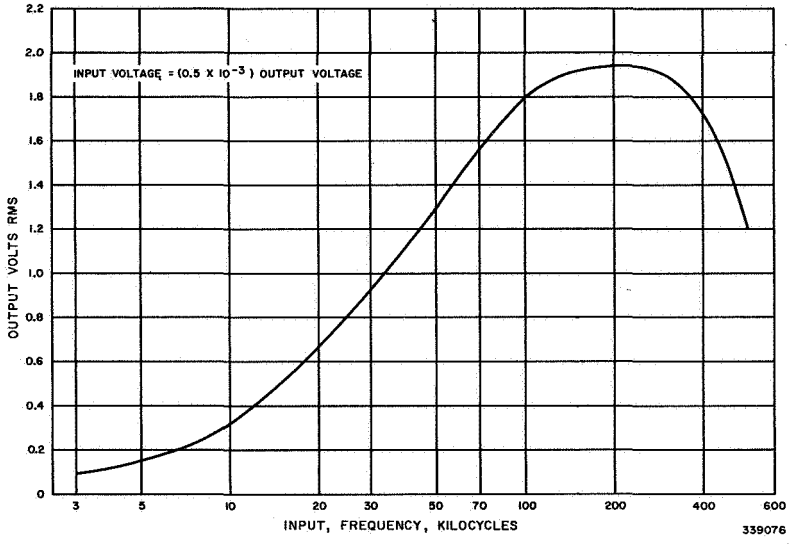

Figure 46. Video Playback Amplifier Response Curve

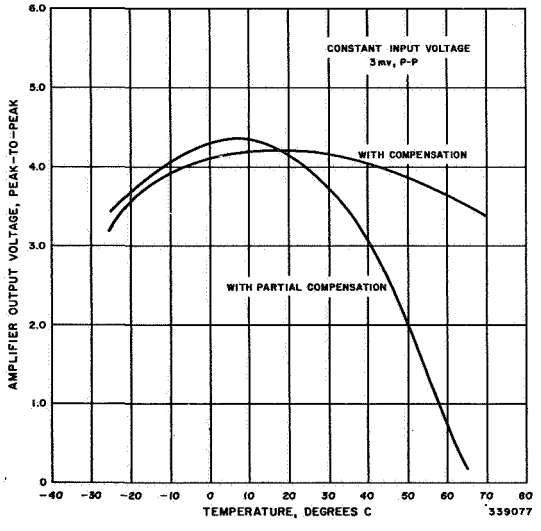

Figure 47. Playback Amplifier Temperature Characteristics

The transmitters were Model 3115-1C units manufactured by Radiation, Inc. A complete description of these transmitters and their operation, as well as a parts list and illustrations is contained in "Handbook of Instructions — FM Telemetry Transmitter — Models 3115-1C, 3115-2C" published by the manufacturer.

Essentially, each transmitter provided two watts (minimum) output in the 235 Mc band and had a video response of 10 cps to 200 kc ± 3 db. Physically, each unit weighed two pounds and occupied a space of approximately 6 by 3-3/4 x 1-3/4 inches.

(b) Selection of a Transmitter

At the start of the TIROS contract, considerable time had been spent investigating TV transmitters. Early system studies had been made to determine rough specifications for power output, frequency band and type of modulation. On the basis of these requirements, two commercially available transmitters were chosen to be tested and evaluated.

The first unit tested was a Telechrome Model 1472 FM transmitter. This unit had a video response rating of ± 3 db from 100 to 80,000 cps. Because the camera required a video response for frequencies up to 147 kc, this unit was tested first for video response. It performed well within its specified range but the type of modulator used, produced large variations in response above 100 kc and it was not apparent how this response could be extended without performing major modification.

The second unit tested was a Radiation, Inc., Model 3115-1 transmitter. The modulator in this unit was down only 3 db at 200 kc and required no modifications to produce this response. Because this unit met all of the system requirements, a series of detailed tests were made to ensure that the unit would pass all required environmental specifications. An additional reason for choosing this transmitter was that it had been recommended by ABMA as a reliable unit used in missile programs.

In early mechanical tests on the Model 3115-1 transmitter, a resonance survey was made. With 10 g acceleration applied to the baseplate, the unit was vibrated for 10 minutes at each of 10 resonant frequencies in three mutually perpendicular planes. This was a much more severe test than required, but the only damage noted was the fatiguing of several small components which were supported only by their wire leads; a break occurred in only one of these leads. These faults were corrected by relocating several of the components and by cementing others in place with epoxy cement.

During subsequent electrical tests, several resistors and tubes were found to be operating outside of the specification limits. These variations were reported to the manufacturer who indicated that this had been corrected in the later models which were then being produced.

Tests were made to determine voltage variations of the series string tube heaters. The 25-volt model of the transmitter showed a heater voltage variation of from 5.4 to 6.7 volts across the nominally 6.3-volt heaters. Initially, it was suggested that the manufacturer change the series-connected heaters to a parallel-series strapping

connection, but because this was non-standard, it was decided to provide a source of 6.3 volts a-c in the transmitter d-c to d-c converter. A transmitter with paralleled heaters was then ordered. Other changes in the later model transmitters included the use of teflon wire insulation and sleeving, ascertaining that the VR tube fired at a supply voltage of 235 volts, and performing a complete electrical check at the manufacturer's plant after a vibration test.

The Model 3115-1C units (see schematic diagram, Figure 48§) were selected and procured for actual use in the satellite. Environmental tests for the prototype of this model were performed in accordance with the satellite final test specifications given in Appendix C. Also in accordance with this specification, each flight unit received the standard flight-model test.

(c) Acceptance Tests

Each transmitter was subjected to a complete acceptance test at RCA. Typical transmitter performance data, obtained during these tests, are shown in the following lists:

TYPICAL TV TRANSMITTER PERFORMANCE DATA

1. Alignment Check — Satisfactory
2. RF Power Output (2 W Minimum) — 2.2 Watts
3. RF Frequency (235 ± 0.02 mc) — 234.9890 mc
4. Video Fidelity Response:

Video Frequency (Cycles)	DB
10	-3.8
20	-1.3
30	-0.5
50	0
400	0
1,000	0
5,000	0
10,000	0
50,000	-0.1
75,000	-0.4
100,000	-0.8
150,000	-1.4
200,000	-1.8

§ This illustration is printed on a foldout page, located at the rear of this volume.

5. Frequency Deviation Linearity ($\Delta f = F_m \times 2.404$)

Δf	Voltage (RMS)	F_m
72,000	0.6	30,0892
98,000	0.8	40,917
125,000	1.0	52,012
133,500	1.1	55,699
145,000	1.2	60,876
171,000	1.4	72,386
196,000	1.6	83,377
220,000	1.8	92,918
246,000	2.0	102,381

6. Power Input:

a. Filament Power	8.6 Watts	(1.4 A, 6.3 VAC)
b. Plate Power	28.0 Watts	(117 ma, 240 VDC)
c. Total Power	36.6 Watts	

7. Power Amplifier Grid Voltage at Telemetering Terminal: -1.9 VDC (20 K load)

8. Frequency Stability:

Temperature (°C)	RF Frequency (Mc)
-10	234.9870
Approximately 23 (Room Temperature)	234.9874
50	235.0002

9. Modulation Linearity:

E_{in} (VDC)	RF Frequency (Mc)
23.600	234.8290
24.000	234.8520
24.400	234.8954
24.800	234.9212
25.200	234.9672
25.600	235.0038
26.000	235.0414
26.400	235.0794
26.800	235.1188
27.200	235.1614

10. Storage Test (80°C) for 6 Hours

(d) Modifications by RCA

Several modifications were made on the Model 3115-1C transmitter. The plug-in Winchester connector was removed and a solder terminal board installed. Resistor R1 (originally 450 ohms) was changed to 330 ohm, 5W. Dalohm. This change was made to ensure firing of the VR tube at the lower limits of the plate supply voltage. Resistors R28 and R29 were added to provide telemetering of the final amplifier grid voltage. These modifications are shown on the transmitter schematic diagram in Figure 48.

The final specifications for the transmitter were as follows:

Electrical

Power output:	2 watts (min.) into a 50 ohm load
Output frequency:	235 Mc ± .01% (from 10° to 50°C)
Video response:	10 cps 6 db (1000 cps reference)
Video response:	150 kc 3 db (1000 cps reference)
Modulator input impedance:	3800 ohms ± 20%
Deviation sensitivity:	± 150 kc for (3.1 volts p-p input)

Physical Size

Dimensions:	6.2 x 3.8 x 1.8 inches
Weight:	2 pounds

(4) Command Receivers

(a) General

Two identical command receivers were employed in the satellite to provide for the reception of command signals from the ground stations. One receiver was used for each camera channel: The inputs of both were connected to the common command antenna, but their outputs were conducted to separate control programmers.

The receivers were specially designed by RCA for satellite operation. They were light-weight, compact, transistorized units which could be operated continuously because their power requirements were negligible. A complete description of the command receivers is given in the classified supplement to this report.

(5) Programming and Control System

The programming and control system is described in the classified supplement of this report.

SECTION III A. 3.

3. The Telemetry and Tracking Subsystem

a. General

The design objectives of the telemetry and tracking system were: (1) to provide a 108-megacycle continuous-wave beacon signal from the satellite to aid in the acquisition and tracking of the satellite by stations of the TIROS ground complex; (2) to provide this signal redundantly from two beacon transmitters, thereby ensuring reliability of the subsystem; and (3) to provide a method for telemetering satellite operational and temperature parameters redundantly via the beacon transmitters.

Prior to the initiation of work on TIROS I, RCA had completed development of 20 milliwatt beacons for use in project SCORE. The SCORE beacons utilized a subcarrier oscillator connected to a simple thermistor for temperature measurement. Since these beacon units had performed well in the SCORE satellite, it was decided to use a modified (improved) version of the same general design for TIROS I. Modifications needed were: a better heat sink for the r-f transistors, to stabilize power output with temperature; provision for plus and minus d-c signal inputs to the subcarrier oscillator; and changes to the mounting.

b. Functional Description

The current and voltages of critical electronic circuits, and temperatures at significant locations in the satellite, are sampled periodically, and the information obtained is transmitted to a ground station. (Figure 49 is a block diagram of the telemetry and tracking subsystem; Table 1 lists the telemetered parameters.)

Each circuit or thermal check voltage to be telemetered is converted to a d-c voltage in the +2.5 volt to -2.5 volt range. These d-c voltages are sampled for a period ranging from 700 to 850 milliseconds by means of the 40-contact telemetry switch. This switch sequentially connects the d-c pulses to a 1300-cps subcarrier oscillator. The d-c pulses shift the frequency of this oscillator to values ranging between 1200 and 1400 cps, depending on the magnitude and polarity of the pulses. In turn, the subcarrier-oscillator output amplitude-modulates the 108- megacycle beacon. Duplicate systems, one operating at 108.00 megacycles; the other at 108.03 megacycles; receive inputs from the telemetry sensors to provide redundant transmission.

c. Telemetry Sensors

(1) General

The telemetry sensors provided a means of obtaining the temperature profile of the orbiting satellite. RCA's satellite thermal-design studies, with consideration

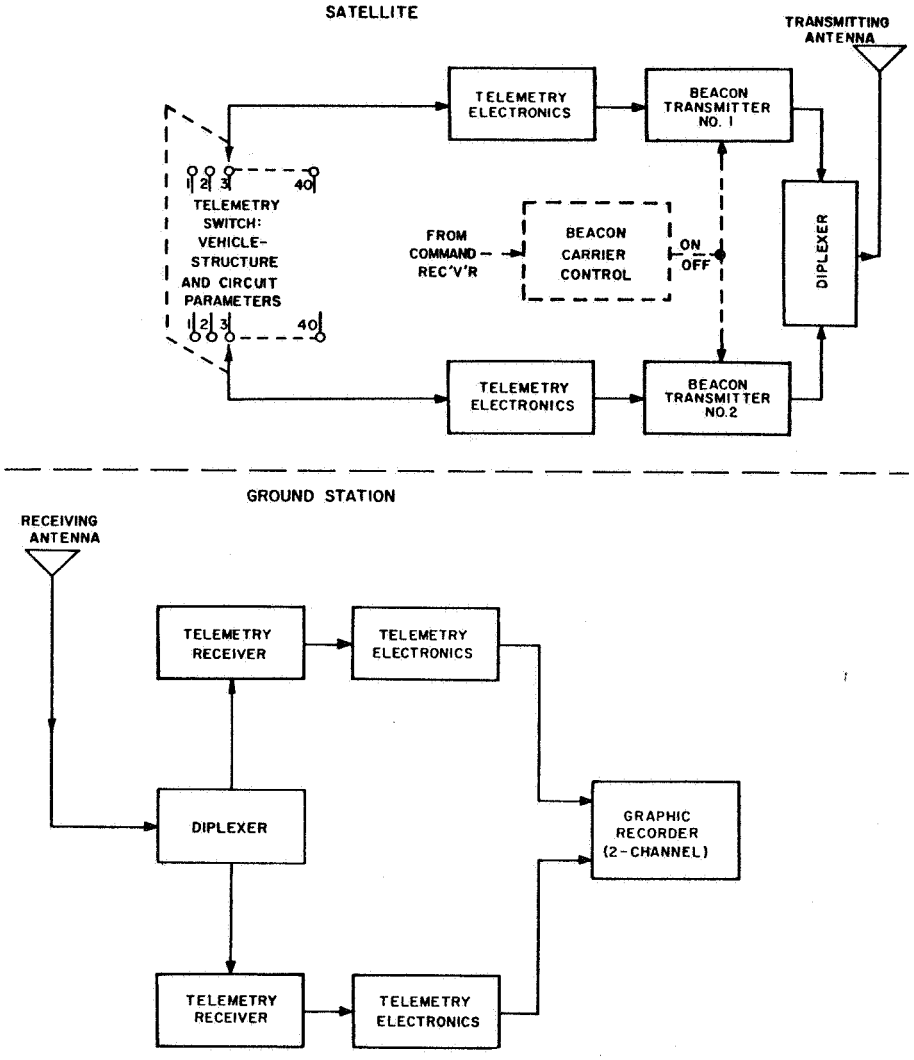

Figure 49. The Telemetry and Tracking Subsystem, Block Diagram

to orbit parameters; and the input signal requirements of the telemetry beacons, were the major factors in formulating the specifications for the design of the telemetry sensors. Secondary factors considered in establishing the specifications were: the number of available telemetry channels, the location within the satellite for temperature data points, the source for transducer polarizing current (if applicable), redundant readings for reliability, minimal power requirements, and the ability to withstand the invoked environmental specifications of vacuum, vibration, shock and acceleration, minimal weight, mechanical form-factor (featuring ease of production installation without the need of time-consuming calibration when installed within the payload).

Once the expected temperature extremes had been established and the number of telemetry channels (and telemetry switch positions) determined, a decision was necessary to determine if a "trade-off" between accuracy of temperature data (expanded scale factor) and the possibility of exceeding the dynamic range of the telemetry input would be justified.

TABLE 1

SATELLITE TELEMETRY SWITCH POSITIONS

Tel. Sw. Pos. No.	Parameter Transmitted Through Beacon No. 1	Parameter Transmitted Through Beacon No. 2
1	Ground Calibrate	Ground Calibrate
2	-2.5 Volts Reference	-2.5 Volts Reference
3	Top Skin Temperature (1)	Base Plate Temperature (40°)
4	Top Skin Temperature (2)	Base Plate Temperature (90°) 19"r.
5	Side Skin Temp. (Top Panel 2)	Base Plate Temperature (190°)
6	Side Skin Temp. (Bot. Panel 2)	Base Plate Temperature (90°) 6"r.
7*	-28 Volts, Battery String "X"	-28 Volts, Battery String "X"
8*	-28 Volts, Battery String "Y"	-28 Volts, Battery String "Y"
9*	-28 Volts, Battery String "Z"	-28 Volts, Battery String "Z"
10	-28 Volts, Main Load Buss	-28 Volts, Main Load Buss
11	Voltage Regulator No. 1, -24.5V	Voltage Regulator No. 1, -24.5V
12	Voltage Regulator No. 2, -24.5V	Voltage Regulator No. 2, -24.5V
13	Voltage Regulator No. 1, -13.0V	Voltage Regulator No. 1, -13.0V
14	Voltage Regulator No. 2, -13.0V	Voltage Regulator No. 2, -13.0V
15	Clock No. 2 Vertical Sync	Transmitter Converter No. 1
16	Clock No. 2 Horizontal Sync	Transmitter Converter No. 2
17	Clock No. 1 Vertical Sync	Transmitter No. 1
18	Clock No. 1 Horizontal Sync	Transmitter No. 2
19	Vidicon No. 1 High Voltage	Vidicon No. 1 High Voltage
20	Vidicon No. 2 High Voltage	Vidicon No. 2 High Voltage
21	Vidicon No. 1 Fil. and Focus Cur.	Vidicon No. 1 Fil. and Focus Cur.
22	Vidicon No. 2 Fil. and Focus Cur.	Vidicon No. 2 Fil. and Focus Cur.
23	Spin-Up Rocket Firing Index	Spin-Up Rocket Firing Index
24	TV Camera No. 1 Video Output	Solar Cells, Top
25	TV Camera No. 2 Video Output	Solar Cells, Side
26	Solar Cells, Top	Recorder Head No. 1
27	Solar Cells, Side	Recorder Head No. 2
28	Motor Power Converter No. 1	Motor Power Converter No. 1
29	Motor Power Converter No. 2	Motor Power Converter No. 2
30	Playback Amplifier No. 1	Playback Amplifier No. 1
31	Playback Amplifier No. 2	Playback Amplifier No. 2
32	Transmitter Converter No. 1	Clock No. 2 Vertical Sync
33	Transmitter Converter No. 2	Clock No. 2 Horizontal Sync
34	Transmitter No. 1	Clock No. 1 Vertical Sync
35	Transmitter No. 2	Clock No. 1 Horizontal Sync
36	Base Plate Temperature (40°)	Top Skin Temperature (1)
37	Base Plate Temperature (90°) 19"r	Top Skin Temperature (2)
38	Base Plate Temperature (190°)	Side Skin Temperature (Top Pan. 2)
39	Base Plate Temperature (90°) 6"r	Side Skin Temperature (Bot. Pan. 2)
40	Home Contact	Home Contact

* The storage battery strings X, Y, and Z are monitored separately by the telemetry subsystem.

It was rationalized that some sacrifice in readout accuracy should be made, since slightly inaccurate temperature data would be better than no data at all, as would be the case if the range of telemetry had been exceeded.

The following is a list of preliminary design specifications for the TIROS I temperature sensing subsystem:

Temperature Range:	-30°C to +100°C
Telemetry inputs:	0 to -2.5 Volts
Single end, full scale @ Z_{in} > 10 K ohms	
Number of channels:	8 (commutators to common input)
Source of polarizing voltage if applicable:	-26 Volts
Telemetry accuracy:	5% full scale
Vibration:	25 g rms., 20 -2000 cps
Shock:	15 g
Acceleration:	50 g
Vacuum:	$\geq 10^{-10}$ mm. Hg.

(2) Development

The telemetry-input scale-factor requirements greatly exceeded that of thermoelectric type devices; at least, it did without amplification of the output of these devices. Thus, resistance thermometers were most applicable and various types were investigated. Of these, thermistors had the advantage of reasonable form factor, together with high-temperature coefficients of resistivity.

Thermistors for resistance thermometry have been effectively utilized in operational systems. However, they have certain deficiencies. For example, they have negative exponential conductance - temperature relationships, and where current from these devices is applied to the constant input resistance of telemetry channels, an exponential voltage-vs-temperature response curve results which has a variable slope. This characteristic, coupled with a constant error for the telemetry channel, produces low resolution of absolute temperature for portions of the response curve, and higher resolution in other portions of the curve. If the temperature is to vary throughout the full scale, it is desirable to have a linear response curve and obtain a constant error in temperature resolution. As an approach to this objective, several types of circuits were devised and their response was analyzed.

The types of circuits analyzed were: a simple circuit, a conductance-compensated circuit, and an active-compensation circuit. The response for each of

the circuits has been derived, and is presented in Appendix K. (Ref. 7) The analysis of the simple circuit demonstrated that its response was inadequate to obtain precise temperature data over the required temperature scale. The analysis of the conductance-compensated circuit showed that it would produce a hyperbolic, rather than a linear, response. The analysis of the active compensation circuit showed that it would produce a linear output. This circuit, therefore, was selected for use as the temperature sensor.

(3) Testing of the Temperature Sensor

It was impractical to apply a step function of heat to the sensors inside a vacuum chamber; therefore, a test thermistor was mounted upon a block and strip heater and power was applied to the strip heater as a step function. The time interval measured until the composite assembly reached a maximum temperature gave some indication of the speed of response. Experimental evidence, (see Figure 50) showed that the response timewas at least better than 3.6 minutesfor $\Delta T = 130°C$ and here actually what was measured was the speed of response of the block and heater, not the sensor unit alone. Therefore, since the time required for this order of temperature change in TIROS I is a matter of months, adequate speed of response was provided by the design. Further investigations proved that ascending and descending time-temperature curves were coincident when crushed silver foil was inserted between sensor and block to eliminate vacuum voids and improve thermal conductance. The reason for the separation between the ascending and descending time-temperature curves, shown in Figure 50, was that the time rate of temperature change was much higher when ascending than when descending.

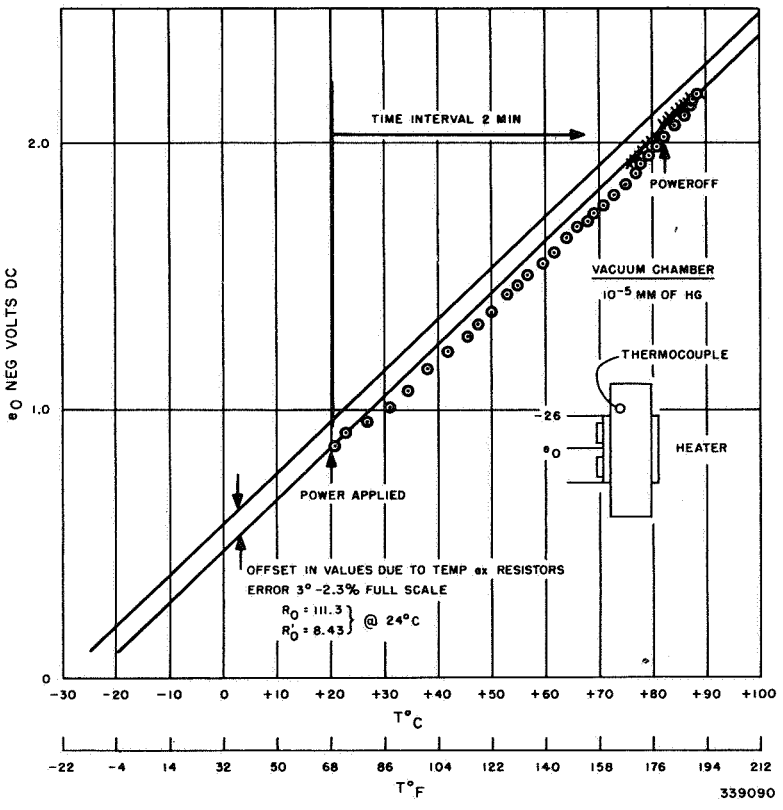

Figure 50. Response Speed of Test Thermistor in Vacuum

The completed assembly showed no impairment of performance when subjected to vibration, shock and acceleration.

(4) Sensor Evaluation

There were no particular problems of integrating the sensors into the system and the initial objectives were met by the design. However, recommendations for future sensor designs, based on the operational performance of TIROS I, are: (1) expand the scale factors, and (2) locate the sensors directly on the satellite's components rather than on the base, side, and top plates.

d. Telemetry Switch

(1) General

Each subsystem development group provided lists of items to be telemetered. These lists were reviewed and thirty-nine items were selected to be telemetered. It was established that all telemetered sources would be d-c, or a-c converted to d-c, with limits of ±2.5 volts dc.

At the start of the project, various time-switching schemes were investigated, including a solid-state commutator. Frequency-division multiplexing was considered but rejected because the inherently low-power beacon (20 to 30 mw) would not supply enough power per channel and also, a large number of subcarrier oscillator units would be required. Time-division multiplexing was considered more feasible, and was therefore chosen. Conventional mechanical telemetry switches were tested and the problem of life and reliability-versus-speed of switch operation was investigated. Since there was no need for fast transmission of the telemetry data, a slow-operating switch was chosen to ensure long operating life and good reliability. For this slow-operating requirement, a geared-down motor versus a ratchet solenoid drive were investigated. An investigation of lubrication problems led to a final design in which the solenoid, the switch, and the electronic drive were packaged as a single hermetically-sealed unit.

The original concept called for continuous rotation of the telemetry switch at about 1 rpm, allowing all Minitrack stations to receive telemetry data. It was later decided to energize the telemetry system on command only, leaving the beacons with an unmodulated output for tracking, thereby saving on power and switch life.

(2) Functional Description

The telemetry switch has 40 contacts, 39 contacts for telemetered channels, the 40th contact used as a "home" or automatic stop circuit. The electrical circuit is shown schematically in Figure 51.

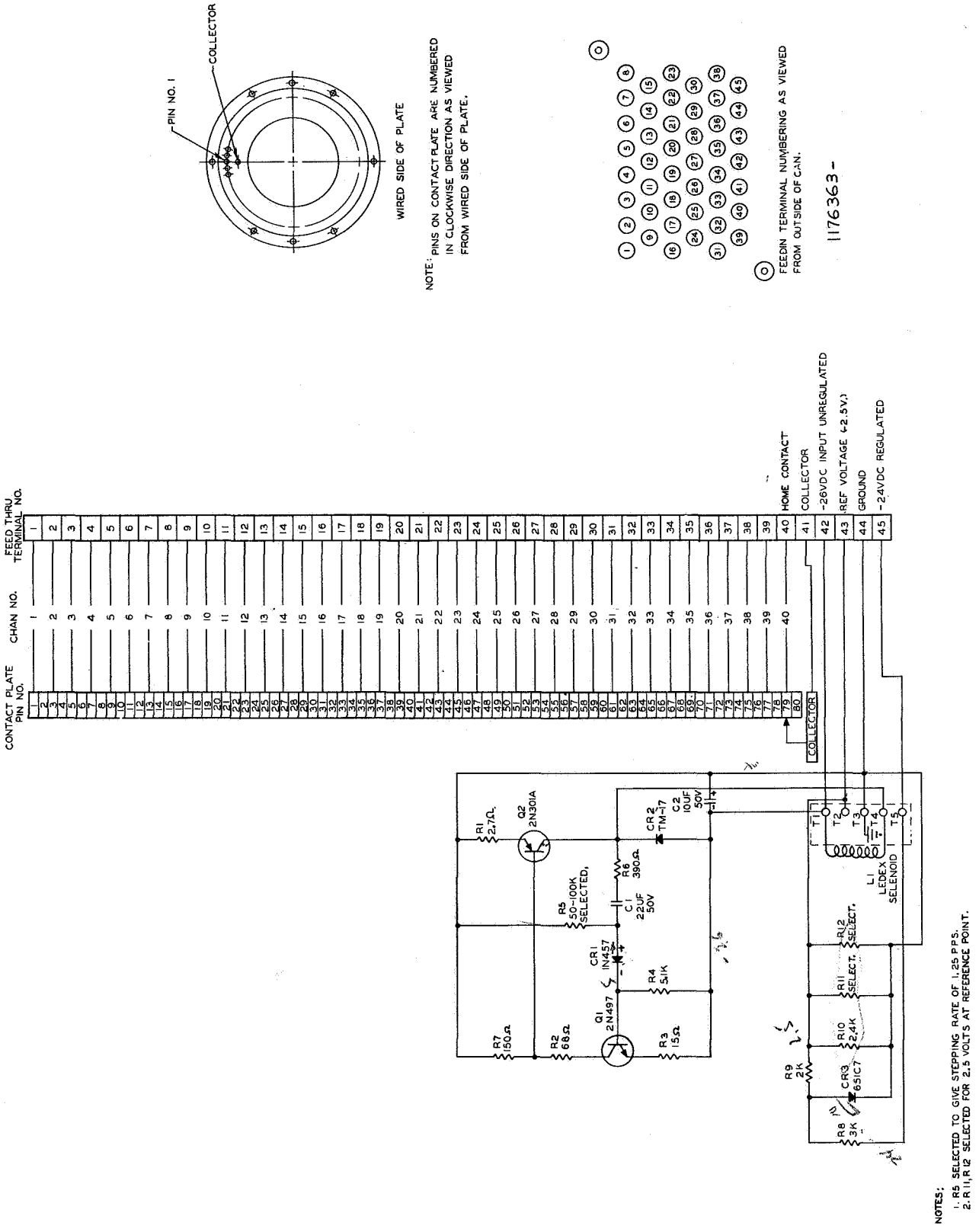

Figure 51. Telemetering Switch with Drive and Voltage Reference Circuitry, Schematic Diagram

Upon receipt of a command for tape playback or direct camera, a relay in the control system is latched up and supplies regulated 24 volts d-c to terminal 45 on the switch. A calibration reference voltage of -2.5 volts ± 1% is supplied to terminal 43 through R8-10-11-12 and CR3, a Zener diode. This voltage is telemetered as channel 2 for reference calibration of the system. Simultaneously -26 v d-c supplied to terminal 42, energizes Ledex solenoid L1 through transistor switch Q2. Transistors Q1-Q2 and time-constant network C1-R6 constitute a flip-flop circuit that turns Q2 on for about 30 msec and off for about 800 msec. The solenoid is therefore energized for 30msec causing it to step the switch one contact point. The switch then dwells on that contact for about 0.8 second before advancing to the following contact. The net power drain is equal to about 30 divided by 800 times 2 amperes, or 2 watts at 26 volts. The unit continues to step automatically at this rate until the switch reaches contact No. 40. This contact discharges a capacitor through a Zener diode located across the subcarrier oscillator input and through a series coil that unlatches the control relay, removing all power from the switch. One rotation of the telemetry switch takes place in approximately a half minute. Two of these switches are provided in the satellite, one associated with each beacon system.

The telemetry switches have performed very well. No failures of any kind have been observed throughout their test and use.

e. Beacon Transmitter (Subcarrier Oscillator Section)

(1) General

The beacon transmitters for TIROS I were constructed by Applied Science Corporation of Princeton (ASCOP). When received by RCA, each transmitter had to be calibrated and adjusted for correct subcarrier center frequency, best linearity, and least center frequency drift of the subcarrier oscillator. The center frequency was adjusted by changing the bias on the reactance modulator and, where necessary, by changing capacitance values in the circuit. The linearity was optimized and the frequency drift was minimized by adjusting the compensating resistors associated with the input transistor stage to the subcarrier oscillator. The final test data (input voltage versus subcarrier frequency) was plotted at three temperatures and calibration curves were prepared for each beacon transmitter. (Ref. 8)

The subcarrier oscillator (SCO) design for TIROS I was based on the SCO used for the SCORE project. On the latter project, each SCO was calibrated for a single temperature sensor; however, on TIROS I, some of the SCO inputs were from high impedance sources. To telemeter the high impedance sources, the SCO input impedance had to remain constant with varying input level.

An example of this characteristic can be seen in Figure 52. To overcome this problem, the input resistance of each of the production SCO units was measured and special low-temperature coefficient padder resistors were installed in each unit so that each SCO would present the same input resistance, within ± 1 percent of 30 thousand ohms.

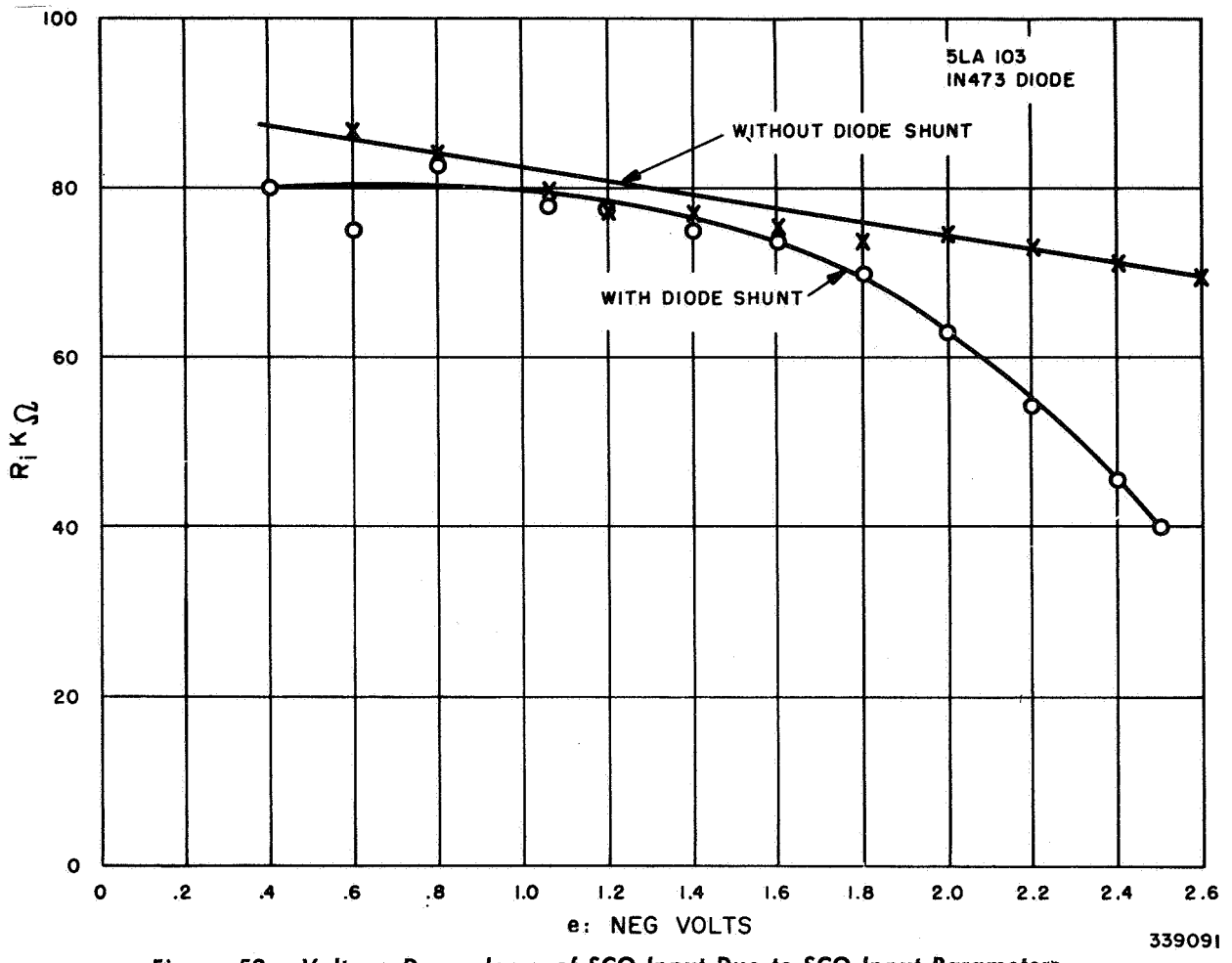

Figure 52. Voltage Dependence of SCO Input Due to SCO Input Parameters

Measurements of temperature coefficient of resistivity of the finalized SCO units, within the range of 0 to +80°C, were found to be .0005 per °C. The input resistance was further shunted to a value of 10 thousand ohms by a fixed low-temperature coefficient resistor in the temperature sensor assembly; the input circuit, therefore, was satisfactory.

(2) Functional Description

The schematic of the SCO is shown in Figure 53. The SCO portion consists of the bipolar input coupling transistor, Q6, driving the reactance modulator, Q1, and the 1300-cps oscillator, Q2. Diode CR4, conducting at plus or minus five volts, protects the input against higher voltages and provides a conduction path for the homing switch release described in (4) above. CR2 compensates for the input impedance change of Q6 when the input polarity reverses. The Zener diode (CR3) regulates the voltage supply for these transistors. Final specifications for the SCO are:

Temperature range:	-10 to +55°C
Center frequency:	1300 cps ± 4 cps

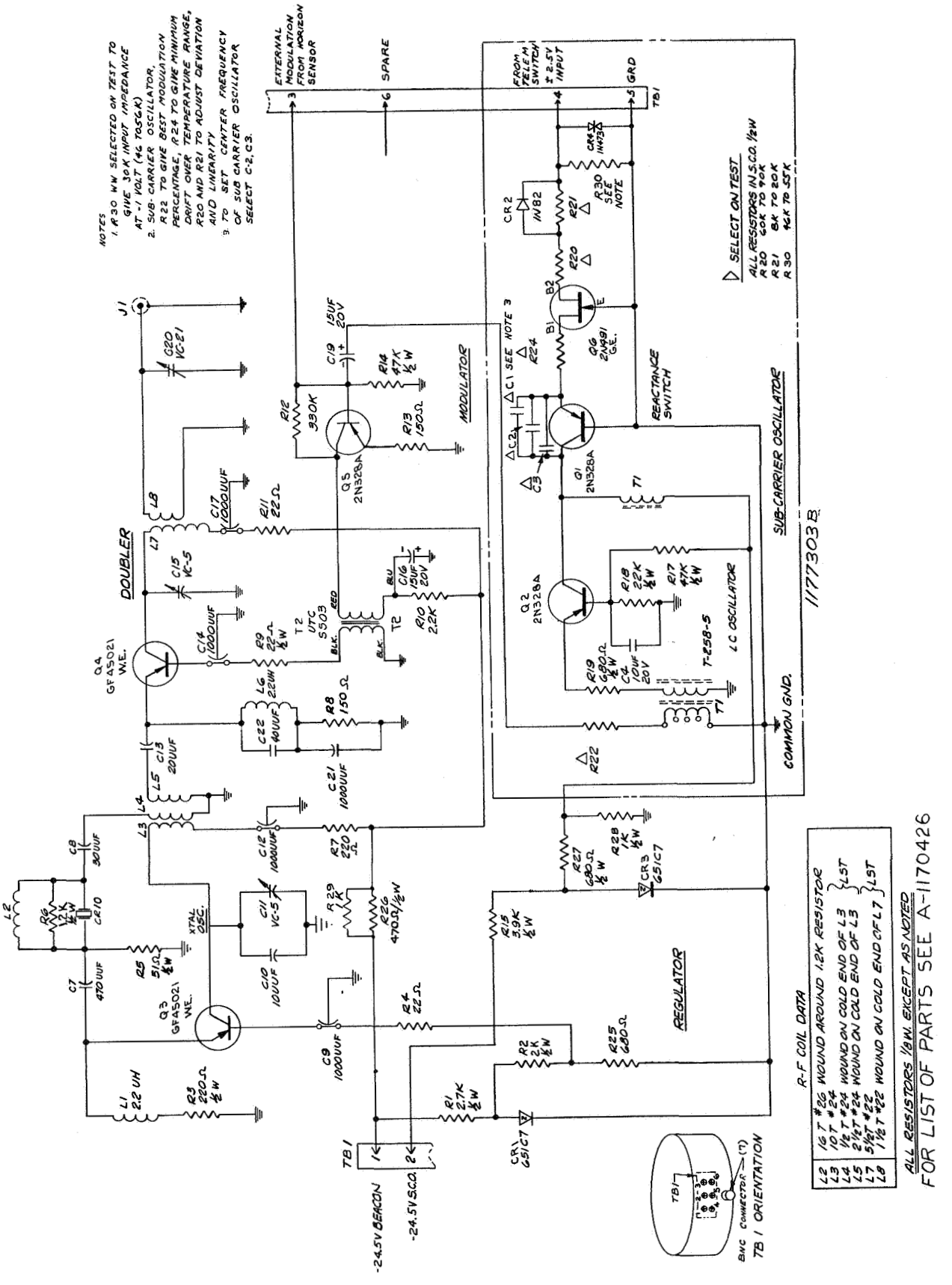

Figure 53. 30-mw Transmitter and Subcarrier Oscillator, Schematic Diagram

Linearity:	± 1% best straight line
Input impedance:	30K ohms ± 1%
Input level maximum:	± 2.5 volts
Frequency shift for ±2.5 volts:	± 100 cps ± 2%
Power drain:	0.123 watt (-24.5 v, 0.005A)

f. Beacon Transmitter (R-F Section)

The schematic diagram of the beacon transmitters is shown on Figure 53. The r-f section consists of crystal-controlled oscillator Q3 and r-f amplifier and doubler Q4. The oscillator, Q3, operates at 54 Mc using series-resonant crystal CR10 in the feedback path from collector to emitter. The doubler-amplifier Q4 is driven at 54 Mc and its collector is tuned to 108 Mc for frequency doubling. Transformer T2, in the common base lead, amplitude-modulates transistor Q4. The modulator, Q5, is driven directly from input terminal 3, the horizon sensor 3000-cps burst signal. In addition, the subcarrier oscillator Q2, on command, feeds the FM subcarrier at 1300 cps to the modulator.

Final Specifications for the Beacon Transmitter are:

Crystal frequencies:	54,000 and 54.015 Mc
Output:	108.000 and 108.03 Mc
Freq. stability:	± .005% -10° to + 55°C
C-W output:	20 mw minimum over -10° to + 55°C
Modulated output:	30 mw minimum over -10° to + 55°C, 80% Modln.
Power drain:	0.49 watt (-24.5 v at 0.02A)

4. Reference Indicator Subsystems

The reference indicator subsystems is the general name given to the North Indicator (Sun Angle) Subsystem and the Attitude Indicator Subsystem, because data from both is required to identify cloud-picture orientation. The sun-angle indicator consists of nine solar-cell sun sensors and associated electronics which provide data from which the north direction of each picture taken can be determined. This data is applied to the TV transmitter for transmission to the ground stations. The attitude indicator consists of an infrared, thermistor sensor and associated electronics which provide data from which the attitude of the satellite spin axis is determined.

a. North Indicator

(1) General

The north direction for a picture received from the TIROS satellite is determined by obtaining: (1) the angular position of the sun with respect to a zero reference-radius on the satellite baseplate, (2) the position of the sun with respect to the earth,

and (3) the position and attitude of the satellite in its orbit with respect to the earth at the time the picture was taken. The nine sun-angle sensor units form the first link in the data chain. Each sensor unit is contained in a special mount, parallel to the spin axis, behind a slit aperture. The mounts are radially mounted 40 degrees apart around the vertical walls of the satellite housing, as shown in Figure 54. As the satellite spins, the slits sweep across the sun, causing the sun sensors to generate "sun triggered" pulses. These pulses trigger coded multivibrators located in the sun-sensor electronics package. Because of the sensor spacing and the 9 to 12 rpm spin rate, two of these coded pulses occur during each two-second picture read-out. The coding is sequenced in such a way that any two pulses uniquely define a sun-sensor location. These pulses are amplified and shaped in the sun-sensor electronics package and applied (in coded form) to the tape-recorder electronics, as shown in Figure 55.

In the electronic circuits, the pulses are transformed into a-c signals. These are portions of a 10-kc wave of time duration equal to that of the pulses are called "tone bursts." If the pictures are being taken in the remote mode (i.e., while the satellite is not in contact with a ground station), the tone bursts are recorded on the tape recorder, along with the corresponding video information, where they are stored until the satellite, in contact with a ground station, is commanded to "playback." The tone bursts (along with the video information) are then "read back" into the electronics. If direct pictures are being taken, this record-playback procedure is deleted.

The tone bursts are then used to modulate the TV Transmitter which sends the information to earth. Here the video and sun-angle information are received by the TV Receiver. The Sun-Angle Bandpass Filter separates the sun-angle information from the video signal, after which the tone bursts are entered into the Sun-Angle Computer. The computer identifies the particular baseplate-referenced sun sensor associated with the tone bursts corresponding to a given bit of video information by using the sensor coding scheme (described in the section on Sun-Sensor Electronics). It then relates the occurrence times of these bursts with the initiation of the video subcarrier, which corresponds to the time at which the picture was taken, and computes the sun angle. Simultaneously, the video information and the sun angle from the computer are displayed visually and photographed. Using the sun angle on a photograph along with orbital data corresponding to the time the TV picture was taken, the north direction can be determined and placed on the photograph.

(2) Sun-Sensor Electronics

(a) Introduction

The first step in determining the north direction for a TV picture taken by the TIROS satellite was to find the angular position of the sun relative to the satellite baseplate reference system. The position of the TV camera, measured in degrees around the baseplate from the zero-reference radius, was known. It was desired to know the position of the sun with respect to this zero reference at the time the picture was taken. This necessitated the use of some sun-sensing device. The device employed in the TIROS satellite is a silicon solar cell which gives an electrical output when light is incident upon its surface. The solar cell and its associated pulse-shaping circuitry

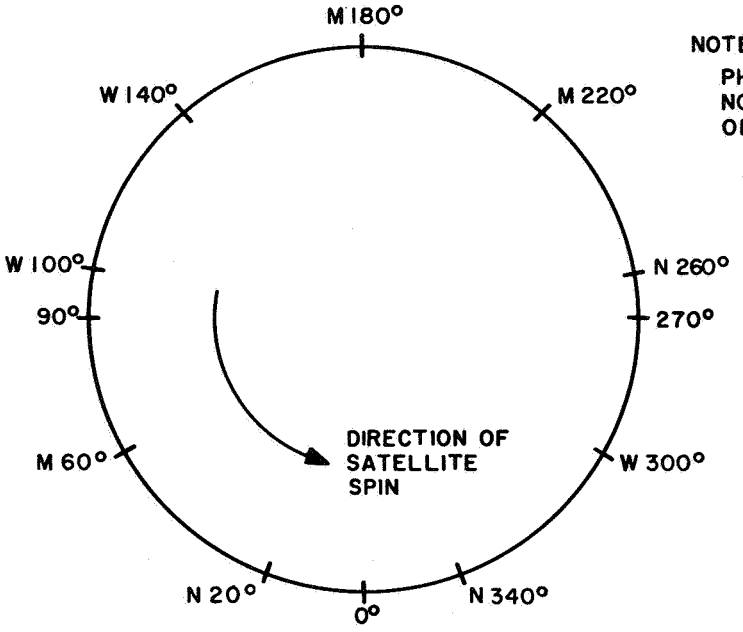

NOTE:
PHYSICAL RESTRICTIONS DID NOT PERMIT A SENSOR TO BE PLACED ON THE 0° REFERENCE LINE

(VIEWED FROM TOP OF SATELLITE)

N: LOCATION OF SENSOR WHICH GIVES A NARROW OUTPUT PULSE
M: LOCATION OF SENSOR WHICH GIVES A MEDIUM OUTPUT PULSE
W: LOCATION OF SENSOR WHICH GIVES A WIDE OUTPUT PULSE

339011

Figure 54. Sun-Sensor Unit Locations on Satellite Baseplate

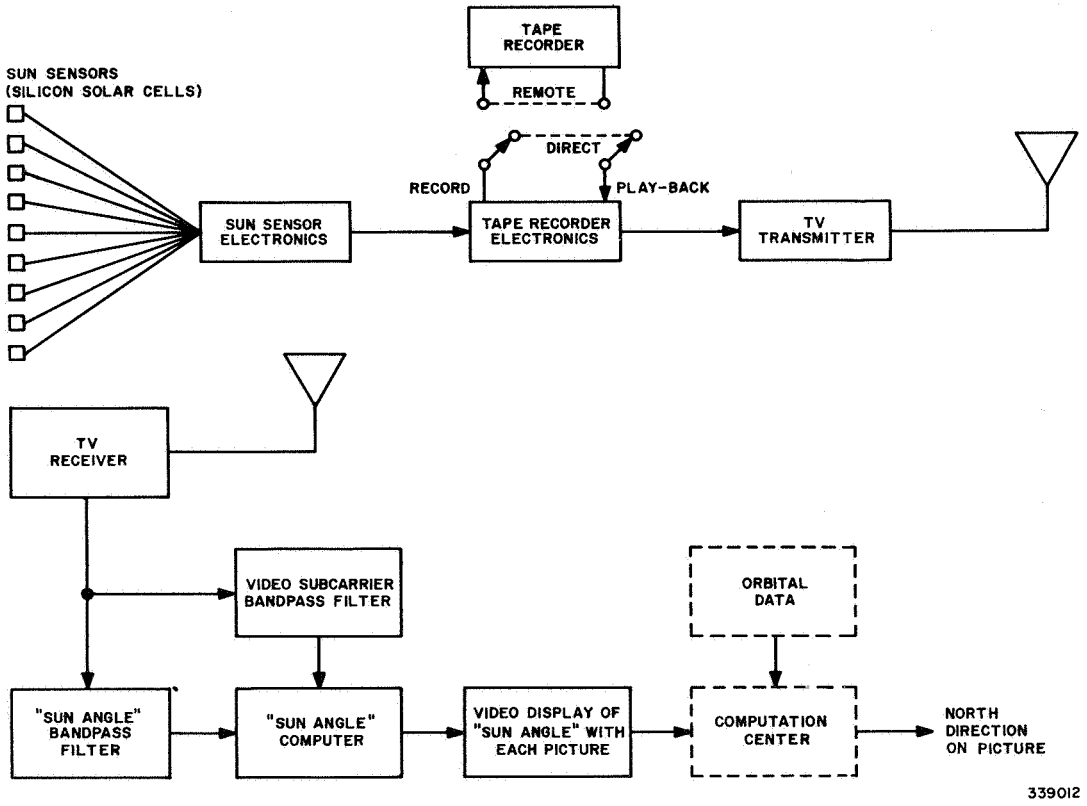

Figure 55. Sun-Angle Data Chain, Block Diagram

comprise the Sun-Sensor Electronics. The type of cell used here is the same as that used for the electrical power subsystem.

(b) Basic Requirements

Because a picture can be taken at any time during one rotation of the satellite, more than one sun sensor must be located around the periphery of the satellite in order to ensure that at least one sensor will "see" the sun whenever a picture is taken. If there is more than one sun sensor, however, a method must be used to determine which sensor "saw" the sun when the picture was taken (i.e., which radial line on the baseplate pointed toward the sun when the picture was taken).

These two requirements: a plurality of sensors, and the need to identify these sensors, made it necessary to develop a coding scheme to determine the location of the sun.

The solution arrived at was to use nine solar cells spaced equally around the periphery of the satellite, which provided a minimum of two sensor outputs for each picture. To determine to which two sensors these outputs correspond, the sensor outputs were coded to form unique pairs. In this way, it was not necessary to make the output of each sensor different from all the others, but only to have three different types of outputs from the nine sensors. It was decided to obtain the three types of outputs by changing the nine equal-duration sensor output pulses into three groups of pulses, each with different widths. A group of three of the sensors would provide narrow-width pulses, another group of three would provide medium-width pulses, and the final group of three would provide wide-width pulses. The resultant coding system is shown in Figure 54.

Another requirement of the sun sensors was to supply the correct inputs to the "tone burst" generators in the Tape Recorder Electronics. These pulses were to be of sufficiently high amplitude with fast rise and fall times. Therefore, the basic requirements on the Sun Sensor Electronics output were that it consist of pulses of sufficient amplitude and rise and fall times, and of different widths.

(c) Development

The pulses from the solar cells do not have the required amplitude nor rise and fall times. Therefore, electronic amplification and shaping was required. However, the different pulse widths could be obtained in either of two ways: physically, by using solar cells of three different physical widths so that the duration of the output pulse would be determined solely by the length of time which sunlight is incident on the cell; electronically, by using the solar-cell outputs to trigger monostable multivibrators ("one-shots"). The multivibrators would provide output pulses with widths determined by their on times. The on times could be controlled by adjustment of an RC network.

These two methods are the physical method and the electronic method respectively. The physical method was attempted first, but the electronic method was later found to be more feasible and was used for the final design.

1. Physical Method. The electrical output characteristics of the solar cells were investigated to determine the amplification and pulse shaping which would be required to satisfy the circuit output specifications, and the optimum loading conditions for the cells. It was found that the response of the cells was rapid enough not to be a limiting factor, but that the actual output from the cells, under normal operating conditions, had rise and fall times which were longer than could be tolerated. This results from the finite times required for the beam of sunlight to fall completely on the cell, and then off the cell, as the satellite rotates. Furthermore, the output from the cell does not maintain an even maximum value, but there are slight fluctuations in the output as the beam of light sweeps across the cell's active surface. Therefore, it was decided to clip and amplify the cell output pulses to obtain clean, "square" pulses as shown in Figure 56.

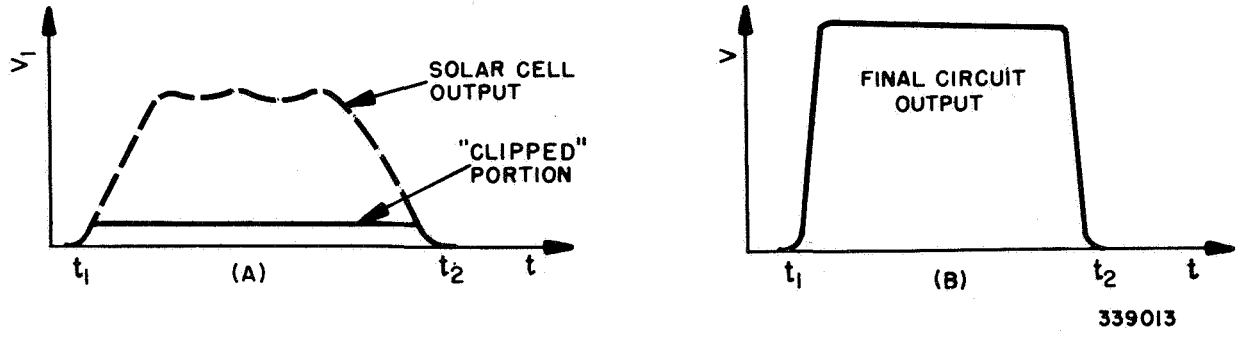

Figure 56. Sun-Sensor and Electronics Pulse Shapes

Initially, the nine solar cells were connected in parallel to the input of a three-stage, transistorized, d-c amplifier. It was desired to have the output of any one of the nine cells produce a final circuit output of the form shown in part (B) of Figure 56. Therefore, the gain of the first two stages had to be sufficient to drive the third stage completely on (i.e., to operate this transistor essentially as a switch). The basic difficulty with arrangement was that the three different pulse widths were being obtained by using solar cells of three different widths. The different width cells generated different amplitude outputs for the same amount of incident light. A "narrow" cell gave an output pulse with an amplitude substantially below that obtained from a "wide" cell or a "medium" cell. If the gain of the amplifier was adjusted to provide sufficient output with a narrow-cell input (as this cell swept across the sun), spurious circuit outputs would be generated when reflected sunlight was incident upon a wide cell. The reflected wide-cell light level which caused these spurious pulses was of the order of that obtained from the earth. Therefore, these cells would actually generate a spurious "sun pulse" as they swept across the earth.

Another problem which was encountered was that the cell efficiency varied between cells. For the same light input, two cells of the same width gave different amplitude outputs even though the pulse widths were the same.

An attempt to eliminate these difficulties was made by using a separate preamplifier for each individual cell. It was hoped that nearly identical amplitude pulses could be obtained from the nine preamplifiers, and that these pulses could be further amplified by a common two-stage d-c amplifier.

Associated with each cell was a load resistor and a Type 2N335 transistor. These nine transistors shared a common output circuit, being connected in parallel to the remainder of the amplifier. Each of the first-stage transistors was selected in an attempt to obtain the same amplitude pulse between its collector and emitter such that equal-amplitude pulses were fed to the succeeding amplifier. This match was attempted by connecting high-output cells to low-beta transistors, and vice versa.

Testing was performed outdoors by using sunlight, and indoors by using artificial, collimated light which simulated the intensity of the sun. The solar cells were mounted in their housings around the periphery of a large aluminum disc so that the cell arrangement was a full-scale reproduction of that to be used in the satellite. The disc or wheel was rotated at 10 rpm, and oriented with respect to the light source so that the angle between the light rays and the axis of rotation ranged between 30 and 90 degrees; the variation in the angle between the sun's rays and the spin axis (the "α angle"), expected during the operation of the satellite. It was found that a change in the α angle did not produce a uniform variation in the solar-cell outputs.

Finally, uniform circuit operation could not be obtained over the required temperature range (-10 degrees C to +60 degrees C). Cell efficiency changes with operating temperature, but this change is not the same for each cell. The transistor characteristics also vary with operating temperature; therefore, biasing became a problem in the d-c amplifier.

The many problems encountered with this approach (non-uniformity in solar-cell performance, cumbersome selection of components, sensitive-circuit adjustment, etc.), indicated that an entirely new design was required. It was decided to use the solar-cell outputs merely as initial signals and to obtain the desired pulse characteristics of amplitude, rise and fall times, and widths completely by electronic means.

2. Electronic Method. With this design, the solar-cell output pulses are used to "trigger" an electronic circuit which generates the desired sun-angle (north-indicator) pulses. The solar cells employed are the same as those which were used with the physical method (i.e., there are nine cells equally spaced around the periphery of the satellite, three narrow-width

cells, three medium-width cells, and three wide-width cells). The same cells were used because they were available, and some had already been mounted in housings. Theoretically, standard- (wide-) width cells would be used because these give the greatest signal output for a given light input, but the different width cells all gave outputs (within the desired operating range) which were sufficient to trigger the electronics.

The required output-pulse widths had been established from considerations concerned with the physical approach, and although more desirable widths may exist for this new type of design, the electronics were designed to give the original pulse widths since the Sun Angle Computer design had already been based on these widths.

The Sun-Sensor Electronics for TIROS I are made up of three basic building blocks, a preamplifier, a one-shot multivibrator and a summing circuit. These are integrated as shown in the block diagram of Figure 57.

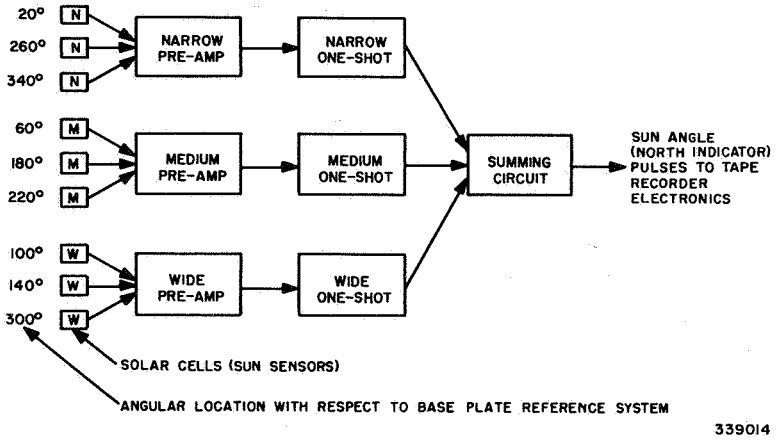

Figure 57. Sun-Sensor Electronics, Block Diagram

(d) Functional Description

1. General. The operation of this system is as follows: When sunlight falls on one of the cells, its electrical output pulse is fed to the corresponding preamplifier. Here the pulse is differentiated and amplified. The leading edge of this amplified pulse is used to trigger the corresponding "one-shot". The output pulse from the "one-shot", with a width corresponding to the "triggering cell", is then fed to the summing circuit where it is applied to a common output lead.

A more detailed description of the circuit operation follows.

2. Detailed. The three narrow cells are connected in parallel to the narrow preamplifier, the three medium cells to the medium preamplifier, and the three wide cells to the wide preamplifier. (See Figure 58.) The resistor, R12, in each of the three preamplifiers and the internal imped-

ance of the three cells constitute the d-c load on the three paralleled cells, across which the initial electrical signal is generated.

Consider the operation of the "narrow branch" of this system. As the satellite rotates, sunlight falls on a narrow cell through a thin slit aperture, and the beam of light travels across the cell as shown in Part (A) of Figure 59. Part (B) through (H) of Figure 59 represents the a-c waveforms at various points in the Sun-Sensor circuitry in an approximate and simplified manner, in order to give a qualitative insight into the circuit operation. (The waveforms are not "rigorous," but are meant only as visual aids.) A maximum amplitude is reached when the entire width of the beam is on the cell and is maintained until the beam begins to fall off the cell. As shown in Part (B) of Figure 59, the amplitude decreases to zero as the incident light goes to zero. The solar-cell output pulse is differentiated, amplified, and inverted by the preamplifier. The resulting positive trigger pulse (shown in Part (F) of Figure 59), which corresponds to the leading edge of the sun pulse, is then applied to the one-shot. The positive trigger pulse is amplified and inverted by Q1. The resulting negative pulse is coupled to the input of Q2 through C1 and R4, where it is amplified and inverted. This resulting positive pulse is fed to the input of Q1 through the voltage divider consisting of R2 and R1 where it adds to the effect of the original positive trigger pulse. After a sufficient charge has built up on C1, Q2 begins to turn off. This produces a negative pulse at the base of Q1, which shuts off. The resulting positive pulse at its collector is coupled through C1 and R4, turning Q2 completely off.

The on-time for the one-shot is determined by the time required for C1 to charge. This time can be varied by changing the RC time constant of the charging path. This can be accomplished by adjusting the value of R4 in each of the three one-shots to give the desired output pulse widths. The value of R4 in the narrow one-shot is less than the value of R4 in the wide one-shot; therefore, the on time (the output pulse width) is greater for the wide circuit than for the narrow circuit because the charging rate (the other resistances being constant) of C1 is inversely proportional to the resistance of R4. R4 is of intermediate value in the medium one-shot.

The Summing Circuit combines the outputs of the three one-shots to provide for a common output, and provides decoupling between the Sun Sensor Electronics and the Tape Recorder Electronics. It consists of an emitter follower with an "OR gate" input. The diodes CR4 and CR7, CR5 and CR8, and CR6 and CR9 couple the negative one-shot output pulses directly to the base of transistor Q4, and prevent the output pulse from one triggered one-shot from feeding back into the other two untriggered one-shots. Since the emitter of Q4 follows its base, the one-shot output pulse is reproduced across resistor R13 with very little decrease in amplitude, and constitutes the Sun-Sensor Electronics output which is the "Sun-Angle" pulse. (See Figure 60 for comparison of input and output pulses.)

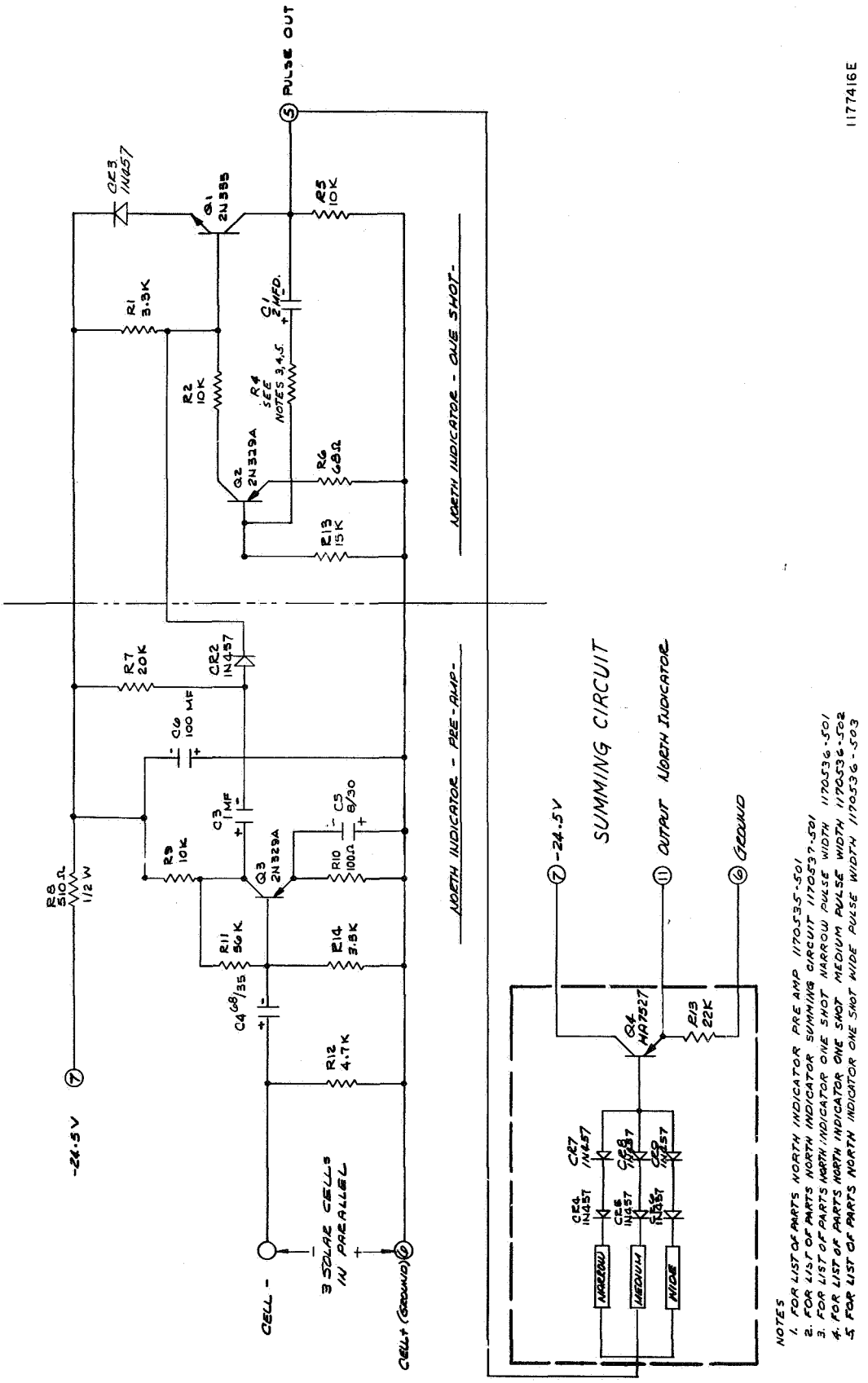

Figure 58. Preamplifier, One-Shot Multivibrator and Summing Circuit, Schematic Diagram

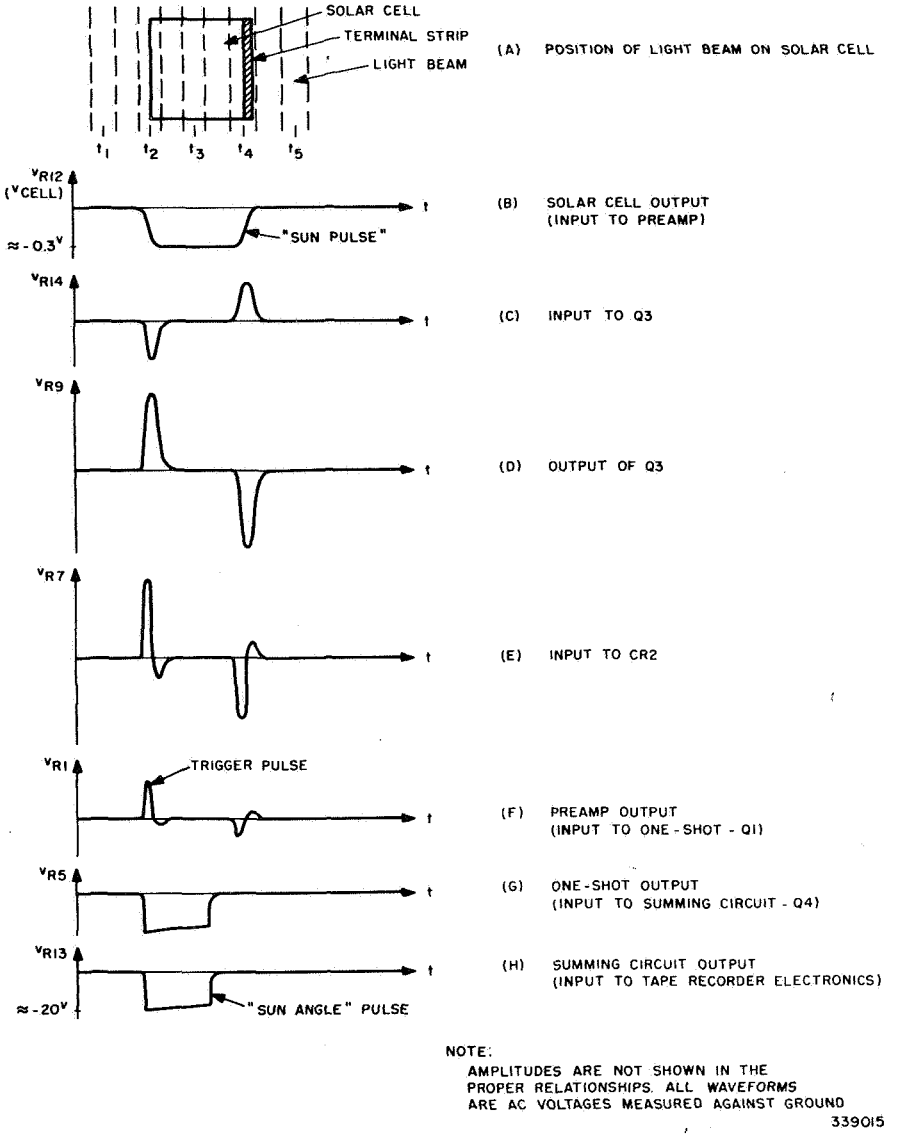

Figure 59. Light-Bear Positions versus Output Waveforms (Nominal)

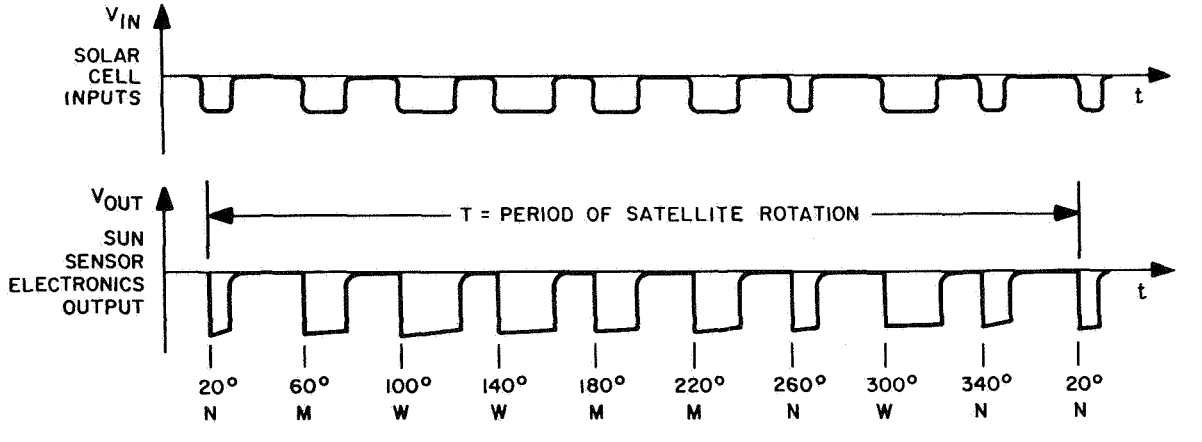

Figure 60. Sun-Sensor Input and Output Pulses

(e) Tests

The Sun-Sensor Electronics package met all environmental test requirements. The output-pulse widths varied as the operating temperature of the circuitry was changed because the characteristics of the circuit elements are effected by temperature. These widths were held within the required limits, however, by proper selection of the "timing resistor" (R4), which affects the RC time constant of each one-shot. The Sun-Angle Computer can "recognize" a pulse as a narrow, medium, or wide pulse if the width of this pulse complies with the pulse-width requirements listed in the following table.

Pulse Width Requirements		
Pulse	Operating Temperature (degrees C)	Required Pulse Width (milliseconds)
N	-10	> 50
	+25	67
	+60	< 85
M	-10	> 120
	+25	145
	+60	< 175
W	-10	> 205
	+25	250
	+60	< 290

Proper circuit operation was obtained using first, actual sunlight, and then artificial, collimated light, which simulated the sun's intensity, to trigger the circuitry. The electronics package was temperature tested, first with the solar cells at room temperature. This was done to make sure the circuitry would operate correctly over the temperature range when the "triggering geometry" was the same as it would be in the satellite. The triggering geometry (that is, the physical arrangement of the solar cells and the manner in which they would be swept across the sun) was simulated by using the large rotating wheel (described previously) and the artificial sunlight. With this design, the variation of solar-cell characteristics with temperature contributes a negligible amount to the change in circuit output because of the operating-temperature variation. One-shot triggering became more difficult as the temperature decreased, but under normal operating conditions the solar-cell outputs were sufficient to produce triggering over the entire temperature range. After satisfying the requirements of this test, the electronics and the solar cells were mounted in their housings. In the tests which followed this initial temperature test, the solar cells were triggered by chopping the light from a spotlight which was aimed at the cells through their apertures. This light was merely chopped by hand with a card. Therefore, in these tests the proper triggering geometry was not simulated, but solar-cell outputs were obtained so that the electronics could be tested. The entire system (solar cells, preamplifiers, one-shot multivibrators, and summing circuit) was then subjected to the temperature test by mounting the nine housings on a rotating test jig in a Tenney temperature chamber and shining the spotlight through a glass window in the chamber.

After the temperature test, the Sun-Sensor Electronics were put through vibration, shock, and acceleration tests, during which the circuits were not energized, but after which they were checked for proper operation. Following these tests, the system was subjected to a space environment in a thermal-vacuum test. The Sun-Sensor housings, contained the solar cells and their associated electronics, were mounted on a test jig in a bell-jar vacuum chamber. With the pressure maintained at 5×10^{-5} mm Hg, the ambient temperature of the electronics was cycled three times between -10°C and +55°C. The solar cells were triggered, using the spotlight, and the circuit output was monitored at temperatures of -10°C, +25°C, and +55°C for each cycle.

Finally, the system was put through a baking test. This consisted of maintaining the system at a temperature of +80°C for six hours, and then checking the circuit operation at +50°C.

Six complete electronics packages, each consisting of three preamplifiers, three one-shots, and one summing circuit, were assembled. Five of these were actually installed in the two prototype and three flight vehicles which were built. The sixth served as a spare set. Only five sets of housings and solar cells were constructed, one for each satellite. The probability of a failure of a solar cell or a housing was negligible, and if any of the circuits failed (the likelihood of which appeared remote judging from the test results), it could be replaced by one of the spare circuits. All sets met the required specifications and passed all environmental tests. (The spare set of electronics was subjected to only the temperature test because this did not have a corresponding set of housings and solar cells.) No failures occurred in any of the finished circuits.

After installation in the vehicles, the five sets were given a Go, No-Go check with the spot light, and all functioned properly.

The Sun-Sensor Electronics operated successfully after launch and throughout the operating lifetime of the orbiting TIROS I satellite. There were some problems concerned with the handling of the received information by the Sun-Angle Computer, but these were not related to the performance of the Sun-Sensor Electronics.

(3) Sun Sensors

(a) Basic Requirements

1. General - The sun-sensor system must, during any two-second remote or direct-mode picture readout, sense the angle of the sun with respect to the baseplate coordinate system. (See Figure 61.) It must be capable of sensing this angle to an accuracy of ± 0.25° when the α angle (the angle between the sun and the vehicle spin axis) varies from 30 to 90 degrees.

2. Number of Sensors. To satisfy the requirement that the system sense the "sun angle" during a two-second picture readout, nine sensors were installed. These were spaced at 40 degree intervals to ensure that at the lower spin rate (9 rpm) at least two sequential pulses occur during a two-second interval. (At 9 rpm the vehicle rotates 108° about

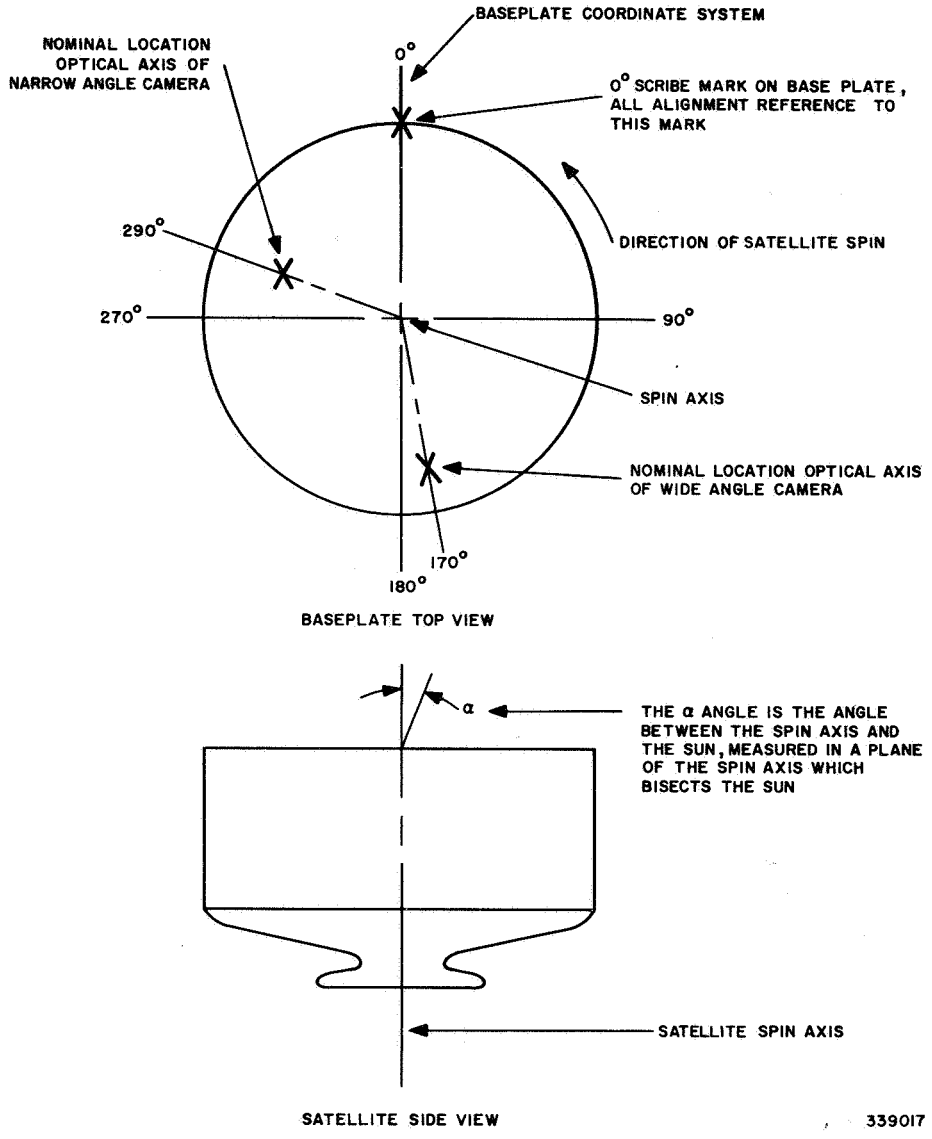

Figure 61. Satellite Coordinates

its axis in two seconds.) The system will meet this requirement at spin rates as low as 7 rpm.

3. Sensor Field-of-View Parameters. The sensor system must: (1) provide a measuring accuracy, in the plane of the baseplate, of ± 0.25° and (2), accommodate α angles of from 30 to 90 degrees. To meet the sensitivity requirement, the sensitive axis (Figure 62) of each sensor must lie along the appropriate radial line (20°, 60°, 100°, etc.) and the sensor must be so designed that it triggers when its sensitive axis passes through the center of the sun. Note that the sun subtends an angle of 0.5° when viewed from earth or from a low-altitude orbit; therefore, at a vehicle spin rate of 12 rpm, approximately 4 milliseconds will be required for the sensors sensitive axis to sweep from one edge of the sun to its center.

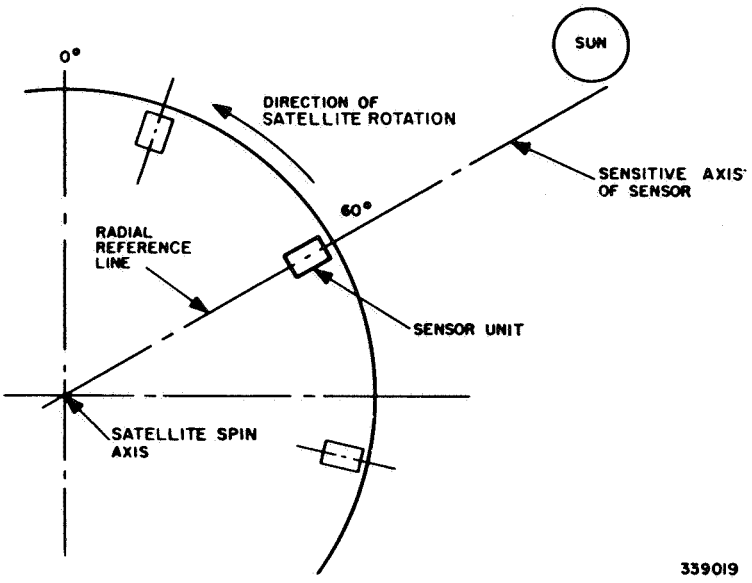

Figure 62. Sensor Alignment Requirements

To meet the α angle range requirement, the vertical field of view of the sensor units must extend from an elevation angle of 0° to +60°; this elevation angle range corresponds to an α angle range of from 90 to 30 degrees respectively. (See Figure 63.)

(b) Development of Subsystem

1. Sensor Optical Mechanical Design. To facilitate studies of the response characteristics of standard 1 x 2 cm solar cells, when the surface is swept by a narrow band of sun rays, a test housing, as shown in Figure 64, was constructed. This test housing was installed on an equatorial mount and rotated in the sun at rates that simulated light-band sweep rates which would be encountered by the sensors when mounted in a vehicle spinning within the acceptable spin-rate range.

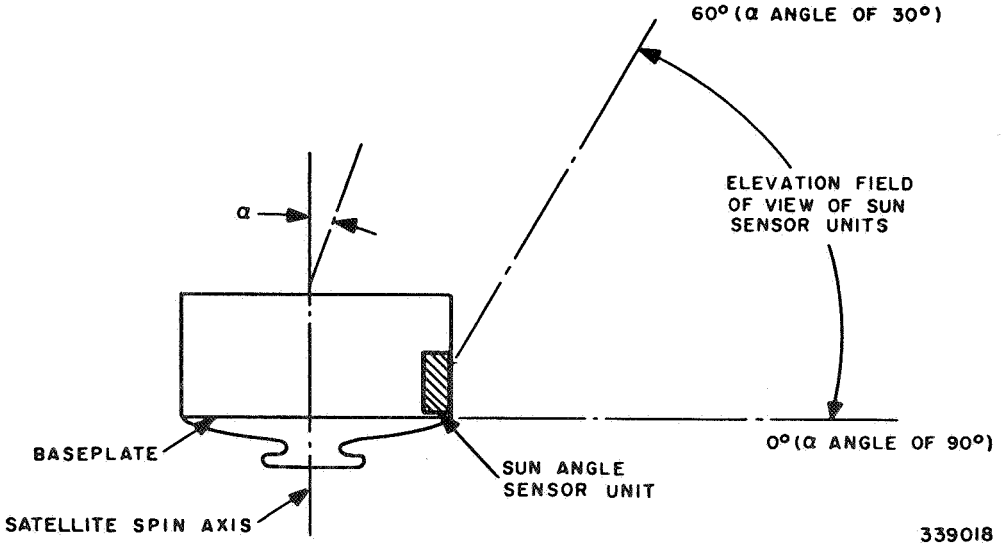

Figure 63. Sun-Angle Sensor Orientation

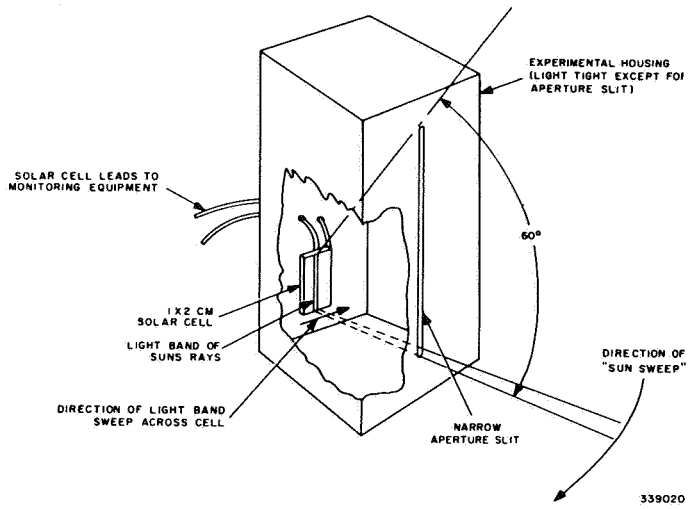

Figure 64. Experimental Sun-Sensor Unit

Note that the slit aperture on the outer surface of the housing is of sufficient height to permit complete vertical illumination of the solar cell when the "sun-ray" angle varies over a 60° range. This variation corresponds to an α angle of from 30° to 90°. During these studies a number of test-parameter variations were investigated, and their effects on the cell outputs were observed. These variations included: (1) α angle, (2) aperture to cell distance, (3) aperture width, and (4) effective cell width and height.

The results of these studies were closely coordinated with the development of the associated amplifier and pulse-forming circuitry to select the most advantageous match between cell output and the required circuit inputs.

From a study of the results of the described investigation with the test housing and a relatively rigorous analysis of the geometric relationships between such parameters as aperture slit width, effective cell width, etc., the physical design parameters were established. These basic parameters were as follows:

Aperture width: .025 inch

Aperture to cell distance (perpendicular distance from plane of slit aperture to cell surface): 1.500 inches

Effective cell width*

Narrow: .050 inch

Medium: .180 inch

Wide: .360 inch

*These three effective cell widths correspond to cell output-pulse widths of (1) 0.050 to 0.085 sec., (2) 0.120 to 0.175 sec., and (3) 0.205 to 0.290 sec. respectively. (Value of width in range depends on spin rate and α angle.)

To provide "coded" cells, standard 1 x 2 cm solar cells were modified as shown in Figure 65. The term "effective cell width" refers to that portion of the modified cell which generates the output pulse.

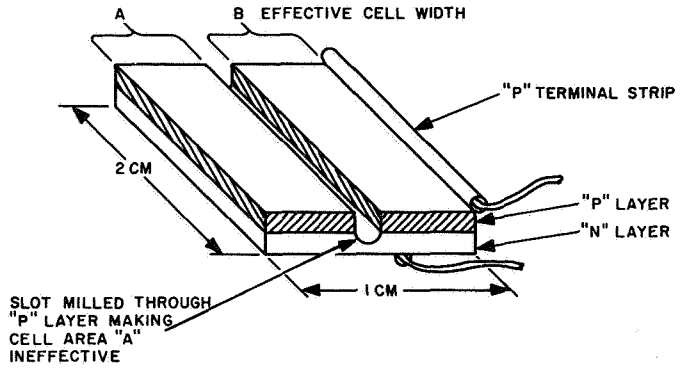

Figure 65. Modified (coded) Solar Cell

For purposes of discussion, the coding method which utilizes cells with three different effective widths will be termed the physical coding system.

To properly evaluate a complete sun-sensor system, a group of nine prototype sensor housings were fabricated. The configuration of these housings was essentially the same as the test housing shown in Figure 64 with the necessary refinements to facilitate accurate alignment of the aperture and cell within the housing and of the housing within the satellite structure. Figures 66 and 67 show exploded and cutaway views of the prototype housing. Note that the electronic circuit for each sensor is contained in the sensor housing.

2. Selection of Coding System. As described in Paragraph 4. a. (2) (c), two coding techniques were proposed; the physical method and the electronic method. From a mechanical design viewpoint, the two designs are essentially the same, except that with the physical method, the physical width of the cell determines the width (time interval) of the coded pulse and with the electronic method, the leading edge of the cell merely triggers the electronic circuit which determines the width (time interval) of the coded pulse.

The decision to employ an "electronic coding" system had little effect on the optical mechanical design of the sensor units. From an alignment standpoint, there was no significant difference between the two approaches, because in either case, only the alignment between the slit aperture and the leading edge of the cell was important. Because of scheduling requirements, the mechanical fabrication of the sensors preceded the decision to use the electronic coding method; therefore, the sensors were built with cells of different physical widths. For the final design, these different widths were of no significance because only the leading edge of each cell triggered the appropriate "one-shot". The only significant requirement imposed upon the mechanical design by the selection of the

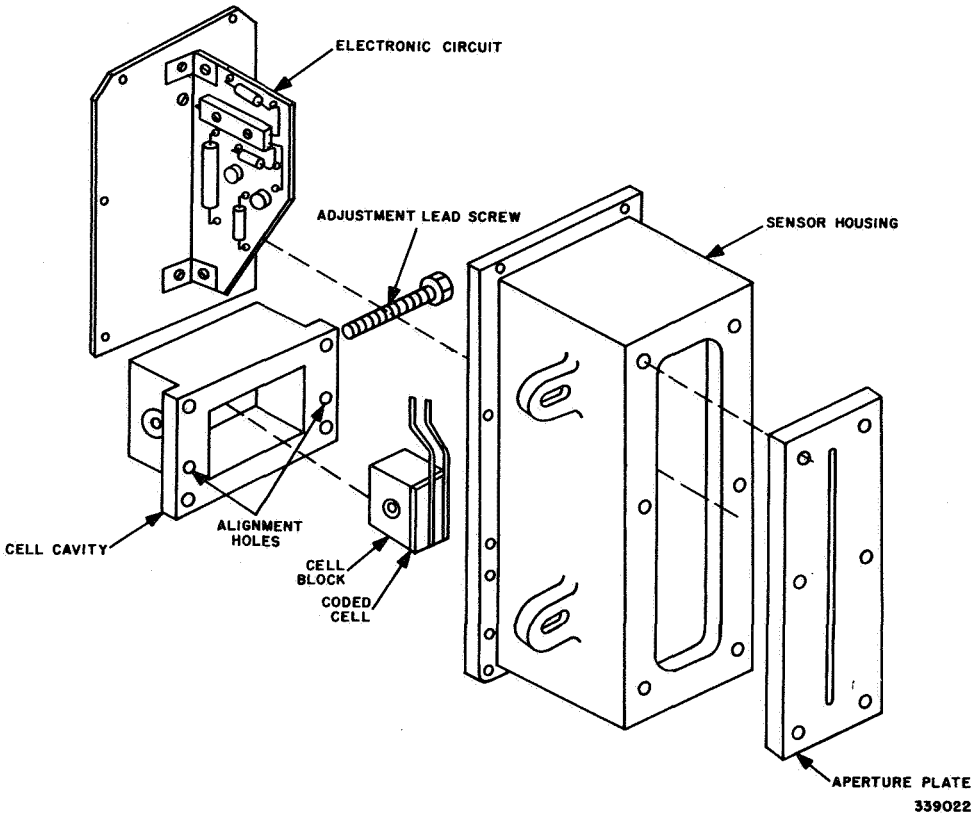

Figure 66. Sun Sensor Housing, Exploded View

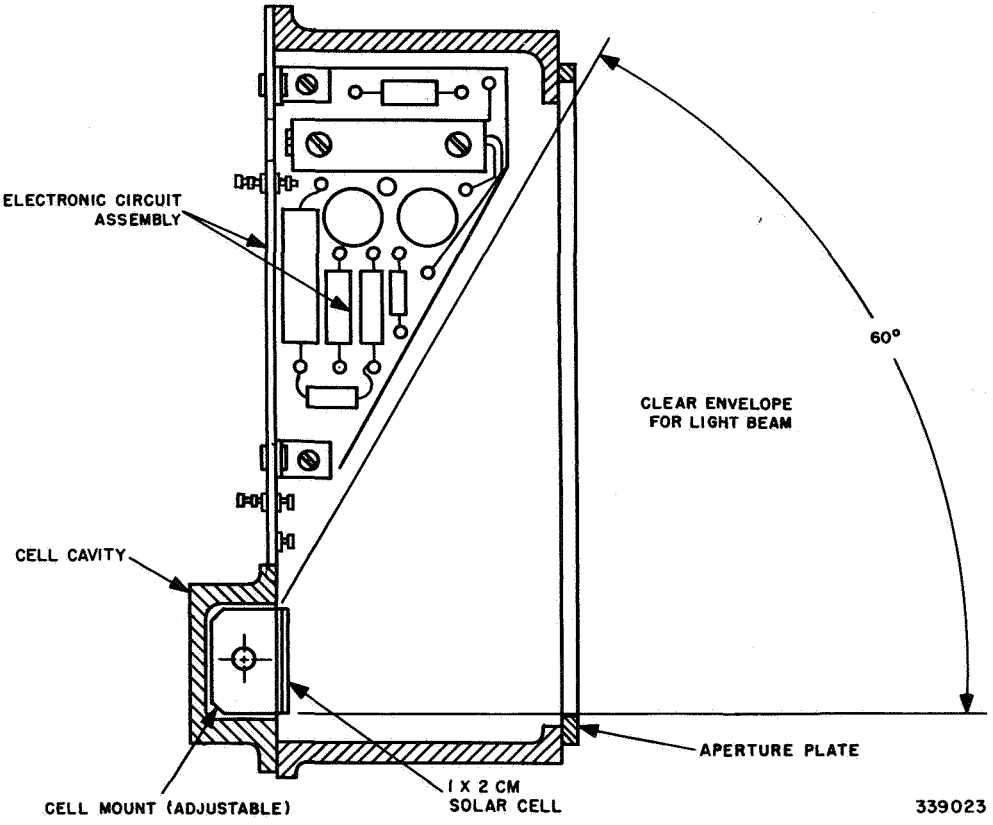

Figure 67. Sun Sensor Housing, Cutaway View

electronic coding system, was that of packaging the additional circuits. Figure 67 shows that each housing can accommodate a moderate amount of transistorized circuitry. The natural divisions of the required circuits (three preamplifiers, three one-shots, and a "summing" circuit) lent itself to physical divisions among six of the sensor housings.

(c) Alignment and Alignment Verification Tests

The first step in meeting the sun-sensor unit alignment requirements was to set up certain alignment parameters in the assembly of the mechanical components of the sensor, (i.e., the slit aperture, the cell cavity, and the cell itself). Some of the pertinent alignment requirements of the assembly (Figure 66) are as follows:

> The planes of the coded cell and the aperture must be parallel. (Non-parallelism will cause "keystoning" of the light beam which sweeps the cell and which would have an adverse effect on alignment.)
>
> The planes must remain parallel when the cell block is traversed across the cell cavity by the lead screw; therefore, high accuracy in lead-screw thread fit, relative parallelism, etc., is required. The cell to aperture distance was held close for the physical coding system although this became less important when the electronic coding system was adopted.

1. Sensor Housing Assembly, Pre-Alignment. Before the sensor units were installed in the satellite, the elements of each housing were pre-aligned. During this procedure, the unit was placed on an optical bench. It was positioned so that the center line through the two alignment holes in the cell cavity was horizontal, and the plane of the aperture plate was perpendicular to the line of sight of the alignment and collimating telescope. Next, the aperture plate was adjusted until the "triggering edge" of the slit was vertical and lay midway between the centers of the two alignment holes. Finally, the cell block was traversed by the lead screw until the leading edge of the cell was aligned with the triggering edge of the slit aperture. This procedure ensures that the sensitive axes of the sensor lay in a plane which was perpendicular to the front face of the aperture plate, midway between the center lines of the two alignment holes.

2. Sensor-Housing Assembly, Vehicle-Structure Alignment. The nine sun-sensor housings were mounted in the cover assembly of the satellite, and mechanical-assembly procedure was set up to ensure that the optical axes of the nine sun-sensor units were properly aligned in the cover assembly. A zero-reference mark was transferred from the baseplate to the cover. This mark was used to align a fixture which attached to the sensor housing at the cell-cavity alignment holes. The fixture was accurately positioned along the appropriate radial line by means of an indexing head mounted at the mechanical axis of the cover assembly.

3. Alignment Verification. As part of the final calibration of each satellite, the alignment of the nine sun-sensor units was verified. At the completion of the camera-alignment test, which is described in some detail in the Alignment and Calibration book for each satellite, the optical alignment of the "20°" sun-sensor unit was checked with respect to the zero-reference mark on the baseplate. This 20° sensor was then used as a reference in checking the alignment of the other eight sensors. A high-speed "paper-tape" recording of the nine sensor output pulses was made, and by measuring the relative spacing of the sequential pulses and translating this physical spacing into degrees of vehicle rotation, the accurate alignment of each sensor with respect to the 20° reference sensor was verified to be well within the specified tolerance of ± 0.25°.

4. Environmental Testing. The sun-sensor housings were subjected to the complete TIROS component-test program, including shock, vibration, acceleration, etc. There were no mechanical failures, loss of alignment, or degradation of performance in the units as a result of these tests.

b. Attitude Indicator

(1) General

The purpose of the satellite-borne portion of the attitude indicator is to supply data from which the satellite spin-axis attitude can be determined at the ground station. It basically consists of a horizon sensor and electronic circuitry to prepare the sensor output for transmission to earth, as shown in Figure 68. The horizon sensor, which contains an infrared detector, is mounted radially on the satellite. As the satellite spins,

339108

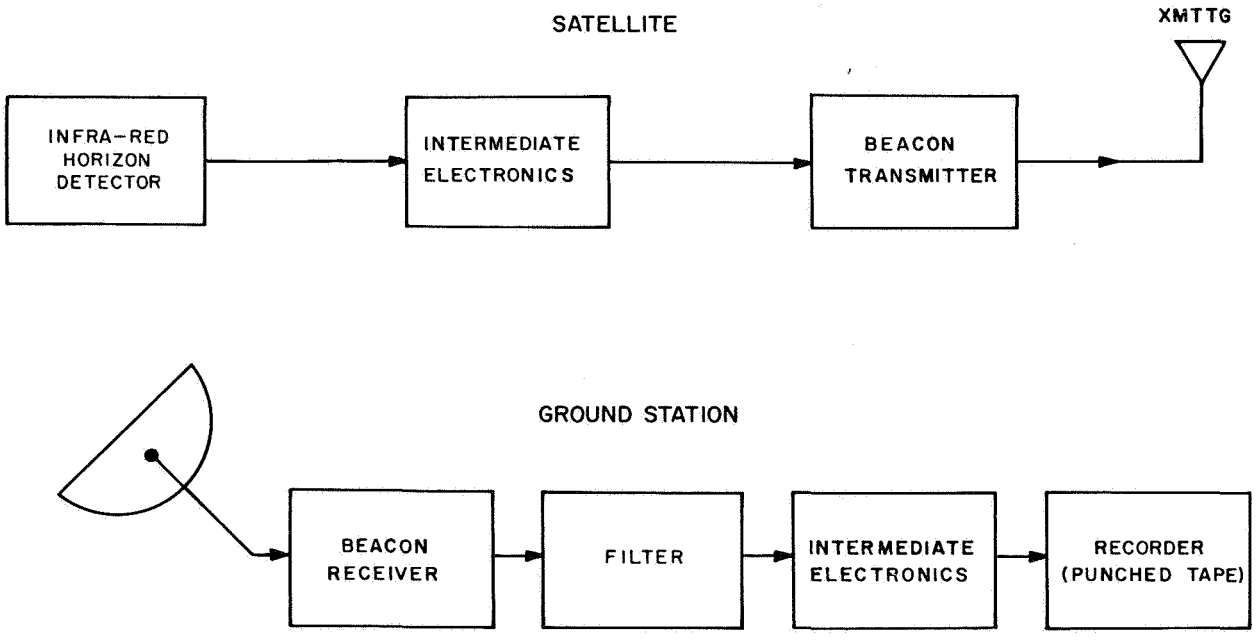

Figure 68. Attitude Indicator Data Chain, Block Diagram

the horizon scanner scans the earth and sky. As it sweeps the earth, the infrared sensor detects the infrared heat radiation and generates an output pulse, the width of which is equal to the earth scan duration. This pulse is applied to the horizon pulse shaper and processing electronics which provides, as modulation to the beacon transmitter, a 3-kc output "pulse", at those times corresponding to the leading and trailing edges pips of the earth-scan pulse. The beacon signal is received by the beacon receiver at the ground station and the "horizon" pips positive and negative pulses which correspond to the leading and trailing edges of the earth-scan pulse are separated from the beacon signal by a filter. The pips are shaped and amplified and applied to an Elapsed Time Counter and Scanner Unit which measures the intervals between the pips. The time interval measurement is then recorded on a punched paper teletype tape. This data, when eventually processed, provides the elevation angle (θ) of the satellite spin axis.

(2) Basic Requirements

The attitude indicator subsystem was basically required to detect deviations in the vehicle's attitude from that indicated by the orbital position of the vehicle and the assumed stability of its spin axis in space. This was to be accomplished by accurately determining the time period required for a radially-oriented infrared sensor to scan the earth's surface from horizon to horizon. (The detailed requirements of the attitude indicator subsystem are contained in the "Specifications for the RCA TIROS Exploratory Meteorological Satellite" dated July 1, 1959.)

(3) Development

Prior to early October 1958, the spin-axis of the TIROS satellite had been presumed fixed in space at some known orientation, which would be established at orbit injection and held relatively fixed thereafter. It was recognized that small external forces would act to precess the axis, but partly because of earlier planning, based on only a 14-day useful life, detailed consideration of the long-term effects of these forces had not been made. While investigating the effects of magnetic-field interaction on the spin rate, it was shown that magnetic forces would cause considerable precession of the spin axis. It was then apparent that, for adequate programming of picture-taking and for worthwhile analysis of both photographic and infrared data, some means of measuring and predicting satellite orientation must be incorporated. The earliest proposals included the use of the pictorial and infrared data themselves to determine orientation. Neither of these ideas was dropped, but because of reservations as to the speed (in the case of pictures) and the accuracy (in the case of infrared) of attitude determination by these methods, a supplementary system was considered desirable. Sun followers and gryoscopes were considered and discarded because of their complexity, power, and weight requirements. The method chosen was infrared horizon-scanning, which employed a narrow-field sensor and relatively wide-band data transmission in comparison to the functional (i.e., experiment-package) infrared detection system.

The scanner axis would be perpendicular to the spin-axis of the satellite, and provide attitude data by successive, independent determinations of the angle

subtended by the earth in the plane of the scanner motion. Each such determination in itself is a measurement of the quasi-instantaneous angle between the satellite's spin axis and the local vertical; this angle is defined as the "nadir" angle. Numerous independent determinations, over a period of time during which the axis is relatively stable, such as several orbits, theoretically permit determination, by least-squares fitting, of the actual or average spatial orientation of the body during the data interval. The time-lag deficiency, ascribed to attitude determination from the television pictures, was to be circumvented by automatic processing of the horizon-scanner data.

The attitude indicator system originally was to have been a relatively inexpensive and simple by-product of the shutter-timing control system for the side-looking camera, which later was discarded. In it, two infrared sensors were to have been employed: one sensor was to be used to measure the current value of the angle subtended by the earth and to provide system reset and warmup and tape-recorder start signals; the second sensor was to be used to actually trigger the camera shutter. Originally these sensors were to be employed for attitude determination by using the amplified shaped output from either one to directly amplitude modulate the beacon transmitters. Ten-millisecond duration pulses were to have been generated at the beginning and end of each earth scan, in connection with the camera-control functions described above, and these pulses would have been used to partly or completely gate the 108-megacycle carriers off.

At this point, analysis was performed to establish the optimum characteristics of a sensor to accomplish both camera-control and attitude-determination objectives, and a brief error analysis was performed on the expected accuracy of attitude determination by this method. (Ref. 9 and 10)

The choice of sensor field was established primarily by the requirements of the camera-control function; a precision of ±two degrees had been specified as tolerable in the actuation of the side-looking shutter, and, in consideration of signal-to-noise ratio and horizon-height uncertainty, a one-degree field was selected. An infrared specialist concern, Barnes Engineering Co., was contacted for information about available sensors and optical systems, and the parameters were tentatively established as follows:

Sensor Type:	Thermistor flake
Size:	0.9 x 0.9 mm
Time Constant:	4 milliseconds
Optics:	2-inch focal length, f/2
Field:	1° x 1°
Signal (220°K) to Noise Ratio:	22.5 db

With these parameters (affected principally by field of view and slightly by time constant), the accuracy of measuring attitude by recording long sequences of

horizon-interval measurements was established somewhere between 4.5 and 11 degrees, for data gathered during one full orbit. Subjective estimates that this calculation was overly conservative, combined with the philosophy that this was only a supplementary method and that the attitude would not change to any great extent, caused acceptance of the principal system parameters in the above form. In addition, the requirement to store continuous data during each orbit was discarded on the basis that essentially independent data must be obtained, in any event and both could be gathered by a network of monitoring stations recording real-time data. No ready method of storing data for a full orbit was available nor was the complexity of providing one considered justified; it was also felt that continuously-radiated data was superior in the respect that each observation could easily be referenced to the absolute time of its occurrence.

The establishment of the feasibility of the method and the selection of the basic satellite implementation and parameters were followed by further refinements. The direct modulation of the beacon was discarded because of the possibility of: (1) confusing the signal fades or antenna nulls with data, (2) the interference to Minitrack tracking, and (3) the relatively poor transmission signal-to-noise properties. A system employing a 3-kilocycle subcarrier, gated on by the 10-millisecond pulses, to amplitude modulate the beacon transmitter was substituted for direct modulation. This permitted improvement of the signal-to-noise ratio by audio filtering, provided a unique identification of TIROS radiations, and permitted aural determination of spin rate on the launch trajectory. The choice of the 3-kc subcarrier frequency was dictated by Minitrack tracking requirements.

The next modification of the satellite-borne system detail specification was a change in pulse duration. There was a brief period during which the use of 5-millisecond pulses was considered, but laboratory tests on the first horizon-scanned units from Barnes Engineering showed that the dynamic response of the amplifier supplied produced significant ringing for a period of about 60 milliseconds after the initiation of a thermal step at the input. At this time, analysis showed that the shortest meaningful horizon-width pulse duration* was of the order of 250 milliseconds. It was then decided to circumvent the amplifier-response problem by generating pulses with a 100-millisecond duration. This was the pulse duration used.

The spectral response of the bolometer was desired to be flat at lengths of from 12 to 30 microns, with substantially no response at wavelengths of less than 12 microns. In the course of development, it was found that this response would be difficult to achieve, so relaxed specifications were granted to the vendor to save time and expense. The first official specification (RCA-AED Specification TIROS TPS-D-232.01, Jan. 28, 1959) called for a spectral response from 7 to 30 microns. A subsequent relaxation of specifications was granted to permit response at wavelengths from 1.8 to 30 microns. Each such modification in specifications was based on discussions with the vendor, in which assurance was given that the changes would have no effect on the ability to recognize horizon and discriminate against all other changes in thermal input which the sensor was expected to undergo.

* This is defined as the time for the scanner axis to pass from horizon to horizon at an attitude where, at the middle of the scan, the extreme of the sensor field would be tangent to the horizon.

The dynamic response of the amplifier was chosen on the basis of existing rules of decision which were developed in the vendor's experience in infrared detection. Direct reproduction of the thermal input in the electrical output and subsequent clipping and differentiation, to produce the leading- and trailing-edge horizon pulses, was the first desire. An optical chopper was proposed by the vendor, but discarded because of its weight, power, size, and potential unreliability in the space environment. D-c amplification was not practical because of the relatively large drift voltages in the bolometer circuit and in the first stage of the amplifier. Differentiation at the input to the preamplifier was accepted, on the premises that the spectral response would sharply attenuate all extraneous thermal changes in comparison to those generated by scanning from space to earth.

(4) Subsystem Design

A detailed block diagram of the satellite's attitude indicator subsystem is shown in Figure 69. The horizon-sensor unit is a standard Model 13-200 unit, manufactured by Barnes Engineering Company. (Refer to "Instruction Manual for Radially-Oriented Horizon Sensor" Barnes Engineering Company No. BEC 4408.) A filter unit, as shown in Figure 70, was added to the sensor to decouple stray r-f energy. Infrared radiation from the earth's surface is focused, by the lens, on the infrared thermistor detector. The thermistor produces an output-voltage pulse of a duration which is equal to the period of earth scan. This pulse is amplified and differentiated by the a-c amplifier in the horizon scanner and the resulting positive and negative (leading and trailing edge) pips are applied to the paraphase amplifier in the horizon-pulse shaper.

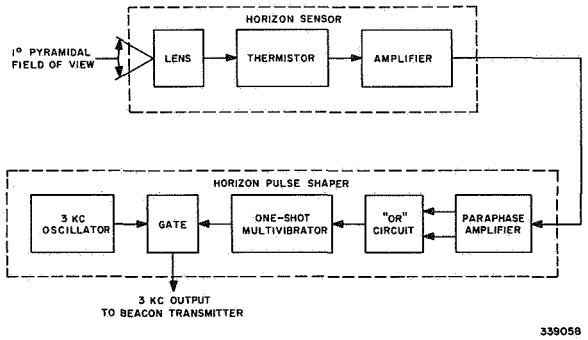

Figure 69. Horizon Scanner, Block Diagram

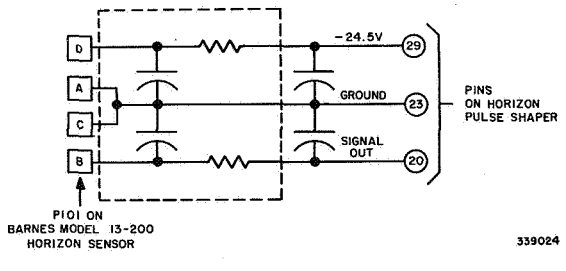

Figure 70. Horizon-Scanner Filter, Schematic Diagram

Differentiated signals from the horizon scanner, representing the transition from sky to earth or vice versa, having amplitudes of approximately 2 volts, rise times of approximately 25 milliseconds, overshoot of approximately 75%, and total duration of approximately 60 milliseconds are applied to the RCA - designed electronics at terminal 20 shown in Figure 71. A regulated voltage of -24.5 volts is applied to terminals 22 and 27. The signal and power-supply grounds are tied to pin 23.

Positive pips from the paraphase amplifier are combined in the OR circuit and applied as trigger signals to the one-shot multivibrator. The one-shot output signal controls the gate which applies a 3-kc burst signal, from the 3-kc oscillator, to the beacon transmitter modulator. These bursts correspond to the leading and trailing edges of the horizon-scanner earth-scan pulses.

The 3-kc oscillator is a 2-stage feedback amplifier with a control tone filter in the feedback loop as the frequency-determining element.

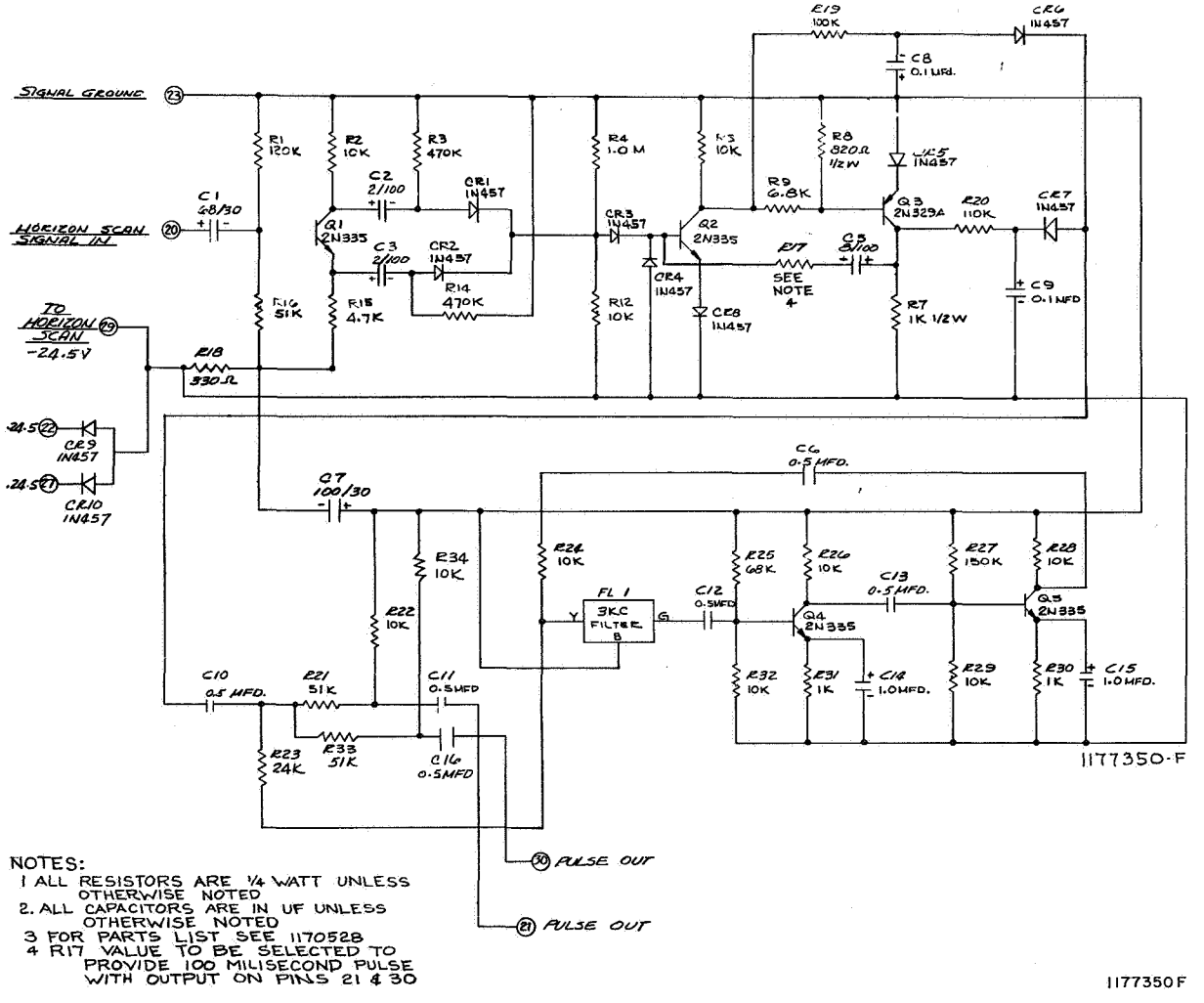

Figure 71. Horizon Pulse Shaper, Schematic Diagram

(5) Tests

Test experience on the sensor units was largely routine. Two of the six bolometers delivered became noisy and were replaced by the vendor. Significant trouble was encountered in the system tests because of r-f pickup in the power-input and signal output leads to the sensor package. The double pi-section, RC filter was incorporated externally, and no further trouble was encountered. Quantitative testing of the units was limited to verification that a 65-degree centigrade source against a room-temperature background produced satisfactory signal levels, and experimental determination of the field of view and optical-axis direction relative to the mounting surfaces. The field of view was found to be approximately 1.3 degrees between 3-db points, and the sensors axes were well within the ± 1/4-degree direction tolerance specified.

(a) Electrical Tests

The sensor output was required to be sufficient to trigger the horizon-pulse shaper with a heat input consisting of a temperature gradient of 15°C with room temperature (23°C) as the reference. The horizon-pulse shaper output was required to be essentially as shown in Figure 72, with a peak-to-peak amplitude between 100 and 150 mv, a nominal pulse width of 100 msec ±10%, and a frequency of 3000 cps ±7.5%.

1. Temperature Test - For the temperature test, as well as for all bench tests, the changing I-R input to the sensor was simulated by filling the field of view of the sensor with a black-body radiator (hot plate covered with a deposit of lamp black) and chopping the infra-red energy with a rotating chopping blade. The linear speed of the leading and trailing edges of the chopping blade and the distance between the plane of the blade and the plane of the thermistor detector were adjusted so that the field of view of the sensor was exposed to and cut off from the heat source at the same rate as the sensor would sweep on-to and off the earth, with the satellite rotating at 10 rpm. The chopping blade was at room temperature (23°C) and the temperature of the black body was maintained at 15°C above this so that the chopping blade simulated space and the radiator simulated earth.

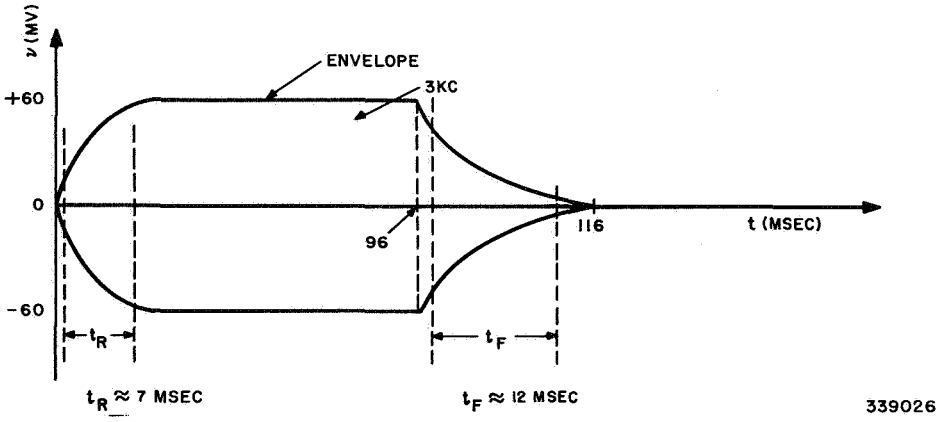

Figure 72. Nominal Characteristics of Horizon-Pulse Shaper Output Pulse

The sensor and horizon-pulse shaper combination was mounted in a Tenney temperature chamber so that the sensor "looked" out through an opening in the side of the chamber at the chopped heat source.

All units passed this test without failure. Proper circuit operation was obtained over the temperature range from -10°C to +60°C. All sensors gave approximately the nominal ±5-v output at +25°C. In general, this output decreased as the ambient (operating) temperature of the sensors changed (both positively and negatively) from this midpoint, but it was always sufficient to trigger the horizon-pulse shaper.

The overshoot on the outputs of two sensors (serial numbers 104 and 105) increased with increasing operating temperature. This was caused by increased loading by the horizon-pulse shapers, to which these particular sensors were more vulnerable.

2. Thermal-Vacuum Test - For the thermal-vacuum test, the sensor and horizon-pulse-shaper combination was mounted in a glass bell jar vacuum chamber. The pressure was maintained at 5×10^{-5} mm Hg, and the ambient temperature was cycled between -10°C and +55°C three times; the circuit operation was monitored at -10°, +25°, and +55°C.

The heat-gradient input was supplied by hand chopping infrared energy which was driven through the bell jar. The proper heat gradient and sweep speed could not be reasonably simulated with this setup, but the circuits had been tested under these actual conditions in the bench and temperature tests. Although a few of the units initially failed this test, all units passed when faulty components were replaced.

3. Baking Test - The setup for the baking test was the same as that for the temperature test. The sensor and horizon-pulse-shaper combinations were baked at +80°C for six hours, after which circuit operation was monitored at a reduced temperature of +50°C. All finished units passed this test.

(b) Mechanical Tests

The RCA Environmental Test Specification TSP-T1-100B, upon which these tests were based, is included in Appendix C. The sensors and horizon-pulse shapers were subjected to the vibration, acceleration, and shock tests individually and in the non-operating condition because they had separate housings. After these mechanical tests, the units were tested electrically. All finished units passed these tests, after some initial failures.

(c) Component Failures and Description

1. Failures

a. Horizon-Pulse Shaper - The only failure was in the "spare" unit. During the thermal-vacuum test this unit "locked on" after being triggered by its sensor. This was caused by a defective timing capacitor (C5) in the one-shot multivibrator. The circuit operated correctly after C5 was replaced.

b. I-R Sensor - The D3 sensor (Serial No. 101) because microphonic and gave an unusually noisy output after the mechanical and thermal-vacuum tests. It was returned to the manufacturer where it was found to have a defective capacitor in its amplifier, and was repaired accordingly.

The "spare" sensor (Serial No. 106) first became noisy during the thermal-vacuum test. It was returned to the manufacturer, where its defective bolometer was replaced. After having been repaired, the unit became microphonic after being put through the mechanical tests. This second failure was caused by a defective capacitor as in the D3 unit. This sensor was again repaired by the manufacturer.

2. Final Unit Assignments and Failure Description - The following table lists the final assignments of the I-R Sensors. Five were installed in satellites; a sixth set was built as a spare.

Final Assignment of I-R Sensors	
Sensor Serial Number	Vehicle Designation
101	D3 (The orbiting TIROS I)
102	D1
103	T1
104	T2
105	D2
106	S

The I-R Sensor (Serial No. 102) when first delivered, gave only half the output of the other sensors (±2.5 v compared to ±5 v). Also, the output of this sensor was reversed; that is, a positive pulse was obtained from a negative heat gradient and a negative pulse was obtained from a positive heat gradient. Both of these difficulties were caused by a reversal of the bolometer connections to the amplifier.

The I-R Sensor (Serial No. 103) was slightly noisy. However, the noise in the output never produced a deterioration of the circuit (sensor and horizon-pulse shaper) performance. Therefore, although the signal-to-noise ratio was slightly below that required, this sensor was never repaired.

At one point in the development of the horizon scanner, an attempt was made to shorten the output pulse width of the 3-kc tone bursts from 100 milliseconds to 10 milliseconds. It was found that the minimum attainable pulse width was 50 milliseconds because the sensor output consisted of a positive (or negative) pulse with an overshoot; the time between the pulse and the overshoot is slightly less than 50 milliseconds. If the one-shot multivibrator on time was made less than 50 milliseconds, both the pulse and its overshoot trigger the one-shot multivibrator, so that two horizon-pulse shaper output pulses were obtained for one heat pulse.

As the sensor sweeps increasingly high temperature differences, its output saturates the amplifier, and the pulse amplitude is limited. However, the overshoot also increases, and approaches the true-pulse amplitude. This condition could result in double horizon-pulse-shaper output pulses. (After the launching of TIROS I, it was learned that the heat gradient from space to earth is equivalent to that between a black body at room temperature (23°C) and a black body at approximately 40°C, rather than at 15°C above room temperature.)

Finally, one other problem was encountered when the horizon scanners were integrated with the satellites. Radio-frequency electromagnetic energy radiated by the TV transmitters was coupled into the sensor amplifier (through the supply and signal leads) even though the electronics were shielded in the sensor housing. This effect was eliminated by placing a specially-shielded RC filter in both the supply and signal leads.

(6) Evaluation

The operation of the horizon-scanner attitude indicator subsystem was not completely successful in the TIROS I satellite. The spin rate determinations were the only useful operational data derived from the subsystem. Several deficiencies prevented utilization of the data for operational attitude determination. The principal source of the difficulty was the improper spectral response of the sensor. If sensor response had been proper, it is reasonable to believe that the system would have worked adequately, although the subjective conclusion that accuracy of considerably better than ± 4.5 degrees was realizable might not have been justified.

The sequence of adversities which resulted from the improper bolometer spectral response is as follows:

1. Transitions from cold cloud to warm earth as seen through the 8 to 12-micron atmospheric window produced electrical signals sufficiently strong to trigger the one-shot multivibrator in the satellite.

2. The computer was not programmed to handle earth intervals consisting of the sum of several shorter intervals; this condition was frequently encountered.

3. The 250-millisecond total recovery time of the one-shot multivibrator in the satellite prevented recognition of the earth-sky transition whenever a strong spurious signal was received close to the horizon.

4. Occasionally, the deluge of spurious pulses caused the counters in the Elapsed Time Counter-Scanner not to be ready to count; (i.e., one counter was still being read out after two subsequent pulses were received).

The effect of these adversities was that perhaps 40 percent of the data points were good, another 20 percent were good if the computer had been programmed generally enough to handle them, and 40 percent were essentially useless, at least where direct determinations of nadir angle were concerned.

There was another significant deficiency in the satellite operation; the reduction in slope of the thermal input pulse to the bolometer, at oblique incidence angles, reduced the amplitude of the differentiated output pulse to the point where no consistent triggering occurred for horizon widths of less than 100 degrees. In the analysis of this phase of the system, it appeared that triggering was sometimes caused by the overshoot following the true pulse rather than by the desired pulse itself, before reaching the point where no triggering occurred at all.

The performance evaluation, which resulted in the above conclusions, had two objectives; one was to permit correction of the system deficiencies for later satellites, and the second, and more urgent at the time, was to exhaust all possibilities of getting useful data from the satellite in flight.

The first objective has been met, and the results will be described later in reports on TIROS II. The second objective was not met in time to use the data for operational attitude determination.

A discussion of the evaluation program is given in the report "Evaluation of the Operational Performance of the TIROS I Satellite."

5. Electrical Power Supply Subsystem

a. General

Electrical power for all of the satellite's requirements was generated by a solar-energy converter, which consisted basically of an array of 9120 silicon solar cells, mounted on the top and sides of the satellite structure. Since the angle of illumination of the cells varied, and the satellite was in the shadow of the earth during part of its orbit, a secondary power supply consisting of 63 nickel-cadmium storage batteries was included in the subsystem, to maintain a continuity of power supply. The storage batteries had a total capacity of approximately 275 watt-hours. The solar-cell array and storage batteries were connected in such a manner that the batteries were charged when the solar cells were active, and excess solar-cell output was used to power the electrical load directly. Precautions were taken to prevent internal circulating currents through the power-source interconnections, and to preclude the total loss of power in the event that a short circuit occurred in one of the cells or batteries. A functional block diagram of the electrical power supply is shown in Figure 73.

The storage batteries were electrically connected in three independent groups, each of which was connected to the solar-cell supply through its own current regulator, which prevented an excessive rate of charge. The excess power was diverted through a by-pass regulator to the main battery-output bus. During the orbital night, when the solar cells were passive, silicon diodes in each series row of solar cells prevented the storage batteries from discharging into the solar cells. Another similar function was played by diodes in each series row of solar cells located on the lateral surface of the satellite. Because the satellite spins about its figure axis, each series row of solar cells on a lateral surface is alternately illuminated and then darkened. The silicon diodes also prevented the darkened solar-cell rows from loading the illuminated rows.

The storage batteries provided a relatively constant voltage across the solar cells, thereby, isolating them from variations in the electrical load. The storage batteries were charged by the solar cells during the orbital day and supplied all equipment loads during orbital night. In addition, during the orbital day, the batteries supplied the difference between peak power requirements and the solar-cell output by the amount that the solar-cell capacity was exceeded by equipment power demands.

b. Development of Subsystem Concepts

The first power supply specification for what ultimately became the TIROS I satellite was written January 1958. The average power required by the system loads was just five watts and the satellite was to carry one television camera and be cylindrically shaped. The power supply consisted of silicon solar cells and nickel-cadmium storage batteries. The solar cells covered approximately 15 inches of the cylinder length. One row of storage batteries, with a nominal four ampere-hour capacity, was to supply peak loads in excess of solar-cell output during daylight and for all nighttime loads.

During 1958, a number of significant changes occurred in the satellite system. Of primary importance was the increase in the number of television cameras to three and

the change of the satellite configuration to the drum or disc shape. The increased number of camera systems and complexity of equipment was accompanied by a significant increase in power requirements. The number of solar cells required increased by several thousand and three parallel rows of batteries were required.

In early 1959, the number of camera systems (and associated equipment) was reduced by one, leaving a two-camera system. The total average power required decreased by significantly less than one-third, however, because many of the power drains were continuous and independent of a specific camera system.

It was decided to have no unfolding, latching or extending mechanisms on this early-generation satellite. This meant that the solar-cell power supply had to be part of the

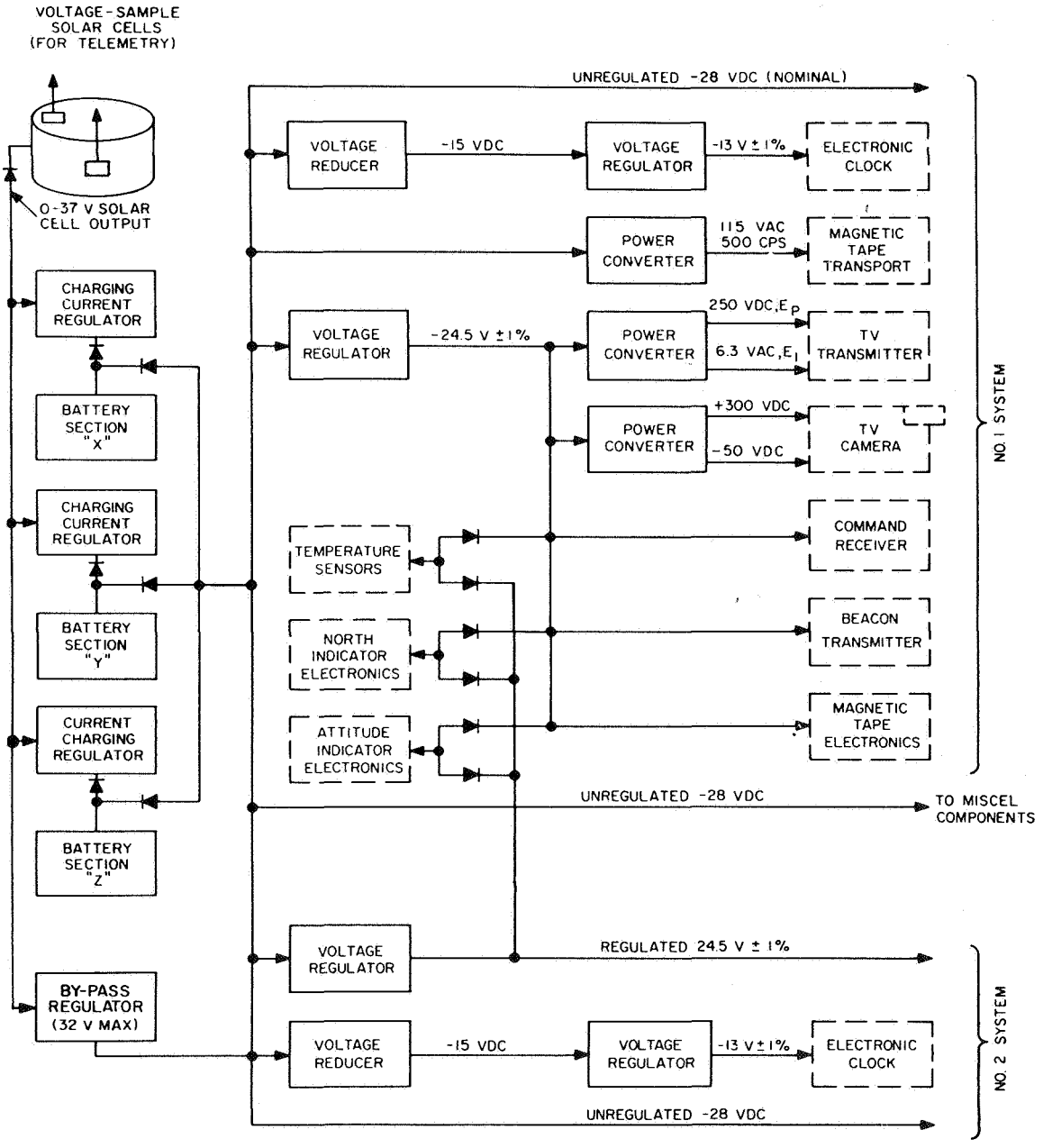

Figure 73. Power Supply Subsystem, Block Diagram

fixed skin which covered the satellite instrumentation. It was also decided that the satellite should be cylindrical in shape and spin-stabilized, with a disc-shaped mass distribution so that it could continue to spin about its figure axis. Furthermore, all thermal control was to be passive and was to be achieved in the design by the selection of proper materials to obtain optimum thermal characteristics for the fixed outer surface, and by the thermal inertia and coupling of the overall system.

As the system concept became more involved and additional power-consuming equipments were added, it became evident that the maximum envelope allowable by the launching rocket would determine the total solar-cell power capability. The design of the power supply was complicated by the fact that the output power of a tight-fitting solar-cell collector is a function of area, while equipment power requirements are roughly a function of volume. As equipments were added, the collector surface began to enclose a progressively greater volume than that of the equipment it was to power. The total satellite equipment power requirements had increased until the solar collector required an area which enclosed all the volume that the nose shroud of the launching vehicle would allow.

An early decision on the TIROS I operational regime fortunately lifted the restraints on the addition of power-consuming hardware. This decision allowed for a portion of the equipments, such as cameras and tape recorders, to be programmed from the ground for immediate or delayed execution of command. It also allowed for variable durations, making it possible to obtain an infinite number of power-versus-time profiles, thus permitting the power supply output to vary considerably. The result of these conditions was to place restrictions on the duty cycle of the instrumentation rather than on the functions it performed.

The general location of the solar cells on the housing "top hat" was determined by the optimum position of the satellite for picture-taking. (The cameras can take good pictures only when the sun is behind them, when they are pointed toward the earth.) With both camera axes parallel to the spin axis and both pointing in the same direction, the solar cells should cover the flat, top surface of the cylinder behind the cameras. Since the sun's rays can be considerably off-parallel with the camera axes for good earth pictures, it became necessary to cover the lateral surface of the cylinder with solar cells, in order to maintain a less-fluctuating projected area. There was no need to cover the bottom surface with solar cells, because if the bottom surface were illuminated, the sun would be looking into the cameras, rendering them temporarily inoperative.

In the earlier forms of the satellite, a single row of storage cells was employed. Initial specifications for the power supply spelled out a regulated supply voltage of 24 volts. When the number of TV cameras increased to three, three rows of storage batteries, with each row containing 20 series-connected storage cells, became necessary. These three rows provided a nominal full-voltage of 26 volts and were paralleled at a point 11 storage cells above ground in order to provide a nominal 13-volt supply. During this phase of the program, the voltage-regulation requirement was dropped; and it was anticipated that the unregulated supply voltage would be 26 ± 1.5 volts.

Because the solar cells covered a great proportion of the top and sides of the "hat" which faced the sun, their thermal surface properties (solar absorptivity and infrared

emissivity) heavily influenced the mean temperature of the components within the satellite. Thermal analysis determined a required value of α/ϵ ratio of around 1.0, with an ϵ of 0.85. Three parallel development programs were started to develop coatings for the solar cells, (whose "bare" α/ϵ ratio is between 2 and 3) to bring the emissivity from around 0.3 up and equal to their absorptivity of 0.9. Transparent plastics, vacuum-deposited inorganics, and bonded transparent covers were all investigated. The organic plastics alone were dropped for radiation and vacuum-sensitivity reasons. A development program with a leading optical firm had not yielded either sufficient sensitive-region transparency or high enough emissivity in time for the decision on coating materials. The result was the selection of a bonded "Micro-sheet" glass-platelet coating, using a vacuum-deposited blue-reflector coating on the glass to protect the transparent epoxy adhesive from darkening when exposed to ultra-violet and near ultra-violet light; also, an anti-reflective coating was used to maximize solar transmission at the cell's peak response wavelength of 0.8 micron. Some time after this coating had been selected, the vacuum-deposition program yielded a direct coating of SiO_2 -Si_2O_3 on the solar cells, which dropped the electrical output power of the solar cels no more than 3%, while raising the emissivity to 0.8-to-0.85. The blue reflector coating has the advantage (over the direct emissivity coatings) of permitting some variation in net absorptivity, with the fixed emissivity of the glass. On the other hand, the direct-emissivity coating permits a variable value of ϵ as a function of thickness, and as recently disclosed, can be augmented with a multilayer blue reflector which gives the flexibility of varying both α and ϵ, and permits dark-side as well as illuminated-side thermal control.

The simplified schematic diagram in Figure 74 shows the power supply at this stage of development (1958). Two solar-cell power supplies were provided. One provided charging energy for the full assembly of storage batteries and restored to the batteries all energy discharged at the nominal 26-volt level. However, energy was additionally discharged at the 13-volt level, so that the 11 storage cells comprising this 13-volt supply required a solar-charging input which replenished the energy discharged at that voltage level.

In early 1959, when the TIROS system became a two-camera system, sufficient storage-battery testing had taken place to demonstrate the need for voltage regulators. Thus, 24.5-volt and 13.0-volt regulation circuits were incorporated. Because these

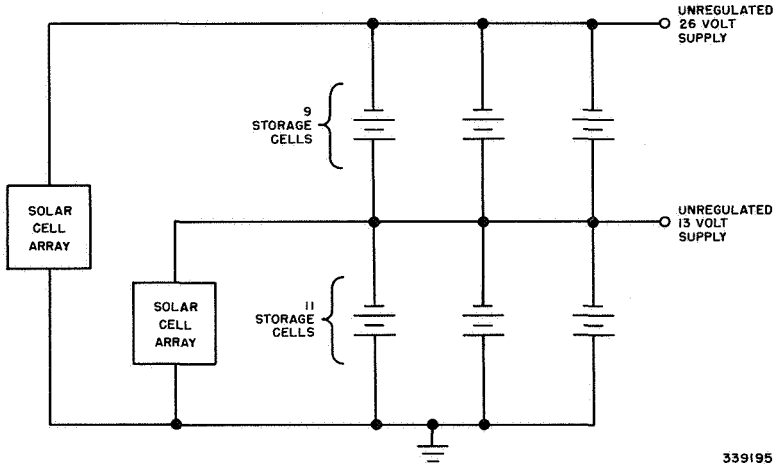

Figure 74. Early Power Supply Circuit, Simplified, Schematic Diagram

regulators required about 1.0 volt to operate, the minimum battery supply voltage could be no less than 25.5 volts at full load. It became necessary to add one storage cell in each row of batteries to achieve this required voltage level. The center-tap position for the 13.0-volt regulator remained unchanged because an excess of voltage already existed at this point. The power-supply configuration then remained essentially unchanged until early 1960 when a major shortcoming of the storage cells themselves (described in the section on storage batteries) required that modifications be made.

The diagram in Figure 75 shows the power-supply circuit before the changes were made. It can be seen that the only charge current to the upper 10 storage cells was that which was contributed by only one solar array, but the total current to the remaining 11 cells was the sum of the outputs of the two arrays. Approximately 100 to 150 milliamperes per row was the calculated additional current in the 11-volt supply storage batteries in actual orbit conditions.

As described in the section on the storage-battery test program, an exhaustive test program and the system-performance requirements put a maximum required limit of 440 milliamperes charging current for each row of batteries. A transistorized charge-current limiter was necessary to ensure that this limit would not be exceeded. Thus, as shown in Figure 75, the 11-volt battery would be the limiting factor, from the standpoint of maximum acceptable charge rate, because of the excess charging current that it carried. This limitation placed a serious restriction on the total energy which could be withdrawn by the system loads at the 26-volt level, because of the essentially lower recharge-current rate which would be in effect at this voltage level. It was decided, therefore, to eliminate the 13-volt tap on the battery and substitute a transistorized circuit to drop the full battery voltage to a 15 or 17-volt level to provide the proper input to the 13.0 volt regulator. No change was made to the 24.5-volt regulator input. A disadvantage of supplying the 13.0-volt energy requirements at the full voltage level was that about 50% of the power so supplied was dissipated as heat in the voltage dropping circuit. However, this was balanced by the fact that only three current limiters, rather than six, were required; this minimized the added weight and power which would have been required to provide a current limiting function.

The overall power supply functional block diagram is shown in Figure 76. One solar array, which was a rewired combination of the two arrays which had been formerly provided, provided energy to the three rows of batteries. A charge-current limiting circuit, which limited at a level of 440 milliamperes, was provided for each row of batteries. The

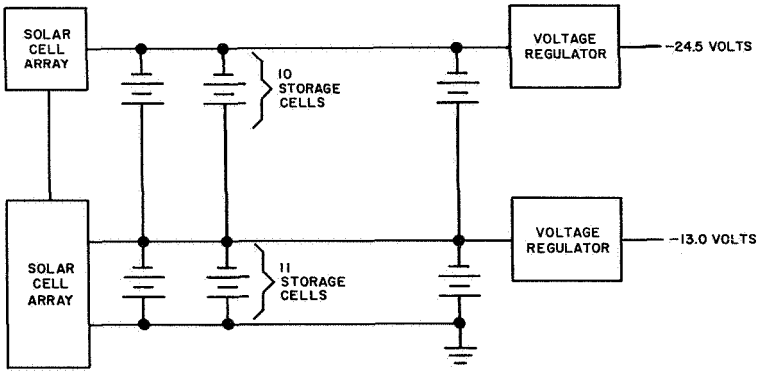

Figure 75. Power Supply Circuit of Early 1960

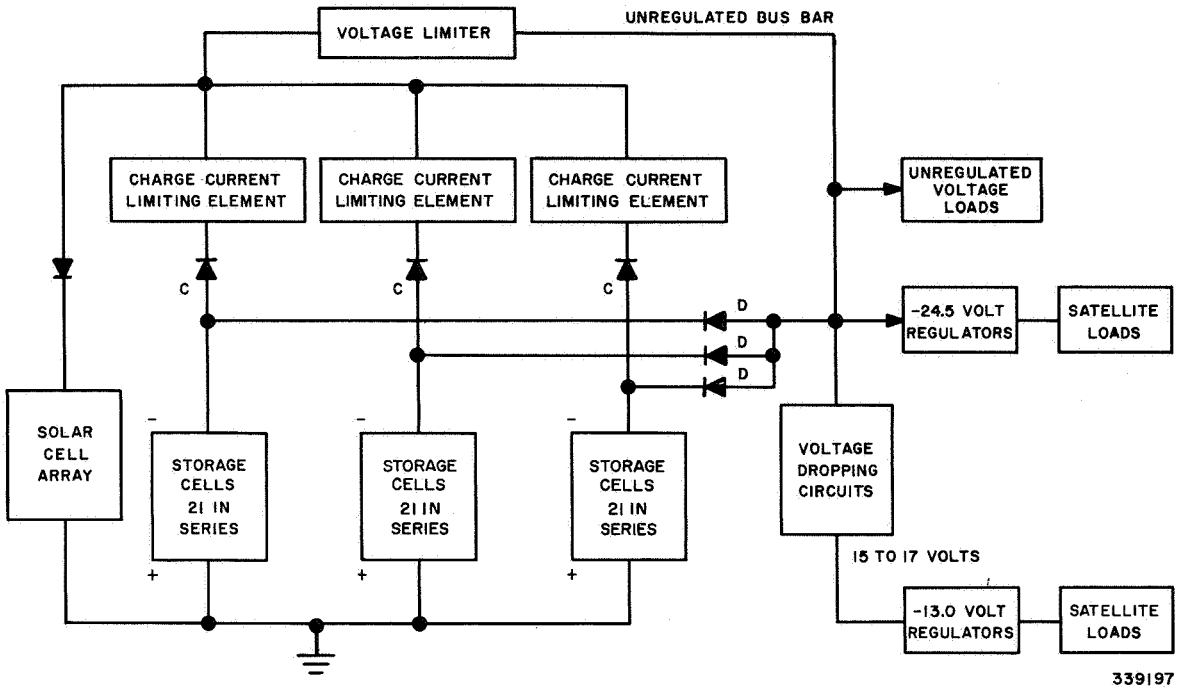

Figure 76. Power Supply, Functional Block Diagram

diodes labeled C and D prevented a shorted row of storage cells from loading the remaining row or rows which had developed no failures. In the event open circuits or high impedances developed in one row, that row was automatically isolated from the other row.

The voltage-limiting circuit prevented the voltage at the unregulated bus bar from exceeding 32 volts.

Not shown in Figure 76 are the circuits for telemetering the battery voltage on each row and the voltage on the unregulated bus bar. In each of these telemetry-sensing circuits, 22-volt Zener diodes compress the voltage scale so that only voltages between 22 and 32 volts are telemetered. This voltage range is sufficient to observe normal operation and detect abnormal conditions when they arise.

c. Power-Source Specifications

(1) Solar Cells

(a) Basic Solar Cell and Five-Cell Shingle

The solar cells used were manufactured by the International Rectifier Corporation. They are 1 x 2 centimeter boron-doped silicon cells, assembled in a

shingle form. Each shingle comprised five of these individual cells in series. A minimum conversion efficiency of 7.5% at a voltage of 1.95 volts ± 5% in voltage at a temperature of 30°C ± 3°C was specified for the basic shingle. Each individual cell of the 5-cell group has a transparent coating bonded to it which greatly improves the thermal emissivity. This permits radiative self-cooling in the spectral region corresponding to the desired cell temperature. The coating consists of a platelet of "microsheet" glass 0.006 inch thick, which is coated with an optical, vacuum-deposited coating. The upper, or outer surface, has an anti-reflective coating which permits the maximum transmission of light in the 800-millimicron range, where the solar cells are most responsive. The inner, or lower surface, has a 15-layer, sharp-cutoff reflector coating which reflects and absorbs all light of wavelengths shorter than 450 millimicrons, and transmits 90 to 95% of the light at wavelengths longer than 450 millimicrons and beyond the solar cells upper response limit of 1100 millimicrons. The platelets are bonded to the individual cells with a transparent epoxy adhesive.

(b) Module Specifications

A module is a flat, epoxy-fiberglass board*, used as the basic building block to simplify the handling and assembly techniques. The size of each module was 3.400 inches by 7.572 inches by 0.036 inch thick. Each module weight approximately 80 grams with the solar cells mounted.**

The module boards are paralleled in clusters of four (i.e., they are electrically connected to one another at the ground), with the one-quarter, one-half, three-quarter, and full-voltage points, respectively, corresponding to 20, 40, 60, and 80 cells in series. This method of interconnection tends to minimize the loss of solar-converter output in the event of failure resulting from open or short circuits in one shingle.

On the top surface of the cylinder, the modules are bonded directly to the satellite skin in electrical groups of four. The lateral area of the satellite was modified from a continuous curved surface to eighteen flat panels to enable simpler mounting of the modules. Four module boards were epoxy-bonded to each aluminum panel; these panels were then bolted to the aluminum vehicle frame.

(c) Array Size

The physical characteristics of the solar-cell array are as follows:

Location	No. of Solar Cells	Active Area (Sq. Ft.)
Top	3560	6.90
Side	5560	10.8
TOTAL	9120	17.7

* MIL-P-18177A.

**For the operating temperature predicted and the load voltage required, 80 series-connected cells (i.e., 16 shingles) were mounted on each module.

The solar collector includes solar cells, with bonded-glass covers, adhesives, standoffs, diodes, wiring, and module boards, but excludes the aluminum surface which was part of the structure. Its weight is 24.5 pounds.

(d) Array Output Power

The instantaneous power output of the solar collector is a function of the alpha angle.* As the alpha angle changes, the total silicon area projected normal to the sun changes; therefore, the solar-cell temperature also changes. As alpha increases, the top area projected normal to the sun decreases, but the average solar-cell temperature also decreases. Simultaneously, the side area projected normal to the sun increases as does its average operating temperature. The combined effect of these area and temperature changes is shown in the following table in terms of the power output of the solar collector corresponding to the average operating temperatures at each value of alpha.

The average power output of the solar collector was obtained by multiplying the instantaneous power output by the ratio of illuminated time to the duration of orbital period (percent sun time). This ratio has a minimum value of 0.65. The average power to the load was approximately 0.68 of the average output of the solar collector, because of losses which occurred in the energy-storage system, voltage regulators, and current limiters.

Alpha Angle	Instantaneous Power In Watts	Average Collector-Power Output In Watts	Remarks
0	34	22	Side solar cells not illuminated.
10	38	25	
20	43	28	
30	47	31	
40	50	33	
45	51+	33+	Maximum collector output.
50	51+	33	
60	48	31	
70	42	27	
80	33	22	
90	27	18	Top solar cells not illuminated.

*The alpha angle (also known as gamma angle) is that measured between the sun vector and the satellite spin axis.

(e) Telemetered Parameters

The output voltage of each of two groups of solar cells, electrically isolated from the solar-cell power supply and each other, but operating into accurately-known resistance loads, was telemetered. The temperatures of the cell groups also were telemetered. The temperature sensors were actually mounted on the satellite skin, behind each of the solar-cell groups.

(2) Storage Cells

The characteristics of the individual storage cells and battery are as follows:

(a) Characteristics

1. Type of cell: Sintered plate glass-to-metal seal; hermetically sealed nickel-cadmium storage cell, F-size, with paper separators.

2. Manufacturer: Sonotone Corporation, New York

3. Electrical characteristics of cell:

a. Ampere-Hour Capacity:

(1) 3.5 ampere-hours at a 1.30-ampere discharge rate at a terminal voltage of 1.20 volts or greater at 25°C.

(2) 3.0 ampere-hours at a 1.30-ampere discharge rate at a terminal voltage of 1.20 volts or greater at 0°C.

(3) 2.3 ampere-hours at a 1.30-ampere discharge rate at a terminal voltage of 1.20 volts or greater at +55°C.

b. Watt-hour capacity: 4.2 watt-hours at 25°C for discharge conditions listed above in (3)(a)1.

c. Watt-hours per pound: 7.6 watt-hours at 25°C for discharge conditions listed above in (3)(a)1.

d. Maximum recharge rate: 0.44 ampere between -10°C and +55°C.

e. Watt-hour efficiency: 60%

4. Physical Characteristics of Cell:

a. Weight: 0.53 to 0.55 pound

b. Dimensions:

Diameter: 1.3 inches

Length: 3.5 inches

Volume: 4.7 cubic inches

(b) Battery Characteristics:

1. Number of F-size cells: 63

2. Number of parallel rows: 3

3. Number of series cells per row: 21

4. Total watt-hour capacity: 265, at discharge conditions defined in (3)(a)1.

5. Total ampere-hour capacity: 10.5, at discharge conditions defined in (3)(a)1.

6. Total weight of 63 storage cells: Approximately 34 pounds

7. Total weight of assembled battery including all packaging: 38.5 to 40.0 pounds

8. Maximum range of output voltage: 25.5 to 33.0 volts

(c) Telemetered Data

The following battery operational parameters are telemetered:

1. The terminal voltage of each of three rows of batteries.

2. The voltage supplied to the input of one of the voltage regulators by the three rows of batteries, each supplying power to the regulator through isolating diodes.

3. The temperature of the satellite baseplate, adjacent to the battery package.

4. The output voltage of two 24.5-v d-c voltage regulators and two 13.0-v d-c voltage regulators.

Each of these parameters is employed to determine whether the storage batteries (or associated equipment) are performing within the tolerated electrical-design specifications.

d. Voltage Regulator Specifications

During March 1959, the initial system tests disclosed need for extensive decoupling and regulation. The battery impedance, which had been considered negligible, was measured and found to increase from 0.13 ohm at 100 cycles to over 10 ohms at 1 megacycle. It was decided to build a common regulator for each system, rather than to have each subsystem decoupled and regulated internally. Four regulators were envisioned; two with a -24.5-volt output, and two with a -13-volt output. The -24.5-volt and -13-volt regulators for each camera system were packaged into a single unit, resulting in two identical units for the two cameras in the satellite.

The initial specifications decided upon are as follows:

(1) Battery-voltage variation: -24 to -32 volts.

(2) Nominal regulated output: -24.5 ± 0.2 volts.

(3) Load current: 0.5 to 5.0 amperes.

(4) Ripple: to be reduced by at least 10 to 1.

(5) Output Characteristics:

Input Voltage Above 25.5 Volts: Impedance less than 0.02 ohm at 5 kc with 5-ampere load.

Input Voltage Below 25.5 Volts: Maximum voltage drop to be less than 1 volt with output voltage following input voltage profile.

A similar regulator circuit for the 13-volt input to the satellite clocks was mounted on the same chassis as the -24.5 volt unit. The initial specifications were:

(1) Input voltage range: -14 to -18 volts.

(2) Load current: 0 to 0.5 ampere.

(3) Output voltage: 13.9 volts ± 1%.

For the complete voltage-regulator specifications, see TIROS Specification SP-100.

e. Solar-Array Power-Availability Studies

(1) Total Energy Calculation

Because the silicon solar cells are located on the top and lateral surfaces of the cylindrically-shaped structure as shown in Figure 77, the total instantaneous active-silicon area projected normal to the sun's rays determines the power collecting capabilities of the satellite. This area is expressed in terms of the angle between the sun's rays and the satellite spin axis (referred to here as the alpha angle) and the silicon area on the top and lateral surfaces. Thus, if the alpha angle is zero, only the top is illuminated; at an alpha angle of 90°, only part of the lateral area is illuminated. Maximum instantaneous solar-cell output is derived at an alpha angle of approximately 45°.

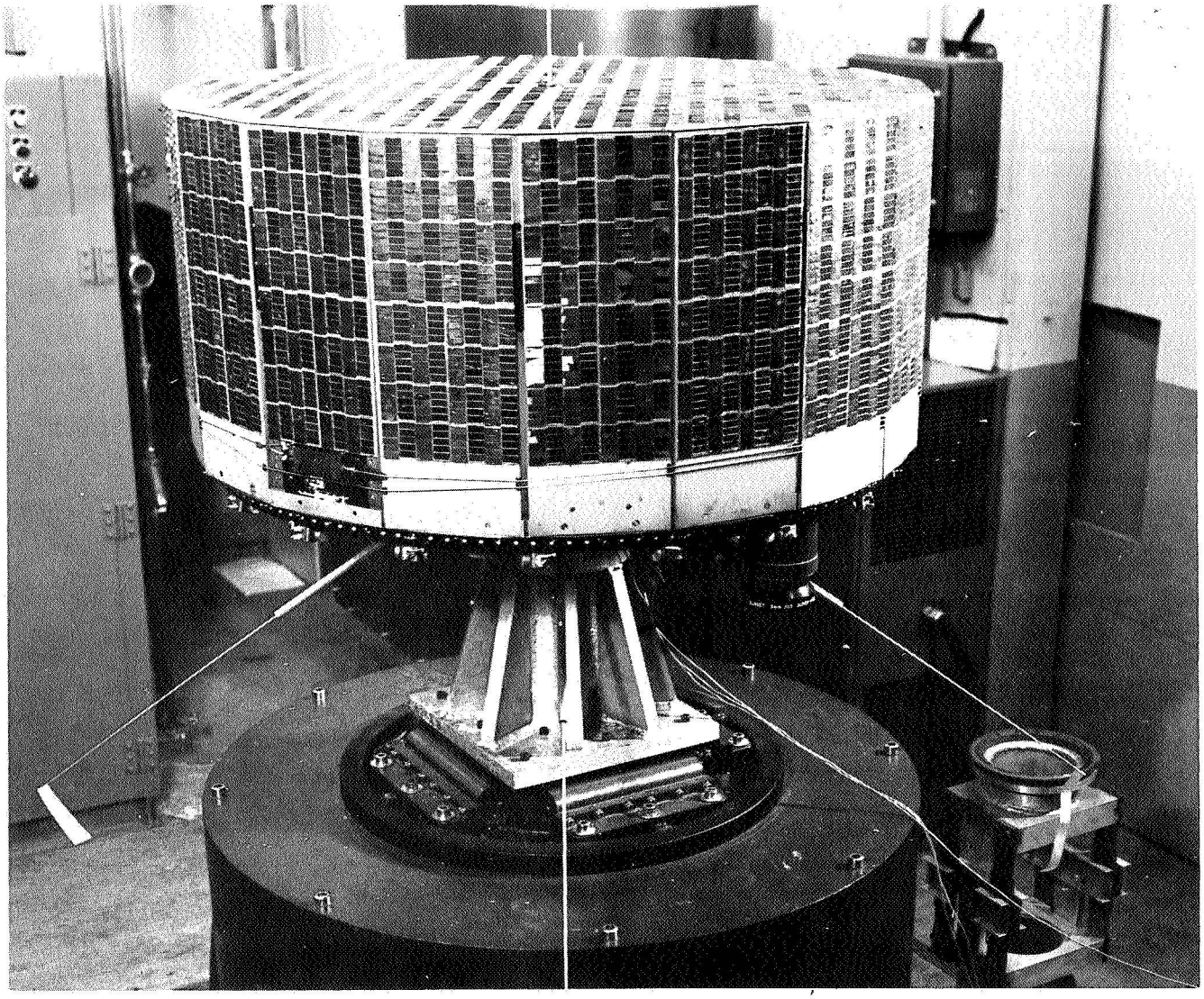

Figure 77. TIROS I Satellite Showing Solar-Cell Location

The original concept of the system was to place in orbit a spin-stabilized satellite whose spin-axis orientation remained essentially fixed in inertial space as the satellite orbited the earth and as the orbit precessed in space. Pre-launch calculations demonstrated that the effect of differential gravity would perturb the spin axis only slightly. Further investigation indicated that eddy currents in the satellite structure and the presence of soft iron in the satellite would similarly affect the orientation. Under these conditions, the major variation in alpha is attributed to the relative motion of the sun and spin axis as the satellite travels with the earth in the yearly orbit of the earth about the sun. For the pre-selected spin-axis orientation, the time of year and time of day launch were to be chosen so that during the initial three months of satellite life, the alpha angle would be favorable for television coverage of the earth, and for power collection and conversion.

A generalized expression for the total energy available to the satellite load can be written as:

$$W_{TL} = 1440\ P_S A_S E_S D_T \psi, \text{ in watt-minutes}$$

with the symbols defined as follows:

W_{TL}	Total energy in watt minutes delivered to the satellite loads in a 24-hour period
P_S	Solar radiation intensity at satellite altitude 0.140 watts/cm^2 = 130 watts/ft^2
A_S	Total silicon area projected normal to the sun's rays in cm^2 of ft^2
E_S	Solar cell efficiency at +30°C
D_T	Accumulated product of degradation factors described below
ψ	Percent of the orbital period during which the solar array is illuminated
1440	Number of minutes in each 24 hour period

The diagram in Figure 78 shows relationship between the satellite spin axis and the sun vector.

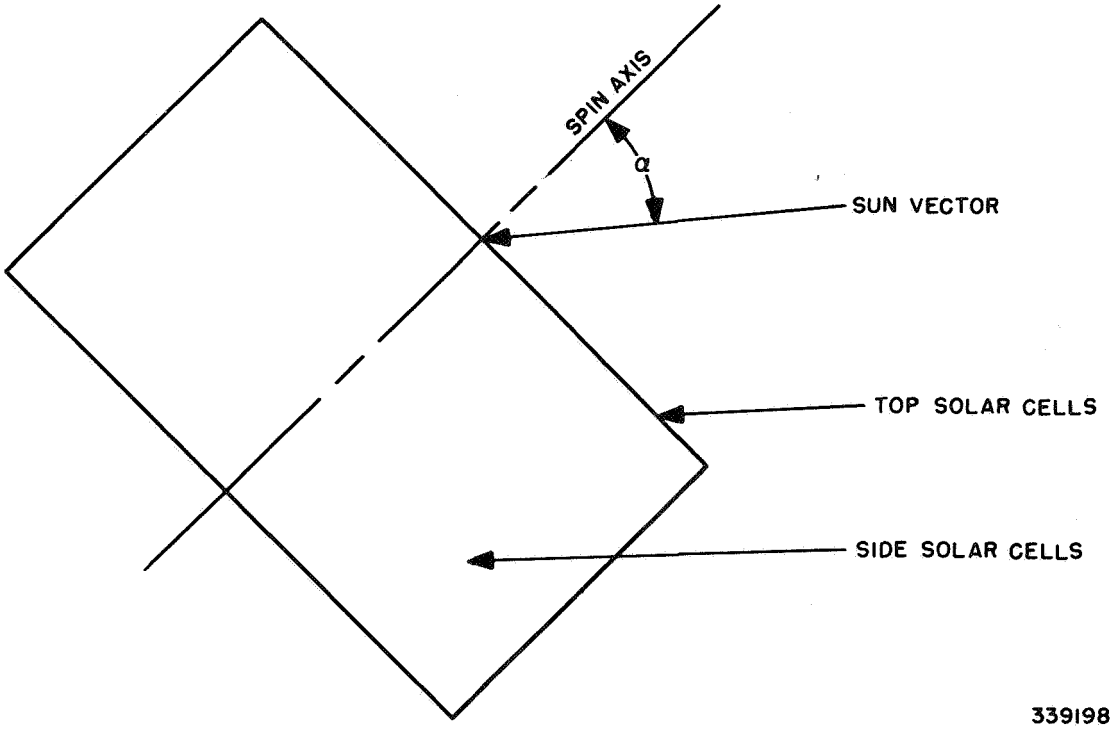

Figure 78. Spin-Axis/Sun-Vector Relationship

If the solar cells on the side of the satellite were distributed evenly about a continuous curved surface, the output of the array would not vary as the satellite spins about its axis. However, the side of the satellite consists of 18 flat panels which provide a slightly varying output with spin. In addition, two panels have less than the maximum number of solar cells, so that an additional small variation in instantaneous area projected to the sun is encountered. Because the satellite makes one revolution in 5 to 7 seconds, it is convenient and sufficiently accurate to calculate an average total projected area over a small period of time such as one minute. This was the approach which was used.

The instantaneous active silicon area projected normal to the sun vector is expressed as follows:

$$\text{Effective top area} = (A_{TOP})\ (\cos 1.05\ \alpha)$$

$$\text{Effective side area} = (A_{SIDE})\ (0.304 \sin 1.05\ [\alpha\ \psi]\ ).$$

Where: A_{TOP} is the total active silicon area on the top of the satellite or hat; A_{SIDE} is the corresponding quantity for the side solar cells; and cos 1.05 α gives the effective projected top silicon area normal to the sun's rays. The 1.05 multiplier is an experimentally-determined quantity which accounts for the non-sinusoidal output of a glass covered silicon solar cell as a function of a changing angle of incident illumination, and 0.304 sin 1.05 ($\alpha\ \psi$) is a similar expression for the solar-cell effective area. The 0.304 factor is a combination of a geometrical factor, which accounts for the illumination of a projected area of $\frac{1}{\pi}$ of the total area on a cylindrical surface, and the experimental non-sinusoidal response of the glass-covered solar cells.

Values of A_{TOP} and A_{SIDE} are given in a subsequent paragraph.

The quantity E_S as used in these calculations, is the efficiency of the entire solar-cell array - which includes the power losses due to transmission of glass cover slides, diodes, and series-parallel connection of the solar cells. For the TIROS satellites, E_S = 7.3%.

(2) Spectral Transmission Loss Resulting from Glass Cover and Coatings

The use of this special glass cover to control the radiative self-cooling capabilities of the solar cells introduced a spectral transmission loss. Laboratory measurements made by RCA and the technical information available indicated that a 6-mil glass coated with blue-reflecting coating passes a minimum of 96% of the solar spectrum. In actual solar-cell efficiency measurements, the total percentage reduction in electrical output was actually less than the 4% indicated.

(3) Power Loss Caused by Diodes

In order to prevent the solar cells from loading the batteries during the orbital night, silicon diodes were connected in each series row of solar cells, as shown in the block diagram, Figure 79. These diodes consume power in the order of 2%, causing a

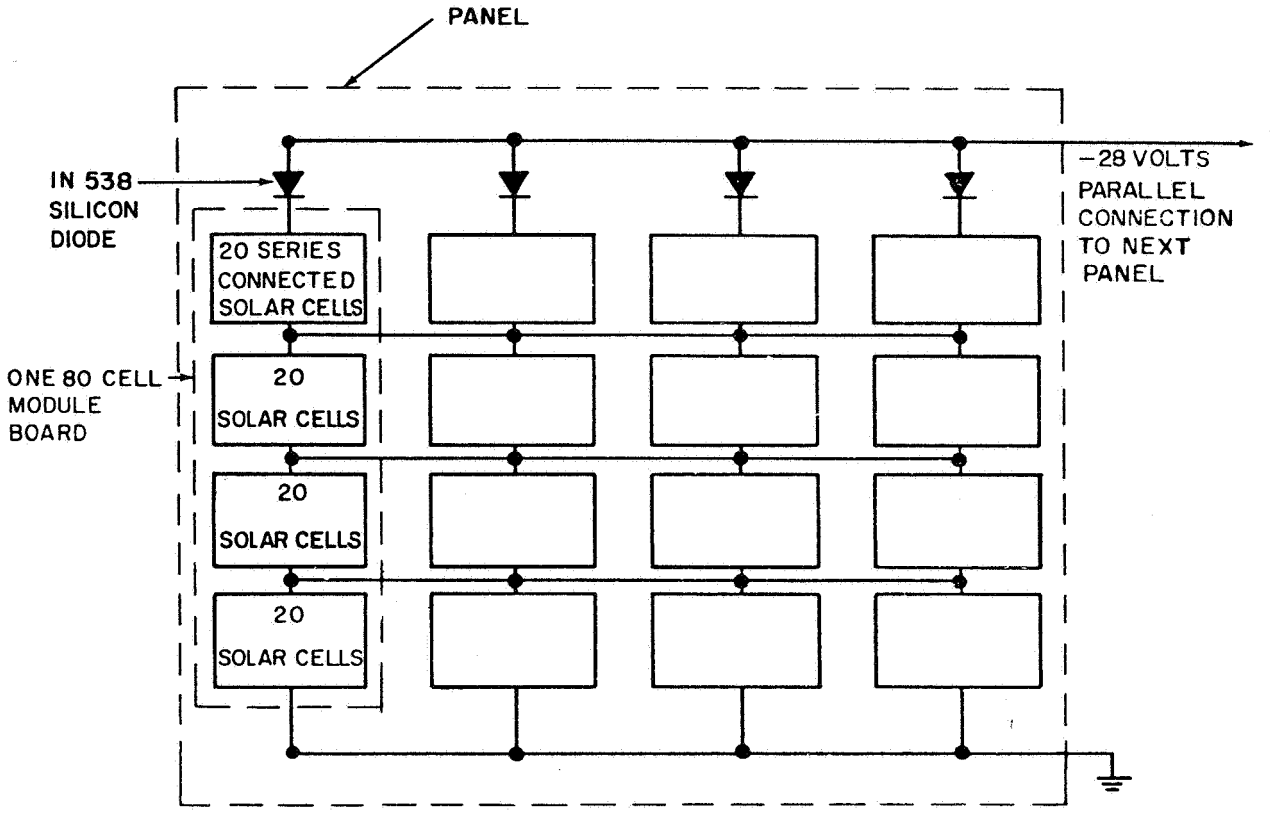

Figure 79. Solar-Cell Interconnection, Block Diagram

reduction to 98% of the total power otherwise available. The voltage drop across each diode is approximately 0.75 volt at 25°C. The effect of this voltage drop must be allowed for in the determination of the optimum-voltage operating point of the solar cells, and is one of the considerations that is part of the analysis leading to the efficiency degrading factor listed in the following paragraphs.

(4) Series-Paralleling Losses

The effect of series-paralleling the shingles into modules, the modules into panels, and the panels into the entire array, produced approximately a 2.5% loss in efficiency as determined from the measurements program. The degradation factor, D_T, allowed for the solar-cell array performance characteristics which reduced the effective efficiency of the array from the value of E_S. These performance factors are each expressed as efficiencies, and their product is the quantity D_T. Efficiency degrading factors were used in sizing the solar power supply. The radiation shift of the satellite altitude was assigned a value of 0.86. The efficiency E_S employed above was the solar-cell efficiency as measured on the earth's surface at air mass one (m=1) under an integrated sunlight intensity of 100/mw/cm^2. In going from a standard-day sea-level solar spectrum to a satellite altitude spectrum, a spectral shift toward the shorter wavelengths is encountered. Because of this shift, the solar-cell responsive wavelength band, which peaks between 0.8 and 0.9 micron, contains a smaller proportion of the total solar flux

and a poorer distribution of this flux at satellite altitudes than at sea level. Therefore, at the satellite altitude, this phenomenon results in a reduction of solar-cell efficiencies from the sea level efficiency. Thus, for a specific assumed solar-cell spectral response, a 7.5% solar cell as measured under sea-level conditions is only 0.86 times as efficient (or 6.45%) at satellite altitudes.

(5) Micrometeorite Bombardment Effects

When design decisions were made for the power supply, little data was available concerning the numbers, intensity, and particle size of micrometeorite particles at satellite altitudes. The sprinkling of data from the first satellites produced a decision not to provide a protective transparent shielding against such particle showers. For the purposes of power estimating, however, it was assumed that a 20% loss in output caused by micrometeorites would occur in one year at a linear rate. Expressed as normalized power, the power after days in orbit was therefore: 1.000-0.000548x = normalized power. Thus, after 90 days in orbit, only a 5% (approximately) loss in power would be expected. It was planned that, after launch, telemetered solar-cell data would be constantly analyzed to detect indications of gradual degradation in solar-cell output power and to correct predicted energy available accordingly.

(6) Effects of Temperature and Storage-Battery Voltage Variations

Peak power is delivered by a solar cell at a specific voltage which is, to a great extent, independent of illumination over wide variations of intensity below the level encountered at satellite altitudes, but is critically dependent upon operating temperature. Because a solar cell under given illumination can operate over a wide range of voltages, the voltage across a series row of the cells and across the individual cells that comprise the row, is forced to follow the storage battery voltage as it varies during the charge and temperature cycles. The above variations reduce solar-cell output power of the solar cells by 5%.

(7) Deterioration of Output Power with Increasing Temperature

As the operating temperature of a solar cell increases from +30°C, for example, the power developed at every operating voltage decreases. At each temperature, there is a different specific voltage at which maximum power is generated. This maximum power deteriorates at a rate of 0.5 to 0.6% per degrees C above +30°C, and the maximum-power voltage decreases at a rate of 2.0 to 2.3 millivolts per degrees C. In the power supply, however, the voltage at which the solar array operates is determined by the sum of the voltages across the batteries and current-limiting transistor which undergoes a total variation of only ±10%. The effect of this variation in power is described above. This discussion is presented to show that the variation in power as temperature of the array varies for a solar cell operating at a fixed voltage of 0.39 volt. From the solar-cell current-voltage characteristics as a function of temperature, an expression was derived for normalized power over the range of average temperature of the solar cells predicted throughout the initial 90 days of satellite life.

For the range of average solar-cell temperatures predicted, the normalized power for the top solar cells is = 5.79 - 0.0155T°K, where T°K is the average solar-cell temperature in degrees Kelvin occurring in daylight. This expression is valid between +40°C and +70°C. For the side solar-cell temperature in daylight; this expression is valid between -20°C and +20°C. From the thermal analysis, a day-by-day plot of these average solar-cell temperatures for the top and side was obtained for specific launch date and launch conditions; linear approximations were made for these temperatures (shown in Figure 80); and these substituted in the above expressions for normalized power. The results of these calculations and substitutions appear in RCA-AED Technical Memo 212-17, Page 2, and there are terms in parenthesis which are labeled $T_{TOP} = T_T$ and $T_{SIDE} = T_S$.

(8) Energy Transfer Efficiency

The term "transfer efficiency," E_T, was adopted to express energy loss in transferring energy from the solar array to the satellite equipment loads, and is defined as:

$$E_T = \frac{\text{Total Energy Delivered To Satellite Equipment Loads}}{\text{Total Energy Supplied by Solar-Cell Array}}$$

This quantity, when evaluated and multiplied by the total available energy from the solar array, provides the total energy available to the load W_{TL}.

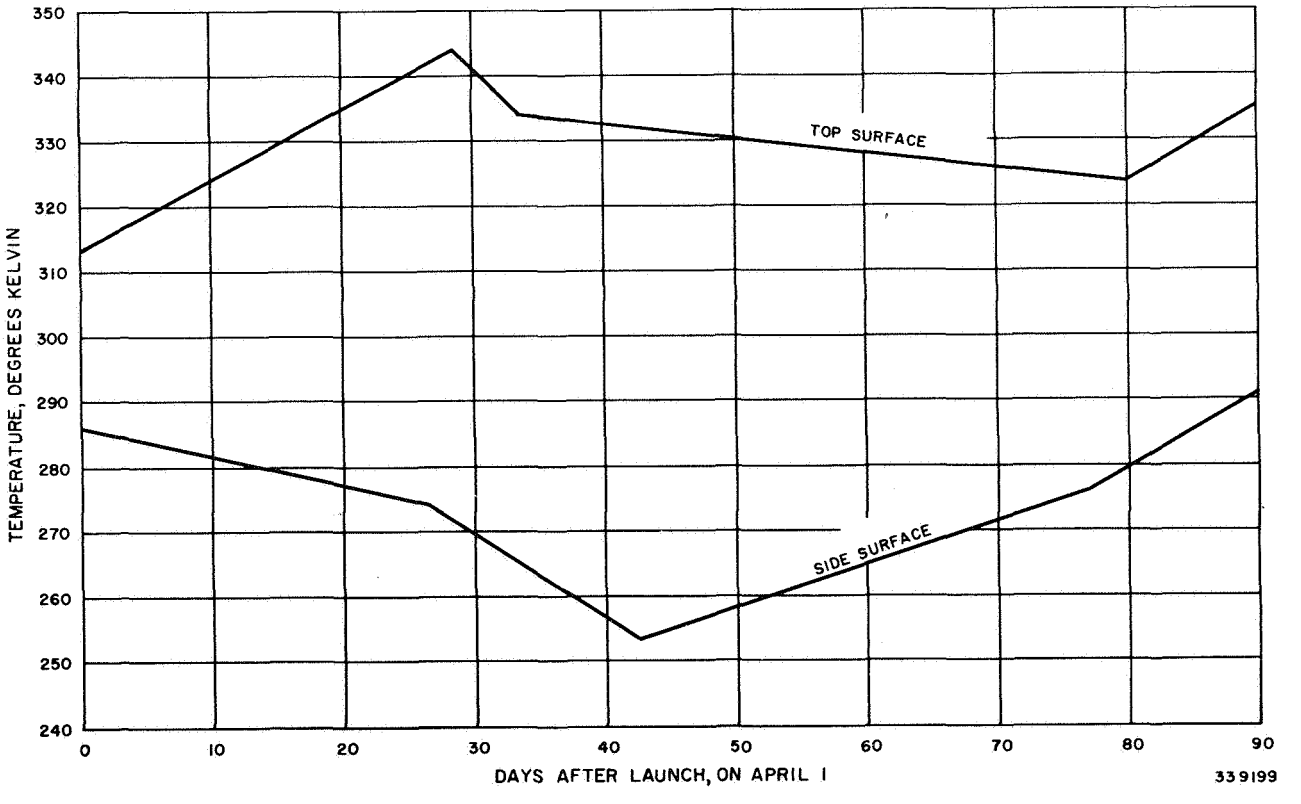

Figure 80. Plot of Average Solar-Cell Temperatures

The magnitude of E_T is less than unity because of energy losses resulting from the inefficiency of the energy-storage system, the voltage regulators, and current limiters.

An average value of E_T was calculated for a number of different equipment power-drain profiles. For example, the typical program modes in this analysis included the following power profiles:

(1) The entire system in the standby mode for an entire orbit.

(2) An orbit in which both camera systems are programmed for the remote and playback modes and in which the direct-alternate camera modes are programmed. For each of the load profiles considered, average voltage levels were assumed for the solar array and storage batteries, as were average voltage drops across current-limiting elements in order to permit calculation of the efficiency of the transfer of power through series elements in the power-transfer paths.

Using a value of battery efficiency of 60%, an average value of $E_T = 0.68$ was calculated.

The overall product of the degradation factors is substituted in the equation for W_{TL} above together with the following values:

$$W_{TL} = 1440\ P_s\ E_s\ \psi\ D_T\ A_{TOP}\ (\cos 1.05\alpha) + A_{SIDE}\ (0.304 \sin 1.05\ [\alpha\ \psi])$$

$$E_S = 0.073;\ A_{TOP} = 6408\ cm^2;$$

$$A_{SIDE} = 10,008\ cm^2 \text{ and } P_S = 0.140\ watts/cm^2.$$

The final expression for W_{TL} is given on Page 2 of RCA-AED Technical Memos 212-17.

RCA-AED Technical Memos 212-16A, 212-17, and 212-18 used together provide sufficient data to determine the total energy available to the load from the solar-cell array for any day after launch, and the total energy required by the instrumentation for various equipment programs.

The graph shown in Figure 81 is a plot of W_{TL} evaluated for specific pre-launch variation of α. Pre-launch variations in α and ψ are given in the Figures 82 and 83.

f. Development of Protection Circuits

(1) General

Because a common power supply was used for both of the TV camera systems, a method of protecting the power supply from damage or depletion, in the event of one

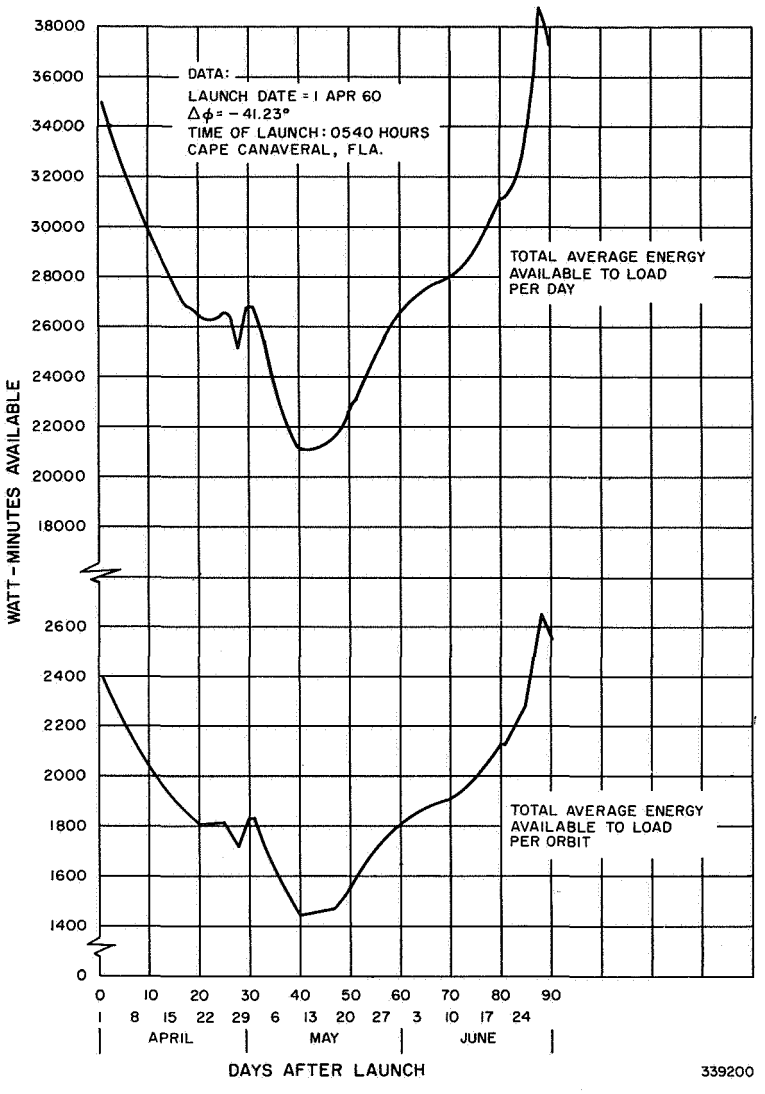

Figure 81. Plot of Energy Available to Load

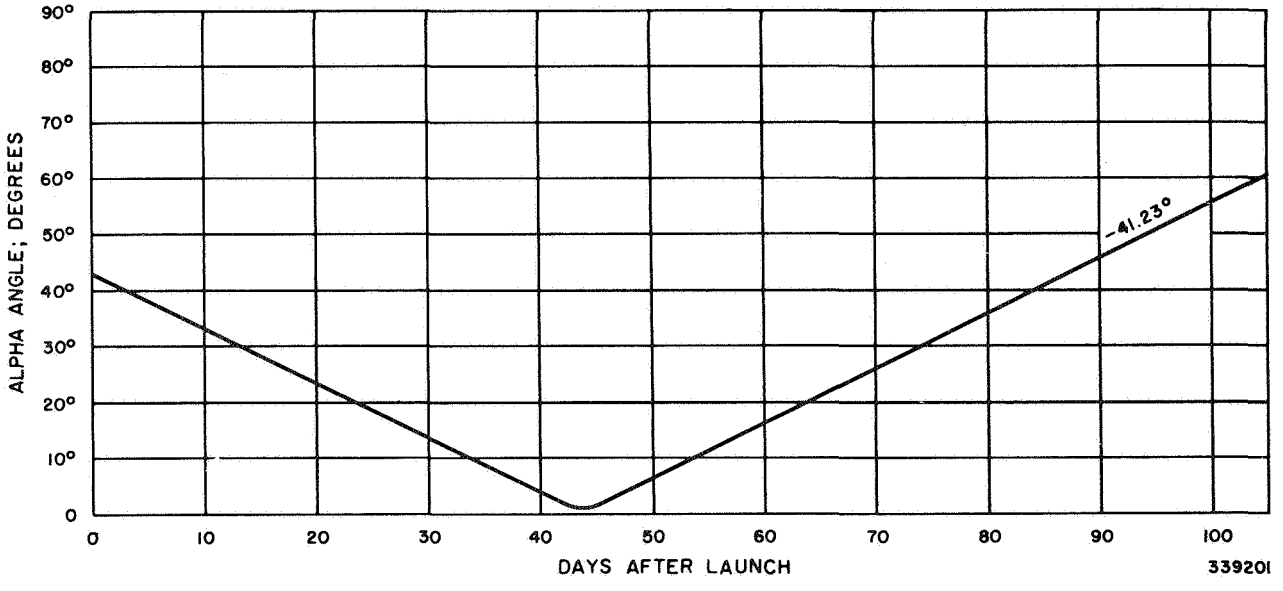

Figure 82. Plot of Pre-Launch Alpha Variations

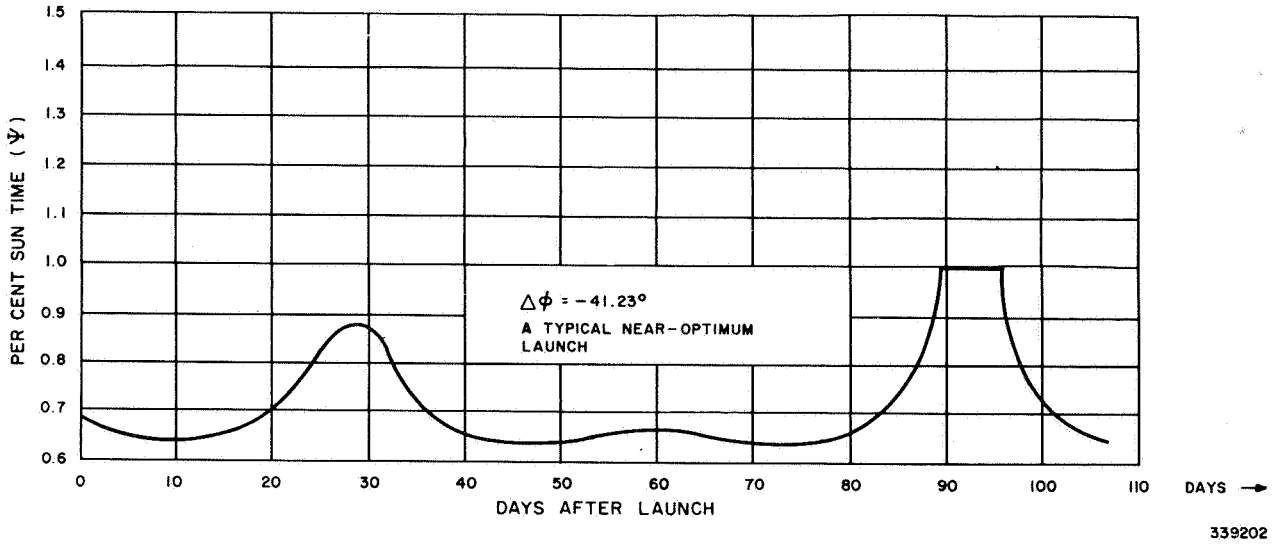

Figure 83. Plot of Pre-Launch Sigma Variations

subsystem failure, was needed to permit the operation of the other TV system and sustain a reduced mission. Also, it was necessary to devise a method of preventing damaging circulating currents from flowing when the three storage-battery strings were connected in parallel to form the composite battery.

In the initial power supply configuration, each - 26-v cell string was tapped at the - 14-volt point. The three - 14-volt taps were connected together to provide a - 14-volt bus and the three - 26-volt terminals were similarly connected to provide a - 26-volt bus. This represented an unfavorable condition because a string of cells with a slightly lower terminal voltage would tend to be charged by the other two strings, which would result in an internal circulating current within the battery pack. Initially, this current results in discharging two strings while overcharging the third, but a balanced condition may be expected within a short time and at only a slightly lower terminal voltage level with only a minor loss of available power. However, if a short circuit were to have developed in any of the three strings, the circulating current would then become equal to the differential voltage divided by the network impedance (12 amperes for the loss of a 1.2 volt cell with a 0.1-ohm composite resistance). Circulating currents and the resulting terminal voltage drops of this magnitude were intolerable; therefore, the fuse circuit shown in Figure 84 was evolved. It can be seen that a shorted cell in any one of the strings would result in a circulating current supplied by the other two strings. Under nominal conditions, twice as much circulating current flows in the string with the shorted cell as in either of the other two strings which supply this current. This tends to cause the fuse in the shorted string to blow first, eliminating the circulating current.

A problem arose during system tests, which indicated that the cell impedance, and, therefore, the battery-string internal impedance, varied considerably from unit to unit. Thus, the current load was not shared equally by the two good strings. In fact, under tests with a simulated shorted cell, the fuse in the best of the three strings sometimes blew first, causing the battery to be reduced to one high-impedance string in parallel with one shorted cell string. The circulating current remained and the battery reserve was considerably reduced.

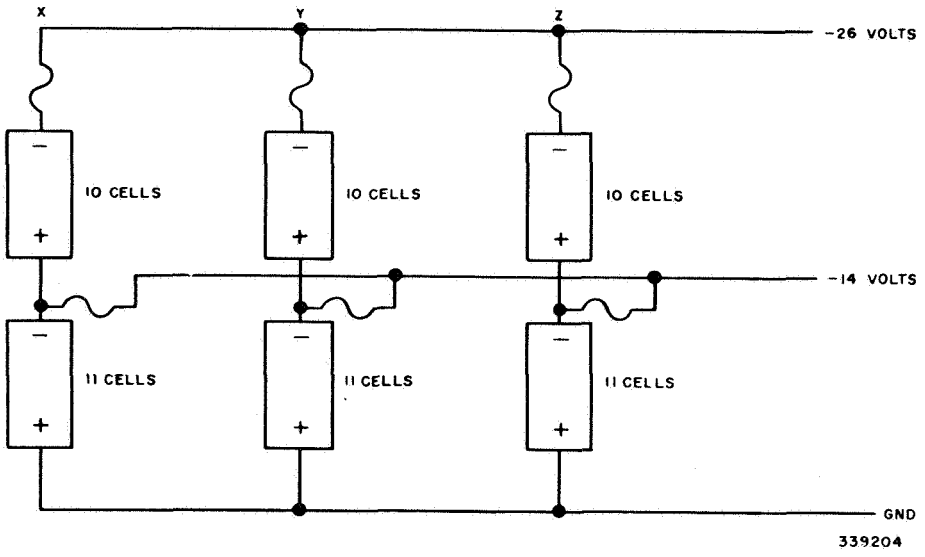

Figure 84. Storage-Battery Fuse Circuit, Schematic Diagram

This problem was solved by installing diodes in parallel with the fuses. These diodes were oriented in such a direction that, if the fuse in a good string of cells blew first, the diode would continue to carry the current and blow the fuse in the defective string. The circuit with the diodes added is shown in Figure 85. If the fuse in a string containing a shorted cell blew, the circulating current through that string would cease. The defective string could deliver current to the load, however, if the terminal voltage of the other two strings dropped to the point at which the diode in the defective string became forward biased. This could have happened if the other two strings either lost one cell each or developed a high internal impedance. Therefore, the modified version ensured that the best string would remain useful and allow a defective string to deliver current if the entire pack degraded to a lower terminal voltage.

A search for a suitable fuse was conducted and several likely samples were tested under vibration and vacuum. Standard aircraft-type, antivibration fuses were tested and proved to be unreliable under the expected 25-g launch-vibration level.

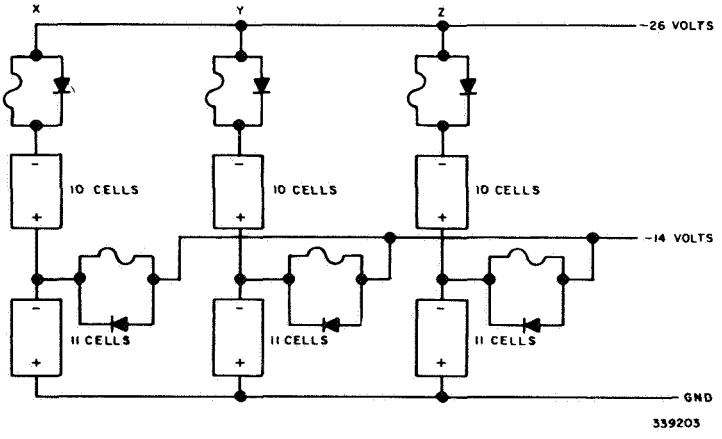

Figure 85. Storage-Battery Circuit with Diodes Added, Schematic Diagram

Early in 1959, literature describing a pyrophoric fuse wire was obtained from Sigmund Cohn Corporation. This fuse consisted of an aluminum core with a palladium jacket, drawn to wire form. Sizes ranging from 0.020 to 0.001 inch were available with current ratings which were inversely proportional to the square of the diameter. When heated to the melting point of Aluminum (660°C), an exothermic alloying action takes place resulting in temperatures approximately 2500°C. The fuse wire effectively disintegrates into tiny particles of alloy and a deposit of aluminum and palladium oxides, if it fuses in an atmosphere containing oxygen. The reaction also takes place equally well in vacuum or inert atmosphere, but with different current ratings. Samples of the fuse wire were tested in vacuum to determine the proper size for the 12-ampere fuse and for the 1.2-ampere fuse.

The fuse board configuration is shown schematically in Figure 86 and represents the design chosen for TIROS I as of September 1959. In addition to the circulating current protection shown in Figure 85, load protection was added in the form of six additional fuses. The unregulated - 26-volt lines to camera system 1 and camera system 2, as well as the regulated lines to each camera system, contain 12-ampere fuses in series. The normal currents in these wires were on the order of 3 to 4 amperes. This provided a 60% derating to allow for transients and short-time overloads before cutting the power to that circuit permanently. The input lines to the - 13-volt regulators contain 1.2-ampere, 0.004-inch fuses of the same material as the 12-ampere 0.020-inch fuses. The normal currents in the 1.2-ampere fuses were also one third of the fuse rating or approximately 400 milliamperes.

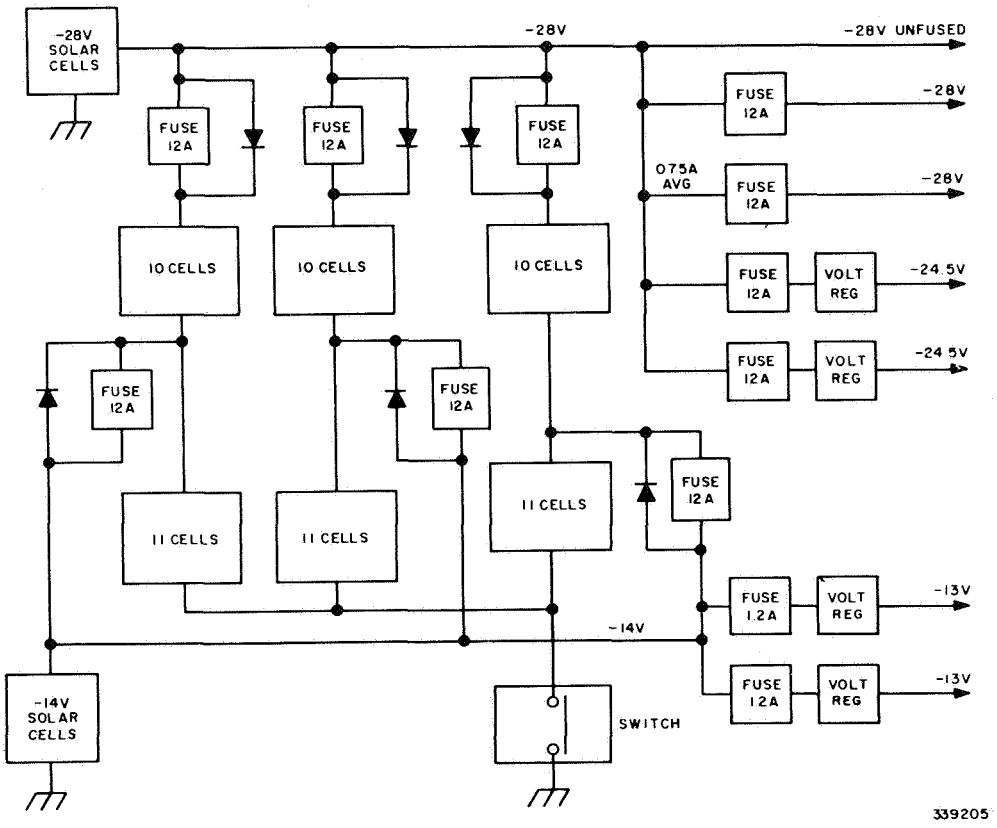

Figure 86. Fuse Board, Schematic Diagram

In December 1959 during early environmental tests, several battery packs failed. Several contributory causes were found during a complete investigation into the battery situation. One of the causes of failure was found to be uncontrolled charge rates in each of the three parallel strings. It had been assumed that the charging current would divide equally between the three strings; however, this assumption was incorrect. Also, the total safe charge rate for the battery pack had not been accurately determined. Several sources of technical assitance were contacted (i.e., the battery manufacturer and the Signal Corps battery-evaluation group at Fort Monmouth). The composite conclusion, based upon limited tests by both groups, was to limit the charging current to 400 milliamperes per string or 1.2 amperes to the entire pack. The other cause of failure seemed to be moderate but long term circulating currents, which did not blow the fuses but did overheat the cells. Some cells expanded when overheated and overcharged; this caused the destruction of the thermal bond to the battery-pack structure. These cells then became even hotter, causing destructive deterioration of the cell separators which, in turn, resulted in shorted cells.

(2) Regulators

(a) General

After the failure of the battery packs, the TIROS Payload Integration Group undertook the redesign of the battery-protection circuits to include charging-current limitation, and an improved protection against circulating currents. The redesigned battery protection circuitry which resulted is shown schematically in Figure 87. Four new circuits or concepts were incorporated. These were: charging-current regulators, load-coupling diodes, - 14-volt regulators, and a bypass regulator.

The solar cells or external charger provide a voltage source at -40 to -28 volts with the capability of supplying up to 2.2 amperes to the satellite. A good approximation of the solar-cell supply for ground testing has been a 40-volt supply with a 5-ohm resistance connected in series. At 2.2 amperes then, the voltage supplied to the satellite would be 29 volts, which is approximately the nominal battery terminal voltage under light load.

(b) Current Regulators

The current regulators limit the current in each string to 400 milliamperes ±10% over the temperature range and over a differential charging-bus, battery-voltage range of from 1 to 14 volts. Because the charging current is limited to 1.2 amperes total, one ampere is available for direct use by the satellite loads.

The bypass regulator limits the voltage supplied to the load bus to a maximum of -32 volts to protect the circuits which use unregulated voltages. It will pass up to one ampere at input levels of from -40 to -28 volts, with a minimum voltage drop of less than one volt. The -14-volt charging inputs and load-output taps were eliminated from the battery strings in order to reduce unequal charging above and below the taps. Two simple, auxiliary voltage regulators were then added to drop the - 26-volt load bus

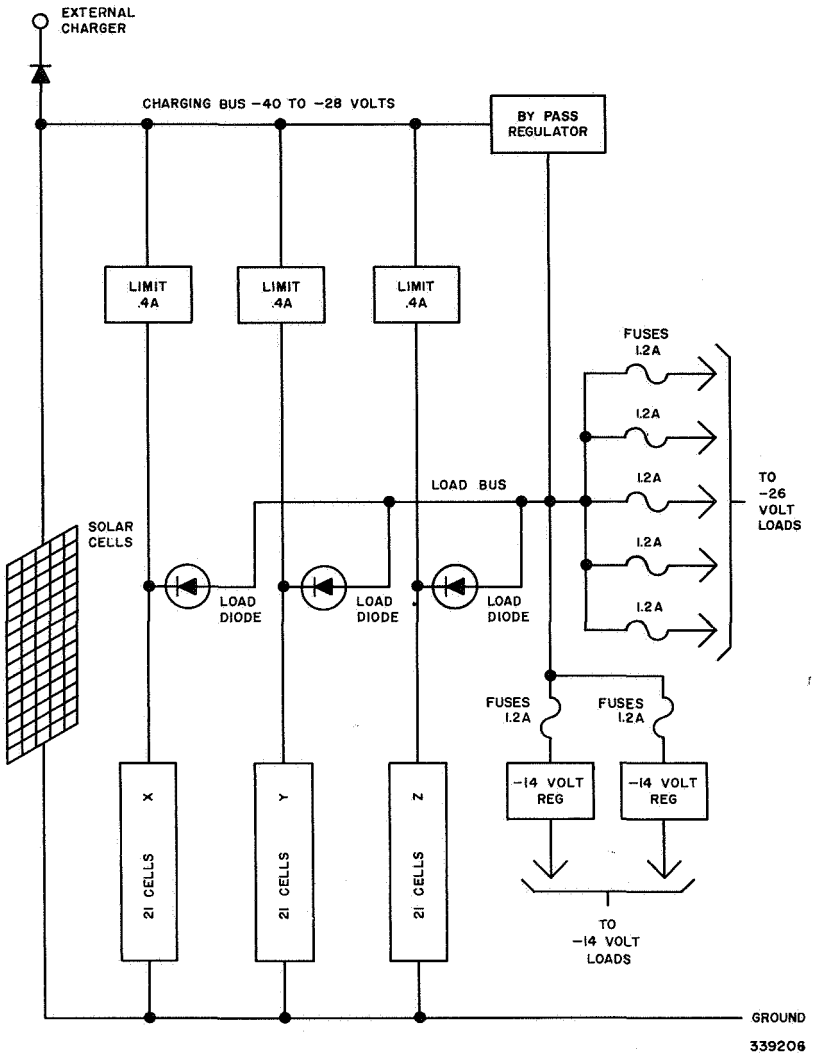

Figure 87. Battery Protection Circuits, Schematic Diagram

voltage to -14 volts for the input to the two - 13-volt regulators. The power loss, which originally was wasted in overcharging the upper cell bank of each battery string, was then dissipated (by the auxiliary voltage regulator) directly into the baseplate rather than into the battery. The solar-cell wiring was changed to provide extra capacity at the - 40-volt level by using the panels formerly delivering - 14-volt power.

The load-coupling diodes consist of large power transistors connected as diodes (base to collector) with forward drops ranging from 0.1 volt at light loads up to 1.0 volt at full load. The improvement in circulating current protection due to the excellent isolation was considered to be worth the small voltage drop.

(c) Charging Current Limiter

In December 1959, the need for a limiting of the battery current became apparent. The initial objectives were to limit the cell-string charging current to 500 milliamperes and to maintain a low series impedance for all lower values of charging

current. An initial approach is shown in Figure 88(a). If the base-emitter voltage on a transistor is held constant, the collector current will be almost constant and only a small function of the collector-emitter voltage. A practical circuit is shown in Figure 88(b). The Zener diode stabilizes the emitter-base voltage of the power transistor, establishing the nearly constant voltage desired. Initially, a silicon, NPN, power transistor (RCA Type 2N1068) was used as the series element. Tests with this configuration, assuming several cells shorted in the string, indicated a possible power dissipation in excess of the capabilities of the Type 2N1068 transistor. Because of the extreme necessity for a reliable circuit, the feasibility of using a larger silicon transistor was investigated. The Signal Corps had procured several thousand development models of the RCA Type 2N1070 transistor. The increased power-handling capabilities (30 watts at 100°C) and lower forward saturation resistance of this transistor were important factors in its ultimate selection. Several thousand transistors were tested at Fort Monmouth, and approximately fifty selected units were delivered to RCA for use in the current regulators. These units were baked for 100 hours at 100°C in order to further stabilize the gain drift at high temperatures.

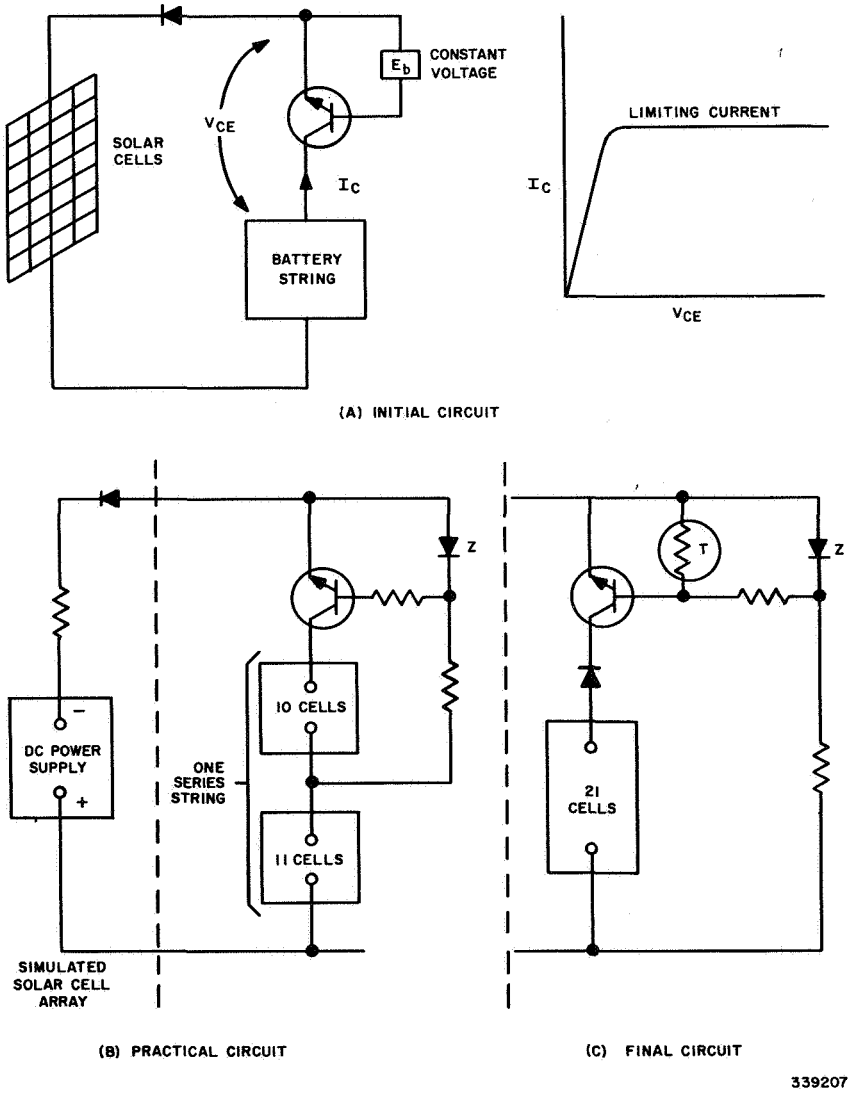

Figure 88. Charging-Current Limiter Circuit Configurations

Upon recommendation from the battery manufacturer and the Signal Corps battery group, the battery-charging current was reduced to 400 milliamperes (from the initial 500-milliampere value). The final regulator-circuit configuration is shown in Figure 88(c). The Zener-diode dropping resistor was connected directly to ground when the - 14-volt tap was eliminated, and a thermistor, shunting the base of the power-transistor, was installed to provide temperature compensation. An additional diode, in series with the power-transistor collector, was included to provide protection against emmiter-base breakdown when the three battery strings were connected to the three current regulators. The current limiters were tested in thermal-vacuum under operating conditions. In thermal testing, the limiters held the charging current to a nominal value of 400 milliamperes ±10% from -10°C within a range of limiter voltage drop of 1 to 14 volts. Unit vibration tests were made with no adverse results. The current limiter required no further modifications after system integration on the satellite.

(d) Bypass Regulator

Under favorable conditions, the solar cell supply can deliver up to 2.2 amperes to the satellite. The charging-current limiters pass 1.2 amperes to the batteries, leaving 1.0 ampere available for direct use by the loads. A simple two-transistor bypass regulator was designed to prevent the voltage level of the excess solar-cell power from exceeding 32 volts. When the input drops below 32 volts, the bypass regulator functions as a diode with a forward drop of approximately 1.0 volt and passes the current to the load without regulation. No problems were encountered with this regulator design either during subsystem testing or in system integration.

(e) Voltage Regulators

A block diagram, Figure 89, of the regulator circuit is shown. It consists of a series regulating element, a d-c amplifier, an error detector, and a bridge which is nulled for the desired output voltage.

The first voltage-regulator design utilized two large, germanium, power transistors, connected in parallel, as the series regulating element. Load-current equalizing resistors of 0.1 ohm were connected in the emitters of each transistor. The base current was supplied by a silicon emitter-follower stage driven by a two-stage d-c amplifier, utilizing two Zener diodes in a bridge circuit with an error detector.

The initial voltage drop was in excess of 2 volts. This was primarily caused by the drop errors in the silicon emitter-follower stage. This transistor was then changed to a large germanium power type. The unit then exhibited a marked tendency to oscillate at approximately 100 kc. Some gain-frequency compensation was added and several RC networks were added to shape the gain characteristics to eliminate the undesirable oscillations.

A major problem arose during thermal vacuum testing; under long-time loading, the -24.5-volt regulator was found to go out of regulation in a form of thermal "run-away". The temperatures of the power-transistor cases were monitored during subsequent testing, and case temperatures in excess of 80° were found to be coincident with the loss of regulation. (This temperature is critical for these germanium transistors

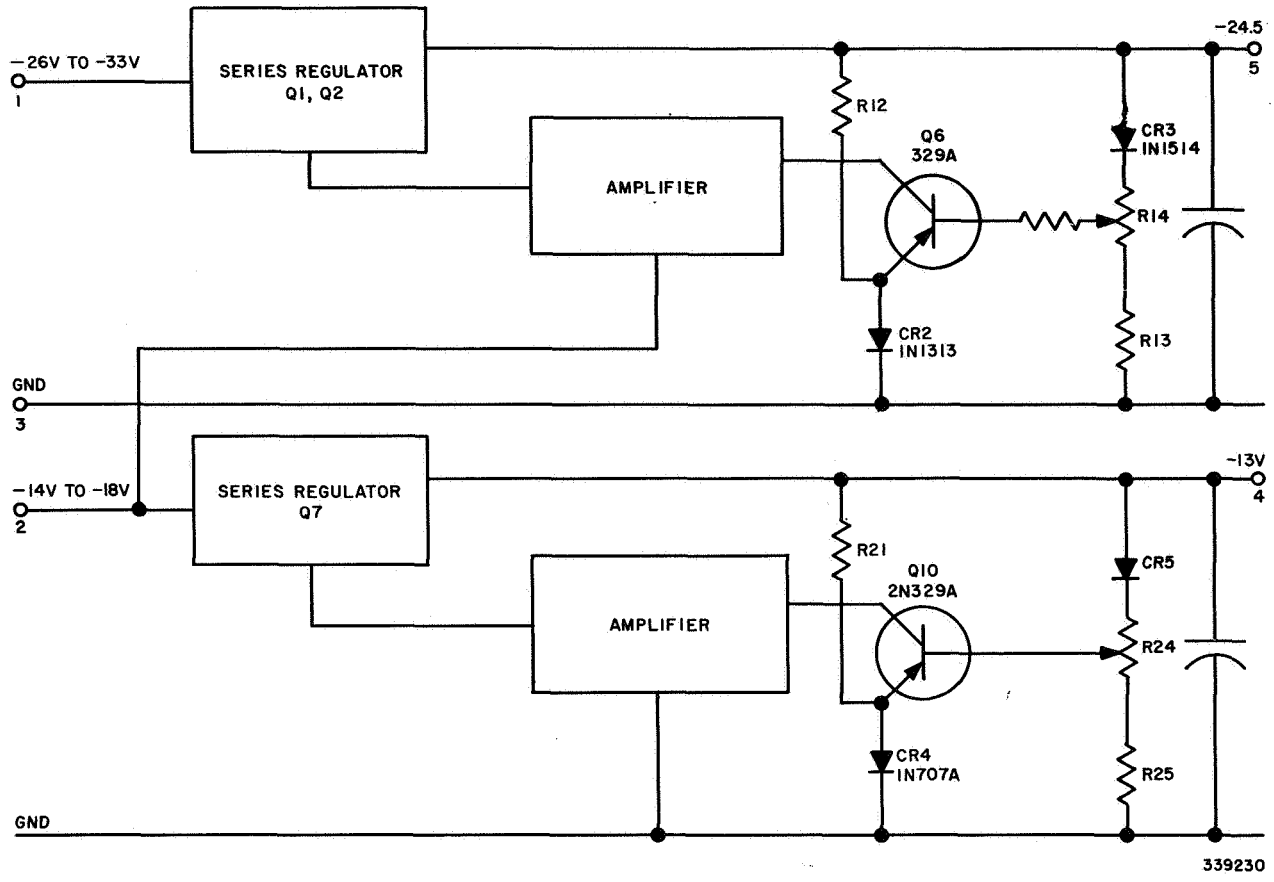

Figure 89. Voltage Regulators, Block Diagram

because the leakage current increases exponentially with temperature and other parameters undergo drastic change with higher temperatures.) To provide better transistor cooling, several means of providing a more intimate contact from transistor case to regulator chassis were tried. The chassis was milled flat and a thin, mica washer was installed. A considerable, but not a sufficient, improvement of the thermal gradient was noted. A final approach was the use of a 1/4-inch thick aluminum heat sink with an area of approximately eight square inches. The high-power transistors were mounted directly to the heat sink; this provided an intimate contact with a low thermal gradient. The entire heat sink was then bonded to the regulator chassis with alumina-filled epoxy resin. Further thermal-vacuum tests indicated satisfactory heat transfer and elimination of the high junction temperatures for the expected thermal environment.

A similar regulator circuit for the - 13-volt input to the satellite clocks was mounted on the same chassis as the - 24.5-volt unit. The reduced current requirement permitted the use of one transistor as the series element in this circuit. This was driven by a similar transistor and two low-power, d-c amplifiers. R-C frequency compensation was included in the amplifier stage to eliminate undesirable oscillations. No problems were encountered in adding the - 13-volt circuit because the proven design features of the - 24.5-volt unit were utilized wherever possible. The thermal problem was not encountered with this regulator because the maximum load current was only 0.5 ampere; therefore, normal power-transistor mounting (with a mica washer for electrical isolation) were used.

The final voltage-regulator chassis contained one - 24.5-volt and one - 13-volt regulator. The schematic diagram of these regulators is shown in Figure 90. Two such units were installed in the satellite.

The regulator chassis was placed in the small vacuum chamber for thermal-vacuum tests. An external nickel-cadmium battery, with characteristics similar to the satellite battery pack, was used as a power source. Charging was maintained and the battery was discharged through the regulator under test, utilizing a program similar to actual orbit conditions with regard to amplitude and duration of cycling the load current. No complications arose during the unit testing. When the regulator units were subjected to standard unit-vibration tests, each unit performed satisfactorily; therefore, no circuit changes or redesign were necessary.

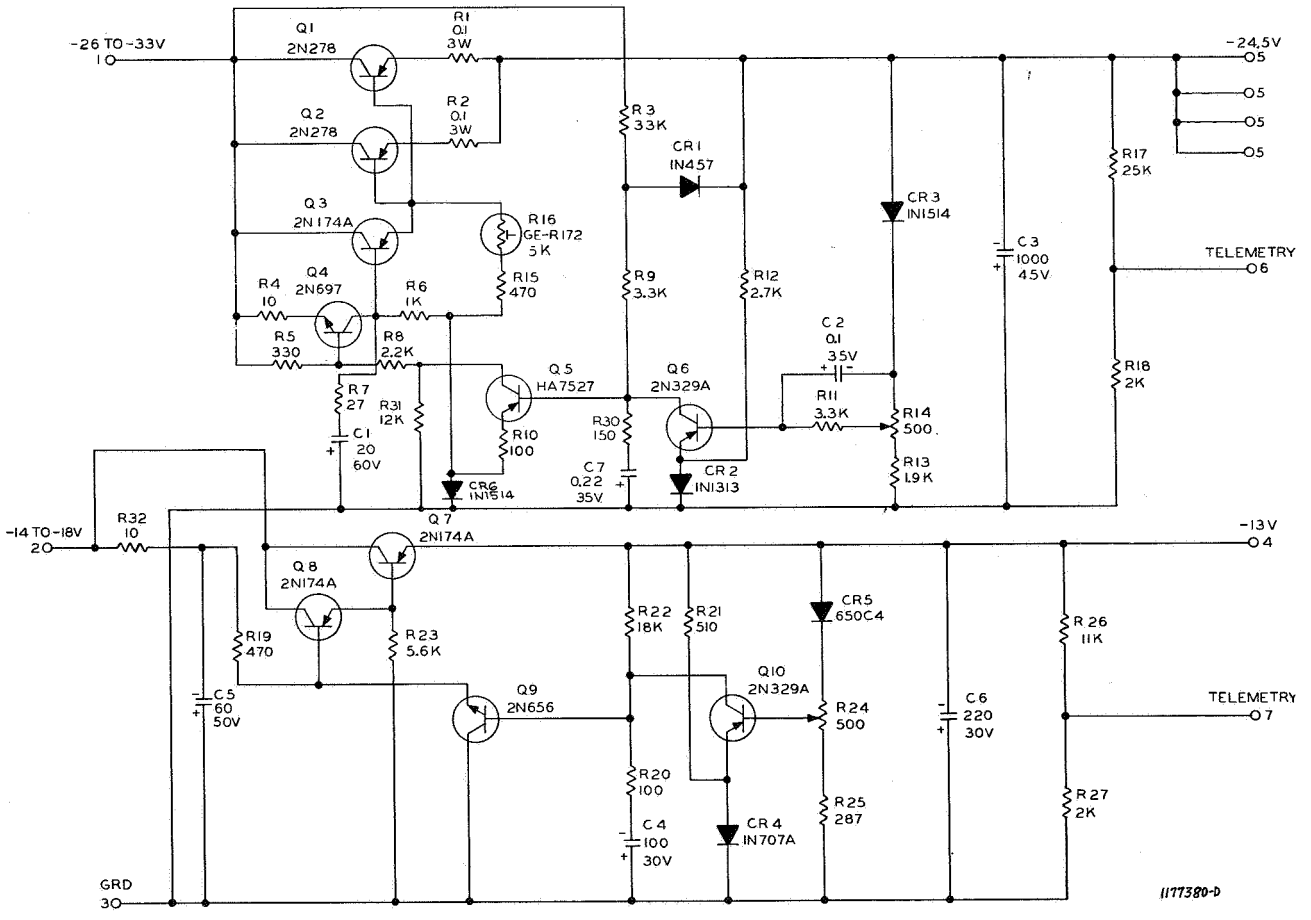

NOTE:
ALL CAPACITORS IN UF UNLESS OTHERWISE NOTED.
ALL RESISTORS IN OHMS UNLESS OTHERWISE NOTED.
BOARD & CHASSIS - 1176238
PARTS LIST SEE A-1170437

Figure 90. Voltage Regulators, Schematic Diagram

The voltage regulator sub-system performed in accordance with the initial specifications. (Ref. 11) The noise on the output line was considerably reduced. Requirements for voltage stabilization, in each subsystem operating from the regulator, were eased. This resulted in improved operation for various critical-gain and time-constant circuits. The effective power-supply impedance was reduced to the point where it caused no major problems.

(f) Auxiliary Voltage Regulator

The - 14-volt taps on the battery pack had been eliminated to simplify the charging paths and to provide equal charge in all cells in a particular series string. The maximum input voltage that could be applied to the - 13-volt regulators, for the satellite clocks, was approximately -18 volts. A one-stage, single-transistor regulator was designed to be placed in series with the input lead to the clock regulator. Two of these regulators, one for each satellite system (identified as VR-2), are packaged together and are shown in Figure 91 schematically. The circuit is actually a high-power emitter-follower configuration in which the load voltage follows the base voltage. The Zener diode maintained the base at -15 volts, which is approximately the same voltage that is supplied to the standard satellite regulators. This design proved to be ample for providing the 0.5-ampere clock current without further modification. The standard vibration and thermal-vacuum tests were completed without any need for modification.

(3) Load Protection Fuses

The current limiters and load diodes eliminated six of the fuses which were formerly used in the power-supply subsystem. In the final design, seven pyrophoric fuses were used to protect the power supply in the event of a subsystem or component failure. Five 12-ampere fuses were used in the two unregulated and two regulated lines for the TV camera systems, with a common fuse in the line for the auxiliary-control functions. A 1.2-ampere fuse was used in series with each of the power circuits for the clocks. An unfused line was provided for the lift-off switch for ordnance firing which followed the separation sequence of payload from the third-stage rocket.

Some speculation arose concerning the actual rating of the fuse wire installed. Repeated tests were performed in a vacuum, with low values of current, for longer periods of time than had been used previously. The results indicated that the actual rating of the fuses, after handling, soldering, and aging, was approximately one half the expected value. The fuses were then rewired, using two conductors in parallel for each 12-ampere fuse and three conductors in parallel for each 1.2-ampere fuse.

g. Final Design

The battery protection circuits, as shown in Figure 91[§], represent the final circuit configuration used for the satellite. All of the objectives established, after abandoning of the initial concept in December 1959, have been successfully fulfilled. The three series-strings of cells in the battery were adequately isolated during charge as well as discharge. Charging current was regulated and an equal state of charge could be maintained in each usable cell in the battery pack. Circulating currents were eliminated

[§] This illustration is printed on a foldout page, located at the rear of this volume.

through the use of six diodes in the charge and discharge paths. The loads were drawn through fuses designed to withstand a considerable short-time overload before breaking the circuit to the defective subsystem and subsequently allowing the satellite to operate on a reduced-mission basis. The voltages of each battery string and the load bus were telemetered to the ground station. Observation of this telemetry report has indicated successful operation of the power supply during the useful life of the satellite.

h. Storage-Battery Procurement and Evaluation

(1) General

Prior to the start of the satellite project, a few "silicon solar-cell, nickel-cadmium storage battery" power supplies had been successfully operated. The Signal Corps designed such a supply for the Vanguard satellite and the Bell Telephone Company supplied auxiliary power for a rural telephone system in Georgia.

Nickel-cadmium storage cells were employed primarily because of the relatively high number of charge-discharge cycles they could provide compared to other storage systems. In addition, their sealed construction obviated vacuum and electrolyte problems. Other storage systems such as silver-zinc, silver-cadmium, nickel-iron, and lead-acid batteries were eliminated from consideration because of one or more of these reasons: (1) low cycle life, (2) vented construction which allows gassing, (3) requirements of periodic maintenance, and (4) poor low-temperature performance.

In the spring of 1958, an order was placed for the Gulton Industries 4.0 ampere-hour, sintered-plate, nickel-cadmium storage cell. This cell was rectangular in shape. Internally, the electrodes were flat plates separated by a paper material which also served the essential function of holding the electrolyte (potassium-hydroxide solution) in intimate contact with the plates. On the top of the cell, positive and negative terminals were brought out from the plates. Between these terminals on the cell top, there was an opening through which electrolyte was introduced to the cell. This filler vent was sealed by means of a rubber washer which was held securely in place by a screw.

The nominal capacity of this cell was 4.0 ampere-hours or more at discharge rates of up to 4.0 amperes. The nominal cell weight was 181.6 grams (0.40 pound).

In mid-1958, a number of battery tests were planned for the succeeding months. Some of these tests were performed by the Applied Science Corporation of Princeton under the technical direction of RCA. The storage cells successfully passed the vibration, shock, and acceleration tests. However, at the conclusion of a storage test at 10^{-5} mm Hg for 100 hours at 26°C, corrosion was observed to have occurred about the filler cap of one cell and leakage was observed around the negative terminal of a second cell. In addition, it was found to be extremely important that both electrical terminals be securely tightened to prevent leakage or corrosion.

The RCA tests consisted of delivering a constant-current charge to bring the storage cells to a state of full charge, followed by a constant current discharge. Tests were run at normal atmospheric-pressure temperatures of +20°C, +40°C, +60°C, and +80°C. The results of these tests are listed in the following table.

Storage Cell Temperature °C	Constant Continuous Charge Rate in Amperes	Total Ampere-Hour Input	Constant Continuous Discharge Rate In Amperes	Total Amp.Hours Including All Energy Delivered At 1.20 Volts	Total Cells Tested
80°	1.0	5.0	3.7	0.77	10
60°	1.1	5.5	3.8	2.54	10
40°	1.0	5.0	3.7	3.35	10
20°	1.1	6.0	3.85	3.85	5

Two major defects with the Gulton cell became apparent as a result of the testing program. First, corrosion and/or leakage occurred at the electrical terminals and at the filler cap. Secondly, the sides of the cell bulged severely at charging rates of 0.50 ampere and above.

These problems caused an additional investigation of the availability of sealed nickel-cadmium batteries. In December of 1958, RCA contacted the Sonotone Battery Corporation in Elmsford, New York. Sonotone revealed that they had developed a hermetically-sealed, F-size storage cell with an all-welded steel case and a glass-to-metal seal. The cell was cylindrically shaped, with essentially flat ends, making it a superior pressure vessel to the rectangular-shaped storage cell. The nominal capacity of this F-cell was 4 ampere-hours when discharged at a 0.8-ampere rate to an end voltage of 1.20 volts. At this time, Sonotone indicated that the F-cell was capable of withstanding considerable overcharge, perhaps by 10 to 100 times the energy required to fully charge the battery, with safety. These apparent advantages overcame such disadvantages as a weight per cell of about 0.5 pound (227 grams) which was 25% heavier than the Gulton storage cell, and the poor packing factor resulting from the cylindrical shape.

The electrodes of the F-cell consist of a spiral wrap of two positive and two negative plates separated from one another by a cellulose-acetate (paper) separator. In the assembly of the cell, this spiral wrap or core is forced into the cold-rolled steel (nickel-plated) drawn can (nominally 0.032-inch thick). A nickel tab was welded to the negative plates at the bottom of the core (end near the bottom of the drawn can). With the core in place, two thin welding rods were passed through a small opening in the core center, and the nickel tab at the core bottom was "blind welded" to the bottom of the drawn can. Similarly, another tab, welded to the positive plates, was located at the top of the core. This tab was visually welded to a metal pin or lug, supported by a glass-to-metal seal in a steel cover, which fit snugly into the can. The mating surfaces of the can and cover were welded closed. Nylon discs, with openings to permit passage of the nickel tab, were located at the top and bottom of the cell to prevent shorting of the plates to the can. An F-cell which has been cut open is shown in Figure 92.

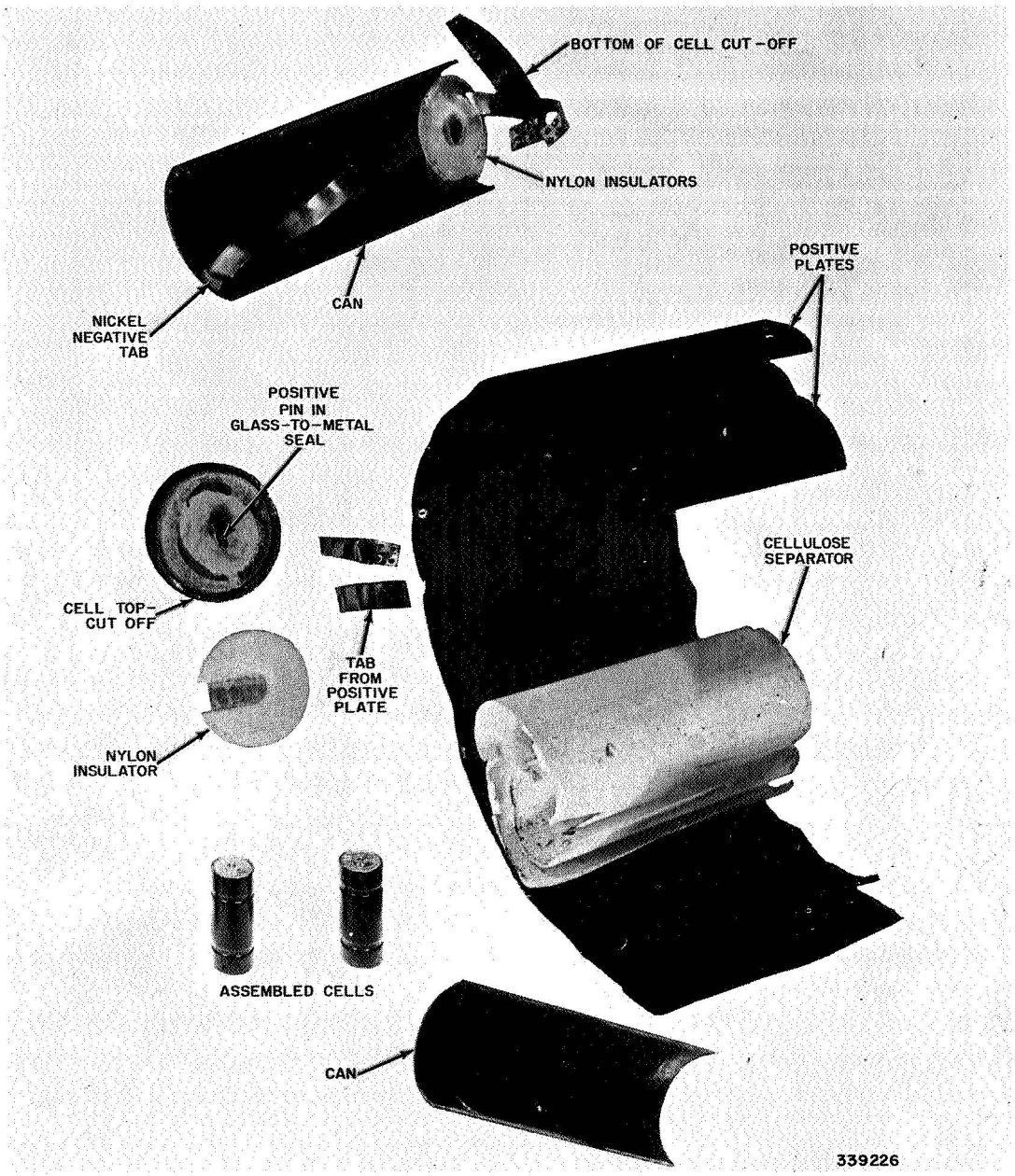

Figure 92. Cut-Open View of F-Cell

In early 1959, a large quantity of Sonotone storage cells were ordered, and testing was initiated in April of that year. These tests consisted of the following phases:

1. Each cell was dimensioned, visually inspected for leaks, and placed in a vacuum for several hours to ensure soundness of weld area.
2. Each cell received flight-satellite component vibration in accordance with Environmental Specification TSP T1-100B.
3. Storage cells were placed in oven or cold box to establish the battery temperature to be maintained throughout test. Tests were run at 0°C, +25°C, +40°C, and +60°C.

4. After the desired temperature was attained, a constant-current charge was delivered to the storage cells until full charge was reached.

5. Immediately upon conclusion of the charge, a constant-current discharge was initiated and maintained until the total row-voltage fell below an average of 1.20 volts per cell.

6. Those cells which performed according to specifications were accepted for satellite use.

In June 1959, the first indications of major problems with the F-cell became evident. Three rows of cells, each with 21 in series and receiving a total charge rate of 3.0 amperes or 1.0 ampere/row at 0°C, were under test. After 5.5 hours of charge, one cell developed a terminal voltage of 5.3 volts which was about 3.6 volts greater than any other cell under test. When the discharge was initiated, its terminal voltage went negative, indicating that a high internal resistance had developed inside the cell.

In July 1959, a group of 63 cells was charged at an average rate of 1.0 ampere at 25°C. Two storage cells developed abnormally high terminal voltages, (i.e., 2.70 and 1.95 volts). Each of these cells were cut open and inspected. It was observed that the weld, where the tab which connects the negative plate to the case, was not secure, and was making only pressure contact to the case, producing a high internal resistance. An additional group of 33 cells was charged at 1.0 ampere for 6 hours at +25°C. One cell developed 2.43 volts and another 1.61 volts upon charge. Each of these cells also exhibited a loose negative tab instead of a secure weld to the case.

Over 200 storage cells were fully charged and then discharged at 60 amperes to determine if high internal resistance was present. A poor electrical contact was observed by measuring an unusually large internal resistance voltage drop which occurred at a 60-ampere discharge rate and by heating at the bottom of the cell where the poor contact was located. The acceptable terminal voltage of storage cells was 0.35 volt after a nine-second discharge with no local heating. Unacceptable cells developed zero voltage within the nine seconds, became warm locally, or could not support a 60-ampere discharge.

The cell was redesigned through the cooperative efforts of RCA and Sonotone. The tab from the negative plate was still to be blind welded to the can as before, but the tab length was to be increased so that it could run up the side of the can. A second, but visual weld of the tab to the can was made at the top of the can. This ensured good mechanical and electrical contact. All cells which were subsequently purchased from Sonotone received a 60-ampere discharge, after being fully charged, for nine seconds. At the end of this time, the terminal voltage under load was required to be no less than approximately 0.5 volt, and no temperature rise greater than 30°F was to occur anywhere on the cell. The terminal voltage of 0.50 volt or greater corresponds to an internal voltage drop of 0.9 volt or less at a 60-ampere rate. Because a normal cell possessed approximately 10 to 15 milli-ohms internal resistance, it was reasonable to expect, at 60 amps, a loss of 60 (0.010) = 0.6, to 60 (0.150) = 0.9 volt. Testing of this improved cell was initiated in August of 1959.

The battery test procedure, described above, was modified because of this accelerated pace of the entire satellite program. Full charge-discharge tests were carried out at 0°C, 25°C, and +60°C. The ampere-hours required of each storage cell was 3.1, 3.5, and 2.5 at a discharge voltage of 1.20 volts or more per cell, at 0°C, +25°C, and +60°C, respectively.

In October 1959, the battery package in the T2 satellite was found to be defective upon the conclusion of prototype vibration. Each of the three rows showed open-circuit voltage, but when an attempt was made to load the battery, the terminal voltage decreased immediately toward zero. The battery was then removed from the satellite. Wiring and solder joints were carefully checked to ensure that the cause was not external to the storage cells. The storage cells were removed from the structure. It was observed that a large number of the cells had bulged bottoms; these cells had been bulged in a full-charge/discharge test approximately two months earlier. One of the bulged cells was cut open as shown by the dotted lines in Figure 93. Both sections A and B fell free from their tabs without an external force being applied. Thus, it was reasoned that the positive tab was merely in a pressure contact with the positive pin which gave rise to a high-resistance connection. Although the section labeled "B" came loose from the negative tab, the second connection at the cell top, described earlier, still provided adequate connection from the external negative termination to the negative plates. A second bulged cell was placed on charge at 500 milliamperes and shaken simultaneously by hand along the axis of the cell. During this light vibration, the charge current became intermittent, varying between zero and 500 milliamperes, indicating alternate making and breaking of the internal storage-cell circuit. A total of 51 of the 63 cells, comprising the T2 battery, were inspected; forty were found to be bulged. Of these, it was determined, by hand vibrating each cell, that 34 had loose cores. Thirteen of these cells charged intermittently when hand vibrated. The remaining 11 cells were not bulged, but five had loose cores and one of these charged intermittently when it was hand vibrated.

The problem, therefore, was clear. A storage cell with a flat bottom could have a loose core which could cause, during vibration, the fatiguing and breaking of the internal positive-tab connection ot the positive pin. Secondly, bulged cells are more susceptible to the development of loose cores because of the added room available for motion of the core when the bottom is bulged out. In this case, internal connection to

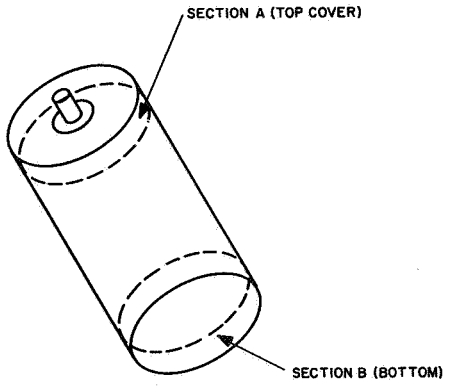

Figure 93. Positions at which Storage Cells were Cut to Determine Connection Integrity

the positive pin would also fail. In the case of all cells which were cut open and inspected, secure connection of the negative tab, from the plates to the can, was always present.

Immediately, the Sonotone Corporation was consulted about the failure and methods of correcting it. It was decided that two grooves should be rolled circumferentially into the can to hold the core securely in place. The location and depth of the grooves were decided upon and appear in Figure 94. Sonotone began production of these revised F-cells which were called crimped cells.

Meanwhile, at RCA, tests were underway to determine if crimping would hold the core securely in place. Seven cells with flat bottoms were mounted in the submodule battery structure and subjected to a 25-g random-noise vibration at frequencies of from 20 to 2000 cps along the thrust axis of the submodule package. Similarly, seven bulged and seven crimped, unbulged cells were so tested. Table 2 summarizes pre- and post-test findings. During the vibration test, the storage cells were charged continuously at about 0.500 ampere. Individual cell voltages were automatically and continuously recorded. In this way, the development of an open-circuited or high internal-resistance cell was observed almost immediately.

The test results indicated that vibration of a cell which had a bulged bottom was certain to result in the production of a broken internal contact, and cells which had flat bottoms also permitted relative motion of the can and core which also resulted in a borken internal contact. The crimped cells, however, showed no evidence of failure during or after the vibration tests.

After initial shipments of crimped cells were received from the manufacturer, additional vibration tests were performed. Two groups of seven cells each were prepared. One consisted of bulged cells which were crimped, and the other consisted of flat crimped cells. Each group was vibrated at a 25-g random noise level at frequencies from 20 to 2000 cps for 32 minutes while under charge. No unusual performance was observed in these two tests; the effectiveness of the crimp holding the core was clearly demonstrated.

These tests demonstrated the ability of the crimp to hold the core securely in place and to prevent breaking of the internal connections between the positive plates

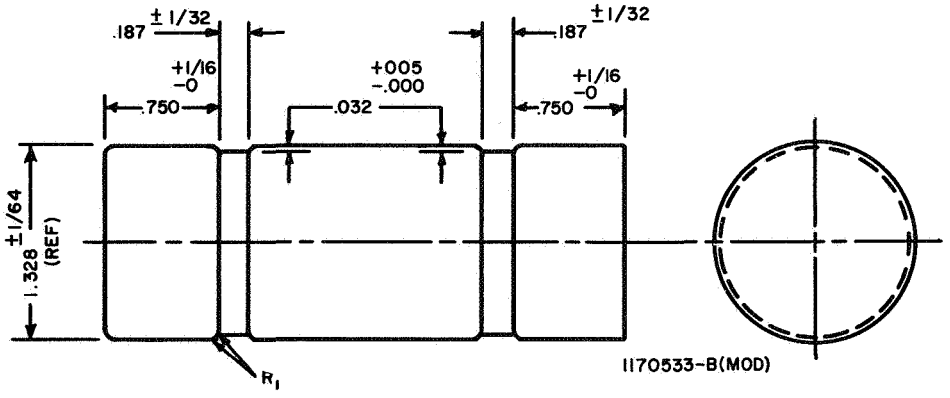

Figure 94. Location and Dimensions of Crimped Grooves

Table 2. Vibration Tests of Various Storage-Cell Types

	Cell No.	Pre-Vibration Characteristics		Time to Failure* During 25 g Vibration	Post Vibration Characteristics
		Core	Charge		Core
Flat Cells Uncrimped	562	Loose	Steady when vibrated**	13 minutes	Loose
	535	Secure	Steady when vibrated	10 minutes	Loose
	546	Secure	Steady when vibrated	(did not fail	Loose
	571	Secure	Steady when vibrated	after 30	Secure
	557	Secure	Steady when vibrated	minutes)	Secure
	559	Loose	Steady when vibrated	13 minutes	Loose
	558	Loose	Steady when vibrated	10 minutes	Loose
Bulged Cells Uncrimped	517	Secure	Intermittent when vib**	All cells	Loose
	536	Loose	Intermittent when vib	failed	Loose
	518	Loose	Steady when vibrated**	within	Loose
	539	Loose	Steady when vibrated	one	Loose
	547	Secure	Steady when vibrated	minute	Secure
	520	Loose	Steady when vibrated		Loose
	528	Secure	Steady when vibrated		Secure
Crimped Not Bulged Cells	863	All	Steady when vibrated**	No cell	All
	797	cores	Steady when vibrated	failed in	cores
	790	were	Steady when vibrated	30 minutes &	securely
	872	secure	Steady when vibrated	15 seconds	held
	793		Steady when vibrated	of vibration	
	778		Steady when vibrated		
	798		Steady when vibrated		

* Failure is defined as the occurrence of a high internal resistance or open circuit.

** Vibration in this case was a shaking of the cell, by hand.

and the positive terminal. It was the consensus, on the part of Sonotone and RCA personnel, that the occurrence of bulging was, therefore, no longer detrimental to storage-cell performance.

On 14 December 1959, long after three flight and two prototype satellites had been supplied with storage batteries, the final major failure occurred. The storage battery on the T2 satellite failed after a few days in a thermal vacuum at +55°C. The three rows of storage batteries developed total voltages, on open circuit, of 23.1, 21.9 and 20.3 volts instead of a nominal value between 26 and 28 volts. The electrical characteristics of each of the individual cells were then measured; eleven cells were found to be shorted internally. An additional 39 cells showed unusually high terminal voltage when charged at 1.0 ampere at +25°C. A considerable number of these cells were cut open in the presence of RCA, Fort Monmouth, NASA, and Sonotone representatives. Every cell which was cut open contained a deteriorated separator material. The cellulose-acetate separator had a "cheese" consistency which accompanied a loss in strength and reduced ability to hold the potassium-hydroxide electrolyte.

At this time, it was felt that a comprehensive re-evaluation of storage battery requirements, performance, and failures was called for. A comprehensive program was initiated to attempt to reproduce the conditions which surrounded the failures, and initiate a redesign which would again permit confidence in future battery performance.

(2) Comprehensive Storage Battery Test Program

(a) Purpose of Test

Following the failure of the storage battery in the T2 satellite, it was decided to subject the T1A vehicle to a vacuum-thermal environment while duplicating both the programming and charging-duty cycles of the satellite. The purpose of this orbital simulation test was to reproduce the T2 failure, detect the cause of the failure, and observe the sequence of events which led to the bulging and electrical deterioration of the batteries.

(b) Thermal and Electrical Equilibrium Test

1. Purpose - The initial test performed preceded the orbital-simulation test, and was designed to establish electrical and thermal equilibrium of the battery package.

2. Test Conditions - The storage batteries were charged at the full-voltage level at a total of 1.0 ampere to the three rows (or 0.33 ampere average per row). No charging was carried out at the half-voltage level.

One direct mode and one playback every two hours.

a. Direct Mode: Seven minutes duration with shutter pulses every 30 seconds.

b. Remote Mode: Two systems.

c. Playback Mode: Duration of about three minutes; include setting of two clocks.

The baseplate temperature was raised to +50°C and the satellite was operated at the above conditions until the thermal and voltage conditions became repeating for four hours.

3. Test Results - The results of the thermal- and electrical-equilibrium tests are listed here.

Elapsed Time After Start of Test In Hours	Baseplate Temperature Average Value In Degrees C	Battery Temperature Average Value In Degrees C
1 1/2	46	46
4	48	48

Thermal equilibrium was established, and the battery data (not shown) indicated that the power supply (excluding solar cells) was performing satisfactorily.

(c) First Orbital Simulation Test

1. Test Conditions - At the full-voltage level the charge rate was 1.5 amperes total to the three rows (or 0.500 ampere average per row). At the half-voltage level, the charge rate was 0.45 ampere total to the three rows (or 0.150 ampere per row). The total orbit time was 100 minutes (period of a satellite at 380 nautical miles circular orbit). The satellite was considered to be illuminated 80% of the time or 80 minutes. Thus, each orbit consisted of 80 minutes of charging at the rates given above and 20 minutes of no charge.

One direct mode and one playback in every orbit.

a. Direct Mode: Duration of five minutes per orbit.

b. Remote Mode: Two systems

c. Playback Mode: Two systems playback for about 4 minutes; set both clocks.

Programming of these modes was carried out only during the 80-minute charge period.

Because this orbital-simulation test followed without interruption the thermal- and electrical-equilibrium test, the baseplate had an initial temperature of approximately 50°C.

2. Test Results - The data recorded with time = zero at the start of this second test are as follows:

Elapsed Time After Start Of Test In Hours	Baseplate Temperature In Degrees C	Battery Temperature In Degrees C
2 1/2	44 to 50°C	50 to 53°C
4 1/2	43.3 to 49.4°C	51.1 to 60°C

The temperature values given show the maximum and minimum readings of the various thermocouples which were used to read the temperatures of the baseplate and batteries.

Note that the battery temperature exceeded the maximum baseplate temperature by as much as 10.6°C. These high temperatures occurred simultaneously with, and were related to, the electrical failure of five storage cells in one of the three rows of batteries. Upon removal of the satellite from the chamber, it was observed that the failure of the cells was due to the shorting of wires on the instrumentation employed to monitor the individual cell voltages in this test. The cause of the instrumentation failure was attributed to human error.

(d) Second Orbital Simulation Test

The instrumentation which failed during the first orbital simulation test was repaired and the orbital-simulation test resumed.

1. Test Conditions - These are the same as those given under the first orbital simulation test. Orbital simulation in programming was started when the baseplate attained a 50°C temperature orbit.

2. Test Results - The data recorded is summarized in Tables 3 and 4. Interpretation of Table 3 - The column headeds''Orbit Number'' gives the identifying number of the specific orbit or range of orbits for which temperature and battery data are provided. Various orbits, such as 2-5 and 10-19, are grouped together whenever these orbits had common programming loads and/or included those time intervals when the baseplate was undergoing a temperature change. With the excep-

TABLE 3. SECOND ORBITAL SIMULATION TEST

Orbit Number	Baseplate Temperature, °C				Battery Temperature, °C			Full Battery Voltage		Half Battery Voltage		Type of Program
	Range	Avg.	When Taken	Remarks	Range	Avg.	When Taken	Max.	Min.	Max.	Min.	
1	43-39	46	Start of Orbit 1		47-48	47.5	Start of Orbit 1	28.4		15.0		Remote, Direct Playback
2-5	44-49	47	End of 5		52-54	53	End of 5	529.6	27.1	14.5	15.6	Remote, Direct Playback
6-8	44-49	46	End of 8		51-55	52.5	End of 8	29.5	28.5	15.7	15.0	None
9	No Significant Changes From #8							29.6	28.0	15.6	14.8	Remote, Direct Playback
10-19	0-7	2	End of 19	Temp. lowered to 0°C	8-12	10	End of 19	In Orbit 19 Only 30.7	28.4	16.3	15.1	Remote, Direct Playback
20	-1 to +8	3	In 20		10-13	11.5	In 20	33.0	28.0	15.4	15.0	Remote, Direct Playback
21-23	-1 to +8	2.5	End of 23		13-19	15.5	End of 23	32.6	28.9	17.1	15.3	None
24	No Significant Changes From No. 23							32.2	28.0	16.7	14.7	Remote, Direct Playback
Interruption of Orbital-Simulation Test for Three hours	During This Three Hour Period One Row of Batteries Was Charged Continuously at a 1.5-Ampere Rate. Data From This Test Appears in The Table #4. The Other Batteries Were Not Charged in This Period.											
25	1.5-10	No data	In 25		14-28	No data	In 25	29.0		15.3		Remote, Direct Playback
26	4-7	5	In 26	Raise to Temp. to 50°C	16-25	18.5	In 26	28.3		14.9		Remote, Direct Playback
27-30	48-53	51	In 30		44.51	46.5	In 30	27.6	27.0	14.6	14.4	Remote, Direct Playback

tion of the interruption of the orbital-simulation test which is noted in the table, the separate orbits were run consecutively. The column headed baseplate temperature provides the following data:

(1) The maximum and minimum baseplate temperatures.

(2) The average value of the baseplate temperature.

(3) The specific orbit or part of the orbit where the temperature data was recorded.

(4) The column headed "Remarks" is used to indicate when changes in the baseplate temperature were initiated.

The column headed "Battery Temperature" provides data in the same manner as described for the baseplate.

The columns headed "Full Battery Voltage" and "Half Battery Voltage" give the maximum and minimum battery voltages for the specific orbit or range of orbits indicated in the orbit number column.

The column headed "Type of Program" indicates the nature of the programming load for the specific orbits for which temperature and electrical data are given.

(e) Summary of Storage-battery Tests

From Table 3 it can be seen that, during the first nine orbits, with a maximum baseplate temperature of +49°C, the batteries reached an equilibrium temperature of about +53°C. Terminal voltages were generally stabilized even though programmed loads varied between the extremes of no loading for three consecutive orbits to normal programming outlined in the test procedure. Between orbits 19 and 24, with an average baseplate temperature of +3°C, the storage batteries were stabilized at a minimum of +8°C. Again, battery terminal voltages were relatively stable, Between orbits 24 and 25, an attempt was made to bulge the storage batteries by charging at a 0.5-ampere rate per row continuously. In orbit 26, the baseplate temperature was raised rapidly to +50°C, and in orbits 27 to 30, the average battery temperature was +46°C. The battery voltages were normal throughout this period. The results of orbits 1 through 9, and 19 through 24 demonstrated that battery thermal equilibrium had been established with the baseplate at +49°C and +3°C respectively. Even when all loading was cut off so that the batteries received an overcharge, thermal equilibrium was maintained. Thus, although the battery was undergoing over-charge and the entire input energy was being converted into heat, thermal equilibrium was maintained. The purpose of the continuous three-hour charge at 0°C was to cause bulging of the storage-cell bottoms. It was hypothesized that bulging of the storage cells in the T2 satellite, at 0°C, had broken the aluminum-loaded epoxy, thermal path from the batteries to the baseplate, and when the baseplate was subsequently run at +55°C, the batteries were unable to "dump" the internally generated heat into the baseplate. This presumably caused the interior of the storage cells to run extremely hot (+55°C) and broke down the cellulose separator.

TABLE 4. CONTINUOUS THREE-HOUR CHARGE TEST AT 0° C

Time After Start of Test In Hours	Baseplate Temperature, °C Range Average	Battery Temperature °C				Type of Program
		Temperature of Cells Under 1.5-A Average Charge	Average of 4 Cells	Temperature Range of Cells Not Under Charge		
				Range	Average	
1	2-9 4	21, 29, 35, 38	31	14-21	16	None
3	0-9 3	22, 32, 40, 44	34.5	17-25	19	None

However, in the test of the T1A battery, no such failure sequence was observed when the baseplate temperature was subsequently raised to +50°C.

This test reaffirmed the soundness of the battery-jacket thermal design approach, but the T2 failure condition was not reproducible. The reason for the T2 failure became apparent, however, in the weeks which followed. During this period, it was decided, however, to redesign the battery submodule packages so that the bottoms of the storage cells would bulge into a recess and not cause damage to the thermal heat sink arrangement for the storage cells.

When inspected, the cellulose separators of the Sonotone storage cells, which were removed from the T2 battery package which failed, showed a deteriorated condition. NASA, the Signal Corps, Sonotone, and RCA decided that a series of systematic tests were required to determine the safe maximum charge rate for +55°C operation. In January of 1960, these tests were initiated at the Sonotone Corporation in Elmsford, New York.

The first of thest tests was designed to determine the effect of soaking the separator in a potassium-hydroxide (KOH) solution at different temperatures. Soak temperatures of 40°C, 50°C, 55°C, 60°C, 75°C, and 85°C were tried. After soaking in the KOH solution for 64 hours at 85°C, some reduction in separator strength was observed with a somewhat lower loss in strength at 75°C. At 60°C and lower, no significant loss in strength was observed after a seven-day soak period. These tests demonstrated that, at temperatures of +55°C or lower, soaking of the separator in a KOH solution causes little deterioration in separator properties within a period approximately equal to that in which the T2 battery had failed.

The second test was designed to determine the effect of simultaneous battery charging (at a 660-milliampere rate) and operation at different discrete temperature levels upon the performance of the storage cell. The 660-milliampere rate was selected because this was the absolute maximum rate at which any row of storage batteries would be charged in actual flight, and it was approximately the same charging rate which was employed in thermal-vacuum tests. Four groups of batteries, each containing five cells, were employed in the test. Each group of cells was maintained at a different fixed temperature, including +35°C, +40°C, +45°C, and +55°C. At 35°C and 40°C, little, if any, deterioration in performance occurred after 14 days of continuous charging. At 45°C, however, extremely high terminal voltages were developed after five days, and the existence of unusually high internal pressures was evidenced by bulging of the tops of most of the storage cells (caused by 1600 PSI) and bulging of the bottom of the cells (caused by 400 PSI). After 13 days, three cells showed a terminal voltage of nearly zero. The remaining two cells had a considerably reduced ampere-hour capacity. By this time, all cells were bulged at the top and the bottom. At +55°C, all five of the cells developed a very high terminal voltage, all bulged at the top and the bottom, and three had unusually low ampere-hour capacities. Electrically, the cells from the 50°C and 55°C tests exhibited the same characteristics as the T2 storage cells. From these tests, it became apparent that operation of the cell with the paper separator, at temperatures in excess of 45°C for periods of two weeks at a charge rate of about 600 to 700 milliamperes, is detrimental to performance.

Finally, one additional test was performed: the purpose of this test was to find the maximum safe charging rate at +55°C. Five groups of storage cells were assembled, and five different charge rates, (250, 350, 450, 550, and 660 milliamperes were employed. After five days, none of the cells exhibited deteriorated electrical performance during charge or during a short discharge. In addition, no bulging was observed. After 12 days, degraded performance had occurred in all groups except the group which was charged at the 250 milliampere charge rate. There was a prevalence of bulging in the groups at the lower charge rate; this was not expected. It was apparent that the small sample size, that is, five cells per group, was yielding poor statistical results. After 21 days, the number of bulged cells and the degree of bulging increased with increasing charge rates.

These test results can be summarized as follows: Storage batteries with cellulose separators which were subjected to high charge rates, at temperatures in excess of 45°C, developed excessively high internal gas pressure (caused by the combination of the high charge rate and high temperature) which can cause bulging of the cell bottoms and tops. Bulging at the cell top can cause shattering of the glass-to-metal seal, extreme gassing, and deterioration of performance. More important, the high temperatures which are developed inside the cell at the high charge rate, in combination with the oxygen gases formed during overcharge, will oxidize and deteriorate the cellulose separator. The resulting failure was shown by the occurrence of very high or low voltages during charge and very low voltage during discharge. This indicated that some cells were internally shorted whereas others had developed high internal resistances.

On the basis of the Sonotone test program and calculation of the current rates necessary to recharge the storage batteries for the equipment-programming rates expected in actual orbit, it was decided to limit the maximum recharge rate, for each row of batteries, to 440 milliamperes. The Sonotone tests were continuous-charge tests, interrupted only periodically for short discharges, and, as such, represent a greater stress on the storage cell than vacuum-thermal tests or actual orbital conditions, where the charge is interrupted in the main for about 30 minutes out of every 1.5 hours. To obtain this limiting function, a charge-current limiting circuit was incorporated into each of three rows of storage batteries.

i. Solar-Cell Test Program

(1) Physical Inspection

Solar cells, in five-cell shingle arrays were used to convert the solar radiation to electrical energy. Each satellite had a total of 1824 shingles bonded to the top and side structure.

Because the dimensional tolerances on the length, width, and the positive and negative locations were rather close on the shingle, a small, master Go, No-Go test fixture was fabricated to check dimensions. The shingles were received from the vendor (International Rectifier Corporation) in small shipments of 50 to 300 pieces. Each shingle was visually inspected for cracks and blemishes in the cover glass. Then each

shingle was carefully inserted into the Go, No-Go fixture to ensure proper dimensions and tab location. In this initial inspection phase, the quality of the shingles was very poor. Most of them were found to have blemishes under the glass covers. Because time was an important factor, these blemished shingles could not be returned, but had to be considered acceptable.

A sample quantity of shingles from each shipment also had to undergo a simple, supported-beam bending test in which they were supported at the extreme edges of opposite sides while a 250-g force was applied at their centers. If the individual cells in the shingle did not separate at the solder joints, the shingles were considered acceptable.

After the mechanical and visual inspection, each shingle and its individual plastic shipping case was numbered.

(2) Electrical Tests

The next phase of the operation was the electrical acceptance test. A special mass solar-cell test fixture was designed, developed, and built in the model shop. The text fixture consisted of the following:

1. a light source consisting of a 24- by 24-inch board with provisions for mounting a maximum of 25 Tungsten-filament lamps (150-W and 300-W) regulated by a 5-kw, a-c voltage regulator.
2. a water filter, to absorb most of the lamp's infrared spectrum.
3. a sheet of pyrex glass.
4. a universal mounting board in the illuminated test area which was able to accommodate four racks of 15 shingles each, a mounting board with four modules, or a complete panel assembly.

The first and most time-consuming phase of the shingle-testing program was the achievement of a uniform illuminated area in the test fixture. A standard test shingle was calibrated with the use of a standard solar cell, which in turn was cross-checked and calibrated with solar illumination, Tungsten-lamp illumination, and International Rectifier Corporation standard cells. The standard shingle was then mounted on a slide rack and positioned in the illuminated area. At each location that a test shingle would occupy, the short-circuit current of the standard shingle was recorded. A total of 60 short-circuit readings were taken and then analyzed. High readings indicated illumination hot-spots. By a combination of aiming the lamps, adjusting the lamp voltages, and judicious use of clear Mylar tape to diffuse the light, a highly uniform, illuminated test area was achieved to within less than 1% variation. Because the short-circuit current readings (a measure of light intensity) are somewhat insensitive to temperature, the uniform light field was achieved first. Next, the test area had to be temperature controlled. The test area was made part of a plenum chamber, and with proper venting, ducting, and a room air conditioner, a temperature scan was made. A thermocouple was attached to the positive strip of the standard shingle. The shingle was inserted into the lighted area and allowed to stabilize. A temperature was recorded for each position that a test shingle would occupy. The temperatures varied from 26°C to

32°C. This was considered adequate for testing because the shingle conversion efficiency is rated at a temperature of 30° C ± 3° C. All of the adjustments were made only once. After the adjustment, each day of testing solar cells was preceded by a light-intensity scan with the standard shingle to check and determine the illumination level.

During the course of the shingle testing, the water filter became a source of major trouble. Initially, the water tank had provisions to continually circulate fresh water, but dirt in the incoming water necessitated a redesign. It was decided to fill the tank with distilled water and cool it with a heat exchanger. Copper tubing was installed along the top, sides, and bottom of the tank to provide a continuous flow of cold water within the tubes. This greatly improved the dirt problem; however, a bubble formation along the sides of the tank altered the intensity pattern of light uniformity. The final modification resulted in complete removal of the water-tank filter.

The individual shingles were carefully loaded in the test racks which were inserted into the illuminated test area. Cables were connected to the racks, and each shingle was tested at 1.85, 1.95 and 2.05 volts. The power at these three load points was recorded on shingle test-data sheets. From a set of efficiency charts, the conversion efficiency of each shingle was recorded on the data sheets. The shingles were then removed from the test racks, replaced in their plastic cases, and then sorted according to their efficiency value at a particular voltage.

(3) Assembly and Light Tests

Sixteen equal efficiency shingles rated at the same voltage were assigned to a module. A module was placed on an assembly fixture. Pre-cut pieces of glass-cloth epoxy were placed on the printed-circuit board, and the shingles were then carefully positioned on the epoxy. A fixture weight was placed on the shingles, and the assembly was placed in a 200°F curing oven for five hours.

After the curing process, the shingle tabs which protrude through the back of the printed boards and the exposed copper wiring of the boards were cleaned. The tabs were then bent to make contact with the printed circuit, and the 32 contact points were then carefully soldered, so that excessive heat would not be applied to the joint and cause the wiring to separate from the fiber-glass board.

The modules were then light tested. Current readings were recorded for voltages of 29.6, 31.2, and 32.8 volts, and the corresponding efficiencies, taken from the efficiency charts, were also recorded. Four modules of like efficiencies at the same voltage were assigned to a panel.

The bare panel was bolted to a fixture to prevent bowing. Pre-cut sheets of glass-cloth epoxy were placed on the panel. The modules were set on the epoxy, making certain that the module wiring pins were not in contact with the edges of the clearance holes in the panel. Mylar tape was placed over the modules to prevent the individual modules from slipping on the panel. The panels were placed in a 200°F oven for 5 hours.

After the oven curing process, the space between the shingles on the module board and the space between individual modules on the panel were filled in with a clear

epoxy (Hysol 6232). This was allowed to cure at room temperature. Also to prevent possible peeling at the edge of the modules, the four corners of each module were lashed down with 0.010-inch diameter steel wire and covered with clear epoxy.

Figure 95 shows a 1 x 2 cm solar cell, a five-cell shingle, a bare printed-circuit board, an assembled module board with 16 shingles, and an assembled side panel with four module boards.

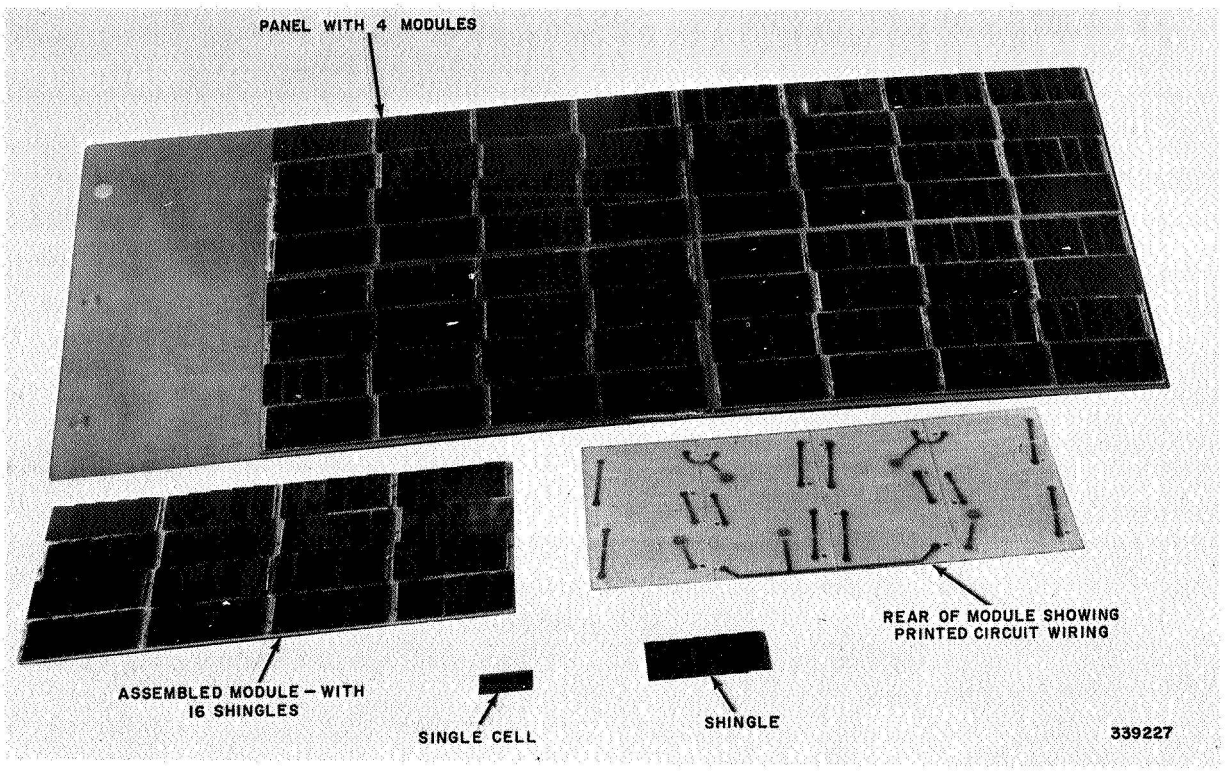

Figure 95. Solar-Cell Assembly Configurations

The panel was light tested, following the same procedure as for the individual module test, to ascertain that the module performance had not been altered during the final assembly and curing process. All four module boards on the panel were then wired in parallel.

To assemble the modules to the top surface of the satellite, a large template was made to accurately locate the module wiring pins with relation to the pre-drilled clearance holes. Pre-cut sheets of glass-cloth epoxy were then placed on the top surface, and the modules were set on this adhesive. To prevent any movement of these modules during the curing process, they were held in place by adhesive tape. The entire top was then placed in the large oven to cure for 5 hours at 200°F.

To enable light testing of the individual modules on the top surface, a portable light tester was designed and built to illuminate one module at a time. The light source consisted of two Tungsten bulbs (300 watts each), connected to a regulated a-c power supply. A glass filter was placed at some distance from the lamps to diffuse the light. A blower was mounted on the fixture and aimed at the module to be tested in an attempt

to keep the solar-cell temperatures near 30°C. A removable adaptor slide-board was used for mounting the standard solar-cell shingle to permit scanning of the illuminated test area in order to determine the uniformity and light-intensity level. This slide-board was removed, the light tester was positioned to illuminate one module, and the outputs for various voltages were recorded. The light was then moved and positioned on the next module. This procedure was repeated until all of the modules on the top had been tested.

The module connecting pins on the underside of the top surface and the back side of the panel were color tested to facilitate the correct parallel wiring of the modules.

After the wiring was completed, another light test was performed on each wired panel and on each sub-group of four modules on the top surface.

The following is a brief summary of the results indicated by the light tests on the solar cells:

1. the average conversion efficiency of a group of more than 10,000 shingles tested was approximately 7.8% at 30°C
2. the average conversion efficiency of a group of more than 600 module boards tested was approximately 7.5% at 30°C
3. The assembled panel average conversion efficiency was approximately 7.3%. It should be realized that this number includes the effects of diodes in the circuit, filter covers on the solar cells, and the inevitable mismatches in the individual current-voltage characteristics of the shingles.

(4) Final Tests

The final test was performed out of doors on a clear, cloudless, bright, sunny day. By making connections to the main connector plug, any number of panels could be tested individually or in groups. By positioning the panel normal to the sun's rays, using a "standard" calibrated solar cell to give instantaneous readings of the illumination level, fairly accurate tests of the panels were accomplished. These results verified the results obtained from the indoor tungsten-light tests. In addition, two other tests were performed. After covering the side surface and positioning the top surface normal to the sun's rays, the total output of the top solar cells was measured and recorded. Next, the top surface was covered, the side surface was positioned normal to the sun's rays, and the total output of the illuminated projected area of the side panels was measured and recorded.

One additional indoor test, the telemetry module calibration test, was performed An 80-cell module board on a side panel, and a 60-cell module board on the top surface were assigned solely for voltage sampling of the output of the solar-cell collector. The main indoor solar tester was modified so that the telemetry modules could be cycled over wide temperature extremes. It was decided to read the voltage of the telemetry module across a fixed, calibrated resistor, for various illumination intensity levels and a wide range of temperatures. For intensity levels of 90 to 130 mw/cm^2, the voltage was recorded for temperatures over the range of -10°C to +70°C and a graph of these values was constructed.

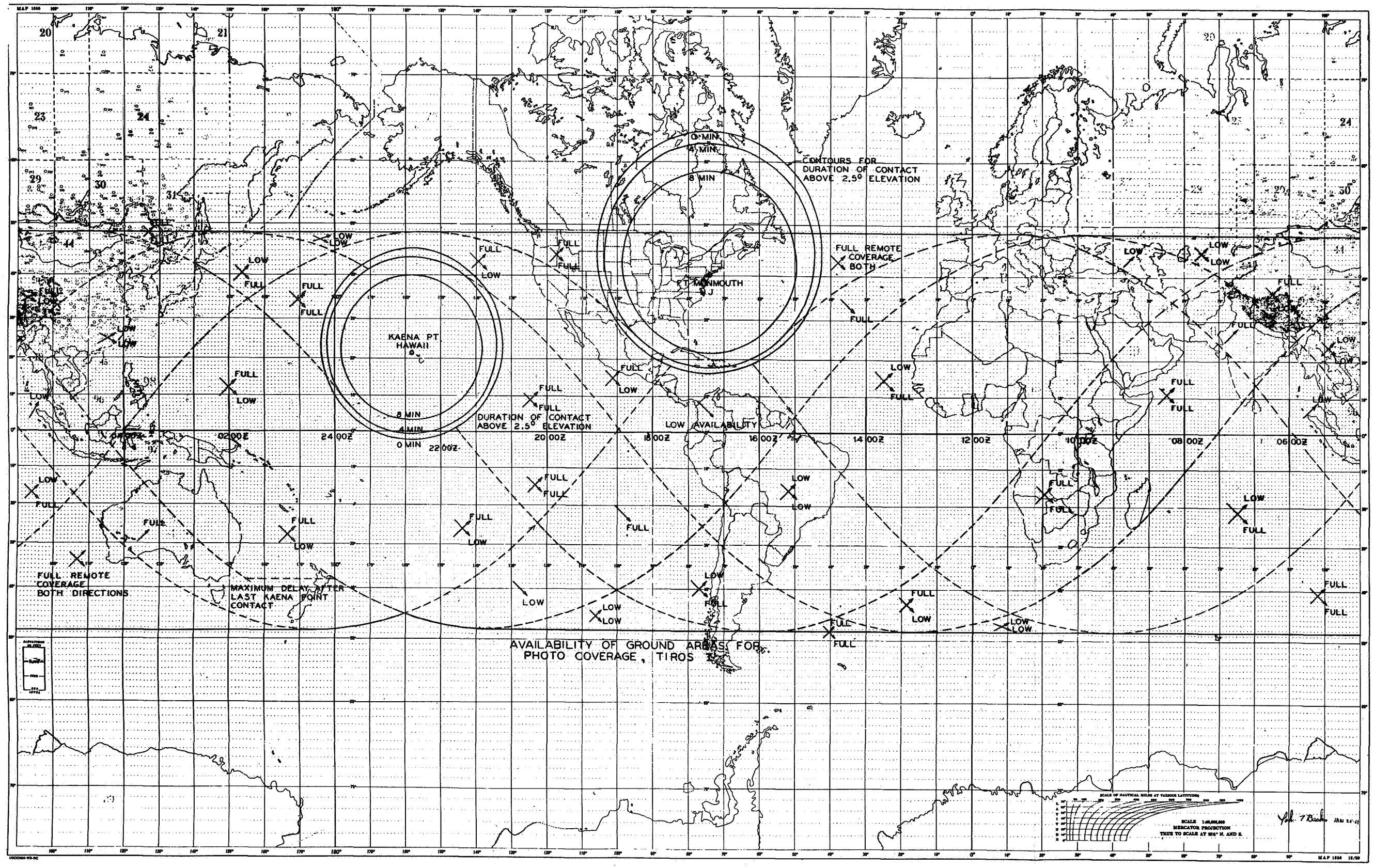

1173250

Figure 25. Availability of Ground Areas for Photo-coverage, TIROS I

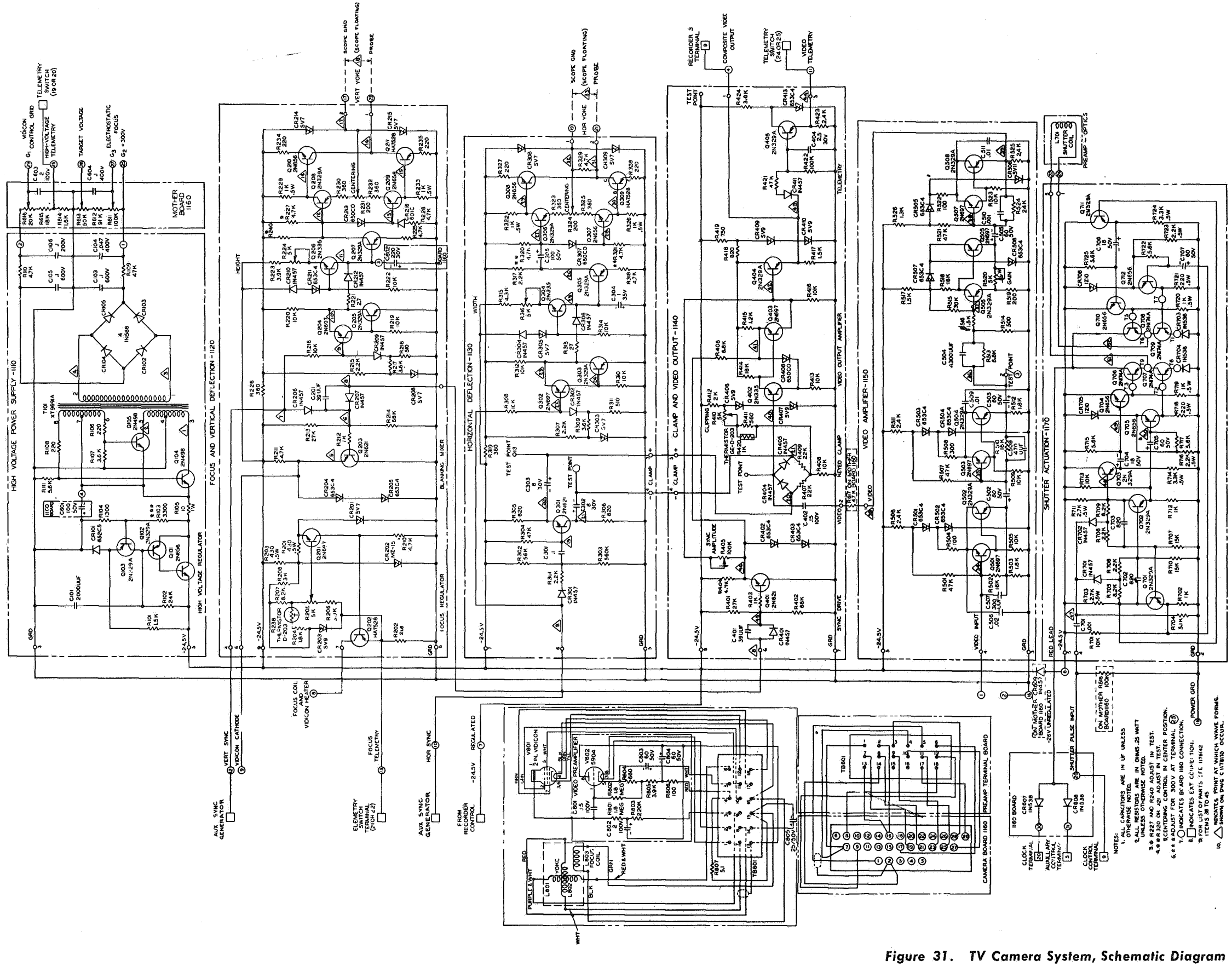

Figure 31. TV Camera System, Schematic Diagram

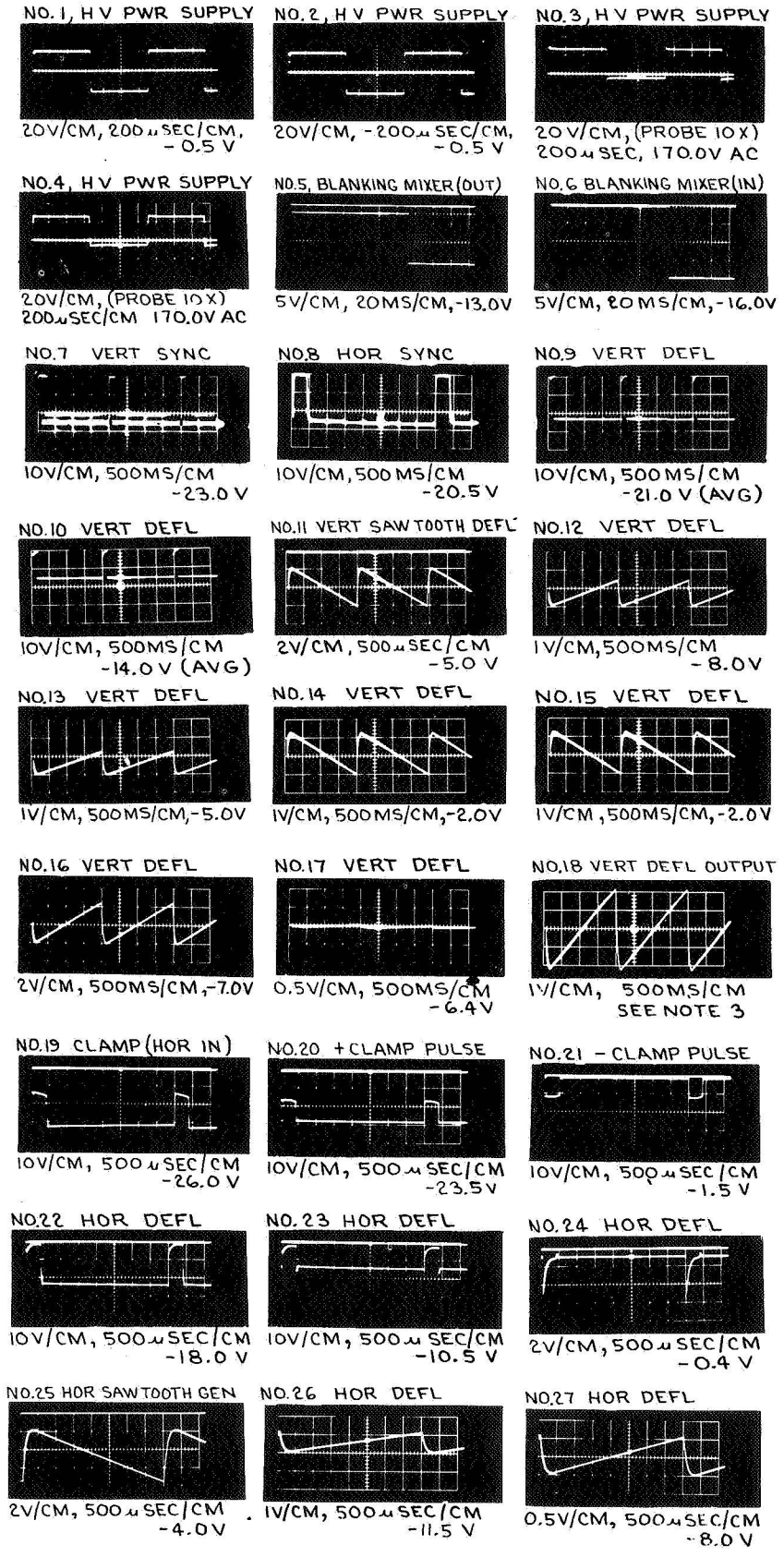

NOTES:

1. SET-UP OF OSCILLOSCOPE IS SHOWN BELOW EACH WAVE FORM. SCOPE ON DC VOLTAGE MEASURED TO GROUND.
2. ALL VOLTAGES ARE D C UNLESS OTHERWISE SPECIFIED.
3. SCOPE GROUND TO NUMBER 17. PROBE TO NUMBER 16. EQUAL DEFLECTION EACH SIDE OF CL. CL GROUND LEVEL.
4. SCOPE GROUND TO NUMBER 32. PROBE TO NUMBER 31. EQUAL DEFLECTION EACH SIDE OF CL. CL GROUND LEVEL.
5. WAVE FORMS ARE OBTAINED AT INDICATED POINTS ON E 1173027

1178170

Figure 32. Waveforms, TV Camera Electronic Circuits

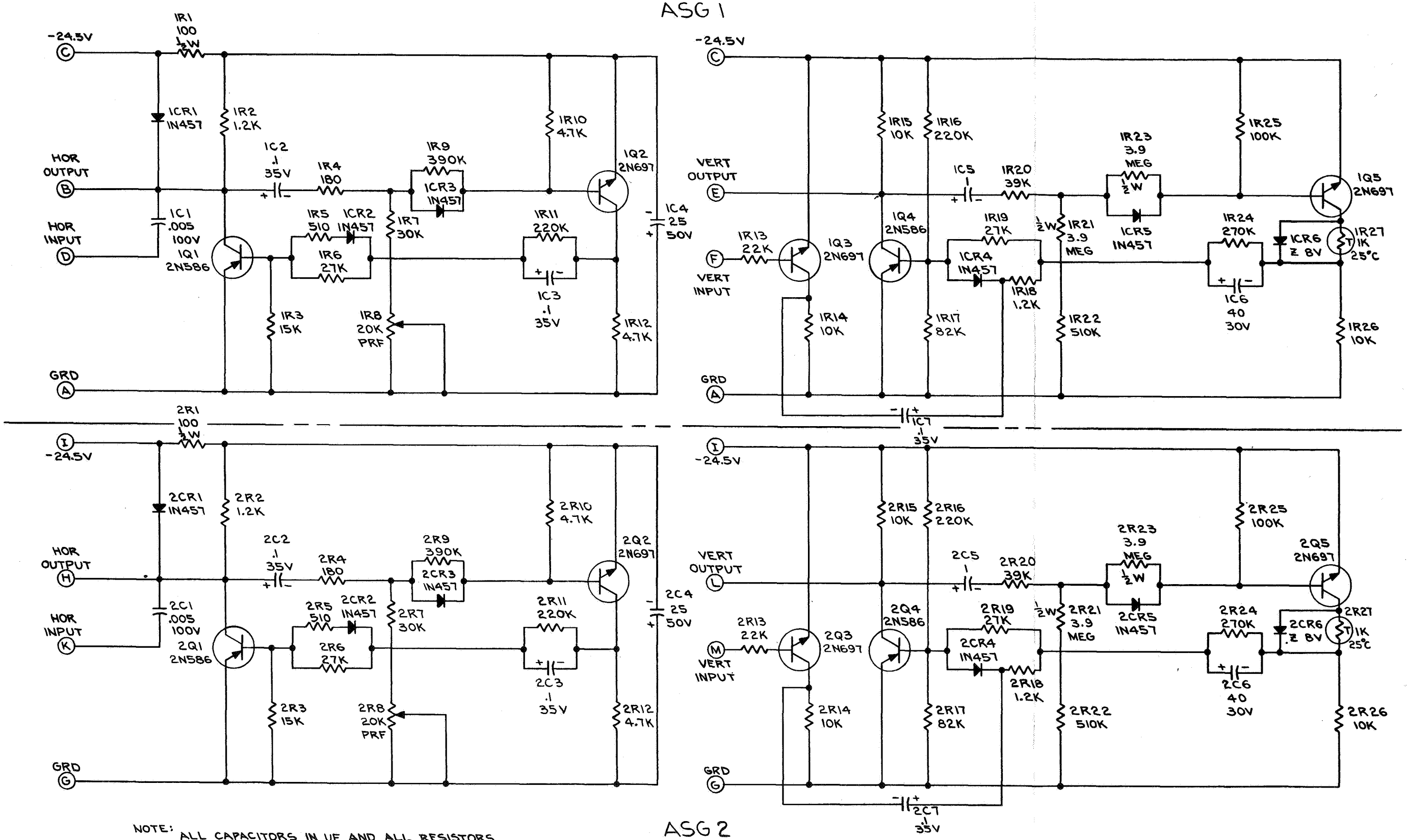

NOTE: ALL CAPACITORS IN UF AND ALL RESISTORS IN OHMS ½W UNLESS OTHERWISE NOTED.

1177 576

Figure 33. Auxiliary Sync Generator, Schematic Diagram

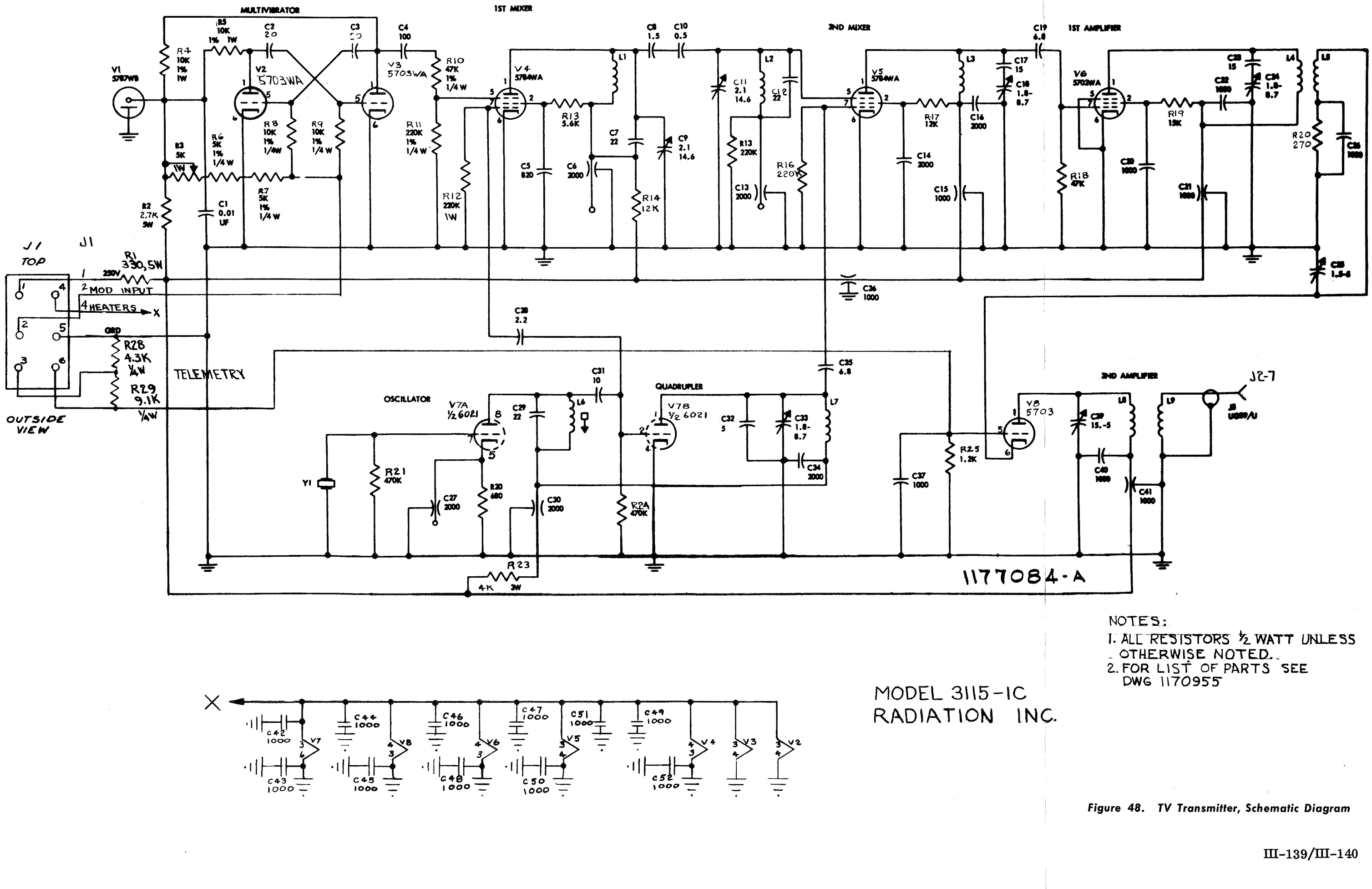

NOTES:
1. ALL RESISTORS ½ WATT UNLESS OTHERWISE NOTED.
2. FOR LIST OF PARTS SEE DWG 1170955

MODEL 3115-1C
RADIATION INC.

Figure 48. TV Transmitter, Schematic Diagram

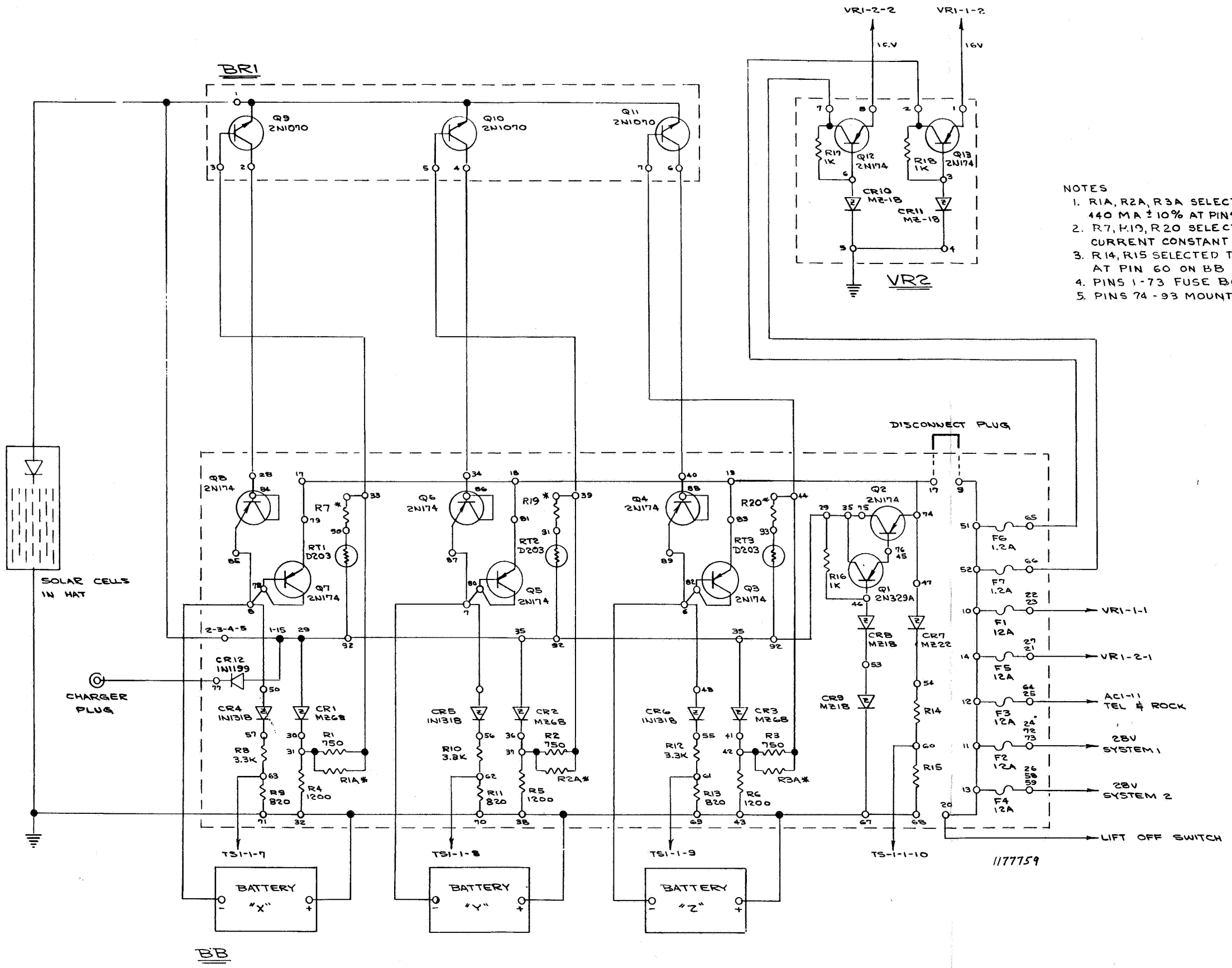

NOTES
1. R1A, R2A, R3A SELECTED TO GIVE 440 MA ± 10% AT PINS 2,4,6 ON BR1
2. R7, R19, R20 SELECTED TO KEEP CURRENT CONSTANT AT 0°C TO 55°C
3. R14, R15 SELECTED TO GIVE 1 VOLT AT PIN 60 ON BB
4. PINS 1-73 FUSE BOARD
5. PINS 74-93 MOUNTING BOARD

Figure 91. Power Control Units, Schematic Diagram